Theoretische Physik

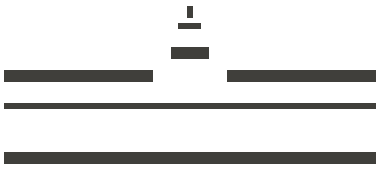

Westfälische
Wilhelms-Universität
Münster

Double parton scattering in jet production processes at the LHC

Inaugural-Dissertation
zur Erlangung des Doktorgrades
der Naturwissenschaften im Fachbereich Physik
der Mathematisch-Naturwissenschaftlichen Fakultät
der Westfälischen Wilhelms-Universität Münster

vorgelegt von
Oleh Fedkevych
aus Zjurupynsk, Ukraine
- 2019 -

Theoretische Physik

Double parton scattering in jet production processes at the LHC

Inaugural-Dissertation
zur Erlangung des Doktorgrades
der Naturwissenschaften im Fachbereich Physik
der Mathematisch-Naturwissenschaftlichen Fakultät
der Westfälischen Wilhelms-Universität Münster

vorgelegt von
Oleh Fedkevych
aus Zjurupynsk, Ukraine
- 2019 -

Dekan:	Prof. Dr. Gerhard Wilde
Erste Gutachterin:	Prof. Dr. Anna Kulesza
Zweiter Gutachter:	Apl. Prof. Dr. Christian Klein-Bösing
Tag der mündlichen Prüfung:	.....
Tag der Promotion:	.....

Abstract

The composite nature of hadrons implies that more than two partons can be involved in several hard, semi-hard or soft interactions in one hadron-hadron collisions. Such processes are known as *multiple parton interaction* (MPI) processes. The *double parton scattering* (DPS) is a process involving two hard interactions per one hadron-hadron collision which provides a cleanest MPI system. Moreover, the DPS is the most often occurring type of MPI at high transverse momenta of the observed final state. The DPS, among others, constitutes an important background to many Standard Model, as well as Beyond the Standard Model processes. In particular, DPS plays a crucial role for the specific kinematic regions of multi-jet pair production. Theoretical studies of DPS phenomena indicate a fundamental connection between DPS and various partonic correlations. Experimental measurements of DPS performed at the Tevatron and the LHC suggest a presence of non-trivial correlations between proton's constituents. However, the nature of these correlations needs to be better understood. Therefore, studies of the DPS phenomena can provide valuable insights into proton's structure and dynamics of its constituents.

In the main part of this thesis we discuss the phenomenology of the four-jet DPS production in *proton-proton* (pp) and *proton-nucleus* (pA) collisions. We present simulations of the four-jet DPS signal performed with our standalone DPS Monte Carlo code. We provide a detailed study of the DPS and the *single parton scattering* (SPS) contributions to the the four-jet production in pp collisions. In particular, we study the relative importance of both contributions for different jet cuts and collision energies. We show how one can combine DPS events generated with our DPS code at the partonic level and the *initial and final state radiation* (ISR and FSR) simulations implemented in the `Pythia` event generator. We present necessary checks of an interface between our DPS code and the `Pythia` event generator and study the impact of the ISR and FSR effects on our four-jet DPS simulations. Our DPS code allows to use different models of *double parton distribution functions* (dPDFs). In particular, we study the impact of the Gaunt & Stirling dPDFs (GS09) on the four-jet DPS production in pp collisions and identify the regions of the final state phase space where GS09 effects become important. After discussing DPS in pp collisions we extend our DPS calculations to pA collisions using the framework proposed by Strikman & Treleani. We study the interplay between the DPS signal and the SPS background in pA collisions and estimate the overall impact of the *nuclear parton distribution functions* (nPDFs) on the four-jet DPS productions in pA collisions.

In the remaining part of this thesis we provide a detailed comparison between the formalism we have used to describe DPS in pp and pA collisions against models used in the `Pythia` event generator. First, we study in detail similarities and differences between the GS09 approach and modelling of dPDFs in `Pythia` and the role of momentum and number correlations induced by dPDFs sum rules proposed by Gaunt & Stirling. Furthermore, we study the role of momentum and number correlations induced by GS sum rules in the phenomenology of the four-jet DPS production. Secondly, we provide a detailed comparison between the predictions of Strikman & Treleani against the predictions of the `Angantyr` model of pA collisions which was recently implemented into the `Pythia` event generator.

Zusammenfassung

Die zusammengesetzte Natur der Hadronen impliziert, dass mehr als zwei Partonen an mehreren harten, halbharten oder weichen Wechselwirkungen in einer Hadron-Hadron-Kollision beteiligt sein können. Solche Prozesse werden als *Multiparton-Wechselwirkung* oder MPI bezeichnet. Die *Doppelpartonstreuung* (DPS) ist ein Prozess, die zwei harte Wechselwirkungen pro Hadron-Hadron-Kollision umfaßt. Sie stellt eins der reinsten MPI-Systeme dar. Außerdem ist die DPS die am häufigsten vorkommende MPI-Art bei hohen Transversalimpulsen des beobachteten Endzustands. Die DPS bildet unter anderem einen wichtigen Hintergrund für viele Standardmodell- und Jenseits-des-Standardmodell-Prozesse. Insbesondere spielt die DPS für die spezifischen kinematischen Bereiche der multiplen Jet-Paar-Produktion eine entscheidende Rolle. Theoretische Untersuchungen von DPS-Phänomenen weisen auf eine fundamentale Verbindung zwischen DPS und verschiedenen partonischen Korrelationen hin. Experimentelle Messungen der DPS, die am Tevatron und am LHC durchgeführt wurden, legen nahe, dass nichttriviale Korrelationen zwischen den Protonenbestandteilen bestehen. Die Art dieser Zusammenhänge muss jedoch noch besser verstanden werden. Deshalb können Untersuchungen der DPS-Phänomene wertvolle Einblicke in die Struktur des Protons und die Dynamik seiner Bestandteile geben.

Im Hauptteil dieser Dissertation wird die Phänomenologie der Produktion von vier Jets in *Proton-Proton-* (pp-) und *Proton-Kern-* (pA-)Kollisionen diskutiert. Wir präsentieren Simulationen des Vier-Jet-DPS-Signals, die mit unserem eigenständigen DPS-Monte-Carlo-Computerprogramm durchgeführt wurden. Wir legen eine detaillierte Studie der Beiträge der DPS und der *Einfachpartonstreuung* (SPS) für die Vier-Jet-Produktion in pp-Kollisionen vor. Insbesondere vergleichen wir den Einfluss beider Beiträge in Abhängigkeit verschiedener Jetparametrisierungen und Kollisionsenergien. Wir zeigen, wie man auf partonischem Niveau DPS-Ereignisse, die mit unserem DPS-Program generiert wurden, mit dem *Partonen-Schauer* des `Pythia`-Ereignisgenerators kombinieren kann. Wir diskutieren Tests einer Schnittstelle zwischen unserem DPS-Programm und dem `Pythia`-Ereignisgenerator und untersuchen die Auswirkungen der Partonen-Schauer-Effekte auf unsere Simulationen der Vier-Jet-Produktion. Unser DPS-Programm ermöglicht die Verwendung verschiedener Modelle von *Doppelpartondichtefunktionen* (dPDFs). Insbesondere untersuchen wir den Einfluss der Gaunt & Stirling-dPDFs (GS09) auf die Vier-Jet-Produktion in pp-Kollisionen und identifizieren diejenigen Bereiche des Endzustand-Phasenraums, in denen GS09-Effekte wichtig werden. Nach Erörterung der DPS für pp-Kollisionen dehnen wir unsere DPS-Berechnungen auf pA-Kollisionen unter Verwendung des von Strikman & Treleani vorgeschlagenen Modells aus. Wir untersuchen das Zusammenspiel zwischen dem DPS-Signal und dem SPS-Hintergrund für pA-Kollisionen und schätzen den Gesamteinfluss der *Kernpartondichtefunktionen* (nPDFs) auf die Vier-Jet-Produktion bei pA-Kollisionen. Im verbleibenden Teil dieser Dissertation stellen wir einen detaillierten Vergleich zwischen dem Formalismus, den wir zur Beschreibung der DPS in pp- und pA-Kollisionen verwendet haben, und Modellen, die im `Pythia`-Ereignisgenerator verwendet werden, an. Wir untersuchen erstens detailliert Ähnlichkeiten und Unterschiede zwischen dem GS09-Ansatz und der Modellierung der dPDFs in `Pythia`. Außerdem untersuchen wir die Rolle derjenigen Impuls- und Zahlenkorrelationen, die durch die von Gaunt & Stirling vorgeschlagenen dPDF-Summenregeln induziert werden. Darüber hinaus untersuchen wir die Rolle derjenigen Impuls- und Zahlenkorrelationen, die durch GS-Summenregeln in der Phänomenologie der Vier-Jet-DPS-Produktion

induziert werden. Zweitens bieten wir einen detaillierten Vergleich zwischen den Vorhersagen von Strikman & Treleani und den Vorhersagen des `Angantyr`-Modells für pA-Kollisionen, das kürzlich in den `Pythia`-Ereignisgenerator implementiert wurde.

Acknowledgements

I would like to being by thanking to my supervisor, Anna Kulesza, for accepting me as a PhD student, providing me an interesting research topic and for all her help and guidance during the work on this thesis. I also would like to thank her for all her support, encouragement and suggestions provided whenever I was facing difficulties during my PhD time.

I am very grateful to Michael Klasen and Christian Weinheimer as well as to all the other board members the Research Training Group "GRK 2149: Strong and Weak Interactions - from Hadrons to Dark Matter" for accepting me as a GRK student. My PhD training within the framework of "GRK 2149" included a three months experimental research project dedicated to the study of various aspect of the simulation of multiple parton interaction signals with the `Pythia` event generator. I want to thank to my second supervisor, Christian Klein-Bösing, for guiding me during the work on this experimental project as well for the useful comments and discussions.

My research in the period of time 01.10.2018 - 31.01.2019 has received funding from European Union's Horizon 2020 research and innovation programme as part of the Marie Skłodowska-Curie Innovative Training Network MCnetITN3 (grant agreement no. 722104). I express my gratitude to all members of the MCnet advisory board for accepting me for the Marie Skłodowska-Curie Early Stage Researcher short-term research project which was performed at the Lund University, Sweden. I express my gratitude to Leif Lönnblad, Torbjörn Sjöstrand and Johannes Bellm for supervising me during the work on my Marie Skłodowska-Curie project as well as for interesting and productive discussions. I am also very grateful to Torbjörn Sjöstrand for introducing modifications to the `Pythia` code necessary to combine my simulations with `Pythia`, and to Jonathan Gaunt for providing me grids with GS09 dPDFs covering the range of parameters relevant for my research.

I also would like to express my gratitude to Christian Bierlich, Peter Christiansen, Gösta Gustafson, Karol Kovařík, Olivier Mattelaer, Stefan Prestel, Christian Reuschle, and Harsh Shah for fruitful and useful discussions. I also acknowledge all members of the Institute of Theoretical Physics at the University of Münster and all members of the Theoretical Particle Physics Group of the Lund University for warm and friendly atmosphere.

Last but not least I would like to thank my family - my parents Tatyana and Oleh, my wife Mariia, my uncles Sergei and Igor, my parents-in-law Ekaterina and Vladislav, my grandparents Tamara, Lubov and Nikolai, and my cousin Angelina. All of them have supported me in their own way over the years.

Declaration

All diagrams in this thesis unless the opposite is explicitly stated were created with the JaxoDraw code [304]. All plots with our results were created by means of the Matplotlib [305], NumPy [306] and SciPy [307] libraries. The code we developed to simulate DPS processes is using GSL [294] and LHAPDF6 [296] libraries.

Contents

Chapter 1

Introduction to QCD

In this chapter we shall review the main formulae and concepts of the *quantum chromodinamics* (QCD) we need to describe double parton scattering. Since we are going to talk about well established ideas we shall not give any proofs. The details can be found either in the existing textbooks, for example [1] - [5], or in original publications.

1.1 The QCD Lagrangian

A concept of symmetry can be seen as a cornerstone of modern particle physics since the requirement to have a theory being invariant under the action of a certain symmetry group automatically constrains the number of possible terms in a Lagrangian. Moreover, due to the Noether's theorem, each continuous symmetry leads to a conserved current and a corresponding quantum charge. Therefore, a commonly used approach is to request first a certain symmetry of a new theory and then write down all possible invariant terms.

Let us illustrate this idea by demonstrating how the Lagrangian of *quantum electrodynamics* (QED) can be constructed using the Lagrangian of a free Dirac field as a starting building block. The Lagrangian for the free Dirac field is given by

$$\mathcal{L}_{free} = \bar{\psi}\left(i\partial\!\!\!/ - m\right)\psi, \tag{1.1}$$

where $\partial\!\!\!/ \equiv \gamma^\mu \partial_\mu$, ψ is a four-component Dirac spinor and $\bar{\psi} \equiv \psi^\dagger \gamma^0$ is its Dirac conjugate. This Lagrangian is invariant under so called *global gauge transformations* $\psi(x) \to e^{ie\theta}\psi(x)$, where θ is a constant number and e is a coupling constant. However, if we promote θ to an arbitrary function of a space-time (so called *local gauge transformations*), the Lagrangian will not be invariant any more. One can restore the invariance by changing the four-derivative ∂_μ to a new object called *covariant derivative* $D_\mu = \partial_\mu + ieA_\mu$, where an auxiliary field A_μ, also called a *gauge field*, transforms under the local gauge transformation as $A_\mu \to A_\mu - \frac{1}{e}\partial_\mu\theta$, and hence the new Lagrangian

$$\mathcal{L}_{int} = \bar{\psi}\left(iD\!\!\!/ - m\right)\psi = \bar{\psi}\left(i\partial\!\!\!/ - m\right)\psi - e\bar{\psi}A\!\!\!/\psi \tag{1.2}$$

is invariant under the local gauge transformation $\psi(x) \to e^{ie\theta(x)}\psi(x)$.

Now, if we would like to identify the field A_μ with a physical field we also need to add to Eq. 1.2

a term which will describe the propagation of the field A_μ in the absence of interactions. Therefore,

$$\mathcal{L}_{QED} = \bar{\psi}\left(i\not{D} - m\right)\psi - \frac{1}{4}F_{\mu\nu}F^{\mu\nu}, \tag{1.3}$$

where $F_{\mu\nu} = \partial_\mu A_\nu - \partial_\nu A_\mu$ is a gauge-invariant antisymmetric tensor of the second rank also called *electromagnetic tensor*.

The considerations above show how the requirement to have a Lagrangian being invariant under a certain set of transformations give rise to a new theory. Using a group theory language one can say that the requirement of the invariance of the free Dirac Lagrangian $\mathcal{L}_{free}$ is equivalent to the requirement of the invariance of the $\mathcal{L}_{free}$ under the action of the *abelian* U(1) symmetry group on its fermionic fields. The local gauge transformation $\psi(x) \to e^{ie\theta(x)}\psi(x)$ therefore describes how the Dirac field transforms under the action of the U(1) symmetry group. The U(1) symmetry group, in turn, is a simplest member of an infinite family of *non-abelian Lie groups* SU(N)[1]. It is therefore very tempting to try to construct Lagrangians being invariant under the action of another members of SU(N) family, *e.g* SU(2) or SU(3), and to investigate the properties of outcoming theories. In 1954 Yang and Mills [6] built a gauge theory invariant under the SU(2) symmetry group and used it to explain the isopin conservation in nucleon-nucleon interactions. This approach turned up to be very fruitful for the description of fundamental interactions. In particular, in 1973 Fritzsch, Gell-Mann and Leutwyler [7] proposed to describe strong interactions with the Yang-Mills theory based upon SU(3) symmetry group. In the same year Politzer [20] and independently Gross and Wilczek [21] published their groundbreaking papers where the asymptotic freedom was discovered. Therefore, 1973 can be seen as a year when a modern theory of strong interactions was born. In the rest of this section we will briefly sketch main concepts of this theory we will need later in this thesis.

The transformation of a Dirac field ψ under the action of the SU(3) symmetry group can be written as $\psi(x) \to e^{i\alpha^a t^a}\psi(x)$ where t^a are the generators of the SU(3) group (see Appendix A) and a sum over all repeating indices is assumed. Replacing a partial derivative ∂_μ in Eq. 1.1 by a covariant derivative $D_\mu = \partial_\mu - igA^a_\mu t^a$ one can write

$$\mathcal{L}_{QCD} = \bar{\psi}\left(i\not{D} - m\right)\psi, \tag{1.4}$$

and, therefore, the transformation law of the field A^a_μ is now given by

$$A^a_\mu \to A^a_\mu + \frac{1}{g}\partial_\mu\alpha^a + f^{abc}A^b_\mu\alpha^c, \tag{1.5}$$

where f^{abc} are the SU(3) group structure constants. The last term in Eq. 1.5 was absent in the case of QED and emerges due to the non-abelian nature of the SU(3) symmetry group.

The tensor $F^a_{\mu\nu}$ also acquires the additional term proportional to the structure constants f^{abc}:

$$F^a_{\mu\nu} = \partial_\mu A^a_\nu - \partial_\nu A^a_\mu + gf^{abc}A^b_\mu A^c_\nu, \tag{1.6}$$

[1] In this thesis we give only a necessary minimum of SU(N) properties essential to perform LO QCD computations, see Appendix A. A more detailed description can be found, for example, in [3], [5].

and, finally, the QCD (Yang-Mills) Lagrangian is [2]

$$\mathcal{L}_{QCD} = \bar{\psi}\left(i\not{D} - m\right)\psi - \frac{1}{4}F^a_{\mu\nu}F^{a\mu\nu}. \tag{1.7}$$

The fermions and bosons described by the QCD Lagrangian are called *quarks* and *gluons* respectively. The tensor $F^a_{\mu\nu}$ in Eq. 1.7 being contracted with itself will give, among others, terms involving products of three and four gauge fields A^a_μ. Such terms give rise to new types of Feynman graphs shown in Fig. 1.1 b) and c) which were absent in QED.

1.2 QCD Feynman rules

The quantization of non-abelian gauge theories is a highly non-trivial task which requires special procedures. The first results for one-loop diagrams were obtained by Feynman in 1963 [8] and De Witt in 1964 [9]. Three years later Faddeev and Popov proposed a general way to quantize non-abelean gauge theories valid for all orders in perturbation theory [10]. This procedure adds new unphysical anti-commuting scalar fields to the QCD Lagrangian called *Faddeev-Popov ghosts*. The ghosts give rise to negative probabilities that compensate unphysical contributions from the longitudinal parts of the gauge boson propagator and thus restore the unitarity and the gauge-invariance[3].

However, the necessity to use diagrams with Faddeev-Popov ghosts appears only in loop computations and in the case of tree-level scattering processes one can evaluate matrix elements without taking ghosts into account.[4] In this thesis we construct DPS processes out of two $2 \to 2$ *leading order* (LO) QCD processes and therefore in this section we provide only QCD Feynman rules necessary for such computations. Therefore, the QCD Lagrangian can be separated into two parts: the first part contains an interaction term proportional to $\bar{\psi}\not{A}^a t^a \psi$ and gives rise to the graph similar to the QED vertex which is shown in Fig. 1.1 a) and the second part contains new triple and quartic terms which give rise to so called *gluon self-interaction graphs* shown in Fig. 1.1 b), c). In addition to new vertices one also has to know Feynman rules for quark and gluon propagators. The form of a gluon propagator depends on a gauge chosen to quantize QCD Lagrangian. In Fig. 1.2 we list quark and gluon propagators for commonly used *covariant* and *axial gauges*.

1.3 Asymptotic freedom of QCD

One of the most common application of the field theory is evaluation of amplitudes which correspond to a probability of transition between two different states, say $|k_m\rangle$ and $|p_n\rangle$ where $\{k_m\}$ and $\{p_n\}$ are two sets of four momenta with m and n elements correspondingly. The amplitude for the transition between $|k_m\rangle$ and $|p_n\rangle$ is given then by the eigenvalues of a certain operator $\hat{\mathrm{S}}$ called *scattering matrix*. Therefore, one has to evaluate the following quantity $\langle k_m|\hat{\mathrm{S}}|p_n\rangle$ called also the

[2] Here we omitted a term proportional to $F^a_{\mu\nu}\tilde{F}^{a\mu\nu}$ where $\tilde{F}^{a\mu\nu} = \varepsilon^{\mu\nu\rho\delta}F^a_{\rho\delta}/2$. This term leads to a non-trivial QCD vacuum structure and violation of CP symmetry which was not observed experimentally (so called *strong CP problem*, see [12]).

[3] The De Witt-Faddeev-Popov method is based upon so called *path integral formulation* of gauge theories. Later gauge theories were also quantized in the *covariant operator formalism*, see [11].

[4] This depends on the diagrammatic technique being used to evaluate diagrams with triple gluon vertex. See, for example, Peskin and Schroeder [5] Chapter 17.2 and Problem 17.3.

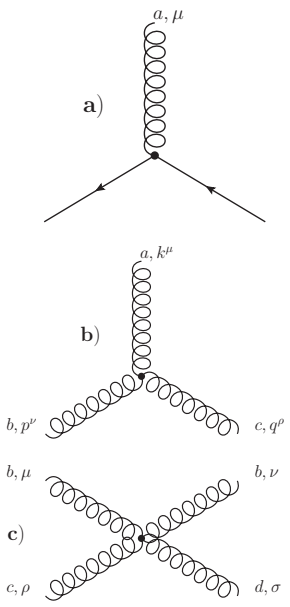

$$ig\gamma^{\mu}t^{a}.$$

$$gf^{abc}\left[g^{\mu\nu}\left(k-p\right)^{\rho}+g^{\nu\rho}\left(p-q\right)^{\mu}+g^{\rho\mu}\left(q-k\right)^{\nu}\right].$$

$$\begin{aligned}&-ig^{2}f^{abe}f^{cde}\left(g^{\mu\rho}g^{\nu\sigma}-g^{\mu\sigma}g^{\nu\rho}\right)+\\&-ig^{2}f^{ace}f^{bde}\left(g^{\mu\nu}g^{\rho\sigma}-g^{\mu\sigma}g^{\nu\rho}\right)+\\&-ig^{2}f^{ade}f^{bce}\left(g^{\mu\nu}g^{\rho\sigma}-g^{\mu\rho}g^{\nu\sigma}\right).\end{aligned}$$

Figure 1.1: Basic QCD graphs and corresponding vertex factors. The triple gluon vertex factor depends on four-momenta of gluons and therefore on the direction of the momenta flow. Here we choose all four-momenta to be flowing towards to the center of the vertex.

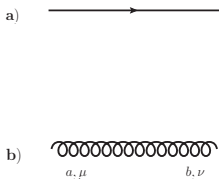

$$\frac{i}{\not{p}-m+i\varepsilon}.$$

$$\begin{aligned}&\frac{i}{q^{2}+i\varepsilon}\left[-g_{\mu\nu}+(1-\lambda)\frac{q_{\mu}q_{\nu}}{q^{2}+i\varepsilon}\right]\delta^{ab}\,(\text{covariant gauge}),\\&\frac{i}{q^{2}+i\varepsilon}\left[-g_{\mu\nu}+\frac{n_{\mu}q_{\nu}+n_{\nu}q_{\mu}}{n\cdot q}-n^{2}\frac{q_{\mu}q_{\nu}}{(n\cdot q)^{2}}\right]\delta^{ab}\,(\text{axial gauge}).\end{aligned}$$

Figure 1.2: Fermion and gluon propagators in QCD.

S-matrix element. It is remarkable that one can relate S-matrix elements with a Fourier transform of quantities called *n-point Green functions* using so called LSZ[5] reduction formula [13]:

$$\langle k_1\dots k_m|\hat{\mathrm{S}}|p_1\dots p_n\rangle \Longleftrightarrow \langle\Omega|\hat{\mathrm{T}}\left\{\phi(x_1)\dots\phi(x_n)\phi(y_1)\dots\phi(y_n)\right\}|\Omega\rangle, \tag{1.8}$$

where sets of variables $\{x_n\}$ and $\{y_n\}$ are Fourier conjugates of four-momenta $\{p_n\}$ and $\{k_n\}$, $\hat{\mathrm{T}}$ is a time-ordering operator, $\phi(x_1)\dots\phi(x_n)\phi(y_1)\dots\phi(y_n)$ is a certain combination of the field operators and $|\Omega\rangle$ is a ground-state of the theory under consideration. There are different methods to compute Green functions. One of the most commonly used approaches is the expansion of $\langle\Omega|\hat{\mathrm{T}}\left\{\phi(x_1)\dots\phi(x_n)\phi(y_1)\dots\phi(y_n)\right\}|\Omega\rangle$ in perturbation series in powers of a coupling constant g. This approach allows to get many important results, in particular it allows to derive equation which governs the evolution of the QCD coupling constant which was verified experimentally, see Fig. 1.6. The concept of the running coupling is related to the so called *renormalization* procedure which we briefly describe below. As a starting point let us consider a toy ϕ^3 model with the Lagrangian given

[5] After Lehmann, Symanzik and Zimmermann who derived it at the first time.

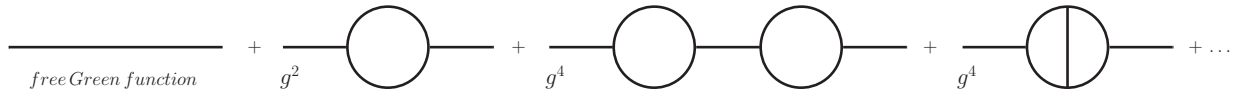

Figure 1.3: Perturbation series for two-point correlations function for the ϕ^3 model.

by

$$\mathcal{L}_{\phi^3} = \frac{1}{2}\left(\partial_\mu \phi\right)^2 - \frac{1}{2}m^2\phi^2 - \frac{g}{3!}\phi^3. \tag{1.9}$$

In the ϕ^3 theory one can write the two-point Green function $\langle\Omega|\hat{\mathrm{T}}\left\{\phi(x)\,\phi(y)\right\}|\Omega\rangle$ in form of a series with diagrammatic representation shown in Fig. 1.3. Careful examination of the diagrammatic expansion allows to identify subseries of diagrams with similar structures as in Fig. 1.4. It was shown by Dyson [14] that one can sum up such subseries in all orders of g^2 in a way similar to the summation of the geometric series. Therefore, for the subseries shown in Fig. 1.4 one has to evaluate only a contribution of the order of g^2 and then perform a summation of the whole subseries. This summation, however, comes at cost. Namely, such summation procedure will lead to a redefinition of parameters in a starting Lagrangian. For example, a sum of the series shown in Fig. 1.4 will result in a correction to the pole of the propagator of the scalar field ϕ:

$$\frac{i}{p^2 - m^2 + i\varepsilon} \longrightarrow \frac{i}{p^2 - m^2 + i\varepsilon} \times \sum_{n=0}^{\infty}\left(\frac{\Sigma(p)}{p^2 - m^2 + i\varepsilon}\right)^n = \frac{i}{p^2 - m^2 - \Sigma(p) + i\varepsilon}, \tag{1.10}$$

where Σ is a contribution of the term of the order of g^2 in Fig. 1.4. We see that summation of the subseries shown in Fig. 1.4 in all orders of perturbation theory "shifts" the pole in the propagator of the scalar field ϕ from m^2 to $m^2 + \Sigma(p)$ which can be seen as a redefinition of the "bare" mass parameter m^2. One can find similar series which being summed will lead to the redefinition of the coupling constant g and of the normalization of the field operator ϕ. The redefinition of the mass, coupling constant and normalization of the field operators is called *renormalization procedure* and it can be performed in different ways. In practice one fixes the form of the redefined parameters by imposing so called *renormalization conditions*. In the case of $\Sigma(p)$ one can, for example, require

$$\Sigma(p)\Big|_{p^2=-\mu^2} = 0, \tag{1.11}$$

$$\frac{d}{dp^2}\Sigma(p)\Big|_{p^2=-\mu^2} = 0, \tag{1.12}$$

where μ is a certain parameter called *renormalization scale*. The arbitrary choice of the renormalization scale, however, should not affect predictions of the theory. Solution to this problem brings us to the concept of the running mass and the running coupling, where both parameters become functions of the renormalization scale μ such that the variation of the Green function with respect to μ is compensated by the variation of mass and coupling constants. Theories where such redefinition of parameters is possible at all orders in the perturbation expansion are called *renormalizable*.

In 1970 Callan [15] and Symanzik [19] generalized the aforementioned ideas and derived a differential equation which provides a connection between the renormalized n-point Green function

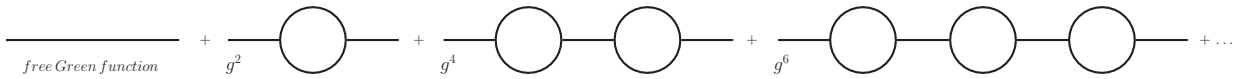

Figure 1.4: Example of the Dyson series for the two-point correlations function for the ϕ^3 model.

and the renormalization scale μ:

$$\left[\mu\frac{\partial}{\partial\mu}+\beta(g)\frac{\partial}{\partial g}+n\gamma(g)\right]\langle\Omega|\hat{\mathrm{T}}\left\{\phi(x_1)\dots\phi(x_n)\phi(y_1)\dots\phi(y_n)\right\}|\Omega\rangle=0, \tag{1.13}$$

where $\beta(g)$ and $\gamma(g)$ are certain functions which compensate the changes in n-point Green function due to the changes in the renormalization scale μ. For example, one can show that the β-function[6] in Eq. 1.13 describes the speed of change of the coupling constant g with the renormalization scale μ:

$$\beta(g)=\mu\frac{\partial}{\partial\mu}g. \tag{1.14}$$

This equation is called *renormalization group equation* and its solution determines the dependence of the coupling constant g on the renormalization scale μ.

We shall note here that so far we were not discussing the structure of terms in the perturbation series shown in Fig. 1.3. However, the evaluation of the contribution of the order of g^2 shown in Fig. 1.4 gives an infinite value of $\Sigma(p)$. The corresponding expression for $\Sigma(p)$ is proportional to the integral over the loop four-momentum q:

$$\Sigma(p^2)\sim\int\frac{d^4q}{[(p+q)^2-m^2+i\varepsilon]\,[q^2-m^2+i\varepsilon]}, \tag{1.15}$$

where p and q are four-momenta assigned as in Fig. 1.5. Since the value of the four-momentum q is not fixed by the energy-momentum conservation, the integration in Eq. 1.15 runs over the whole four-volume d^4q which at high values of q yields

$$\int\frac{d^4q}{[(p+q)^2-m^2+i\varepsilon]\,[q^2-m^2+i\varepsilon]}\approx\int\frac{d^4q}{q^4}\sim\int\frac{dq}{q}, \tag{1.16}$$

which is a logarithmically divergent quantity. The divergence in Eq. 1.16 can be regularized in different ways. One can, for example, impose an upper integration limit Λ which makes the integral over d^4q convergent. Another commonly used method is so called *dimensional regularization* [17]. According to this approach one makes the loop integrals as in Eq. 1.16 functions of the dimensionality of the space-time d by changing the integration measure as $d^4q\to d^dq$. For the sufficiently small values of d the integral in Eq. 1.16 will become convergent which allows to evaluate the loop integral in d-dimensions. After performing the integration in d-dimensions one restores the correct dimensionality by taking the limit $d\to4$. The final expression should have a well defined limit as $d\to4$.

[6]The modern name β-function was introduced in paper of Callan [15] and Symanzik [19]. However, the idea of scaling behaviour was first developed in the earlier paper of Gell-Mann and Low [18] and in the PhD-thesis of Petermann written under the supervision of Stueckelberg [16]. A pedagogical introduction to the Callan-Symanzik equations and to the concept of running coupling can be found, for example, in [5].

However, the regularization of the loop integrals introduces to a theory a new scale called *regularization scale*. For example, if one regularizes the loop integrals by imposing an upper integration limit then the new scale is given by the cutoff parameter Λ. In case if one uses dimensional regularization the new scale is given by the parameter $\varepsilon = 4 - d$ which appears in the final expressions after taking the limit $d \to 4$. Therefore, one could expect that β- and γ-functions in the Callan-Symanzik equation would depend on the regularization scale. However, the remarkable property of the renormalizable theories is that both functions appear to be independent on the regularization scale in all orders of the perturbation theory. To prove this statement for each theory is a non-trivial task. The representative selection of proofs is given in the monograph of Collins [4]. The concrete form of β- and γ-functions has to be found by solving Eq. 1.13 at the given order in the perturbation theory. After computing the β-function one can substitute it into Eq. 1.14 and solve it for the coupling g which will give the evolution equation for the coupling constant as a function of the renormalization scale μ. In QED at the one-loop accuracy level the solution of Eq. 1.14 yields

$$g^2(\mu^2) = \frac{g^2(\mu^2_{QED})}{1 - \frac{g^2(\mu^2_{QED})}{12\pi^2} \log\left(\mu^2/\mu^2_{QED}\right)}, \tag{1.17}$$

which describes the evolution of g from the initial value of the renormalization scale μ_{QED} up to the higher values of μ. We see that in QED the increase of μ leads to the increase of the g^2. In case of the QCD the behaviour of the coupling constant, however, changes. In early seventies of the past century theoretical physicists started to understand that the theory of strong interactions, in order to be able to explain experimental data available at that time, must have the coupling constant which behaves inversely to the QED coupling. According to the monograph of Steven Weinberg [22], Chapter 18.7, one of the first scientists who came up with this idea was Anthony Zee. However, he did not publish this observation. In 1972 Gerardus 't Hooft developed the *background field* method and with its help demonstrated that in QCD $\beta(g) < 0$. In June 1972 at the conference on gauge theories in Marceille 't Hooft reported his results which, however, were not published, see [22], Chapter 18.7. One year later Gross and Wilczek [21] and independently Politzer [20] demonstrated that in the SU(N) non-abelian gauge theory at one-loop accuracy level

$$\beta(g) = -\frac{g^3}{(4\pi)^2}\left(\frac{11}{3}C_A - \frac{4}{3}N_f \mathrm{T_R}\right), \tag{1.18}$$

where N_f is a number of fermion species, C_A is the SU(N) group invariant and and $\mathrm{T_R}$ fixes normalization of the SU(N) generators, see Appendix A. In the case of the SU(3) symmetry group this equation becomes

$$\beta(g) = -\frac{g^3}{(4\pi)^2}\left(11 - \frac{2}{3}N_f\right), \tag{1.19}$$

which is always a negative quantity as long as $N_f \leq 16$.

After evaluation of the β-function one can solve the equation for running coupling constant

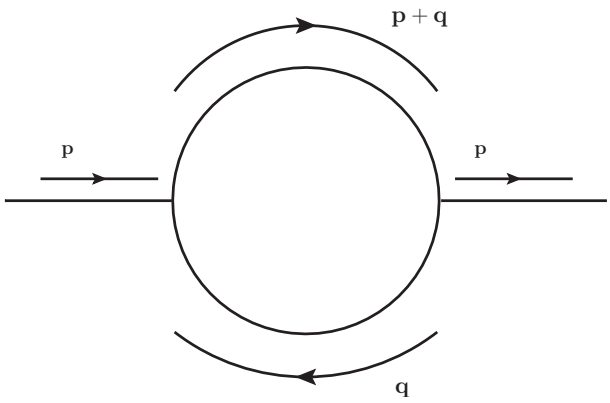

Figure 1.5: One loop contribution to $\Sigma(p)$ in the ϕ^3 model. Arrows here represent "circulation" of four-momenta inside the loop.

which at one-loop accuracy level yields

$$g^2(\mu^2) = \frac{g^2(\mu^2_{QCD})}{1 + \frac{g^2(\mu^2_{QCD})}{(4\pi)^2}\left(11 - \frac{2}{3}n_f\right)\log(\mu^2/\mu^2_{QCD})}, \tag{1.20}$$

or

$$\alpha_s(\mu^2) = \frac{\alpha_s(\mu^2_{QCD})}{1 + \frac{\alpha_s(\mu^2_{QCD})}{12\pi}\left(33 - 2n_f\right)\log(\mu^2/\mu^2_{QCD})}, \tag{1.21}$$

where $\alpha_s = g^2/4\pi$. We see that as soon as $n_f \leq 16$ the coupling constant of QCD *decreases* with the growing of the renormalization scale μ. This phenomenon is called *asymptotic freedom* and it is confirmed by various experimental measurements, see Fig. 1.6. In this thesis we will concentrate on the evaluation of the *leading order* (LO) DPS cross section and, therefore, through this thesis we will use one-loop expression for the running α_s given by Eq. 1.21. The details on higher order computations of the β-function and on α_s measurements can be found in [23], [24].

1.4 Factorization theorem and parton model

We have now constructed the QCD Lagrangian using formal considerations which were quite far away from the application to experimental results. In this section we shall briefly discuss two key ingredients, namely *parton model* and *factorization theorem*, that make a comparison between predictions of QCD and experimental data possible.

Let us start with a brief historical introduction to the parton model. According to its main assumption, a proton is a composite particle which consist of many point-like particles called *partons*. A strong indication that protons are of composite nature can be obtained from a comparison between proton and electron magnetic moments. If proton was an elementary particle its magnetic moment would be the same as the magnetic moment of an electron which is not the case[7]. In early sixties Gell-Mann [30] and Zweig [31] postulated proton to be a bound state of three new particles with

[7]The g-factor of a proton is $g_p \approx 5.96$ which is almost three times bigger than the g-factor of an electron. For the first measurements of the proton g-factor see [25], for the recent measurements see [26].

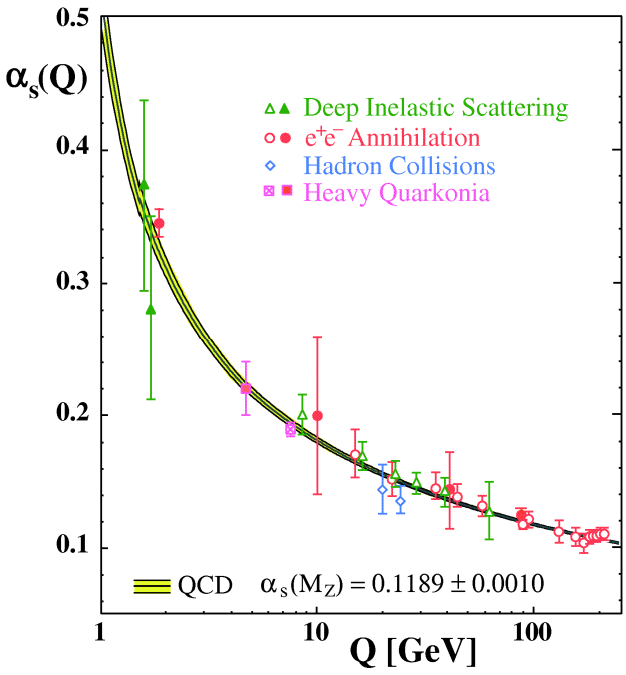

Figure 1.6: The combined measurements of α_s as a function of the renormalization scale $\mu \equiv Q$, from [23].

fractional electric charge called quarks. Later, to avoid spin-statistic violation, a new quantum number called *colour* was proposed by Greenberg [32] and by Han and Nambu [33] [8]. Assuming electrons being point-like particles, one could try to test the composite nature of proton studying the electron-proton collisions. In 1966 Bjorken [36] demonstrated that electron-proton cross sections for composite and point-like protons are of comparable size and, therefore, the composite nature of proton could be tested at the Stanford Linear Accelerator Center (SLAC-MIT experiment). A few years later first pioneering experimental studies took place [45] - [49]. We will not discuss the details of these measurements which can be found in the original publications and, for example, in the reviews [29] and [38]. Instead we briefly sketch main results and their role for the verification of the parton model.

As a starting point let us consider a process in which an electron scatters on a proton elastically:

$$e(k_1) + p(k_2) \to e'(k_1') + p(k_2'), \tag{1.22}$$

where k_1, k_2 (k_1', k_2') are four-momenta of the electron and proton before (after) the scattering. In the case of the point-like particles the cross section for this process is given by the well known Mott formula corrected for the scattering of two spin 1/2 particles[9]:

$$\frac{d\sigma^{elastic}_{point-like}}{d\Omega} = \left(\frac{d\sigma}{d\Omega}\right)_{Mott} \left[1 - \frac{q^2}{2M}\tan^2\left(\frac{\theta}{2}\right)\right], \tag{1.23}$$

[8] In parallel to the research done in the cited papers, many interesting results, *e. g.* existence of the colour charge, were obtained independently by Struminsky and by Bogoliubov, Struminsky and Tavkhelidze [35]. Unfortunately, these results were never published in regular journals and exist only in form of preprints. The translation of the paper of Struminsky is given in [34].

[9] The details can be found, for example, in [42], [43].

where M is a proton mass, q^μ is a four-momentum transferred $q^\mu = (k_1' - k_1)^\mu = (k_2' - k_2)^\mu$ and θ is a scattering angle. In 1950 this formula was generalized by Rosenbluth [39] for the case of the non-point-like proton

$$\frac{d\sigma^{elastic}}{d\Omega} = \left(\frac{d\sigma}{d\Omega}\right)_{Mott} \left[\mathcal{F}_1^2(Q^2) - \frac{\kappa Q^2}{4M^2}\mathcal{F}_2^2(Q^2) - \frac{Q^2}{2M^2}\left(\mathcal{F}_1(Q^2) + \kappa\mathcal{F}_2(Q^2)\right)^2 \tan^2\left(\frac{\theta}{2}\right)\right], \quad (1.24)$$

where κ is a parameter which describes the deviation of the proton g-factor from the g-factor of an electron $g_p = 2(1+\kappa) \approx 5.96$ and $q^2 = -Q^2 < 0$ is a virtuality of a photon being exchanged between the electron and the proton in the scattering process. The form-factors $\mathcal{F}_1$ and $\mathcal{F}_2$ are functions of only the absolute value of the four-momentum transferred between the electron and the proton. The linear combinations of $\mathcal{F}_1$ and $\mathcal{F}_2$ gives the spatial distribution of charge $G_E(Q^2)$ and magnetic moment $G_M(Q^2)$ of the proton in the momentum space:

$$G_E(Q^2) = \mathcal{F}_1(Q^2) + \frac{\kappa Q^2}{4M^2}\mathcal{F}_2(Q^2), \quad (1.25)$$

$$G_M(Q^2) = \mathcal{F}_1(Q^2) + \kappa\,\mathcal{F}_2(Q^2), \quad (1.26)$$

also called *Sachs form-factors*. By measuring $d\sigma^{elastic}/d\Omega$ one can extract the form-factors $\mathcal{F}_1$ and $\mathcal{F}_2$ out of the data, as it was first done by Hofstadter *et al.* [40], [41].

The approach of Rosenbluth turned out to work well at the low scattering energies. However, the growth of the momentum transferred in the elastic scattering process will lead to a decrease of the de Broglie wave-length of a photon exchanged between the electron and the proton. Following the analogy between the wave optics and the quantum mechanics, one could expect that a photon with a short de Broglie wave-length would resolve proton constituents if there are any. Therefore, it is natural to expect that at high value of the four-momentum transferred the electron in Eq. 1.22 will stop to interact with a whole proton but instead will interact with one of its constituents. Moreover, one would expect that the interaction of a such type will lead to the destruction of a proton. Schematically it can be written as

$$e(k_1) + p(k_2) \to e'(k_1') + X(k_2'), \quad (1.27)$$

where X stands for all possible unobserved final states as it shown in Fig. 1.7. Such scattering process is called *deep inelastic scattering* (DIS) and its differential cross section is described by so called *hadronic tensor* [10]:

$$W_{\mu\nu} = -\left(g_{\mu\nu} - \frac{q_\mu q_\nu}{q^2}\right) W_1\left(Q^2, \nu\right) + \frac{1}{M^2}\left(p_\mu - \frac{p\cdot q}{q^2}q_\mu\right)\left(p_\nu - \frac{p\cdot q}{q^2}q_\nu\right) W_2\left(Q^2, \nu\right), \quad (1.28)$$

where p_μ is a four-momentum of the proton, M is a proton mass, $\nu = E - E'$ is the difference between energies of outgoing and incoming electrons and q_μ is the four momentum of the virtual photon. These parameters are connected through $M\nu = p \cdot q$.

With the help of the hadronic tensor one can express the differential cross section for the process

[10] This parametrization of the hadronic tensor does not account for the spin of the target in DIS processes. For the parametrization of the hardonic tensor for the case of spin 1/2 targets see [44].

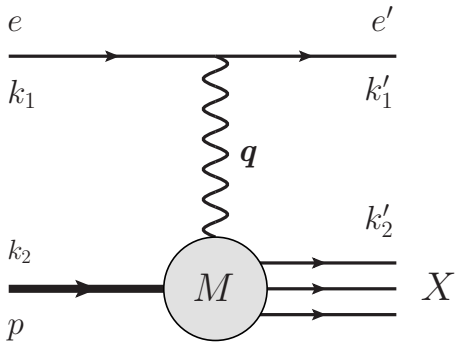

Figure 1.7: A schematic picture of electron-proton scattering studied in the SLAC-MIT experiment.

$e + p \to e' + X$ in the rest frame of a proton as

$$\frac{d\sigma^{\mathrm{DIS}}}{d\Omega} = \left(\frac{d\sigma}{d\Omega}\right)_{Mott} \left[W_2(Q^2,\nu) + 2W_1(Q^2,\nu)\,\tan^2(\theta/2)\right], \tag{1.29}$$

see [36], [38]. The form-factors W_1 and W_2, also called *structure functions*, are of a non-perturbative nature and thus have to be extracted out of the scattering data. Unlike the form-factors $\mathcal{F}_i(Q^2)$ in the Rosenbluth formula for the elastic cross section, the structure functions W_i depend on the virtuality of the exchanged photon q^2 and the change of its energy $\nu = E - E'$. Therefore, one can expect a strong difference in behaviour of the elastic and the DIS cross sections given by Eq. 1.24 and Eq. 1.29 correspondingly.

In 1969 first measurements of DIS processes were reported by the SLAC-MIT collaboration [45], [46]. The measured DIS cross section as a function of Q^2 is shown in Fig. 1.8. We see that the DIS cross section measured for different values of the invariant mass of the proton decay products W drastically differs from the elastic electron-proton cross section given by the Rosenbluth formula Eq. 1.24. We also see that the DIS cross section dominates over the elastic cross section for values of $Q^2 > 1$ GeV and that the DIS cross section demonstrates a mild dependence on the value of the invariant mass of the proton decay products. In the same year Bjorken analyzed the experimental data and demonstrated that in the limit when $Q^2 \to \infty$ and $\nu \to \infty$ such that the ratio Q^2/ν is fixed the form-factors W_1 and W_2 are functions only of a single variable $x = Q^2/2M\nu$ [37]:

$$\begin{aligned} \lim_{Q^2\to\infty,\,\nu\to\infty} MW_1(Q^2,\nu) &= F_1(x), \\ \lim_{Q^2\to\infty,\,\nu\to\infty} \nu W_2(Q^2,\nu) &= F_2(x), \end{aligned} \tag{1.30}$$

which was verified experimentally, see Fig. 1.9.

Moreover, in 1969 Callan and Gross [51] demonstrated that in the Bjorken limit $F_1(x)$ and $F_2(x)$ are not independent and are related through

$$2xF_1(x) = F_2(x), \tag{1.31}$$

which was also confirmed by the SLAC experiment, see Fig. 1.10. The Callan-Gross relation was derived using so called *current algebra methods*, see [53]. Within this approach one can derive Eq. 1.31 from the commutator of parton currents which depends on the spin of partons. The

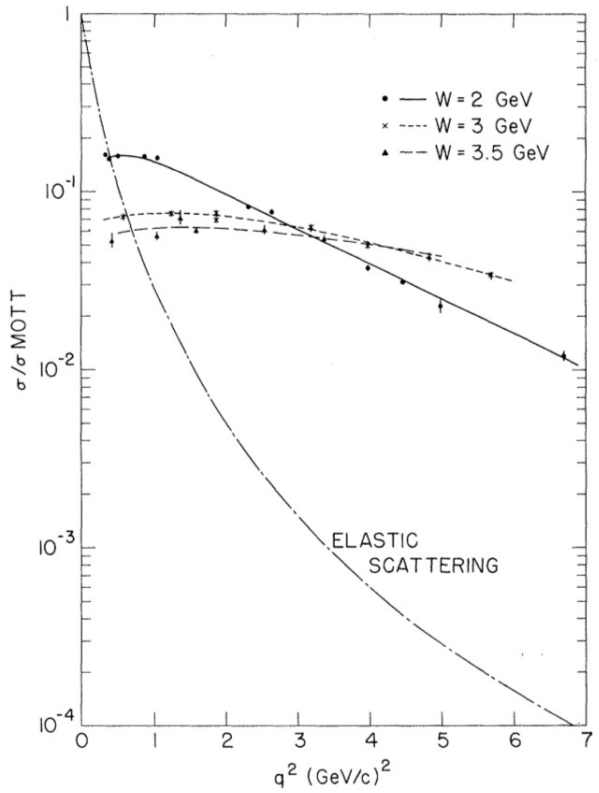

Figure 1.8: Deep inelastic scattering cross section measured by the SLAC-MIT collaboration for the different values of the invariant mass of the proton decay products W = 2, 3 and 3.5 GeV. The data is normalized to the Mott cross section, from [46].

Callan-Gross relation was derived assuming that partons have the spin equal to 1/2. Additionally, it was demonstrated that for the partons with the spin equal to 0 or 1 in the Bjorken-limit $xF_1 = 0$ [51]. Therefore, the experimental verification of the the Callan-Gross relation demonstrated that proton consist of the partons with the spin 1/2 which was the first step towards to the discovery of quarks and establishment of the modern theory of strong interactions.

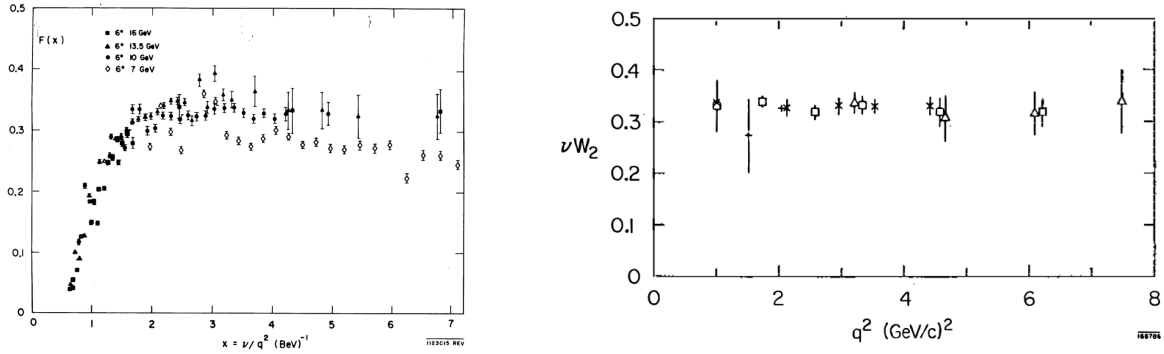

Figure 1.9: a) The experimental test of Bjorken scaling, from [50]. b) $\nu W_2(q^2, \nu)$ as a function of q^2 from $W > 2$ GeV at the fixed value of Bjoken variable $Q^2/2M\nu = 4$. The plot is taken from [49]. The data shown in the plot is from [45], [46], [47].

The parton model based upon results of Bjorken, Callan and Gross despite its success had a significant disadvantage. Namely, this model did not account for the interaction between partons

and, therefore, needed to be improved. In 1969 Adler and Tung [54] considered an improved parton model consisting of an SU(3)-triplet of fermions and an SU(3)-singlet massive gauge boson. It was shown that due to the interactions between partons in a such model the Bjorken limit does not exist. In the same year Jackiw and Preparata [55], independently from Adler and Tung, obtained similar results. However, the models of the interaction between partons considered in [54] and [55] were not asymptotically free. In 1973 Gross and Wilczek [56] suggested that in the asymptotically free theories the Bjorken scaling will hold up to the logarithmic corrections. The appearance of the logarithmic corrections to the Bjorken scaling was demonstrated in the same year by Callan and Gross [57]. The results obtained by Callan and Gross in [57] together with the discovery of the asymptotic freedom of QCD [20], [21] allowed to build the so called *QCD-improved parton model*. The detailed historical review of the foundation and verification of the QCD and the QCD-improved parton model can be found in [58] - [60]. The detailed description of the state-of-the art of the QCD and QCD-improved parton model is given in the monograph of Collins [1]. From now on we will assume that interactions between partons are described by the QCD Lagrangian discussed in Chapter 1.1. In the rest of this section we will describe how one can connect the scattering amplitudes computed in perturbation theory in QCD with the experimental data by means of the *factorization theorem*.

As we have discussed at the beginning of this section, the DIS cross section can be expressed in terms of the structure functions W_1 and W_2 or, in the Bjorken limit, in terms of F_1 and F_2. Therefore, in order to test the QCD-improved parton model one has to compute W_i or F_i in QCD. However, the main obstacle here is that the structure functions W_1 and W_2, as well as F_1 and F_2, are non-perturbative objects and, therefore, cannot be computed by means of the perturbation theory. One could circumvent this issue by postulating that one can express the structure functions F_i as convolutions of perturbative and non-perturbative pieces. For example,

$$F_1(x) \;=\; \sum_a \int_x^1 \frac{d\xi}{\xi} f_{a/h_A}(\xi) H_{1a}\left(\frac{x}{\xi}\right), \tag{1.32}$$

where the functions $f_a(\xi)$ are called *parton distribution functions* (PDFs) and the functions H_{1a} are called *hard scattering coefficients*. The product $f_a(\xi)d\xi$ in Eq. 1.32 is a probability to find a parton of a type a in a hadron of a type h_A carrying a fraction ξ to $\xi + d\xi$ of the hadron's longitudinal momentum. The factorization of the structure function F_1 as in Eq. 1.32 is equivalent to a separation into a long-distance physics (non-perturbative piece described by PDFs) and short-distance physics (perturbative piece described by the hard scattering coefficients). By writing F_1 as in Eq. 1.32 we also assume that the interaction between a virtual proton and a hadron occurs at the time-scales short enough to consider all hadrons' constituents have a definite momentum and that a virtual photon interacts only with one parton during the DIS process. However, a detailed theoretical study based upon field-theoretical definitions of the PDFs and hard scattering coefficients H_{1a} tells us that Eq. 1.32 is not correct and requires some important modifications, see [1], [61]. First of all, the separation of the scattering process into the short- and long-distance pieces as in Eq. 1.32 leads to UV-divergent parton densities which have to be regularized. As a consequence, both PDFs and hard scattering coefficients H_{1a} will depend on a new scale μ_F called *factorization scale*. Moreover, the structure functions F_i and hard scattering coefficients H_{1a} will also depend on another so

called *characteristic scale* Q which leads to the violation of the Bjorken scaling which was observed experimentally, see Fig. 1.11. Therefore, the correct factorization formulae for the DIS structure functions F_i are

$$F_1(x,Q^2) = \sum_a \int_x^1 \frac{d\xi}{\xi} f_{a/h_A}(\xi,\mu_F)\, H_{1a}\left(\frac{x}{\xi}, \frac{Q}{\mu_F}, \frac{Q}{\mu_R}, \alpha_s(\mu_R)\right) + (\text{p.s.c}), \tag{1.33}$$

$$F_2(x,Q^2) = \sum_a \int_x^1 \frac{d\xi}{\xi} f_{a/h_A}(\xi,\mu_F)\, \xi\, H_{2a}\left(\frac{x}{\xi}, \frac{Q}{\mu_F}, \frac{Q}{\mu_R}, \alpha_s(\mu_R)\right) + (\text{p.s.c}), \tag{1.34}$$

where Q^2 is a characteristic scale of the DIS process and (p.s.c) is a term suppressed by the power Q^{-2}. The parameter μ_R is a renormalization scale of hard scattering coefficients H_{1a}, H_{2a} and $\alpha_s = g^2/4\pi$ where g is a QCD coupling constant, see [1], [61].

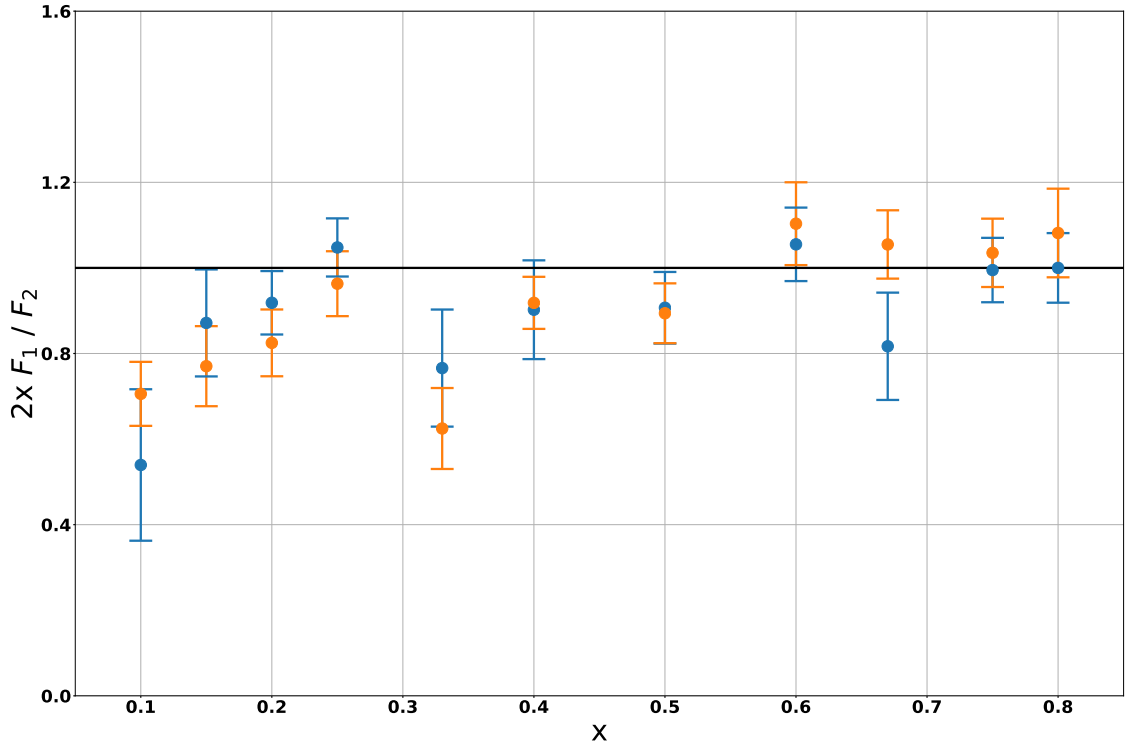

Figure 1.10: The experimental test of the Callan-Gross formula. Different colours correspond to the different measurements. Here we plot the data from [52].

In general, similar statements are proved for some other types of scattering processes (*e.g.* Drell-Yan process [69], for the proof see [70] - [72] and the review [61]), however, due to the complexity of a problem, many scattering processes of experimental relevance still lack the proof of factorization. In the case of the *hadron-hadron* scattering, the factorization theorem (omitting the power suppressed terms) reads

$$\sigma = \sum_{ij} \int dx_1\, dx_2\, f_{i/h_a}(x_1,\mu_F)\, f_{j/h_b}(x_2,\mu_F)\, H_{ij}\left(x_1, x_2, \frac{Q}{\mu_F}, \frac{Q}{\mu_R}, \alpha_s(\mu_R)\right), \tag{1.35}$$

where functions $f_{i/h_a}(x_1,\mu_F)$ and $f_{j/h_b}(x_2,\mu_F)$ are renormalized distribution functions of partons

of type i and j in hadrons h_a and h_b correspondingly. The hard scattering coefficients H_{ij} can be expanded in terms of the coupling constant α_s as

$$H_{ij}\left(x_1, x_2, \frac{Q}{\mu_F}, \frac{Q}{\mu_R}, \alpha_s(\mu_R)\right) = \alpha_s^2 \sum_{m=0}^{n} \alpha_s^m(\mu_R)\, h_{ij}^m\left(x_1, x_2, \frac{Q}{\mu_F}, \frac{Q}{\mu_R}\right), \tag{1.36}$$

which allows to write Eq. 1.35 as

$$\begin{aligned} \sigma &= \sum_{ij} \int dx_1\, dx_2\, f_i(x_1, \mu_F)\, f_j(x_2, \mu_F) \times \\ &\times \alpha_s^2 \sum_{m=0}^{n} \alpha_s^m(\mu_R)\, h_{ij}^m\left(x_1, x_2, \frac{Q}{\mu_F}, \frac{Q}{\mu_R}\right). \end{aligned} \tag{1.37}$$

Several important comments have to be made. First of all, the definition of the renormalized PDFs $f_{i/h}(x, \mu_F)$ depends on a chosen renormalization scheme. Once the scheme is chosen, one can use Eq. 1.33 and Eq. 1.34 to extract $f_{i/h}(x, \mu_F)$ out of the DIS data. One of the most popular renormalization schemes is so called $\overline{\text{MS}}$ *scheme* [64]. The scale dependence of the PDFs renormalized according to the $\overline{\text{MS}}$ scheme is governed by a system of the renormalization group equations called *Dokshitzer - Gribow - Lipatow - Altarelli - Parisi* (DGLAP) equations [66], [67], [68]. In section 1.5 we will discuss it in more details. The factorization scale μ_F is an arbitrary parameter which implies that the renormalized PDFs cannot be interpreted as probability distribution functions any more. Instead, one can think about hard scattering coefficients and renormalized PDFs in Eq. 1.37 as about perturbative and non-perturbative counterparts of the same expression. Due to the arbitrariness of the choice of μ_F, the cross section σ cannot depend on the variations of μ_F. It implies that the variation of renormalized PDFs in Eq. 1.37 leads to a variation of the coefficients h_{ij}^m in the perturbation expansion of H_{ij} such that the cross section σ does not depend on it[11]

$$\frac{\partial \sigma}{\partial \mu_F} = 0. \tag{1.38}$$

In practice, however, one truncates the perturbative expansion in Eq. 1.37 at the certain order in the power of α_s. It means that the dependence on μ_F and μ_R of the cross section evaluated with truncated series will not cancel out. The choice of both factorization and renormalization scales becomes then important. Usually one sets $\mu_F = \mu_R = Q$ where the value of Q is chosen such that the cross section evaluated with truncated series provides the best agreement with the data and is least sensitive to the scale variation.

The factorization theorem, as it is formulated for the DIS Eq. 1.33, Eq. 1.34 and hadron-hadron scattering Eq. 1.35, together with the renormalized PDFs which obey DGLAP evolution equations and hard scattering coefficients computed in QCD are the main components of the QCD-improved parton model. In this thesis, in order to construct *double parton scattering* (DPS) processes, we will use LO QCD $2 \to 2$ scattering processes of a type

$$p\,p \to j_1\, j_2 \,+\, X, \tag{1.39}$$

[11] The same statement is true for the variation with respect to the renormalization scale μ_R which implies $\partial\sigma/\partial\mu_R = 0$.

where $j = g, u, d, s, c, \bar{u}, \bar{d}, \bar{s}, \bar{c}$ and X stands for the other possible final states. In this case, the factorization theorem can be written as

$$\begin{aligned}\sigma &= \sum_{ij} \int dx_1\, dx_2\, f_i(x_1, \mu_F)\, f_j(x_2, \mu_F) \times \\ &\times \alpha_s^2 \sum_{m=0}^{n} \alpha_s^m(\mu_R)\, h_{ij}^m \left(x_1, x_2, \frac{Q}{\mu_F}, \frac{Q}{\mu_R}\right) \approx \\ &\approx \sum_{ij} \int dx_1\, dx_2\, f_i(x_1, \mu_F)\, f_j(x_2, \mu_F) \times \\ &\times \alpha_s^2\, h_{ij}^0\,(x_1, x_2)\,. \end{aligned} \tag{1.40}$$

Note that the the first term in the expansion of the leading order hard scattering coefficient depends only on renormalization scale μ_R and up to the factor α_s^2 coincide with the LO QCD cross section. Therefore, we can write $\alpha_s^2\, h_{ij}^0\,(x_1,\, x_2) = \sigma_{ij}^{\mathrm{LO}}\,(x_1,\, x_2,\, \alpha_s(\mu_R))$. In our computations we set $\mu_F = \mu_R = Q$ which gives us the master expression for the leading order $2 \to 2$ cross section:

$$\sigma = \sum_{ij} \int dx_1\, dx_2\, f_i(x_1, Q)\, f_j(x_2, Q)\, \hat{\sigma}_{ij}^{\mathrm{LO}}\,(x_1, x_2, \alpha_s(Q))\,, \tag{1.41}$$

which we will write in a more compact form as

$$\sigma = \sum_{ij} \int dx_1\, dx_2\, f_i(x_1, Q)\, f_j(x_2, Q)\, \hat{\sigma}_{ij}, \tag{1.42}$$

where x_1, x_2 are Bjorken variables, $f_i(x_1, Q)$ and $f_i(x_1, Q)$ are renormalized parton distribution functions at the factorization scale Q.

1.5 Evolution of parton distribution functions

In section 1.4 we have discussed the factorization theorem and mentioned that the renormalization procedure introduces scale dependent parton distribution functions $f(x, \mu_F)$. We also argued that the renormalization scale μ_F may have an arbitrary value and that the dependence of $f(x, \mu_F)$ on μ_F in the $\overline{\mathrm{MS}}$ renormalization scheme is governed by renormalization group equations also called DGLAP evolution equations. There exist several methods to derive the DGLAP equations. Historically the DGLAP equations were derived by considering the emission of collinear particles by proton's constituents. Within this approach one postulates the "naive" factorization form as

$$F_1(x) = \sum_a \int_x^1 \frac{d\xi}{\xi} f_{a/h_A}(\xi) \hat{\sigma}_{1a}\left(\frac{x}{\xi}\right), \tag{1.43}$$

where $f(\xi)$ are so called "bare" parton distribution functions and $\hat{\sigma}_{1a}$ is a non-regularized partonic cross section[12]. If one will consider then an emission of collinear particles by proton's constituent, one will have to deal with IR-divergent partonic cross sections $\hat{\sigma}_{1a}$. One can regularize these

[12] We shall note here that in general hard scattering coefficients H_{1a}, H_{1b} and H_{ij} as in Eq. 1.33, Eq. 1.34 and Eq. 1.35 do not coincide with partonic cross sections, see, for example, Chapter 7 of [2].

divergences by redefining "bare" parton distribution functions $f(\xi)$ in a such way that the new distributions $f(\xi,\mu_F)$ "absorb" IR divergences due to the emission of collinear particles. The scale dependence of the redefined parton distribution functions $f(\xi,\mu_F)$ is described by the DGLAP evolution equations. The factorization scale μ_F then can be seen as a scale which separates the emission of the collinear particles (which are included into $f(\xi,\mu_F)$) and hard particles which are included into the parton cross section. This approach is also called IR point-of-view on the DGLAP equations. Historically it is the way the DGLAP evolution equations were derived at the first time, see [66], [67], [68]. This approach, though providing correct results, in general, is not correct. One could, for example, consider a field theory where all partons are massive. In this case, according to the IR point-of-view, one would not need then renormalized parton distribution functions $f(\xi,\mu_F)$ which is not correct. Moreover, one can show that the "bare" PDFs defined as products of the field operators "sandwiched" between two hadron states are UV- but not IR-divergent, see [1]. These UV-divergences being renormalized according to the $\overline{\rm MS}$ renormalization scheme give rise to the same DGLAP evolution equation as in the IR approach.

In the rest of this section we will briefly sketch the derivation of the DGLAP equations according to the IR point-of-view. We will follow the pedagogical explanation given in the book of Peskin and Schroeder [5] which is based upon original publications by Dokshitzer [66], Gribov and Lipatov [67] and by Altarelli and Parisi [68]. We also demonstrate how the appearance of the logarithms due to the multiple emission of collinear particles leads to the violation of the Bjorken scaling we mentioned in the previous section. The modern point of view on the DGLAP evolution equations can be find in the monograph of Collins [1]. The connection between the IR and UV approaches to the PDFs is given by the methods described in the monograph of Smirnov [62].

Before discussing the DGLAP evolution equations for QCD, let us consider the processes of emission of collinear particles in QED. Our starting point is to consider a process of an electron splitting as it is schematically shown in Fig. 1.12. Since we are interested in emission of collinear particles we will have to evaluate the matrix element for the process in Fig. 1.12 for the two different kinematic configurations. Namely, we will have to consider situations when one of the final state particles becomes collinear to the initial state electron. Let us consider first the situation when emitted photon becomes collinear. In order to do that we parametrize the momenta of the initial and final state particles as follows

$$p^\mu = (p,0,0,p)\,, \tag{1.44}$$

$$q^\mu = \left(zp, p_\perp, 0, zp-\frac{p_\perp^2}{2zp}\right), \tag{1.45}$$

$$k^\mu = \left((1-z)p, -p_\perp, 0, (1-z)p+\frac{p_\perp^2}{2zp}\right), \tag{1.46}$$

where z is the fraction of the energy of the initial electron that is carried by the photon. The decomposition set by Eq. 1.45 - 1.46 implies

$$q^\mu q_\mu = (zp)^2 - p_\perp^2 - \left(zp-\frac{p_\perp^2}{2zp}\right)^2 = 0+\mathcal{O}(p_\perp^2), \tag{1.47}$$

$$k^\mu k_\mu = (1-z)^2 p^2 - p_\perp^2 - \left((1-z)p+\frac{p_\perp^2}{2zp}\right)^2 = -\frac{p_\perp^2}{z}+\mathcal{O}(p_\perp^4). \tag{1.48}$$

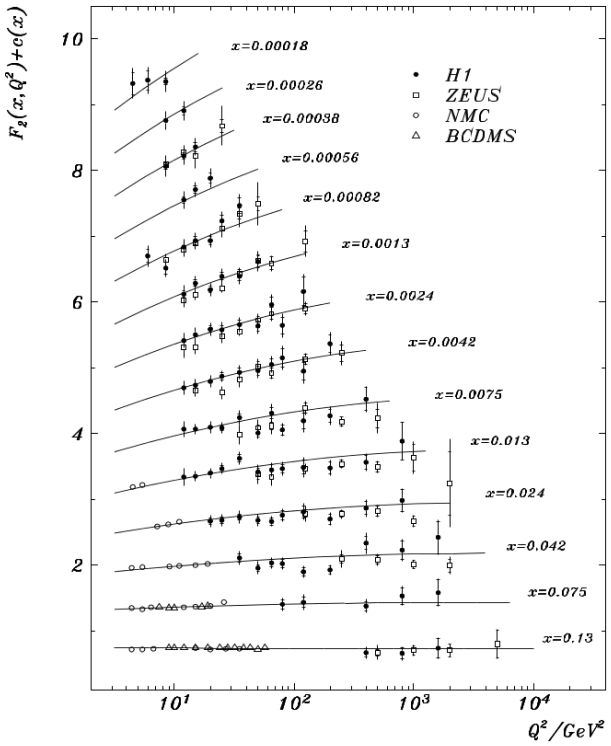

Figure 1.11: Measurements of the DIS at DESY. In order to ease reading of data each measurement was shifted by $c(x) = 0.6(i_x - 0.4)$ where i_x is the bin number starting at $i_x = 1$ for $x = 0.13$, from [63].

We see that according to Eq. 1.47 and Eq. 1.48 in the limit of small $p_\perp$ the emitted photon becomes collinear to the initial state electron and the emitted electron acquires the virtuality $-p_\perp^2/z$. Similar decomposition for the emission of a collinear electron gives

$$k^\mu k_\mu = 0 + \mathcal{O}(p_\perp^2), \tag{1.49}$$

$$q^\mu q_\mu = -\frac{p_\perp^2}{(1-z)} + \mathcal{O}(p_\perp^4). \tag{1.50}$$

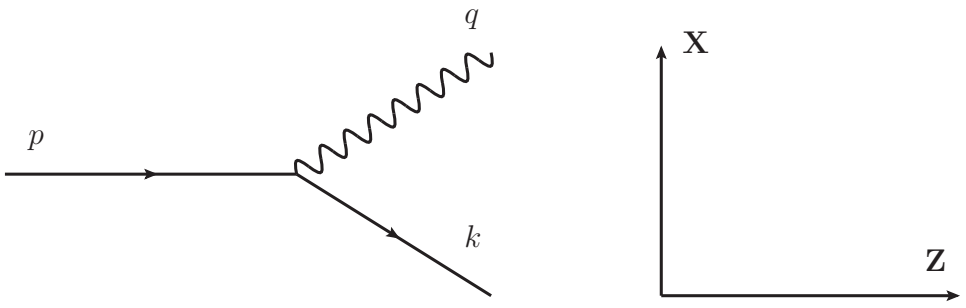

Figure 1.12: Schematic picture of an electron splitting into electron-photon pair.

Using Eq. 1.44 - 1.50 one can evaluate the cross section for the scattering processes with emission of one collinear particle shown in Fig. 1.13. Consider first the scattering process in Fig. 1.13 a). The diagram in Fig. 1.13 a) corresponds to the scattering process where the initial state electron splits into a collinear electron and a virtual photon γ which, in turn, takes part in $\gamma + \mathrm{X} \longrightarrow \mathrm{Y}$

process. At the *leading order* (LO) in perturbation theory the matrix element for the electron splitting into a collinear electron and a virtual photon is given by

$$\frac{1}{2}\sum_{pol}|\mathcal{M}|^2 = \frac{2e^2p_\perp^2}{z(1-z)}\left[\frac{1+(1-z)^2}{z}\right], \tag{1.51}$$

where the sum was taken over all possible polarizations. The cross section for the process in Fig. 1.13 a) is given by

$$\hat{\sigma}(e\mathrm{X}\to e\mathrm{Y}) = \frac{1}{(1+v_\mathrm{X})2p2E_\mathrm{X}}\int\frac{d^3k}{(2\pi)^3}\frac{1}{2k^0}\int d\Phi_\mathrm{Y}\left[\frac{1}{2}\sum_{pol}|\mathcal{M}|^2\right]\frac{1}{q^2}\left|\mathcal{M}_{\gamma\mathrm{X}}\right|^2, \tag{1.52}$$

where v_X is the velocity of the particle X and $d\Phi_\mathrm{Y}$ is the phase space for the final state Y. By substituting Eq. 1.51 in Eq. 1.52 one can write

$$\hat{\sigma}(e\mathrm{X}\to e\mathrm{Y}) = \int_0^1 dz\int_{m^2}^{s}\frac{dp_\perp^2}{p_\perp^2}\frac{\alpha}{2\pi}\left[\frac{1+(1-z)^2}{z}\right]\hat{\sigma}\left(\gamma\mathrm{X}\to\mathrm{Y}\right), \tag{1.53}$$

where α is the fine-structure constant and m is the electron mass. Integrating over $dp_\perp^2$ in Eq. 1.53 we get

$$\begin{aligned}\hat{\sigma}(e\mathrm{X}\to e\mathrm{Y}) &= \int_0^1 dz\,\frac{\alpha}{2\pi}\log\left(\frac{\hat{s}}{m^2}\right)\left[\frac{1+(1-z)^2}{z}\right]\hat{\sigma}\left(\gamma\mathrm{X}\to\mathrm{Y}\right) = \\ &= \int_0^1 dz\, f_\gamma(z)\,\hat{\sigma}\left(\gamma\mathrm{X}\to\mathrm{Y}\right),\end{aligned} \tag{1.54}$$

where we have defined

$$f_\gamma(z) = \frac{\alpha}{2\pi}\log(\hat{s}/m^2)\left[\frac{1+(1-z)^2}{z}\right]. \tag{1.55}$$

One can interpret $f_\gamma(z)$ as a probability to find a photon with momentum zp in an electron with momentum[13] p. The factor $\log(\hat{s}/m^2)$ in Eq. 1.54 and Eq. 1.55 is called *mass singularity* since $\log(\hat{s}/m^2)$ diverges if $m\longrightarrow 0$. Later in this section we will demonstrate how one can resum the mass singularities due to the emission of multiple collinear particles which will give us to the system of DGLAP evolution equations. However, before doing that let us consider a scattering process shown in Fig. 1.13 b) where the initial state electron splits into a collinear photon and a virtual electron which, in turn, takes part in $e+\mathrm{X}\longrightarrow\mathrm{Y}$ process. The corresponding expression is given by

$$\hat{\sigma}(e\mathrm{X}\to\gamma\mathrm{Y}) = \int_0^1 dz\, f_e(z)\,\hat{\sigma}\left(e\mathrm{X}\to\mathrm{Y}\right), \tag{1.56}$$

[13]The function $f_\gamma(z)$ is also called Weizsäcker-Williams distribution function, see [65].

where

$$f_e(z) = \delta(1-z) + \frac{\alpha}{2\pi}\,\log(\hat{s}/m^2)\frac{1+z^2}{(1-z)_+} + \frac{\alpha}{2\pi}\,\log(\hat{s}/m^2)\frac{3}{2}\delta(1-z). \tag{1.57}$$

The first term on the RHS of Eq. 1.57 gives the probability to have a process without a splitting, the second term gives the probability of the perturbative splitting and the last term is due to the contribution of virtual diagrams, see [5]. The "plus" subscript, so called *plus prescription*, was used to regularize the singularity at $z = 1$, and is defined such that

$$\int_0^1 dx\,\frac{f(x)}{(1-x)_+} = \int dx\,\frac{f(x)-f(1)}{1-x} \tag{1.58}$$

holds.

Figure 1.13: Electron scattering process with emission of one collinear particle: a) Emission of a single collinear electron. b) Emission of a single collinear photon.

Expressions given by Eq. 1.54, Eq. 1.55 and Eq. 1.56, Eq. 1.57 describe scattering processes with emission of one collinear particle shown in Fig. 1.13. Now let us discuss the processes with multiple emission of collinear particles. As an example we consider a process with emission of multiple collinear photons which is schematically shown in Fig. 1.14.

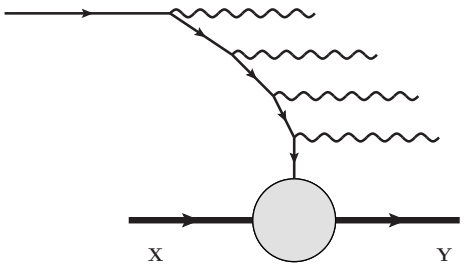

Figure 1.14: Multiple initial state emission of collinear photons.

One can show that if after each emission of a collinear photon the transverse momentum of an intermediate electron becomes smaller, *e. g.* $p_{1\perp} > p_{2\perp} > p_{3\perp}...$, then the n'th emission gives a factor

$$\frac{1}{n!}\left(\frac{\alpha}{2\pi}\right)^n \log^n\left(\frac{\hat{s}}{m^2}\right). \tag{1.59}$$

One can take these multiple emissions into account by considering them as a continuous process and by making distribution functions f_e and f_γ scale dependent. Consider, for example, the probability to find a photon inside of an electron. The differential probability to emit a collinear photon is

equal to

$$\frac{\alpha}{2\pi}\frac{dp_\perp^2}{p_\perp^2}\frac{1+(1-z)^2}{z}. \tag{1.60}$$

Therefore, a probability to find a photon with $p_\perp$ in the range between Q and $Q+\Delta Q$ is given by

$$\begin{aligned} f_\gamma(x,Q+\Delta Q) = f_\gamma(x,Q) &+ \int_0^1 dx' \int_0^1 dz \frac{\alpha}{2\pi}\frac{\Delta Q^2}{Q^2}\left[\frac{1+(1-z)^2}{z}\right] f_e(x',p_\perp)\delta(x-zx') \\ &= f_\gamma(x,Q) + \frac{\Delta Q}{Q}\frac{\alpha}{\pi}\int_x^1 \frac{dz}{z}\left[\frac{1+(1-z)^2}{z}\right] f_e(x/z,p_\perp), \end{aligned} \tag{1.61}$$

and in the limit where $\Delta Q \to 0$ we can write

$$\frac{\partial f_\gamma(x,Q)}{\partial \log Q} = \frac{\alpha}{\pi}\int_x^1 \frac{dz}{z}\left[\frac{1+(1-z)^2}{z}\right] f_e(x/z,Q). \tag{1.62}$$

A similar equation can be written for $f_e(x,Q)$:

$$\frac{\partial f_e(x,Q)}{\partial \log Q} = \frac{\alpha}{\pi}\int_x^1 \frac{dz}{z}\left[\frac{1+z^2}{(1-z)_+} + \frac{3}{2}\delta(1-z)\right] f_e(x/z,Q). \tag{1.63}$$

However, in order to complete this system of integro-differential equations, one has to take into account so called *pair creation processes* where a photon splits into an electron-positron pair. A complete system of such equations was first obtained by Gribov and Lipatov [67] and it is given by

$$\frac{\partial f_\gamma(x,Q)}{\partial \log Q} = \frac{\alpha}{\pi}\int_x^1 \frac{dz}{z}\left\{P_{e\to\gamma}(z)\left[f_e(x/z,Q)+f_{\bar e}(x/z,Q)\right] + P_{\gamma\to\gamma}(z) f_\gamma(x/z,Q)\right\} \tag{1.64}$$

$$\frac{\partial f_e(x,Q)}{\partial \log Q} = \frac{\alpha}{\pi}\int_x^1 \frac{dz}{z}\left\{P_{e\to e}(z) f_e(x/z,Q) + P_{\gamma\to e}(z) f_\gamma(x/z,Q)\right\} \tag{1.65}$$

$$\frac{\partial f_{\bar e}(x,Q)}{\partial \log Q} = \frac{\alpha}{\pi}\int_x^1 \frac{dz}{z}\left\{P_{e\to e}(z) f_e(x/z,Q) + P_{\gamma\to e}(z) f_\gamma(x/z,Q)\right\}, \tag{1.66}$$

where

$$P_{e\to e}(z) = \frac{1+z^2}{(1-z)_+} + \frac{3}{2}\delta(1-z), \tag{1.67}$$

$$P_{e\to\gamma}(z) = \frac{1+(1-z)^2}{z}, \tag{1.68}$$

$$P_{\gamma\to e}(z) = z^2+(1-z)^2, \tag{1.69}$$

$$P_{\gamma\to\gamma}(z) = -\frac{2}{3}\delta(1-z), \tag{1.70}$$

are LO QED splitting functions.

The equations 1.65 - 1.66 have to be solved for the following initial conditions:

$$f_e(x,Q_0) = \delta(1-x), \tag{1.71}$$
$$f_\gamma(x,Q_0) = 0, \tag{1.72}$$
$$f_{\bar{e}}(x,Q_0) = 0, \tag{1.73}$$

which simply state that if no emission happens there is only an initial electron.

The results of Gribov and Lipatov [67] were generalized to the case of QCD by Dokshitzer [66] and by Altarelli and Parisi [68]. The evolution equations obtained in [66], [68] are called DGLAP evolution equations and are given by

$$\frac{\partial f_g(x,Q)}{\partial \log Q} = \frac{\alpha_s}{\pi}\int_x^1 \frac{dz}{z}\left\{P_{q\to g}(z)\sum_f \left[f_f(x/z,Q)+f_{\bar{f}}(x/z,Q)\right]+P_{g\to g}(z)f_g(x/z,Q)\right\}, \tag{1.74}$$

$$\frac{\partial f_f(x,Q)}{\partial \log Q} = \frac{\alpha_s}{\pi}\int_x^1 \frac{dz}{z}\left\{P_{q\to q}(z)f_f(x/z,Q)+P_{g\to q}(z)f_g(x/z,Q)\right\}, \tag{1.75}$$

$$\frac{\partial f_{\bar{f}}(x,Q)}{\partial \log Q} = \frac{\alpha_s}{\pi}\int_x^1 \frac{dz}{z}\left\{P_{q\to q}(z)f_{\bar{f}}(x/z,Q)+P_{g\to q}(z)f_g(x/z,Q)\right\}, \tag{1.76}$$

where $\alpha_s = g^2/4\pi$ and

$$P_{q\to q}(z) = \frac{4}{3}\left[\frac{1+z^2}{(1-z)_+}+\frac{3}{2}\delta(1-z)\right], \tag{1.77}$$
$$P_{q\to g}(z) = \frac{4}{3}\left[\frac{1+(1-z)^2}{z}\right], \tag{1.78}$$
$$P_{g\to q}(z) = \frac{1}{2}\left[z^2+(1-z)^2\right], \tag{1.79}$$
$$P_{g\to g}(z) = 6\left[\frac{1-z}{z}+\frac{z}{(1-z)_+}+z(z-1)+\left(\frac{11}{12}-\frac{N_f}{18}\right)\delta(1-z)\right], \tag{1.80}$$

are LO DGLAP splitting functions.

Since we consider proton as a *uud* bound state, the scale dependent PDFs $f_i(x,Q)$ in Eq. 1.74 - 1.76 obey the following *sum rules*:

$$\int_0^1 dx\, f_{u_v}(x) = 2, \tag{1.81}$$
$$\int_0^1 dx\, f_{d_v}(x) = 1, \tag{1.82}$$
$$\int_0^1 dx\, \left[f_{q_s}(x)-f_{\bar{q}_s}(x)\right] = 0, \tag{1.83}$$

where $f_{u_v} \equiv f_u - f_{\bar{u}}$, $f_{d_v} \equiv f_d - f_{\bar{d}}$ and $q_s = s,c,b,t$. Also, the total longitudinal momentum of all partons has to be equal to the longitudinal momentum of proton, which gives another sum rule

which states the conservation of longitudinal momentum:

$$\sum_{i=g,q,\bar{q}} \int_0^1 dx\, x f_i(x) = 1, \tag{1.84}$$

where $q = d, u, s, c, b, t$.

Like in the QED case, Eq. 1.74 - 1.76 have to be solved with appropriate initial conditions which in the case of QCD are unknown and have to be determined out of the experimental data. After determining initial conditions one can use DGLAP equations to "evolve" PDFs up to an arbitrary factorization scale, see Fig. 1.15.

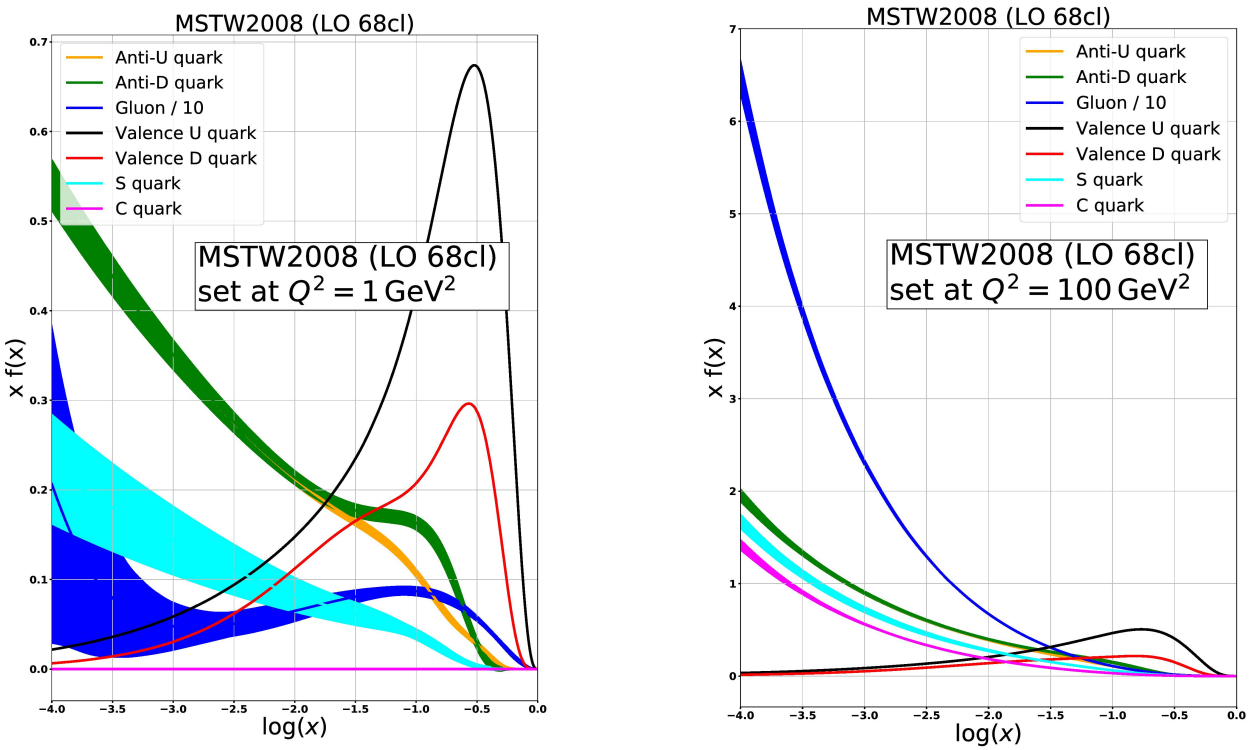

Figure 1.15: MSTW2008 LO PDFs [298] at different values of the factorization scale Q: a) $Q = 1$ GeV, b) $Q = 10$ GeV.

The results described in this chapter form the basis of the QCD and the QCD-improved parton model. In Chapter 2 we will discuss the generalization of the LO DGLAP equations and sum rules given by Eq. 1.81 - 1.84 to the case of the dPDFs we need to describe DPS processes.

Chapter 2

Theoretical foundations of double parton scattering

Since hadrons are composite particles, it is quite natural to consider a possibility that two and more hard scatterings will occur during one hadron-hadron collision. Despite the simplicity of this assumption, a complete theory of such scattering processes is yet to be developed. In this chapter we will briefly describe theoretical foundations of a simplest example of *multiple partonic interaction* (MPI) process, so called *double parton scattering* (DPS) process. We will start with a short historical review of first groundbreaking studies in this field and currently available experimental measurements of DPS. Later in this chapter we will describe the main developments in theoretical description of DPS. In particular, we will discuss the evolution of *double parton distribution functions* (dPDFs), problem of UV-singularities and double counting as well as the role of DPS in *proton-nucleus* (pA) collisions.

2.1 Brief historical review

The "Era of DPS" begins in late seventies - early eighties of the past century. In 1978 Landshoff and Polkinghorne discussed a multi-jet production via MPI mechanism at the first time [111]. One year later, Donnachie and Landshoff studied the process of multiple elastic quark scattering [113]. In the same year Takagi studied the processes of double and triple hard interactions in πA collisions at the first time [112]. In 1980 Goebel, Scott and Halzen published a paper called "Double Drell-Yan annihilations in hadron collisions: Novel tests of the constituent picture" [114]. In Ref. [114] a formula for the double Drell-Yan differential cross section was given for the first time:

$$\begin{aligned}\frac{d^4\sigma_{\rm DPS}}{dM\,dy\,dM'\,dy'} &= \sum_{a_1,a_2,b_1,b_2} \frac{e_i^2\,e_{i'}^2}{\pi R^2}\,\Gamma_{a_1,a_2/h_A}(x_1,x_1')\,\Gamma_{b_1,b_2/h_B}(x_2,x_2')\,\times \\ &\times \frac{d^2\hat{\sigma}}{dM\,dy}\left(a_1\,b_1\to\gamma^*\to l\bar{l}\right)\,\frac{d^2\hat{\sigma}}{dM'\,dy'}\left(a_2\,b_2\to\gamma^*\to l\bar{l}\right), \qquad (2.1)\end{aligned}$$

where $\Gamma_{a_1,a_2/h_A}(x_1,x_1')$ is a probability to find two partons of a type a_1 and a_2 in a hadron of a type A carrying fractions x_1 and x_1' of the longitudinal momentum of h_A. A normalization factor πR^2 takes its origin in the paper on *multiple elastic scattering of quarks* by Donnachie and Landshoff

[113]. The authors of [113], [114] have argued that one can estimate the size of πR^2 using following geometrical considerations: let us assume that we deal with a collision of two hadrons and that R is of the order of a hadron's radius, then the probability that a parton a_2 in one hadron then interacts with a parton b_2 in the other hadron is approximately equal to $\sigma_{a_2,b_2}/\pi R^2$. Therefore, if one hard collision with a cross section σ_{a_1,b_1} already took place one has to multiply it by a probability $\sigma_{a_2,b_2}/\pi R^2$ in order to get the total DPS cross section. Relying on these considerations, one can simply see πR^2 as a transverse area of a hadron expressed in the units of cross section.

Since the distribution functions $\Gamma_{a_1,a_2/h_A}(x_1,x_2)$ are unknown objects, one has to use certain phenomenologically motivated assumptions to model them. In order to make a numerical estimate of the double Drell-Yan cross section, the authors of [114] assumed that one can express $\Gamma_{a_1,a_2/h_A}(x_1,x_2)$ in terms of "standard" collinear PDFs as

$$\Gamma_{a_1,a_2/h_A}(x_1,x_2) = f_{a_1/h_A}(x_1)\, f_{a_2/h_A}(x_2)\,(1-x_1-x_2), \tag{2.2}$$

where the factor $(1-x_1-x_2)$ was added to ensure a smooth suppression of $\Gamma_{a_1,a_2/h_A}(x_1,x_2)$ close to a kinematic boundary $x_1+x_2<1$. Here we shall stress that this approach to model $\Gamma_{a_1,a_2/h_A}(x_1,x_2)$ neglects possible correlations between x_1 and x_2 as well as violates conservation of a number of partons of different flavour. Nevertheless, Eq. 2.2 being combined with Eq. 2.1 allows to make some important predictions; in particular, the authors of [114] computed the double Drell-Yan cross section at the collision energy $\sqrt{S}=25$ GeV and argued that it can be measured experimentally. Additionally, it was predicted that DPS processes should acquire an additional enhancement in pA and *nucleus-nucleus* (AA) collisions [114]. Moreover, it was mentioned that DPS events in pA collisions may originate not only from a collision between a proton and a single nucleon but also from a collision between a proton and two independent nucleons[1] [114]. Also we have to note here that the authors of [113], [114] have argued that the interpretation of πR^2 as a transverse area of a proton is a very rough estimate and a better knowledge of proton structure is required for more precise computations. In fact, there is a deep connection between a structure of proton and a value of πR^2 which will be explained later in this thesis.

In 1980 Politzer [115] proposed an idea to formulate QCD in terms of multiconstituent distribution functions $\Gamma(x_1,x_2,...,x_n)$ which can be seen as a generalization of distribution functions from Eq. 2.1 and, independently from Goebel *et al.*, provided a differential cross section for a double Drell-Yan process. Two years later Paver and Treleani [116] extended ideas of Politzer[2] to the processes of double hard scattering of quarks in hadron-hadron collisions, see Fig. 2.1, and provided a double differential cross section for a four-jet DPS production process:

$$\begin{aligned}\sigma^{\mathrm{DPS}} &= \sum_{a_1,a_2,b_1,b_2}\int\prod_{i=1}^{4} dx_i\, d^2b\,\Gamma_{a_1,a_2/h_A}(x_1,x_2,\boldsymbol{b})\,\Gamma_{b_1,b_2/h_B}(x_3,x_4,\boldsymbol{b})\times \\ &\times\ \hat{\sigma}_{a_1\,b_1\to J_1\,\bar{J}_1}\,\hat{\sigma}_{a_2\,b_2\to J_2\,\bar{J}_2}\,\delta\left(\hat{s}_1+\hat{t}_1+\hat{u}_1\right)\,\delta\left(\hat{s}_2+\hat{t}_2+\hat{u}_2\right).\end{aligned} \tag{2.3}$$

The crucial difference between this formula and Eq. 2.1 is that here a distribution function $\Gamma_{a_1,a_2/h_A}(x_1,x_2,\boldsymbol{b})$ now gives a probability to find two partons of a type a_1 and a_2 carrying

[1] We will discuss the development of this idea in section 2.6 while considering DPS in pA collisions.
[2] In their paper Paver and Treleani do not cite the study of Goebel *et al.*

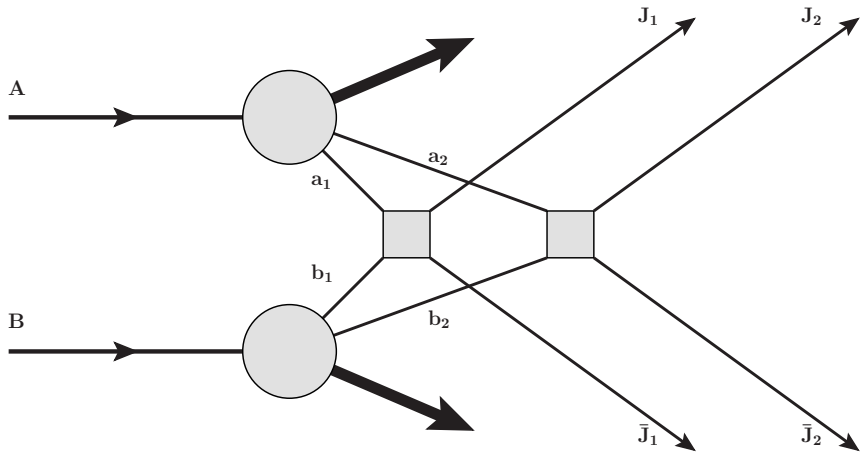

Figure 2.1: A schematic representation of a DPS process.

longitudinal momentum fractions x_1 and x_2 of a hadron h_A separated by a relative transverse distance $|\boldsymbol{b}|$. The connection between $\Gamma_{a_1,a_2/h_A}(x_1,x_2,\boldsymbol{b})$ and factor $1/\pi R^2$ from Eq. 2.1 becomes clear if one assumes that $\Gamma_{a_1,a_2/h_A}(x_1,x_2,\boldsymbol{b})$ can be written as a product of longitudinal- and transverse-dependent functions as

$$\Gamma_{a_1,a_2/h_A}(x_1,x_2,\boldsymbol{b}) \approx D_{a_1,a_2/h_A}(x_1,x_2)\, F(\boldsymbol{b}), \tag{2.4}$$

which implies that Eq. 2.3 transforms to

$$\begin{aligned}\sigma^{\mathrm{DPS}} &= \frac{1}{\sigma_{eff}} \sum_{a_1,a_2,b_1,b_2} \int \prod_{i=1}^{4} dx_i\, D_{a_1,a_2/h_A}(x_1,x_2)\, D_{b_1,b_2/h_B}(x_3,x_4) \times \\ &\times \hat{\sigma}_{a_1\, b_1 \to J_1\, \bar{J}_1}\, \hat{\sigma}_{a_2\, b_2 \to J_2\, \bar{J}_2}\, \delta\left(\hat{s}_1+\hat{t}_1+\hat{u}_1\right)\, \delta\left(\hat{s}_2+\hat{t}_2+\hat{u}_2\right), \end{aligned} \tag{2.5}$$

where

$$\sigma_{eff} = \left[\int d^2b\, F^2(\boldsymbol{b})\right]^{-1}. \tag{2.6}$$

We see that $\pi R^2 = \sigma_{eff}$ and that it depends now on a distribution of partons in a transverse plane of a hadron which is given by the function $F(\boldsymbol{b})$. Later in this thesis, we will discuss a connection between σ_{eff} and $\Gamma_{a_1,a_2/h_A}(x_1,x_2;\boldsymbol{b})$ in more detail. Also, to avoid a clash of different notations, we will always use σ_{eff} instead of πR^2.

In 1983 Paver and Treleani published another paper [118] where numerical estimate of a DPS contribution to the four-jet production was given. In the same year Humbert, expressing $\Gamma_{a_1,a_2/h_A}(x_1,x_2)$ in the form as in Eq. 2.2, evaluated a differential DPS cross section for the four-jet DPS production and gave an estimate of a size of longitudinal parton correlations (correlations in x-space) [120].

In 1984 Humbert and Odorico [121] studied the four-jet production via DPS and *single parton scattering* (SPS) mechanisms. It was found that the four-jet DPS and SPS cross sections for the collision energies $\sqrt{S} = 0.62$, 2, 20 TeV are of competitive size. Moreover, a set of DPS sensitive variables to discriminate between SPS and DPS contributions to the four-jet production was proposed

at the same time [121]. A similar analysis was performed one year later by Ametller, Paver and Treleani [122]. In [122] the four-jet DPS cross section was compared against analytical results for the four-jet SPS cross section from [110]. Finally, in 1986 Halzen, Hoyer and Stirling have published a paper [123] where they have demonstrated that their computations for double Drell-Yan production can explain available at the time data on multimuon production in pp [124] and π^-p [125] collisions measured by the NA3 collaboration.

The aforementioned studies have drawn attention of the experimental community to the DPS phenomena and in 1986 first experimental measurements of DPS were performed. The experimental measurements of DPS, however, rely on various model dependent assumptions. In order to illustrate it, let us rewrite Eg. 2.3 in a slightly different form:

$$\begin{aligned}\sigma_{AB}^{\mathrm{DPS}} &= \sum_{a_1,a_2,b_1,b_2} \int \prod_{i=1}^{4} dx_i d^2b\, \Gamma_{a_1,a_2/h_A}(x_1,x_2,\boldsymbol{b})\, \Gamma_{b_1,b_2/h_B}(x_3,x_4,\boldsymbol{b}) \times \\ &\times \hat{\sigma}_{a_1\, b_1\to A}\, \hat{\sigma}_{a_2\, b_2\to B}, \end{aligned} \tag{2.7}$$

where A and B denote final states in $2 \to 2$ reactions and we omitted $\delta\left(\hat{s}_1+\hat{t}_1+\hat{u}_1\right)$ and $\delta\left(\hat{s}_2+\hat{t}_2+\hat{u}_2\right)$ (from now on we will always assume that condition $\hat{s}+\hat{t}+\hat{u}=0$ holds for both $2 \to 2$ processes). Using Eq. 2.4, one can factorize x- and b-dependent parts and write

$$\begin{aligned}\sigma_{AB}^{\mathrm{DPS}} &= \frac{1}{\sigma_{eff}} \sum_{a_1,a_2,b_1,b_2} \int \prod_{i=1}^{4} dx_i\, D_{a_1,a_2/h_A}(x_1,x_2)\, D_{b_1,b_2/h_B}(x_3,x_4) \times \\ &\times \hat{\sigma}_{a_1\, b_1\to A}\, \hat{\sigma}_{a_2\, b_2\to B}. \end{aligned} \tag{2.8}$$

If we neglect now correlations in x space, namely if we factorize $D_{a_1,a_2/h_A}(x_1,x_2)$ as $D_{a_1,a_2/h_A}(x_1,x_2) \approx f_{a_1/h_A}(x_1)\, f_{a_2/h_A}(x_2)$, we can write

$$\begin{aligned}\sigma_{AB}^{\mathrm{DPS}} &= \frac{1}{\sigma_{eff}} \sum_{a_1,b_1} \int dx_1\, dx_3\, f_{a_1/h_A}(x_1)\, f_{b_1/h_B}(x_3)\, \hat{\sigma}_{a_1\, b_1\to A} \times \\ &\times \sum_{a_2,b_2} \int dx_2\, dx_4\, f_{a_2/h_A}(x_2)\, f_{b_2/h_B}(x_4)\, \hat{\sigma}_{a_2\, b_2\to B}, \end{aligned} \tag{2.9}$$

which can be written in a compact form as

$$\sigma_{AB}^{\mathrm{DPS}} = \frac{\sigma_A^{\mathrm{SPS}}\, \sigma_B^{\mathrm{SPS}}}{\sigma_{eff}}, \tag{2.10}$$

which is sometimes called as "pocket formula of DPS" in the literature.

One important remark has to be made here: if one deals with indistinguishable final states A and B, one has to multiply this formula by a symmetry factor $1/2$, thus[3]

$$\sigma_{AB}^{\mathrm{DPS}} = \frac{1}{1+\delta_{AB}}\, \frac{\sigma_A^{\mathrm{SPS}}\, \sigma_B^{\mathrm{SPS}}}{\sigma_{eff}}. \tag{2.11}$$

Consider now a four-jet production in pp collisions $pp \to 4j$. Obviously, both DPS and SPS can

[3]The symmetry factor $1/2$ in front of the DPS cross section has a different origin in different studies which may lead to a possible confusion. In Chapter 4.2 we will discuss it in more details.

contribute to production of this final state. If we could now somehow discriminate between events produced via $pp \xrightarrow{\text{DPS}} 4j$ and $pp \xrightarrow{\text{SPS}} 4j$ processes, we could measure a DPS cross section and thus find a value of σ_{eff} with a help of Eq. 2.11.

In July 1986 the Axial Field Spectrometer (AFS) collaboration reported first measurements of DPS events in $pp \to 4j$ at $\sqrt{S} = 63$ GeV collision energy and found $\sigma_{eff} = 5\,\text{mb}$ [128]. These analyses, despite their importance, had some deficiencies. First, the uncertainties for σ_{eff} were not provided. Secondly, the exact matrix elements for QCD $2 \to 4$ processes were not used, therefore the estimated SPS background and thus the fraction of DPS events cannot be trusted. In 1991 UA2 collaboration studied DPS events in $p\bar{p} \to 4j$ process at $\sqrt{S} = 630\,\text{GeV}$ and found the lower bound for σ_{eff} to be equal to 8.3 mb [129]. Two years later CDF collaboration studied DPS events in $p\bar{p} \to 4j$ process at $\sqrt{S} = 1.4\,\text{TeV}$ and found $\sigma_{eff} = 12.1^{+10.7}_{-5.4}\,\text{mb}$ [130]. In 1997 CDF studied DPS in $p\bar{p} \to 3j + \gamma$ [131] and in $p\bar{p} \to 3j + \gamma/\pi^0$ processes [132] at $\sqrt{S} = 1.8\,\text{TeV}$ and reported $\sigma_{eff} = 14.5 \pm 1.7^{+1.7}_{-2.3}\,\text{mb}$.

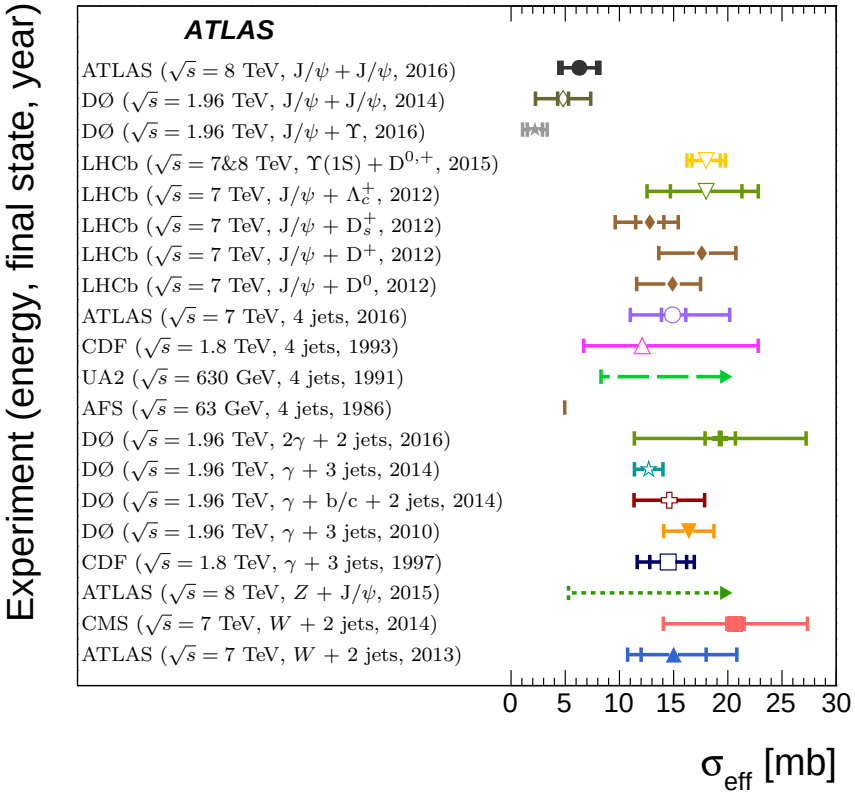

Figure 2.2: Currently available measurements of σ_{eff}, from [134].

After the above mentioned measurements followed a twelve years break. Experimental studies of DPS were resumed in 2009 when DØ collaboration measured DPS in $p\bar{p} \to 3j + \gamma$ production process at $\sqrt{s} = 1.96\,\text{TeV}$ [133]. In 2012 LHCb measured DPS in $pp \to J/\psi + h_X$ production process where $h_x = D^0$, D^+, D_s^+ Λ_c^+ at $\sqrt{S} = 7\,\text{TeV}$ [135]. In 2013 ATLAS and CMS collaborations measured DPS in $pp \to 2j + W(\to l\nu)$ process at $\sqrt{s} = 7\,\text{TeV}$ [136], [137] and CMS collaboration measured DPS in $pp \to 4j$ process [108]. In 2014 DØ collaboration measured DPS for the $pp \to J/\psi + J/\psi$, $\gamma + 3j$ and $\gamma + b/c + 2j$ production processes at $\sqrt{s} = 1.96\,\text{TeV}$ [138], [139], and ATLAS imposed a

lower bound on σ_{eff} in $pp \to J/\psi + Z$ process at $\sqrt{s} = 8\,\text{TeV}$ [140]. In 2015 LHCb collaboration measured DPS in production of bottomonia and open charm hadrons [141] and DØ observed DPS in simultaneous production of J/ψ and Υ mesons [142] and in $p\bar{p} \to 2j + 2\gamma$ [143]. In the same year the CMS collaboration measured DPS production in $pp \to 3j + \gamma$ process [144]. Unfortunately, no clear DPS signal was extracted from the collected data. In 2016 the ATLAS collaboration observed DPS in $pp \to 4j$ [145] and $pp \to J/\psi + J/\psi$ [134] at $\sqrt{S} = 7\,\text{TeV}$ and $\sqrt{S} = 8\,\text{TeV}$ correspondingly. Finally, in 2018 the CMS collaboration measured DPS in $pp \to W^+W^+, W^-W^-$ processes at $\sqrt{S} = 8\,\text{TeV}$ [146]. In these measurements no DPS above the expected SPS background was observed and, therefore, only a 95% confidence level lower limit $\sigma_{eff} > 12.1$ mb was imposed. The short summary on all these measurements apart from [146] is given in Fig. 2.2. We see that within provided statistical and systematic uncertainties most of the measurements of σ_{eff} agree between themselves. Moreover, we see that there is no clear indication of dependence of σ_{eff} on collision energy, see Fig. 2.3.

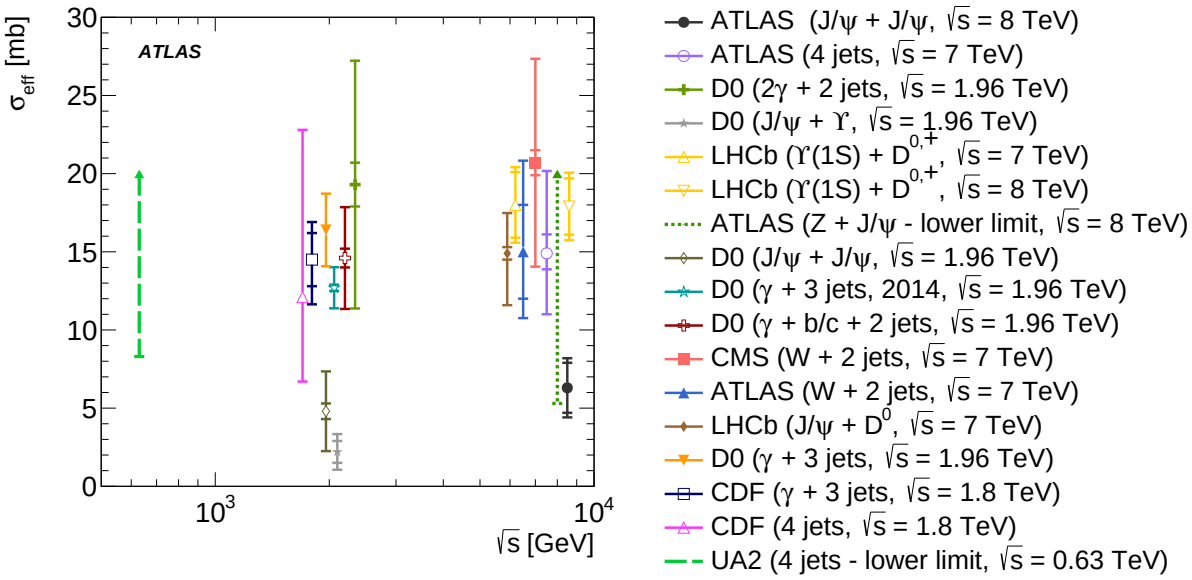

Figure 2.3: Dependence of σ_{eff} on the process and collision energy, from [134].

There are two different experimental techniques to study DPS processes. The first one is a so called "template method". Within this approach one creates SPS and DPS "templates" in the observable of interest and use them later to "split" the experimental data into the SPS and DPS contributions correspondingly. The DPS "templates" are created either with Monte Carlo event generators or by overlaying samples of independent SPS events. For example, one can create a "template" for the four-jet DPS production by overlaying two independent samples of the SPS di-jet events, see Fig. 2.4. Both approaches to create templates have their disadvantages. The Monte-Carlo approach depends on the Monte Carlo model being used to simulate DPS events. The DPS "templates" created by overlaying different data samples are expected to be model independent, however, completely neglect possible correlations between produced final state particles. The template technique can be combined with the machine learning methods as it was done in the ATLAS four-jet DPS measurements [145]. In that paper the artificial neural network "trained" with different DPS "templates" was used to extract the DPS signal out of the collected data. In 2015

the second method so called "inclusive fit" was proposed [147]. According to this approach, one produces MPI tunes for the general purpose event generators using only MPI sensitive distributions as an input. During the fitting procedure only the parameters of the MPI model of a given event generator are tuned to get the agreement with the data. Ones the parameters of the MPI model are fixed one can use them to calculate the value of σ_{eff}, see [147]. Therefore, we can conclude that all available extractions of σ_{eff} can be affected by various model uncertainties. Nevertheless, the available measurements allow to make some important conclusions concerning the existence of the partonic correlations. In order to illustrate it, let us show how one can estimate the value of σ_{eff} assuming no correlations between constituents of a proton. As we have seen before, assumption about factorization of $\Gamma_{a_1,a_2/h_A}(x_1, x_2, \boldsymbol{b})$ into longitudinal and transverse pieces allows to express σ_{eff} in terms of the distribution function $F(\boldsymbol{b})$ which gives a probability to find two partons separate by distance $|\boldsymbol{b}|$ in a transverse plane of a proton, see Eq. 2.6. Using simple models of $F(\boldsymbol{b})$ one can estimate the value of σ_{eff}. For example, if we assume that partons are uncorrelated and distributed in a transverse plane of a proton according to a Gaussian with an average $\langle \boldsymbol{b}^2 \rangle$ then we can find

$$\sigma_{eff} = 4\pi \langle \boldsymbol{b}^2 \rangle. \tag{2.12}$$

Now, taking into account that $\langle \boldsymbol{b}^2 \rangle \sim (0.57\text{fm} - 0.67\text{fm})^2$, we get σ_{eff} in the range between 41 and 56 mb, see the review [161]. However, as one can see in Fig. 2.2 and Fig. 2.3, the value of σ_{eff} evaluated in this way is in a strong disagreement with available experimental measurements. This mismatch was first noticed in 1997 by Calucci and Treleani [148]. Moreover, it was demonstrated that two-body correlations in a transverse plane of a proton can decrease value of σ_{eff} and, therefore, explain its small observed value [148]. This was followed by a series of publications where different correlations mechanisms were explored, see [149] - [160] and the review [161].

The aforementioned mismatch between the observed value of σ_{eff} and estimations based upon Gaussian parametrization of $F(\boldsymbol{b})$, therefore, can be seen as an indication of existence of non-trivial partonic correlations. The origin of this mismatch, however, remains unknown. One should keep in mind that existing experimental techniques to extract σ_{eff} as well as existent theoretical approaches to DPS rely on various assumptions. These assumptions can make exact studies of two-body partonic correlations complicated. Moreover, available theoretical models of DPS are flawed by different uncertainties, *e.g.* ignorance of two-parton distribution functions $\Gamma_{a_1,a_2/h_A}(x_1, x_2; \boldsymbol{b})$ and $D_{a_1,a_2/h_A}(x_1, x_2)$, *etc.*

Finally, we should stress that apart from "first principles approaches" to DPS phenomenon there exist a broad class of Monte Carlo MPI models as implemented in general purpose event generators, *e.g.* `Pythia` [255] - [257], Herwig++ [264] and SHERPA [267]. The detailed description of MPI models being used in `Pythia` and Herwig++ can be found in corresponding publications [258] - [262] and [265], [266]. The MPI model of SHERPA is based upon old MPI model of `Pythia` [259] with some modification as it is described in [267][4]. These MPI models are widely used to simulate DPS processes[5]. The aforementioned Monte Carlo models of MPI were developing in parallel to the "first

[4]There is also a new model of MPI under development, see [268].

[5]Since a typical MPI event contains one hard interaction and several soft interactions the generation of DPS events with the MPI models can be quite time consuming. The `Pythia` event generator starting from version 8 [256], [257] supports a possibility *always* generate two hard interaction in one hadron-hadron collision. Later in Chapter 6 we will discuss the DPS and MPI models of `Pythia` in more details.

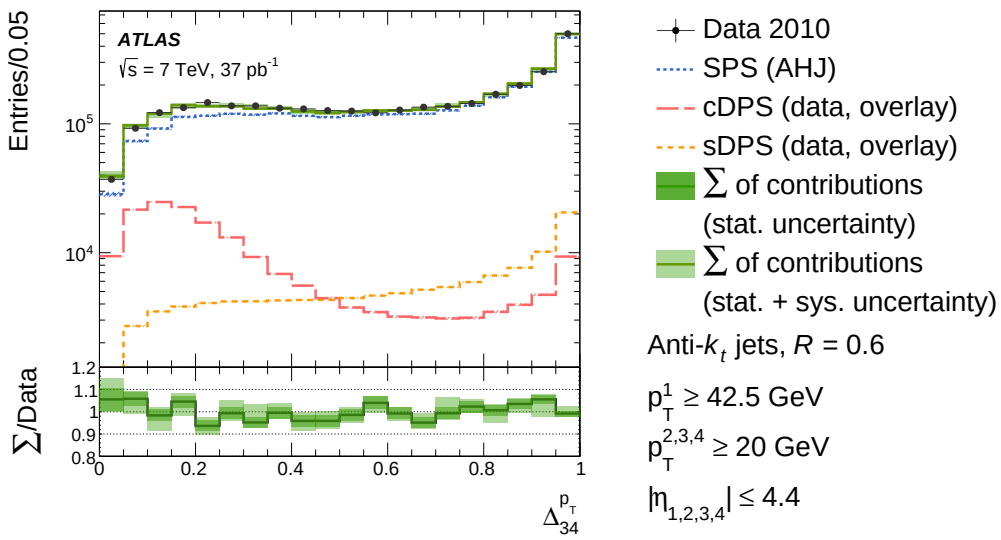

Figure 2.4: Template method to extract the fraction of the DPS events, from [145]. Distribution in terms of the transverse momentum imbalance of the third and fourth jets.

principles" models of DPS and, therefore, significantly differ from them in many places. Whereas the Monte Carlo models are widely used in experimental analysis, the "first principles" DPS models possess a lot of open purely theoretical problems which makes their implementation into Monte Carlo generators complicated.

2.2 Evolution of double parton distribution functions

In the previous section we have seen how the theory of DPS can be formulated in terms of objects $\Gamma_{a_1,a_2/h_A}(x_1,x_2,\boldsymbol{b})$ and $D_{a_1,a_2/h_A}(x_1,x_2)$. In the following we will call $\Gamma_{a_1,a_2/h_A}(x_1,x_2,\boldsymbol{b})$ *generalized parton distribution functions* (gPDFs) and $D_{a_1,a_2/h_A}(x_1,x_2)$ *double parton distribution functions* (dPDFs).

In the previous chapter, we have seen that the emission of collinear particles leads to violation of the Bjorken scaling and to scale dependent PDFs. Therefore, it is natural to try to consider scale dependent dPDFs and to find a system of intergo-differential equations describing their evolution. Such equations were first introduced by Kirschner in 1979 [164] and three years later by Shelest, Snigirev and Zinovev [167], [168] [6]. These equations, also called *double* DGLAP *evolution equations*

[6] Similar evolution equations for quark fragmentation functions were derived in [165], [166].

(dDGLAP), can be written as

$$\frac{dD_{j_1j_2}(x_1,x_2,t)}{dt} = \frac{\alpha_s}{2\pi}\sum_{j_1'}\int\limits_{x_1}^{1-x_2}\frac{dx_1'}{x_1'}P_{j_1'\to j_1}\left(\frac{x_1}{x_1'}\right)D_{j_1'j_2}(x_1',x_2,t) + \frac{\alpha_s}{2\pi}\sum_{j_2'}\int\limits_{x_2}^{1-x_1}\frac{dx_2'}{x_2'}P_{j_2'\to j_2}\left(\frac{x_2}{x_2'}\right)D_{j_2j_2'}(x_1,x_2',t) + \frac{\alpha_s}{2\pi}\sum_{j'}P_{j'\to j_1j_2}\left(\frac{x_1}{x_1+x_2}\right)f_{j'}(x_1+x_2,t)\frac{1}{x_1+x_2}, \tag{2.13}$$

where $f_{j'}(x,t)$ are "standard" collinear PDFs and we have dropped the subscript h_A in $D_{j_1j_2/h_A}$ in order not to overload the notation. Here we use a dimensionless evolution parameter $t = \log(Q/Q_0)$ where Q and Q_0 are final and initial values of the evolution scale respectively. The first two terms on the RHS of Eq. 2.13 involve standard DGLAP LO splitting functions $P_{j_1'\to j_1}(x)$ introduced in Chapter 1.5. Here we note that the first two terms on the RHS of Eq. 2.13, despite presence of two Bjorken variables, essentially have the same structure as standard DGLAP splitting kernels from Eq. 1.77 - 1.80. The last term, however, is new. It couples dDGLAP evolution equations to standard DGLAP equations, Eq. 1.74 - 1.76, and depends on the splitting functions $P_{j'\to j_1j_2}(x)$ which are new objects: if $P_{j'\to j}(x)$ can be interpreted as a probability that a parent parton j' will emit a parton j with $p_\perp^2 \ll Q^2$ carrying a fraction x of the longitudinal momentum of a parent parton j' then the splitting function $P_{j'\to j_1j_2}(x)$ can be interpreted as a probability that the parent parton j' will split into two partons j_1 and j_2 both having $p_\perp^2 \ll Q^2$ and carrying respectively fractions x and $1-x$ of the longitudinal momentum of j'. At the leading order one can express the sum of $P_{j'\to j_1j_2}(x)$ in terms of standard DGLAP splitting functions via

$$P^R_{i\to j}(x) = \sum_k P_{i\to jk}(x), \tag{2.14}$$

where $P^R_{i\to j}(x)$ are given by the real parts of the DGLAP splitting functions Eq. 1.77 - 1.80, see Chapter 2 of [170]. This term effectively includes processes where one parton splits perturbatively into two partons both having $p_\perp^2 \ll Q^2$, for example $g \to q\,\bar{q}$. Therefore, below we will refer to it as to "splitting" term or as to "1v2" term.

In addition to the derivation of dDGLAP equations authors of [164], [167] and [168] demonstrated that the solution of Eq. 2.13 cannot be expressed in a factorized form as

$$D_{j_1j_2}(x_1,x_2,t) = f_{j_1}(x_1,t)f_{j_2}(x_2,t), \tag{2.15}$$

where $f_{j_i}(x_i,t)$ are collinear single parton distribution functions. Moreover, even if we assume the absence of the correlations at the initial scale, or, in other words, if we use a factorization ansatz

$$D_{j_1j_2}(x_1,x_2,t_0) = f_{j_1}(x_1,t_0)\,f_{j_2}(x_2,t_0)\,\theta(1-x_1-x_2) \tag{2.16}$$

as an initial condition to solve Eq. 2.13, the evolution effects will violate this factorized ansatz at higher factorization scales [169]. The first numerical estimates of these effects were given in [171],

[172] where the technique of *Mellin transformation* was used to solve Eq. 2.13. In [169] the impact of the evolution effects on double gluon-gluon dPDFs was shown to be of the order of 10% for the scales of the Tevatron hard processes ($\sim 5\,\text{GeV}$) and of the order of 30% for the scales of the LHC hard processes ($\sim 100\,\text{GeV}$). In [172] the impact of the evolution effects on the DPS production of same-sign W-bosons and $b\bar{b}$ pairs was studied. The impact of the evolution effects on the DPS cross section for the same-sign production of W-bosons was found to be of the order of 40% at 1 TeV collision energy and of the order of 20% at 14 TeV collision energy. In case of the DPS production of the $b\bar{b}$ pairs the impact of the evolution effects on the DPS cross section was found to be of the order of $10-15\%$ at 1 TeV collision energy and of the order of 5% at 14 TeV collision energy.

However, the discussion in [169], [172] did not concern the sum rules for dPDFs. In 2009 Gaunt and Stirling demonstrated that the following sum rules:

$$\sum_{j_1} \int_0^{1-x_2} dx_1\, x_1\, D_{j_1 j_2}(x_1, x_2, t) = (1-x_2)\, f_{j_2}(x_2, t), \tag{2.17}$$

$$\sum_{j_1} \int_0^{1-x_2} dx_1\, D_{j_1 j_2}(x_1, x_2, t) = N_{j_{1v}}\, f_{j_2}(x_2, t), \quad \text{if } j_2 \neq j_1 \text{ or } \bar{j_1}, \tag{2.18}$$

$$\sum_{j_1} \int_0^{1-x_2} dx_1\, D_{j_1 j_2}(x_1, x_2, t) = (N_{j_{1v}} - 1)\, f_{j_2}(x_2, t), \quad \text{if } j_2 = j_1, \tag{2.19}$$

$$\sum_{j_1} \int_0^{1-x_2} dx_1\, D_{j_1 j_2}(x_1, x_2, t) = (N_{j_{1v}} + 1)\, f_{j_2}(x_2, t), \quad \text{if } j_2 = \bar{j_1}, \tag{2.20}$$

where $j_{1v} = j_1 - \bar{j_1}$ $(j_1 \neq g)$ and $N_{j_{1v}}$ is the number of valence j_1 quarks in the proton, are not violated by the dDGLAP evolution if they were preserved at the initial scale t_0 [173]. The first sum rule stands for a conservation of a longitudinal momentum. Its meaning becomes clear if one divides both sides by $D_{j_2}(x_2, t)$. Then one can interpret a ratio $D_{j_1 j_2}(x_1, x_2, t)/D_{j_2}(x_2, t)$ as a conditional probability $\mathrm{P}(j_1, x_1, t \,|\, j_2, x_2, t)$ to find a parton j_1 carrying a fraction x_1 of a proton's longitudinal momentum assuming that there already exist a parton of a type j_2 carrying a fraction x_2 of a proton's longitudinal momentum. Then

$$\sum_{j_1} \int_0^{1-x_2} dx_1\, x_1\, \mathrm{P}(j_1, x_1, t | j_2, x_2, t) = (1-x_2),$$

which has a clear interpretation: the integral on the LHS gives a total longitudinal momentum of all partons apart from j_2. The other three sum rules are generalized "standard" number rules which account for changes in a valence quark content. In the following we will refer to the dPDFs sum rules set by Eq. 2.17 - 2.20 as to *GS sum rules*. The connection between the momentum sum rule and the splitting term on the RHS of Eq. 2.13 was studied in [158], [176]. The GS sum rules were recently proved by Diehl, Plößß and Schäfer [177] in all orders of perturbation theory for "bare" dPDFs and for dPDFs renormalized according to the $\overline{\text{MS}}$ scheme[7]. We also shall notice

[7] In the Appendix C of [170] the GS sum rules were proved within the light-cone wave function framework. However, in [170] the explicit analysis of the UV-divergences and associated scale dependence of dPDFs was not provided.

that GS sum rules are nothing else but constraints which preserve conservation of the longitudinal momentum as well as of the number of valence quarks in DPS processes and, therefore, any realistic model of dPDFs should directly or indirectly obey Eq. 2.17 - 2.20. An example of such model is a model of dPDFs used in the `Pythia` event generator [255], [256], [260]. This model does not include dDGLAP evolution effects and accounts for momentum and number conservation by reweighting single collinear PDFs and by "squeezing" available phase space after each interaction. Later in Chapter 6 we will provide a detailed comparison between both `Pythia` and dDGLAP approaches to dPDFs. In particular, we will study how well both approaches satisfy Eq. 2.17 - 2.20, discuss some recent improvements in `Pythia`'s model of DPS and show how different models of dPDFs affect various DPS distributions.

Since initial conditions for dDGLAP equations are unknown, one can use the GS sum rules, Eq. 2.17 - 2.20, as a guiding tool to constrain dPDFs at initial evolution scale. It is quite natural to assume that the initial conditions can be expressed in terms of single collinear PDFs. However, the authors of [173] also demonstrated that one cannot express the initial conditions for $D_{j_v j_v}(x_1, x_2, t_0)$ as a factorized product of two PDFs without violating sum rules given by Eq. 2.17 - 2.20. They additionally proposed a form of the initial condition for $D_{j_v j_v}(x_1, x_2, t_0)$ which approximately satisfies Eq. 2.17 - 2.20:

$$D_{j_v j_v}(x_1, x_2, t_0) = \frac{N_{j_v} - 1}{N_{j_v}} D_{j_v}(x_1, t_0) D_{j_v}(x_2, t_0)\, \rho^{j_v j_v}(x_1, x_2) - 2g^{j\bar{j}}(x_1 + x_2, t_0), \tag{2.21}$$

where

$$\rho^{j_v j_v}(x_1, x_2) = (1 - x_1 - x_2)^2 \, (1 - x_1)^{-2-\alpha(j)} \, (1 - x_2)^{-2-\alpha(j)}, \tag{2.22}$$

with $\alpha(i) = 0$ if i is a sea parton and with $\alpha(i) = 0.5$ if i is a valence parton, and the function $g^{j\bar{j}}(x_1 + x_2, t_0)$ is defined as

$$g^{j\bar{j}}(x, t_0) = -\frac{\partial D_{\bar{j}}(x, t_0)}{\partial x}. \tag{2.23}$$

After the study of Gaunt and Stirling, an attempt to improve their way to construct initial conditions for dDGLAP equations was made by other authors, see [178] and [179]. However, despite successful solution for double gluon distributions[8], the approach of [178] turned out to have some significant flaws for double quark distributions [179]. Namely, it leads to negative values of dPDFs and introduces asymmetry of dPDFs under simultaneous interchange of Bjorken variables and parton labels, $D_{j_1 j_2}(x_1, x_2, t) \neq D_{j_2 j_1}(x_2, x_1, t)$.

So far, we have discussed only dPDFs with both factorization scales being set to the same value $D_{j_1 j_1}(x_1, x_2, t_1 = t_2 = t)$ which is a reasonable choice for certain DPS processes *e.g.* same-sign W-boson production. However, there exist a variety of DPS processes for which unequal scales dPDFs seem to be a more reasonable choice, *e.g.* four-jet DPS production[9]. The authors of [173] have argued that unequal scale dPDFs can be produced by applying single DGLAP evolution

[8] We also shall notice that recently results of [178] for collinear dPDFs were successfully extended to k_T-depended gluon-gluon dPDFs [181].

[9] We shall stress here that a choice of factorization scales for DPS processes is made by analogy with standard scale choices for SPS. To our knowledge there is no study which could advocate a specific scale choice.

equations to equal scale dPDFs. For example, one can take $D_{j_1 j_1}(x_1, x_2, t_1 = t_2 = t)$ and perform single DGLAP evolution for a given value of x_2 from $t_2 = t$ to a certain value $t_2 > t_1 = t$ keeping x_1 fixed. This procedure can be repeated for all values of x_2 smaller than $1 - x_1$. Using this technique, Gaunt and Stirling have obtained the set of unequal scale dPDFs which we will call GS09 dPDF set [173][10].

In order to produce the GS09 set of dPDFs Gaunt and Stirling have used the LO DGLAP splitting functions given by Eq. 1.77 - 1.80 and Eq. 2.14. Therefore, the GS09 dPDFs were obtained by solving dDGLAP equation at the *leading logarithmic approximation* (LLA) accuracy level. The short overview of the different methods to solve dDGLAP evolution equations at the LLA accuracy level is given in Appendix J. The generalization of the results of [173] to the *next-to-leading logarithmic approximation* (NLLA) accuracy level, however, is a non-trivial task. In 2011 Ceccopieri using so called *"jet calculus rules"* [189] wrote down the dDGLAP evolution equations at the NLLA accuracy level [175]. However, in [175] it was argued that the validity of the results obtained by the "jet calculus" technique have to be confirmed by the first principles calculations. Recently Diehl, Plößl and Schäfer [177] derived the system of the dDGLAP equations for the gPDFs in *momentum space*. The splitting functions in [177] computed at the NLO accuracy level confirmed the results of Ceccopieri [175]. The connection between the dDGLAP evolution equations for the gPDFs in momentum space and gPDFs in position space, however, is non-trivial. Later in this chapter we will discuss it in more details.

In order to close this section, let us note that apart from dDGLAP methods there are other approaches which allow either to model dPDFs or to calculate them from the first principles. Recently, first results on evaluation of the correlation functions of two quark currents in a pion were obtained with the help of the lattice QCD techniques [182]. The dPDFs were also computed within the Light-Front approach [183] - [186], so called "bag model" of a proton [187] and within the AdS/QCD framework [188]. However, the discussion of these methods is beyond the scope of this thesis.

2.3 Two parton distribution functions

The expression for the DPS cross section which includes generalized parton distributions $\Gamma_{a_1,a_2/h_A}(x_1, x_2; \boldsymbol{b})$ was first derived in the pioneer paper of Paver and Treleani for so called "scalar partons" in 1982 [116]. One year later, Mekhfi derived a similar expression where the spin of quarks was taken into account [117]. Later, in 2011, Diehl *et al.* generalized and extended the results of [116], [117] to the case of n-hard interactions [192], [193]. Namely, the results of [192], [193] were obtained using *n-point correlations functions* and generalized parton distributions defined in terms of the light-cone field operators. In this section we will briefly sketch the results of [192], [193] important for our phenomenological studies of the DPS phenomenon.

[10] In Appendix J we provide a short overview of different numerical methods to solve dDGLAP evolution equations.

Let us start with the definition of the *2-parton correlation function*

$$\begin{aligned}\Phi(l_1,l_2,l_1',l_2') &= \left[\prod_{i=1}^{2}\int \frac{d^4\xi_i}{(2\pi)^4}\frac{d^4\xi_i'}{(2\pi)^4}e^{i\xi_i l_i - i\xi_i' l_i'}\right]\times \\ &\times \int \langle p|\bar{T}\left[\phi(\xi_2')\phi(\xi_1')\right]T\left[\phi(\xi_1)\phi(\xi_2)\right]|p\rangle, \end{aligned} \tag{2.24}$$

where T and $\bar{T}$ respectively denote time-ordering and anti-time ordering of the scalar parton filed operators $\phi(\xi)$. The variables ξ_i and ξ_i' give position of initial and final state partons correspondingly. The variables l_i and l_i' are Fourier conjugates of ξ_i and ξ_i' in momentum space. Using the translation invariance of the matrix element $\langle p|\bar{T}\left[\phi(\xi_1')\phi(\xi_2')\right]T\left[\phi(\xi_1)\phi(\xi_2)\right]|p\rangle$ the position of one parton can be fixed yielding

$$\begin{aligned}\Phi(l_1,l_2,l_1') &= \left[\int \frac{d^4\xi_1}{(2\pi)^4}\frac{d^4\xi_1'}{(2\pi)^4}e^{i\xi_1 l_1 - i\xi_1' l_1'}\right]\times \\ &\times \int \frac{d^4\xi_2}{(2\pi)^4}\,e^{i\xi_2 l_2}\langle p|\bar{T}\left[\phi(0)\phi(\xi_1')\right]T\left[\phi(\xi_1)\phi(\xi_2)\right]|p\rangle, \end{aligned} \tag{2.25}$$

where the parton four-momenta l_i and l_i' obey the energy-momentum conservation constraint

$$\sum_{i=1}^{2} l_i = \sum_{i=1}^{2} l_i'. \tag{2.26}$$

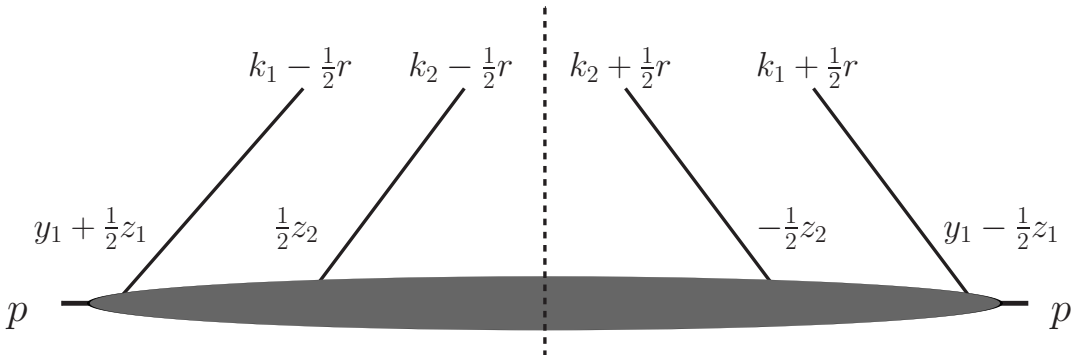

Figure 2.5: Assignment of momentum and position arguments in the multiparton correlation functions and distributions as in [193]. The dashed line denotes the final-state cut.

It is handy to rewrite Eq. 2.24 in terms of the symmetric momentum variables defined as

$$l_i = k_i - \frac{1}{2}r_i, \tag{2.27}$$

$$l_i' = k_i + \frac{1}{2}r_i. \tag{2.28}$$

Using Eq. 2.27 and Eq. 2.28, one can write the energy-momentum constraint $\sum_{i=1}^{2} l_i = \sum_{i=1}^{2} l_i'$ as

$$\sum_{i=1}^{2} r_i = 0, \tag{2.29}$$

which implies $r_1 = -r_2 \equiv r$. The variable r can be seen as a momentum transfer between initial and final state in the cut diagrams in Fig. 2.5.

Using Eq. 2.27 and Eq. 2.28 one can write correlation function $\Phi(l_1, l_2, l_1')$ in terms of k_1, k_2 and r as

$$\begin{aligned}\Phi(k_1, k_2, r) &= \left[\int \frac{d^4\xi_1}{(2\pi)^4}\frac{d^4\xi_1'}{(2\pi)^4} e^{i(\xi_1-\xi_1')k_1 - i(\xi_1+\xi_1')r/2}\right] \times \\ &\times \int \frac{d^4\xi_2}{(2\pi)^4} e^{i\xi_2(k_2+r/2)} \langle p|\bar{T}\left[\phi(0)\phi(\xi_1')\right] T\left[\phi(\xi_1)\phi(\xi_2)\right]|p\rangle. \end{aligned} \tag{2.30}$$

We can rewrite this expression using translation invariance of the matrix element. Therefore, we "shift" $\xi_i \to \xi_i - \xi_2/2$ which gives

$$\begin{aligned}\Phi(k_1, k_2, r) &= \left[\int \frac{d^4\xi_1}{(2\pi)^4}\frac{d^4\xi_1'}{(2\pi)^4}\frac{d^4\xi_2}{(2\pi)^4} e^{i(\xi_1-\xi_1')k_1 - i(\xi_1+\xi_1')r/2} e^{i\xi_2(k_2+r/2)}\right] \times \\ &\times \langle p|\bar{T}\left[\phi(-\frac{1}{2}\xi_2)\phi(\xi_1' - \frac{1}{2}\xi_2)\right] T\left[\phi(\xi_1 - \frac{1}{2}\xi_2)\phi(\frac{1}{2}\xi_2)\right]|p\rangle, \end{aligned} \tag{2.31}$$

where four momenta are assigned to partons as in Fig. 2.5. It is a first "building block" for the DPS cross section. In the following we will need so called *transverse momentum dependent* (TMD) gPDFs which are defined as

$$\begin{aligned}\Gamma(x_1, x_2, \boldsymbol{k}_1, \boldsymbol{k}_2, \boldsymbol{r}) &= \left[\prod_{i=1}^{2}\int \frac{dz_i^-}{2\pi} e^{ix_i z_i^- p^+} \int \frac{d^2\boldsymbol{z}_i}{(2\pi)^2} e^{-i\boldsymbol{z}_i\boldsymbol{k}_i}\right]\left[2p^+\int dy^-\, d^2\boldsymbol{y}_1\, e^{i\boldsymbol{y}_1\boldsymbol{r}}\right] \times \\ &\times \langle p|\mathcal{O}(0, z_2)\mathcal{O}(y_1, z_1)|p\rangle, \end{aligned} \tag{2.32}$$

where

$$\mathcal{O}(y, z) = \phi\left(y - \frac{1}{2}z\right) i\overleftrightarrow{\partial}_+ \phi\left(y + \frac{1}{2}z\right)\Big|_{y^+=z^+=0}. \tag{2.33}$$

The operator $\overleftrightarrow{\partial}_+$ in Eq. 2.33 is defined as $\overleftrightarrow{\partial}_+ = \frac{1}{2}(\overrightarrow{\partial} - \overleftarrow{\partial})$ and the products of operators in Eq. 2.32 are understood to be normal ordered [193]. The variables y_1, z_1 and z_2 describe postion of partons as explained in Fig. 2.5 and "plus" and "minus" subscripts in Eq. 2.32 stand for the plus and minus components of the four-vector in the light-cone coordinates[11].

There is an important connection between the two-parton correlation function $\Phi(k_1, k_2, r)$ and $\Gamma(x_1, x_2, \boldsymbol{k}_1, \boldsymbol{k}_2, \boldsymbol{r})$ [193]. In the frame where the initial state proton has zero transverse momentum it yields

$$\begin{aligned}\Gamma(x_1, x_2, \boldsymbol{k}_1, \boldsymbol{k}_2, \boldsymbol{r}) &= \left[\prod_{i=1}^{2} k_i^+ \int dk_i^-\right] \times \\ &\times (2\pi)^3 2p^+ \int dr^- \Phi(k_1, k_2, r)\Big|_{k_i^+ = x_i p_i^+, r_i^+ = 0}. \end{aligned} \tag{2.34}$$

In section 2.4 we will see how one can derive the expression for the DPS cross section using Eq. 2.31 and Eq. 2.34 in the so called *hard scattering approximation*. We will also discuss how the TMD

[11] For the definition of the light-cone coordinates see Appendix C.

gPDFs $\Gamma(x_1, x_2, \boldsymbol{k}_1, \boldsymbol{k}_2, \boldsymbol{r})$ are related to the gPDFs $\Gamma(x_1, x_2, \boldsymbol{b})$ and the PDFs $D(x_1, x_2)$. In the following we will also need so called *Sudakov form factors* which can be expressed as exponents of the total probability of the parton to decay in the range of virtualities between $\boldsymbol{Q}^2_{\rm min}$ and $\boldsymbol{Q}^2_{\rm max}$:

$$S_q(\boldsymbol{Q}^2_{\rm max}, \boldsymbol{Q}^2_{\rm min}) = \exp\left\{ -\int\limits_{\boldsymbol{Q}^2_{\rm min}}^{\boldsymbol{Q}^2_{\rm max}} \frac{d^2\boldsymbol{k}}{\boldsymbol{k}^2}\,\frac{\alpha_s(\boldsymbol{k}^2)}{2\pi} \int^{1-|\boldsymbol{k}|/|\boldsymbol{Q}_{\rm max}|} dz\, P_{q\to q}(z) \right\}, \tag{2.35}$$

$$S_g(\boldsymbol{Q}^2_{\rm max}, \boldsymbol{Q}^2_{\rm min}) = \exp\left\{ -\int\limits_{\boldsymbol{Q}^2_{\rm min}}^{\boldsymbol{Q}^2_{\rm max}} \frac{d^2\boldsymbol{k}}{\boldsymbol{k}^2}\,\frac{\alpha_s(\boldsymbol{k}^2)}{2\pi} \int^{1-|\boldsymbol{k}|/|\boldsymbol{Q}_{\rm max}|} dz\, [zP_{g\to g}(z) + N_f P_{q\to g}(z)] \right\}, \tag{2.36}$$

where N_f is a number of flavours.

2.4 The DPS cross section

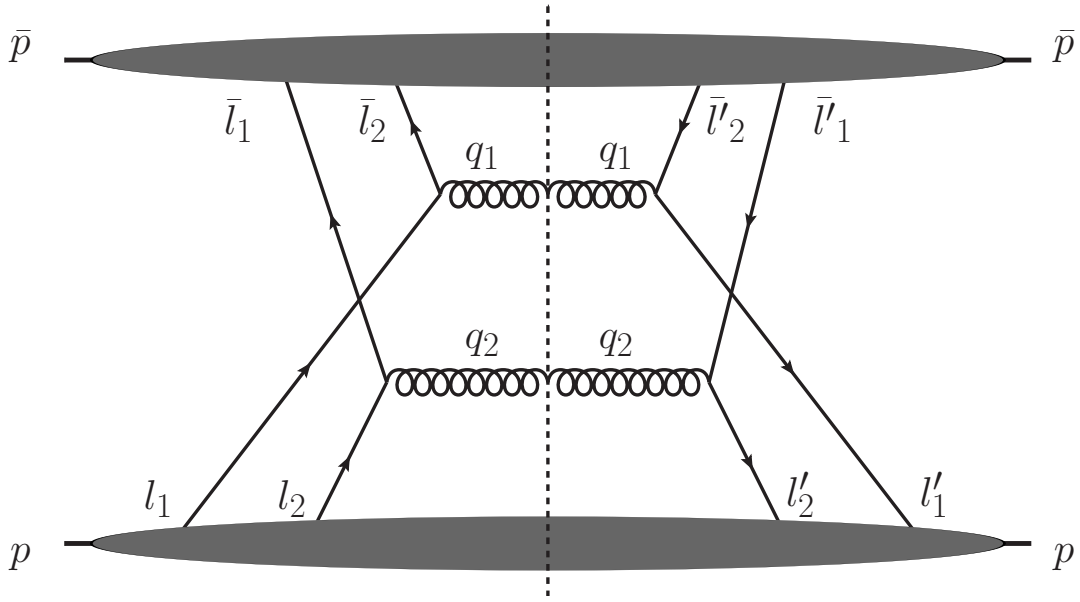

Figure 2.6: Collision of the left moving proton p with the right moving proton $\bar{p}$. The dashed line denotes the final-state cut. The four momenta are assigned as in [193].

Let us consider a cut diagram for the proton-proton collision shown in in Fig. 2.6. In the reference frame where both the left moving proton p and the right moving proton $\bar{p}$ have zero transverse momentum, under the assumption that the squared energy of each interaction q_i^2 is much grater than corresponding transverse momentum $\boldsymbol{q}_i$, one can write the DPS cross section as

$$\begin{aligned} d\sigma &= \frac{1}{C}\frac{1}{4p\bar{p}}\left[\prod_{i=1}^{2}\frac{d^4q_i}{(2\pi)^4}\right]\left[\int d^4k_i d^4\bar{k}_i (2\pi)^4\delta^4\left(q_i - k_i - \bar{k}_i\right)\right]\times \\ &\times \left[\int d^4r d^4\bar{r}\,(2\pi)^4\delta^4(r+\bar{r})\right]\times \\ &\times \left[\prod_{i=1}^{2} H_i(q_i, k_i, \bar{k}_i, r, \bar{r})\right]\Phi(k_i, r)\bar{\Phi}\left(\bar{k}_i, \bar{r}\right), \end{aligned} \tag{2.37}$$

where k_i, r_i and $\bar{k}_i, \bar{r}_i$ are the four-momenta of the left moving proton p and the right moving

proton $\bar{p}$ obtained from $l_i, \bar{l}_i$ according to Eq. 2.27 and Eq. 2.28, $\Phi(k_1, k_2, r)$ and $\bar{\Phi}\left(\bar{k}_1, \bar{k}_2, \bar{r}\right)$ are two-parton correlation functions defined as in Eq. 2.31, $H_i(q_i, k_i, \bar{k}_i, r_i, \bar{r}_i)$ is the squared amplitude of the i'th hard process and C is a combinatorial factor equal to $2! = 2$ for production of two identical final states.

One can simplify this expression using so called *hard-scattering approximation*. Within this approximation, we assume that all hard interactions have a certain characteristic scale Q which is of the order of the center-of-mass energy of each hard interaction $Q^2 \approx q_i^2$. We also assume that all partons which participate in hard interactions shown in Fig. 2.6 have virtualities much smaller than Q^2. Finally, we assume that the transverse momenta of the initial state partons are much smaller than Q. These assumptions allow us to write:

$$k_i^+ \sim r_i^+ \sim p^+ \sim q_i^+ \sim Q, \qquad \bar{k}_i^- \sim \bar{r}_i^- \sim \bar{p}^- \sim \bar{q}_i^- \sim Q, \tag{2.38}$$

$$k_i^- \sim r_i^- \sim p^- \sim \Lambda^2/Q, \qquad \bar{k}_i^+ \sim \bar{r}_i^+ \sim \bar{p}^+ \sim \Lambda^2/Q, \tag{2.39}$$

and

$$|\boldsymbol{k}_i| \sim |\boldsymbol{r}| \sim |\bar{\boldsymbol{k}}| \sim |\bar{\boldsymbol{r}}| \sim |\boldsymbol{q}_i| \sim \Lambda. \tag{2.40}$$

Therefore, in the reference frame where both protons p and $\bar{p}$ have zero transverse momentum, one can write

$$x_i = q_i^+/p^+, \tag{2.41}$$

$$\bar{x}_i = q_i^-/\bar{p}_i^-, \tag{2.42}$$

where x_i and $\bar{x}_i$ are Bjorken variables for the i'th parton in the protons p and $\bar{p}$ respectively. Then the collision energy of protons $\sqrt{S}$ and the collision energies of partons $\hat{s}_i$ are given by

$$S = (p + \bar{p})^2 \approx 2p\bar{p} \approx 2p^+p^-, \tag{2.43}$$

$$\hat{s}_i = q_i^2 \approx 2q^+q^- \approx x_i\bar{x}_iS. \tag{2.44}$$

The constraint $\delta^4(r + \bar{r})$ in Eq. 2.37 can be written as $\delta^2(\boldsymbol{r} + \bar{\boldsymbol{r}})\,\delta(r^+ + \bar{r}^+)\;\delta(r^- + \bar{r}^-)$ which forces r^+ component to be of the same order as $\bar{r}^-$ component:

$$r^+ \sim \bar{r}^- \sim \Lambda^2/Q, \tag{2.45}$$

which is a small quantity. Similarly, $\delta^4(q_i - k_i - \bar{k}_i)$ gives $q_i^+ = k_i^+ + \bar{k}_i^+$ and $q_i^- = k_i^- + \bar{k}_i^-$ which implies

$$q_i^+ \sim k_i^+ + \Lambda^2/Q, \tag{2.46}$$

$$q_i^- \sim \Lambda^2/Q + \bar{k}_i^-, \tag{2.47}$$

or, up to the terms of the order of Λ^2/Q, one can approximate

$$q_i^+ \approx k_i^+, \tag{2.48}$$

$$q_i^- \approx \bar{k}_i^-. \tag{2.49}$$

This approximation fixes the longitudinal momenta in the correlation functions Φ and $\bar{\Phi}$ in Eq. 2.37. Moreover, since all transverse components of k_i, $\bar{k}_i$, r, $\bar{r}$ and q_i are small, we assume that the amplitude squared H_i does not depend on them. Therefore, H_i can depend only on longitudinal degrees of freedom. However, Eq. 2.45 allows to neglect the dependence on r^+ and r^- and Eq. 2.48, Eq. 2.49 reduce a set of independent variables to q^+ and q_i^-. Therefore $H_i(q_i, k_i, \bar{k}_i, r_i, \bar{r}_i) \approx H_i(q_i^+, q_i^-)$. However, H_i has to be invariant under the boost transformation in the longitudinal direction. Because $q_i^2 = 2q_i^+ q_i^- - \boldsymbol{q}_i^2 \approx 2q_i^+ q_i^-$, we can write $H_i(q_i^+, q_i^-) = H_i(q_i^2)$.

We can apply now the aforementioned approximations to Eq. 2.37. First of all, let us write it as

$$\begin{aligned} d\sigma &= \left\{\prod_{i=1}^{2}\dots\right\}\left[\int dk_i^+ dk_i^- d\bar{k}_i^+ d\bar{k}_i^- \,\delta\left(q_i^+ - k_i^+ - \bar{k}_i^+\right)\delta\left(q_i^- - k_i^- - \bar{k}_i^-\right)\right]\times \\ &\times \left[\int dr^+ dr^- d\bar{r}^+ d\bar{r}^- \,\delta(r^+ + \bar{r}^+)\,\delta(r^- + \bar{r}^-)\right]\times \\ &\times \left[\prod_{i=1}^{2} H_i(q_i, k_i, \bar{k}_i, r, \bar{r})\right]\Phi(k_i, r)\bar{\Phi}\left(\bar{k}_i, \bar{r}\right), \end{aligned} \tag{2.50}$$

where $\left\{\prod_{i=1}^{2}\dots\right\}$ stands for

$$\begin{aligned} \left\{\prod_{i=1}^{2}\dots\right\} &= \frac{1}{C}\frac{1}{4p\bar{p}}\left[\prod_{i=1}^{2}\frac{d^4q_i}{(2\pi)^4}\right]\left[\int d^2\boldsymbol{k}_i d^2\bar{\boldsymbol{k}}_i (2\pi)^4\delta^2\left(\boldsymbol{q}_i - \boldsymbol{k}_i - \bar{\boldsymbol{k}}_i\right)\right]\times \\ &\times \left[\int d^2\boldsymbol{r} d^2\bar{\boldsymbol{r}}\,(2\pi)^4\delta^2(\boldsymbol{r} + \bar{\boldsymbol{r}})\right]. \end{aligned} \tag{2.51}$$

The delta functions in Eq. 2.50 reduce the number of integrations, so we have

$$\begin{aligned} d\sigma &= \left\{\prod_{i=1}^{2}\dots\right\}\left[\prod_{i=1}^{2}\int dk_i^+ d\bar{k}_i^- dr^- d\bar{r}^+\right]\times \\ &\times \left[\prod_{i=1}^{2} H_i(q_i, k_i, \bar{k}_i, r, \bar{r})\right]\Phi(k_i, r)\bar{\Phi}(\bar{k}_i, \bar{r})\Big|_{\substack{k_i^+ = q_i^+ - \bar{k}_i^+,\, r^+ = -\bar{r}^- \\ \bar{k}_i^- = q_i^- - k_i^-,\, \bar{r}^- = -\bar{r}^+}}. \end{aligned} \tag{2.52}$$

Within the hard scattering approximation one can write Eq. 2.52 as

$$\begin{aligned} d\sigma &= \left\{\prod_{i=1}^{2}\dots\right\}\prod_{i=1}^{2} H_i(q_i^2)\left[\int dk_i^- dr^-\right]\Phi(k_i, r)\Big|_{k_i^+ = q_i^+, r^+ = 0}\times \\ &\times \left[\int d\bar{k}_i^+ d\bar{r}^+\right]\bar{\Phi}(\bar{k}_i, \bar{r})\Big|_{\bar{k}_i^- = q_i^-, \bar{r}^- = 0}. \end{aligned} \tag{2.53}$$

Now we can use Eq. 2.34, Eq. 2.41 and Eq. 2.42 to rewrite Eq. 2.53 in terms of the distribution functions $\Gamma(x_1, x_2, \boldsymbol{k}_1, \boldsymbol{k}_2, \boldsymbol{r})$. In order to do it we insert into Eq. 2.53 the following ratio:

$$\left[\frac{(2\pi)^3 k_i^+ 2p^+}{(2\pi)^3 k_i^+ 2p^+}\right]\left[\frac{(2\pi)^3\bar{k}_i^- 2\bar{p}^-}{(2\pi)^3\bar{k}_i^- 2\bar{p}^-}\right], \tag{2.54}$$

which gives

$$\begin{aligned} d\sigma &= \left\{\prod_{i=1}^{2}\dots\right\}\prod_{i=1}^{2} H_i(q_i^2)\left[\frac{1}{(2\pi)^3 k_i^+ 2p^+}\right]\left[\frac{1}{(2\pi)^3 \bar{k}_i^- 2\bar{p}^-}\right]\times \\ &\times \left[k_i^+\int dk_i^-(2\pi)^3 2p^+\int dr^-\right]\Phi(k_i,r)\Big|_{k_i^+=q_i^+,r^+=0}\times \\ &\times \left[\bar{k}_i^-\int d\bar{k}_i^+(2\pi)^3 2\bar{p}^-\int d\bar{r}^+\right]\bar{\Phi}(\bar{k}_i,\bar{r})\Big|_{\bar{k}_i^-=q_i^-,\bar{r}^-=0}= \\ &= \left\{\prod_{i=1}^{2}\dots\right\}\prod_{i=1}^{2} H_i(q_i^2)\left[\frac{\Gamma(x_i,\boldsymbol{k}_i,\boldsymbol{r})}{(2\pi)^3 k_i^+ 2p^+}\right]\left[\frac{\Gamma(\bar{x}_i,\bar{\boldsymbol{k}}_i,\bar{\boldsymbol{r}})}{(2\pi)^3 \bar{k}_i^- 2\bar{p}^-}\right]. \end{aligned} \tag{2.55}$$

Regarding that within the hard scattering approximation $q_i^+ \approx k_i^+$ and $q_i^- \approx \bar{k}_i^-$, one can write

$$d\sigma = \left\{\prod_{i=1}^{2}\dots\right\}\prod_{i=1}^{2} H_i(q_i^2)\frac{1}{(2\pi)^6}\frac{1}{4p^+\bar{p}^-}\frac{1}{q_i^+ q_i^-}\Gamma(x_i,\boldsymbol{k}_i,\boldsymbol{r})\Gamma(\bar{x}_i,\bar{\boldsymbol{k}}_i,\bar{\boldsymbol{r}}). \tag{2.56}$$

Now we switch from the short hand notation $\left\{\prod_{i=1}^{2}\dots\right\}$ to the complete expression

$$\begin{aligned} d\sigma &= \frac{1}{C}\frac{1}{4p\bar{p}}\prod_{i=1}^{2}\frac{d^4q_i}{(2\pi)^4}H_i(q_i^2)\frac{1}{(2\pi)^6}\frac{1}{4p^+\bar{p}^-}\frac{1}{q_i^+ q_i^-}\times \\ &\times \left[\int d^2\boldsymbol{k}_i d^2\bar{\boldsymbol{k}}_i\,(2\pi)^4\,\delta^2\left(\boldsymbol{q}_i-\boldsymbol{k}_i-\bar{\boldsymbol{k}}_i\right)\right]\times \\ &\times \left[\int d^2\boldsymbol{r}d^2\bar{\boldsymbol{r}}\,(2\pi)^4\,\delta^2(\boldsymbol{r}+\bar{\boldsymbol{r}})\right]\Gamma(x_i,\boldsymbol{k}_i,\boldsymbol{r})\Gamma(\bar{x}_i,\bar{\boldsymbol{k}}_i,\bar{\boldsymbol{r}}). \end{aligned} \tag{2.57}$$

Using the constraint imposed by $\delta^2(\boldsymbol{r}+\bar{\boldsymbol{r}})$ and cancelling (2π) factors we get

$$\begin{aligned} d\sigma &= \frac{1}{C}\frac{1}{4p\bar{p}}\prod_{i=1}^{2}\frac{d^4q_i}{(2\pi)^2}H_i(q_i^2)\frac{1}{4p^+\bar{p}^-}\frac{1}{q_i^+ q_i^-}\times \\ &\times \left[\int d^2\boldsymbol{k}_i d^2\bar{\boldsymbol{k}}_i\delta^2\left(\boldsymbol{q}_i-\boldsymbol{k}_i-\bar{\boldsymbol{k}}_i\right)\right]\times \\ &\times \int d^2\boldsymbol{r}\,\Gamma(x_i,\boldsymbol{k}_i,\boldsymbol{r})\,\Gamma(\bar{x}_i,\bar{\boldsymbol{k}}_i,-\boldsymbol{r}). \end{aligned} \tag{2.58}$$

The four-volume d^4q_i in the light-cone coordinates can be written as $d^4q_i = d^2\boldsymbol{q}_i dq_i^+ dq_i^-$ or, using Eq. 2.41 and Eq. 2.42, one can write the four-volume d^4q_i as $d^4q_i = p^+\bar{p}^- d^2\boldsymbol{q}_i dx_i d\bar{x}_i$. Substituting

this expression for the four-volume into Eq. 2.58 and using $p\bar{p} = p^+\bar{p}^-$ one can write

$$\begin{aligned} d\sigma &= \frac{1}{C}\prod_{i=1}^{2}\frac{d^2\boldsymbol{q}_i}{(2\pi)^2}dx_i d\bar{x}_i \frac{H_i(q_i^2)}{4q_i^+q_i^-} \times \left[\int d^2\boldsymbol{k}_i d^2\bar{\boldsymbol{k}}_i\, \delta^2\left(\boldsymbol{q}_i - \boldsymbol{k}_i - \bar{\boldsymbol{k}}_i\right)\right] \times \\ &\times \int d^2\boldsymbol{r}\, \Gamma(x_i, \boldsymbol{k}_i, \boldsymbol{r})\, \Gamma(\bar{x}_i, \bar{\boldsymbol{k}}_i, -\boldsymbol{r}) = \\ &= \frac{1}{C}\prod_{i=1}^{2}\frac{d^2\boldsymbol{q}_i}{(2\pi)^2}dx_i d\bar{x}_i \frac{H_i(q_i^2)}{2q_i^2} \times \left[\int d^2\boldsymbol{k}_i d^2\bar{\boldsymbol{k}}_i\, \delta^2\left(\boldsymbol{q}_i - \boldsymbol{k}_i - \bar{\boldsymbol{k}}_i\right)\right] \times \\ &\times \int d^2\boldsymbol{r}\, \Gamma(x_i, \boldsymbol{k}_i, \boldsymbol{r})\, \Gamma(\bar{x}_i, \bar{\boldsymbol{k}}_i, -\boldsymbol{r}), \end{aligned} \tag{2.59}$$

where we have used $q_i^2 \approx 2q_i^+q_i^-$. Because $H_i(q_i^2)$ is an amplitude squared for the i'th hard process and $q_i^2 \approx \hat{s}_i$ we can write $\hat{\sigma}_i(q_i^2) = H_i(q_i^2)/2q_i^2$ which yields the expression for the DPS cross section

$$\begin{aligned} d\sigma &= \frac{1}{C}\prod_{i=1}^{2}\frac{d^2\boldsymbol{q}_i}{(2\pi)^2}dx_i d\bar{x}_i\, \hat{\sigma}_i(q_i^2) \times \left[\int d^2\boldsymbol{k}_i d^2\bar{\boldsymbol{k}}_i\, \delta^2\left(\boldsymbol{q}_i - \boldsymbol{k}_i - \bar{\boldsymbol{k}}_i\right)\right] \times \\ &\times \int d^2\boldsymbol{r}\, \Gamma(x_i, \boldsymbol{k}_i, \boldsymbol{r})\, \Gamma(\bar{x}_i, \bar{\boldsymbol{k}}_i, -\boldsymbol{r}), \end{aligned} \tag{2.60}$$

which can be written as

$$\begin{aligned} \frac{d\sigma}{\prod_{i=1}^{2} d^2\boldsymbol{q}_i dx_i d\bar{x}_i} &= \frac{1}{C}\prod_{i=1}^{2}\frac{1}{(2\pi)^2}\,\hat{\sigma}_i(q_i^2) \times \left[\int d^2\boldsymbol{k}_i d^2\bar{\boldsymbol{k}}_i\, \delta^2\left(\boldsymbol{q}_i - \boldsymbol{k}_i - \bar{\boldsymbol{k}}_i\right)\right] \times \\ &\times \int d^2\boldsymbol{r}\, \Gamma(x_i, \boldsymbol{k}_i, \boldsymbol{r})\, \Gamma(\bar{x}_i, \bar{\boldsymbol{k}}_i, -\boldsymbol{r}). \end{aligned} \tag{2.61}$$

Now, in order to get the formula for the DPS cross section derived first by Paver and Treleani, we have to integrate over $\boldsymbol{k}_i$ and $\bar{\boldsymbol{k}}_i$ and take the Fourier transform with respect to $\boldsymbol{r}$. Let us define the Fourier transform of $\Gamma(x_i, \boldsymbol{k}_i, \boldsymbol{r})$ as

$$\Gamma(x_i, \boldsymbol{k}_i, \boldsymbol{r}) = \int d^2\boldsymbol{b}\, e^{-i\boldsymbol{b}\boldsymbol{r}}\, \Gamma(x_i, \boldsymbol{k}_i, \boldsymbol{b}). \tag{2.62}$$

By applying Eq. 2.62 to Eq. 2.61 we get

$$\begin{aligned} \frac{d\sigma}{\prod_{i=1}^{2} d^2\boldsymbol{q}_i dx_i d\bar{x}_i} &= \frac{1}{C}\prod_{i=1}^{2}\frac{1}{(2\pi)^2}\,\hat{\sigma}_i(q_i^2) \times \left[\int d^2\boldsymbol{k}_i d^2\bar{\boldsymbol{k}}_i\, \delta^2\left(\boldsymbol{q}_i - \boldsymbol{k}_i - \bar{\boldsymbol{k}}_i\right)\right] \times \\ &\times \int d^2\boldsymbol{r}\, d^2\boldsymbol{b}\, d^2\boldsymbol{b}'\, e^{-i\boldsymbol{r}(\boldsymbol{b}-\boldsymbol{b}')}\, \Gamma(x_i, \boldsymbol{k}_i, \boldsymbol{b})\, \Gamma(\bar{x}_i, \bar{\boldsymbol{k}}_i, \boldsymbol{b}') = \\ &= \frac{1}{C}\prod_{i=1}^{2}\frac{1}{(2\pi)^2}\,\hat{\sigma}_i(q_i^2) \times \left[\int d^2\boldsymbol{k}_i d^2\bar{\boldsymbol{k}}_i\, \delta^2\left(\boldsymbol{q}_i - \boldsymbol{k}_i - \bar{\boldsymbol{k}}_i\right)\right] \times \\ &\times \int d^2\boldsymbol{b}\, \Gamma(x_i, \boldsymbol{k}_i, \boldsymbol{b})\, \Gamma(\bar{x}_i, \bar{\boldsymbol{k}}_i, \boldsymbol{b}), \end{aligned} \tag{2.63}$$

where the factor $(2\pi)^2$ was absorbed into the definition of the delta function. The TMD gPDFs $\Gamma(x_1, x_2, \boldsymbol{k}_1, \boldsymbol{k}_2, \boldsymbol{b})$ depend on Bjorken variables of two partons, their transverse momenta $\boldsymbol{k}_1$ and $\boldsymbol{k}_2$, and on the difference between their position vectors in a transverse plane of a hadron $\boldsymbol{b}$. We

can get rid of the dependence on $\boldsymbol{k}_1$ and $\boldsymbol{k}_2$ by performing integration over $\boldsymbol{q}_i^2$:

$$\begin{aligned}\frac{d\sigma}{\prod_{i=1}^{2} dx_i d\bar{x}_i} &= \frac{1}{C}\prod_{i=1}^{2}\hat{\sigma}_i(q_i^2)\times\left[\int d^2\boldsymbol{q}_i\, d^2\boldsymbol{k}_i d^2\bar{\boldsymbol{k}}_i\,\delta^2\left(\boldsymbol{q}_i-\boldsymbol{k}_i-\bar{\boldsymbol{k}}_i\right)\right]\times \\ &\times \int d^2\boldsymbol{b}\,\Gamma(x_i,\boldsymbol{k}_i,\boldsymbol{b})\,\Gamma(\bar{x}_i,\bar{\boldsymbol{k}}_i,\boldsymbol{b}) = \\ &= \frac{1}{C}\prod_{i=1}^{2}\hat{\sigma}_i(q_i^2)\times\frac{1}{(2\pi)^2}\left[\int d^2\boldsymbol{q}_i\, d^2\boldsymbol{k}_i\, d^2\bar{\boldsymbol{k}}_i\, d^2\boldsymbol{z}_i\, e^{-i\boldsymbol{z}_i(\boldsymbol{q}_i-\boldsymbol{k}_i-\bar{\boldsymbol{k}}_i)}\right]\times \\ &\times \int d^2\boldsymbol{b}\,\Gamma(x_i,\boldsymbol{k}_i,\boldsymbol{b})\,\Gamma(\bar{x}_i,\bar{\boldsymbol{k}}_i,\boldsymbol{b}),\end{aligned} \tag{2.64}$$

where we have used the integral representation of the delta function. Now we can rearrange the order of integration and evaluate the integral over $d^2\boldsymbol{q}_i$ which results into a delta function $\delta^2(\boldsymbol{z}_i)$ which, in turn, allows to disentangle integration over $\boldsymbol{k}_i$ and $\bar{\boldsymbol{k}}_i$ so, finally, we have

$$\frac{d\sigma}{\prod_{i=1}^{2} dx_i d\bar{x}_i} = \frac{1}{C}\prod_{i=1}^{2}\hat{\sigma}_i(q_i^2)\int d^2\boldsymbol{k}_i\, d^2\bar{\boldsymbol{k}}_i\, d^2\boldsymbol{b}\,\Gamma(x_i,\boldsymbol{k}_i,\boldsymbol{b})\,\Gamma(\bar{x}_i,\bar{\boldsymbol{k}}_i,\boldsymbol{b}). \tag{2.65}$$

We can define now collinear distributions

$$\Gamma(x_i,\boldsymbol{b}) \equiv \int d^2\boldsymbol{k}_i\,\Gamma(x_i,\boldsymbol{k}_i,\boldsymbol{b}), \tag{2.66}$$

leading to

$$\frac{d\sigma}{\prod_{i=1}^{2} dx_i d\bar{x}_i} = \frac{1}{C}\prod_{i=1}^{2}\hat{\sigma}_i(q_i^2)\int d^2\boldsymbol{b}\,\Gamma(x_i,\boldsymbol{b})\,\Gamma(\bar{x}_i,\boldsymbol{b}), \tag{2.67}$$

which is exactly the same expression as it was obtained by Paver and Treleani in [116]. Before moving to the next section, we shall note that the integral over $\boldsymbol{k}_i^2$ in Eq. 2.66 diverges and requires an appropriate regularization, see [192], [193]. However, the same problem emerges for single parton distributions [204] - [206], therefore we will not describe it here. Instead, we will concentrate on flaws in the theoretical formalism for DPS.

2.5 Problem of double counting and UV-divergences in DPS

In sections 2.2 - 2.4 we have described the key-ingredients of the DPS phenomenology: the DPS cross section, collinear dPDFs and dDGLAP evolution equations. However, as we discuss in this section, the formulation of the DPS in terms of the collinear dPDFs has some flaws. We briefly explain the origin of these flaws as well as exiting solutions to them. The details can be found either in publications we cite or in the review [202].

Let us start the discussion from the dDGLAP evolution equations for the collinear dPDFs given by Eq. 2.13. The splitting term on the RHS of Eq. 2.13 implies that the DPS cross section evaluated with dPDFs which obey dDGLAP evolution equations contains three different contributions which are schematically shown in Fig. 2.7. The "standard" DPS process is shown in Fig. 2.7 a). It involves four partons (two from each of two colliding hadrons) which exist at the non-perturbative

scale. In the following we will refer to such processes as to the "$2v2$" DPS contribution. However, due to the splitting term on the RHS of Eq. 2.13, a situation where one, or even two, initial state partons split perturbatively with a probability given by $P_{j'\to j_1 j_2}(x)$ before two hard interaction take place is possible. Such splittings give rise to new types of DPS processes shown in Fig. 2.7 b) and Fig. 2.7 c). In the following we will refer to them as to "$1v2$" and "$1v1$" DPS contributions, correspondingly.

The aforementioned theory of DPS relies on assumption about factorization of gPDFs into collinear and transverse pieces, see Eq. 2.4. It allows to encapsulate the information about distribution of partons in a transverse plane of a hadron into the parameter σ_{eff} and express the DPS cross section as a convolution of two collinear dPDFs and two hard partonic cross sections, see Eq. 2.8. However, as it was shown in [191], [192], [193], the separation of gPDFs into collinear and transverse pieces is inconsistent with the field-theoretical formulation of DPS and leads to incorrect description of DPS in kinematic regions in which two partons inside a proton originate from a perturbative splitting of a single parton. The problem of the formulation of the DPS theory in terms of the collinear dPDFs was discussed in a series of publications [190], [191], [192], [193], [195], [197], [198], [199], [200]. Several different solutions to it were proposed in [195], [197], [199], [200].

In this section we provide a brief overview of the problem of formulation of DPS in terms of collinear dPDFs and of solutions to it proposed in [195], [197], [199], [200].

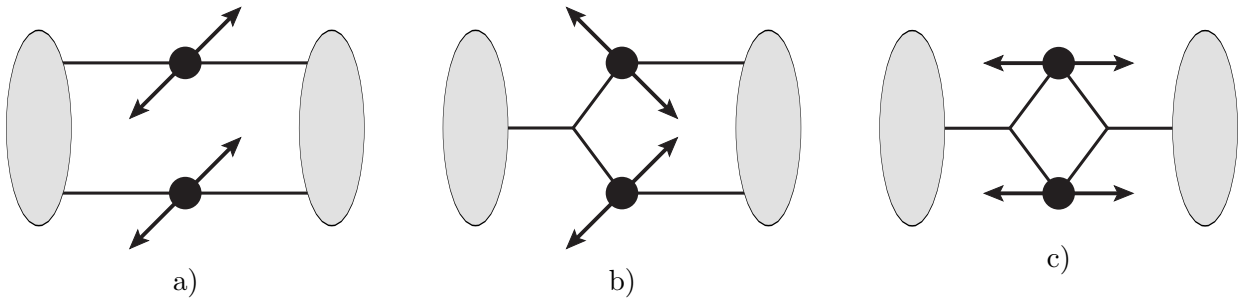

Figure 2.7: Schematic representation of different contributions to DPS. a) "$2v2$" contribution. b) "$1v2$" contribution. c) "$1v1$" contribution.

Let us start the discussion of flaws in factorization of gPDFs into collinear and transverse pieces from the results of Diehl *et al.* [192], [193]. Namely, in [192], [193] Diehl *et al.* computed the "$1v2$" contribution to the distribution function $\Gamma(x_1, x_2, \boldsymbol{b})$ in the limit of small values of $|\boldsymbol{b}|$. For the splitting of a mother parton of a type a_0 into a pair of partons a_1 and a_2 it yields

$$\Gamma^{1v2}_{a_1,a_2;\mathrm{pt}}(x_1, x_2, \boldsymbol{b}) = \frac{1}{|\boldsymbol{b}|^2}\frac{\alpha_s}{2\pi^2} P_{a_0\to a_1 a_2}\left(\frac{x_1}{x_1+x_2}\right)\frac{f_{a_0}(x_1+x_2)}{x_1+x_2}, \tag{2.68}$$

where $P_{a_0\to a_1 a_2}(x)$ is a $1\to 2$ LO splitting kernel defined in section 2.2, $f_{a_0}(x)$ is a standard collinear PDF of a mother parton a_0 and the dependence on factorization scales was not shown for brevity's sake. The $\sim 1/|\boldsymbol{b}|^2$ behaviour of the "$1v2$" contribution to the distribution $\Gamma(x_1, x_2, \boldsymbol{b})$ leads to the *ultraviolet* (UV) *divergences* in the DPS cross section. By substituting Eq. 2.68 into Eq. 2.67 one can see that the integral $\int d^2\boldsymbol{b}\,\Gamma(x_1, x_2, \boldsymbol{b})\,\Gamma(\bar{x}_1, \bar{x}_2, \boldsymbol{b})$ diverges logarithmically for "$1v2$" DPS contributions and quadratically for "$1v1$" DPS contributions. These UV-divergences indicate the failure of the DPS framework described in section 2.4. Their origin becomes clear if one recalls

the assumptions made to derive the DPS cross section given by Eq. 2.67. Namely, that Eq. 2.67 was derived within the hard scattering approximation which, among other things, implies that $|\boldsymbol{r}| \sim |\bar{\boldsymbol{r}}| \sim \Lambda \ll Q$, see section 2.4. The transverse distance $|\boldsymbol{b}|$ is defined as a Fourier conjugate of $|\boldsymbol{r}|$ which means that small values of $|\boldsymbol{b}|$ correspond to big values of $|\boldsymbol{r}|$ and vice versa. The integration over $d^2\boldsymbol{b}$ in Eq. 2.67, or over $d^2\boldsymbol{r}$ in Eq. 2.61, is not constrained and runs over all possible values of $|\boldsymbol{b}|$ and $|\boldsymbol{r}|$. It means that the integral over small values of $|\boldsymbol{b}|$ leads to large values of $|\boldsymbol{r}|$ and, at some point, to violation of the condition $|\boldsymbol{r}| \ll Q$ which was used to derive Eq. 2.67, see [192], [193]. Moreover, the integration over all possible values of $|\boldsymbol{b}|$ leads to the overlap between DPS and SPS contributions. The problem of double counting between DPS and SPS was discussed within different frameworks in [195], [197], [199], [200]. A similar problem for the multijet production was pointed out in [201].

In order to explain the double counting between DPS and SPS processes let us consider two cut diagrams in Fig. 2.8. The cut diagram in Fig. 2.8 a) corresponds to the "$1v1$" DPD contribution involving four partons which were "pulled out" of two gPDFs which is schematically represented by rectangles around upper and lower blobs in Fig. 2.8 a). The cut diagram in Fig. 2.8 b) corresponds to the one-loop SPS process where four quarks in the loop emerge due to the splitting of two initial state gluons into two quark-antiquark pairs. The cross section for the "$1v1$" DPS contribution in Fig. 2.8 a) is derived in the hard scattering approximation which implies that four-momenta of quarks are restricted to the kinematic domain where the hard scattering approximation is valid, see section 2.4. However, in order to compute the one-loop SPS contribution shown in Fig. 2.8, one has to integrate over all values of loop momenta which also include a domain of the DPS contribution which, in turn, leads to the double counting between processes shown in Fig. 2.8 a) and b).

The same problem arises for "$1v2$" DPS contributions. In order to illustrate it consider cut diagrams shown in Fig. 2.9. The cut diagram in Fig. 2.9 a) stands for the "$1v2$" DPS contribution. In this case, the "$1v2$" splitting is included into gPDF $\Gamma(x_1, x_2, \boldsymbol{b})$ which is schematically represented by the rectangle around the upper blob in Fig. 2.9 a). In the case of so called *twist-four contribution* shown in Fig. 2.9 b) the $1 \to 2$ splitting is not included into the parton distribution function of the upper blob and, therefore, the gluon in Fig. 2.9 b) emerges from a single parton distribution function. As it was pointed out in [200], both graphs correspond to the different approximations which are valid for the different values of transverse momenta of partons $\boldsymbol{q}_i$ produced due to the $1 \to 2$ splitting. The graph in Fig. 2.9 a) correspond to the small values of $\boldsymbol{q}_i$ which implies that both partons are almost collinear. On the contrary, the graph shown in Fig. 2.9 b) corresponds to the large values of $\boldsymbol{q}_i$. The cross section corresponding to the Fig. 2.9 a), therefore, does not depend on two-parton distribution functions but on twist-four distributions which correspond to the power suppressed corrections in factorization theorems, Eq. 1.33, Eq. 1.34. More precisely, the hadronic tensor $W^{\mu\nu}$ given by Eq. 1.28, can be expressed as a Fourier transform of a commutator of two quark currents as

$$W^{\mu\nu} = \frac{1}{4\pi} \int d^4\xi \, e^{iq\xi} \, \langle P | \, [J^\mu(\xi), J^\nu(0)] \, | P \rangle, \tag{2.69}$$

where $|P\rangle$ is a hadron ground state and q^2 is a virtuality of a photon exchanged in the DIS process, see [44]. The commutator in Eq. 2.69 can be expanded using so called *operator product expansion*

(OPE) method. This expansion involves operators of different dimensionality each contributing as

$$\left(\frac{1}{Q^2}\right)^t, \tag{2.70}$$

where $Q^2 \equiv -q^2$ and t is so called *twist* of the operator which is defined as $t = d - s$, where d is a dimensionality of a given operator and s is a value of spin it corresponds to. Operators characterized by different values of t in the OPE of Eq. 2.69 being "sandwiched" between $\langle P|$ and $|P\rangle$ give rise to different contributions to $W^{\mu\nu}$. The discussion of the OPE method and its application to calculation of the hadronic tensor $W^{\mu\nu}$ is beyond the scope of this thesis and can be found in Chapter 18 of [5] and in [44]. Here we just note that the twist-two operators give rise to the "standard" single PDFs and that contributions from the twist-four operators is suppressed as $1/Q^4$. Therefore, the problem of double counting between "$1v2$" DPS contribution and twist-four contribution arises only if one goes beyond the leading log approximation of QCD [200].

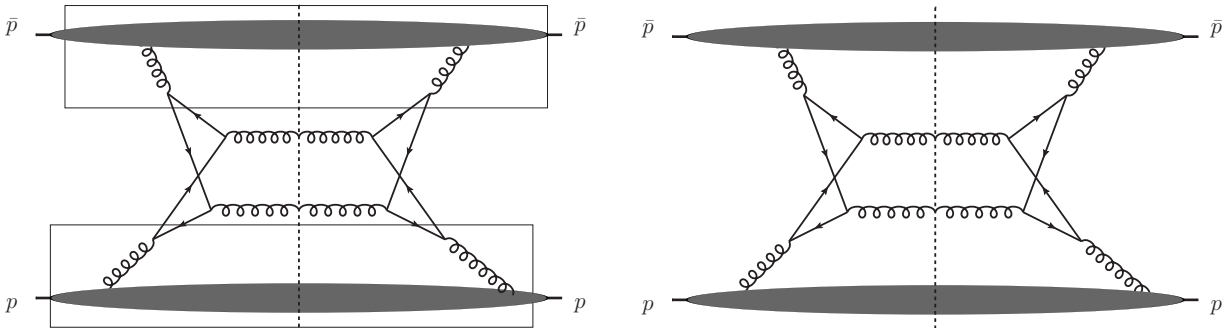

Figure 2.8: DPS and SPS "$1v1$" contributions. The dashed line denotes the final-state cut. a) "$1v1$" DPS contribution. Here the "box" represent double parton distributions. b) one-loop SPS contribution.

The aforementioned problems of the double counting between DPS and SPS contributions as well as the related problems of UV-singularities at low transverse distances obviously require a solution which would allow a consistent treatment of DPS in all orders of perturbation theory. Several different solutions exist in the literature. One of the first solutions was proposed by Blok *et al.* [195] and by Ryskin and Snigirev [197], [198]. The study in these papers was performed for TMD gPDFs $\Gamma(x_1, x_2, \boldsymbol{k}_1, \boldsymbol{k}_2, \boldsymbol{r})$. A starting point of the approach proposed in [195] was to split the distribution function $\Gamma(x_1, x_2, \boldsymbol{k}_1, \boldsymbol{k}_2, \boldsymbol{r})$ defined by Eq. 2.34 into "intrinsic" and "perturbative" parts as

$$\Gamma(x_1, x_2, \boldsymbol{k}_1, \boldsymbol{k}_2, \boldsymbol{r}) = \Gamma^{2v2}(x_1, x_2, \boldsymbol{k}_1, \boldsymbol{k}_2, \boldsymbol{r}) + \Gamma^{1v2}(x_1, x_2, \boldsymbol{k}_i, \boldsymbol{k}_2, \boldsymbol{r}), \tag{2.71}$$

where Γ^{2v2} is the "intrinsic" part which is in charge for "$2v2$" DPS contribution and Γ^{1v2} is the "perturbative" part which is in charge for "$1v2$" DPS contribution. The intrinsic part obeys

homogeneous double DGLAP evolution equations for TMD gPDFs:

$$\begin{aligned}
&\Gamma^{2v2}_{j_1,j_2}(x_1,x_2,\boldsymbol{k}_1,\boldsymbol{k}_2,\boldsymbol{r}) = S_{j_1}(\boldsymbol{k}_1^2,\boldsymbol{Q}^2_{\min})\,S_{j_2}(\boldsymbol{k}_2^2,\boldsymbol{Q}^2_{\min})\,\Gamma^{2v2}_{j_1,j_2}(x_1,x_2,\boldsymbol{Q}_0,\boldsymbol{Q}_0,\boldsymbol{r}) + \\
&+ \sum_{j_1'} \int\limits_{\boldsymbol{Q}^2_{\min}}^{\boldsymbol{k}_1^2} \frac{d^2\boldsymbol{k}}{\boldsymbol{k}^2}\,\frac{\alpha_s(\boldsymbol{k}^2)}{2\pi} S_{j_1}(\boldsymbol{k}_1^2,\boldsymbol{k}^2) \int \frac{dz}{z} P_{j_1\to j_1'}(z)\,\Gamma^{2v2}_{j_1',j_2}\left(\frac{x_1}{z},x_2,\boldsymbol{k},\boldsymbol{k}_2,\boldsymbol{r}\right) + \\
&+ \sum_{j_2'} \int\limits_{\boldsymbol{Q}^2_{\min}}^{\boldsymbol{k}_2^2} \frac{d^2\boldsymbol{k}}{\boldsymbol{k}^2}\,\frac{\alpha_s(\boldsymbol{k}^2)}{2\pi} S_{j_2}(\boldsymbol{k}_2^2,\boldsymbol{k}^2) \int \frac{dz}{z} P_{j_2\to j_2'}(z)\,\Gamma^{2v2}_{j_1,j_2'}\left(x_1,\frac{x_2}{z},\boldsymbol{k}_1,\boldsymbol{k},\boldsymbol{r}\right)
\end{aligned} \tag{2.72}$$

where $P_{j_i\to j_i'}(z)$ are LO DGLAP splitting functions as in Eq. 1.77 - 1.80 without terms proportional to the δ-function. The functions S_{j_i} are Sudakov form factors defined by Eq. 2.35 and Eq. 2.36. The perturbative part $\Gamma^{1v2}(x_1,x2,\boldsymbol{k}_1,\boldsymbol{k}_2,\boldsymbol{r})$ is constructed as a convolution of single collinear PDFs $f_i(x,Q^2)$ and distribution functions $\mathcal{D}^i_j(x,Q_{\rm res},Q_{\rm vir})$ which give the probability to find a parton i at the resolution scale $Q_{\rm res}$ inside of a parton j with a virtuality scale $Q_{\rm vir} < Q_{\rm res}$. The corresponding expression reads

$$\begin{aligned}
&\Gamma^{1v2}_{j_1,j_2}(x_1,x_2,\boldsymbol{k}_1,\boldsymbol{k}_2,\boldsymbol{r}) = \sum_{j_1',j_2',j_3'} \int\limits_{Q^2_{\min}}^{\min(\boldsymbol{k}_1^2,\boldsymbol{k}_2^2)} \frac{d^2\boldsymbol{k}}{\boldsymbol{k}^2}\,\frac{\alpha_s(\boldsymbol{k}^2)}{2\pi}\,\frac{dy}{y^2} D_{j_3'}(y,\boldsymbol{k}) \times \\
&\times \int \frac{dz}{z(1-z)}\,P_{j_3'\to j_1' j_2'}(z)\,\mathcal{D}^{j_1}_{j_1'}\left(\frac{x_1}{zy},\boldsymbol{k}_1,\boldsymbol{k}\right)\mathcal{D}^{j_2}_{j_2'}\left(\frac{x_2}{(1-z)y},\boldsymbol{k}_2,\boldsymbol{k}\right).
\end{aligned} \tag{2.73}$$

The lower integration boundary in Eq. 2.72 and Eq. 2.73 for the integration over $d^2\boldsymbol{k}$ starts from $Q^2_{\min} = \max(Q_0^2,\boldsymbol{r}^2)$ where Q_0 is a starting evolution scale.

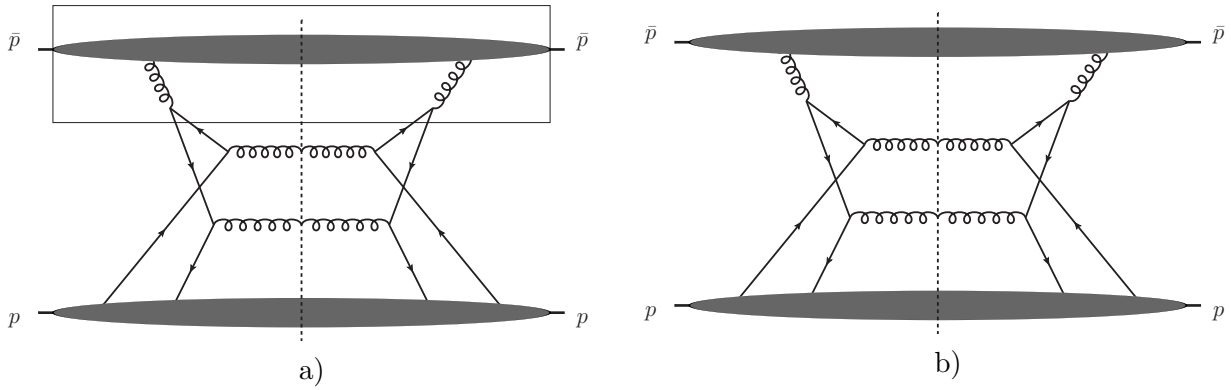

Figure 2.9: "$1v2$" DPS contributions and twist-four SPS contribution. The dashed line denotes the final-state cut. a) DPS "$1v2$" contribution. The "box" here represent double parton distributions. b) Twist-four SPS contribution.

After evaluating "intrinsic" and "perturbative" parts of $\Gamma(x_1,x_2,\boldsymbol{k}_1,\boldsymbol{k}_2,\boldsymbol{r})$ according to Eq. 2.72 and Eq. 2.73 one can substitute them into Eq. 2.60. The resulting combinations of "intrinsic" and "perturbative" pieces resulting from the product $\Gamma(x_1,x_2,\boldsymbol{k}_1,\boldsymbol{k}_2,\boldsymbol{r})\,\Gamma(\bar{x}_1,\bar{x}_2,\bar{\boldsymbol{k}}_1,\bar{\boldsymbol{k}}_2,-\boldsymbol{r})$ give rise to "$1v1$", "$1v2$" and "$2v2$" DPS contributions. As it was argued in [195], the choice of the lower integration boundary $Q^2_{\min} = \max(Q_0^2,\boldsymbol{r}^2)$ in Eq. 2.72 leads to an additional logarithmic

$|\boldsymbol{r}|$-dependence of $\Gamma^{2v2}_{j_1,j_2}(x_1,x_2,\boldsymbol{k}_1,\boldsymbol{k}_2,\boldsymbol{r})$ if $\boldsymbol{r}^2 > Q_0^2$. Since the lower boundary for the integration over $d^2\boldsymbol{k}$ in Eq. 2.73 is the same, the "perturbative" distribution $\Gamma^{1v2}_{j_1,j_2}(x_1,x_2,\boldsymbol{k}_1,\boldsymbol{k}_2,\boldsymbol{r})$ will depend on $|\boldsymbol{r}|$ only logarithmically.

After developing the aforementioned formalism, Blok *et al.* studied how the evolution effects impact the value of the effective cross section σ_{eff} [196], [158]. In this study the additional logarithmic dependence of $\Gamma^{1v2}(x_1,x_2,\boldsymbol{k}_1,\boldsymbol{k}_2,\boldsymbol{r})$ and $\Gamma^{2v2}(x_1,x_2,\boldsymbol{k}_1,\boldsymbol{k}_2,\boldsymbol{r})$ due to the integration boundary $Q^2_{\min} = \max(Q_0^2,\boldsymbol{r}^2)$ was neglected. Therefore, $\Gamma^{1v2}(x_1,x_2,\boldsymbol{k}_1,\boldsymbol{k}_1,\boldsymbol{r}) \approx \Gamma^{1v2}(x_1,x_2,\boldsymbol{k}_1,\boldsymbol{k}_2)$. This approximation, however, does not solve a problem of the UV-divergences in the integral over $d^2\boldsymbol{r}$ at large values of $\boldsymbol{r}$, see Eq. 2.60. This problem was solved by postulating $\boldsymbol{r}^2$-dependence of $\Gamma^{2v2}(x_1,x_2,\boldsymbol{k}_1,\boldsymbol{k}_2,\boldsymbol{r})$ to be described by the two gluon form factor

$$F_{2g}(\boldsymbol{r}^2) = \left(1 + \frac{|\boldsymbol{r}|^2}{m_g^2}\right)^{-2}, \tag{2.74}$$

where parameter $m_g^2 \approx 1.1\,\mathrm{GeV}^2$ was extracted from the FNAL and HERA J/ψ photoproduction data [203]. The usage of $F_{2g}(\boldsymbol{r}^2)$ in the modelling of two-parton distribution functions $\Gamma^{1v1}_{j_1,j_2}(x_1,x_2,\boldsymbol{k}_1,\boldsymbol{k}_2,\boldsymbol{r})$ and $\Gamma^{2v2}(x_1,x_2,\boldsymbol{k}_1,\boldsymbol{k}_2,\boldsymbol{r})$ in fact means introduction of the damping functions into DPS cross section which makes integration over $d^2\boldsymbol{r}$ in Eq. 2.60 finite. The problem of double counting between "$1v2$" and twist-four contributions was not discussed in [194], [196]. Finally, it was argued that "$1v1$" contribution has to be suppressed for the DPS production of two pairs of back-to-back di-jets and, therefore, "$1v1$" contribution was discarded.

A similar study was performed by Ryskin and Snigirev in [197], [198] where, unlike in [196], the "$1v1$" contribution was taken into account. Since, up to logarithmic corrections, the "perturbative" piece $\Gamma^{1v1}_{j_1,j_2}(x_1,x_2,\boldsymbol{k}_1,\boldsymbol{k}_2)$ does not depend on $\boldsymbol{r}^2$, the "$1v1$" DPS correction will diverge quadratically at large values of $|\boldsymbol{r}|$. This divergence was regularized by imposing an upper integration cut off $\min(\boldsymbol{q}_1^2,\boldsymbol{q}_2^2)$ on the $d^2\boldsymbol{r}$ integral.

The connection between the aforementioned UV-divergences and the factorized formula for DPS cross section given by Eq. 2.61 and Eq. 2.63 was studied by Manohar and Waalewijn in [199] by means of the renormalization of the field operators which give rise to different DPS contributions. Namely, it was demonstrated that there is no concept of gPDFs associated with an individual hadron since, unlike the SPS case, the filed operators which give rise to gPDFs involve both hadrons at once as schematically shown in Fig. 2.10 b) and c). In particular, it implies that

$$\left[\int d^2\boldsymbol{b}\,\Gamma_{h_A}(\boldsymbol{b})\,\Gamma_{h_B}(\boldsymbol{b})\right] \neq \int d^2\boldsymbol{b}\,\left[\Gamma_{h_A}(\boldsymbol{b})\right]\left[\Gamma_{h_B}(\boldsymbol{b})\right], \tag{2.75}$$

where $[\ldots]$ means UV-renormalization of the field operators which correspond to gPDFs $\Gamma_{h_A}(\boldsymbol{b})$ and $\Gamma_{h_B}(\boldsymbol{b})$ of hadrons h_A and h_B respectively. Moreover, in Ref. [199] it was shown that the work with the renormalized product of filed operators $\left[\int d^2\boldsymbol{b}\,\Gamma_{h_A}(\boldsymbol{b})\,\Gamma_{h_B}(\boldsymbol{b})\right]$ instead of products of renormalized operators $\int d^2\boldsymbol{b}\,\left[\Gamma_{h_A}(\boldsymbol{b})\right]\left[\Gamma_{h_B}(\boldsymbol{b})\right]$ allows to avoid UV-divergences and double counting between DPS and SPS contributions. However, working within the framework of Manohar and Waalewijn one cannot retain the concept of gPDFs associated with individual hadrons[12]. In

[12] A similar observation was made in the paper of Blok *et al.* [158]. Namely, it was stated that "It is important to stress that in the MPI physics there is *no factorization* in the usual sense of the word.".

2018 Diehl, Gaunt and Schönwald proposed their solution to the problem of double counting and UV-singularities which allows to treat DPS in all orders in perturbation theory consistently, without loosing a concept of gPDFs defined for individual hadrons [200]. The method developed in [200] is based upon classification of space phase regions where one-loop SPS and twist-four contributions overlap with "$1v1$" and "$1v2$" DPS contributions, correspondingly. The double counted contributions are then subtracted by adding corresponding subtraction terms to the sum of the SPS and DPS cross sections. The formalism developed in [200] applies to the TMD gPDFs $\Gamma(x_1, x_2, \boldsymbol{k}_1, \boldsymbol{k}_2, \boldsymbol{r})$ as well as to the collinear gPDFs $\Gamma(x_1, x_2, \boldsymbol{r})$. However, since in this thesis we consider only collinear gPDFs, we will briefly sketch the results of [200] using collinear gPDFs as an example.

Let us consider first the "$1v1$" DPS contribution. In this case the subtraction term $\sigma_{1v1,\mathrm{pt}}$ used to avoid the double counting between "$1v1$" DPS contribution and one-loop SPS contribution is given by

$$\frac{d\sigma_{1v1,\mathrm{pt}}}{\prod_{i=1}^{2} dx_i\, d\bar{x}_i} = \sum_{a_1,a_2,b_1,b_2} \hat{\sigma}_{a_1,a_2}\hat{\sigma}_{b_1,b_2} \int d^2\boldsymbol{b}\, \Phi^2\left(|\boldsymbol{b}|\nu\right)\, \Gamma^{1v2}_{a_1,a_2;\mathrm{pt}}(x_i, \boldsymbol{b})\, \Gamma^{1v2}_{b_1,b_2;\mathrm{pt}}(\bar{x}_i, \boldsymbol{b}), \tag{2.76}$$

where $\Gamma_{1v2,\mathrm{pt}}$ is a short-distance approximation of the splitting part of gPDFs $\Gamma(x_1, x_2, \boldsymbol{b})$ which can be computed by perturbative means, see Eq. 2.68. The cutoff function $\Phi(u)$ is chosen such that $\Phi(u) \to 1$ if $u \gg 1$ and such that $\Phi(u)$ goes to zero at small values of u.[13] The parameter ν in Eq. 2.76 has a dimension of energy and plays the role of the cutoff scale. The short-distance approximation functions were evaluated in [200] by means of dimensional regularization. Their exact form depends on a number of dimensions. For example, in $D = 2$ dimensions $\Gamma_{1v2,\mathrm{pt}}(x_i, \boldsymbol{b})$ is proportional to $\sim 1/|\boldsymbol{b}|$ which allows to write integration over $d^2\boldsymbol{b}$ in Eq. 2.76 as

$$\int \frac{d^2\boldsymbol{b}}{|\boldsymbol{b}|^4}\, \Phi^2\left(|\boldsymbol{b}|\nu\right) = \nu^2 \int \frac{d^2\boldsymbol{u}}{|\boldsymbol{u}|^4}\, \Phi^2\left(|\boldsymbol{u}|\right). \tag{2.77}$$

We see that $\sigma_{1v1,\mathrm{pt}}$ scales quadratically with ν. The complete contribution to the total cross section (DPS + SPS) from the graphs in Fig. 2.8 is given by

$$\sigma^{\mathrm{SPS}} - \sigma_{1v1,\mathrm{pt}} + \sigma^{\mathrm{DPS}}_{1v1}. \tag{2.78}$$

The cutoff scale ν is chosen to be of the order of the factorization scale Q which implies $|\boldsymbol{b}| = 1/Q$. Then, for large values of Q and correspondingly for the small values of $|\boldsymbol{b}|$, one has $\sigma_{1v1,\mathrm{pt}} \approx \sigma^{\mathrm{DPS}}_{1v1}$ which means that at small transverse distances only the σ^{SPS} contribution is present. In this case, the dependence on ν cancels between both contributions. And vice versa at large transverse distances $|\boldsymbol{b}| \gg 1/Q$ we have $\sigma^{\mathrm{SPS}} \approx \sigma_{1v1,\mathrm{pt}}$, so only $\sigma^{\mathrm{DPS}}_{1v1}$ contribution is present. The cutoff dependence does not play a role in this region of the phase space since $\Phi(u) \to 1$ at large values of u.

Similar solution was found for the double counting between the twist-four and "$1v2$" contributions

[13] More precisely, $\Phi(u)$ should reach to zero at small values of u but remain integrable. Therefore, if $u \to 0$ the behaviour should be $\Phi(u) \sim \mathcal{O}(u^{1+\delta})$ with some some $\delta > 0$, see [200].

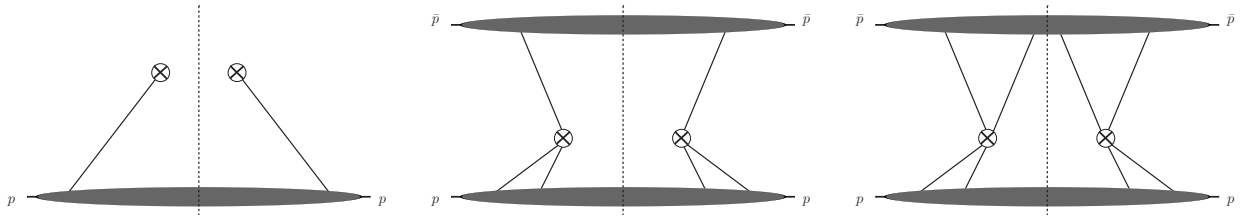

Figure 2.10: Schematic representation of SPS and DPS hadronic operators. a) SPS hadronic operators. b) DPS $1v2$ hadronic operators. c) DPS $2v2$ hadronic operators.

shown in Fig. 2.9. The corresponding subtraction term in this case is

$$\frac{d\sigma_{1v2,\mathrm{pt}}}{\prod_{i=1}^{2} dx_i\, d\bar{x}_i} = \sum_{a_1,a_2,b_1,b_2} \hat{\sigma}_{a_1,a_2}\hat{\sigma}_{b_1,b_2}\, G_{a_1,a_2}(x_1,x_2,x_2,x_1) \times \tag{2.79}$$

$$\times \int d^{D-2}\boldsymbol{b}\, \Phi^2\left(|\boldsymbol{b}|\nu\right) \Gamma^{1v2}_{b_1,b_2;\mathrm{pt}}(\bar{x}_i,\boldsymbol{b}), \tag{2.80}$$

where $G_{a_1,a_2}(x_1,x_2,x_2,x_1)$ is a twist-four distribution and D is a dimension of the integration space. In order to find the ν-scaling of Eq. 2.80 one has to use the technique of integration in $2-2\epsilon$ dimensions. The details can be found in the original publication [200]. The important result is that a *combination* of twist-four contribution and the subtraction term $\sigma_{\mathrm{tw4}} - \sigma_{1v2,\mathrm{pt}}$ scales like $\sim \log(Q/\nu)$. The "$1v2$" DPS contribution, in its turn, scales like $\log(\nu/\Lambda)$. In the combined expression

$$\sigma_{\mathrm{tw4}} - \sigma_{1v2,\mathrm{pt}} + \sigma^{\mathrm{DPS}}_{1v2}, \tag{2.81}$$

the ν-dependence cancels between $\sim \log(Q/\nu)$ and $\log(\nu/\Lambda)$ providing $\log(\nu/\Lambda)$ factor in Eq. 2.81. It is also important to notice that with the scale choice $\nu \sim Q$ the large part of the logarithm is contained only in $\sigma^{\mathrm{DPS}}_{1v2}$ contribution.

The complete expression for the total cross section (DPS + SPS), therefore, reads

$$\sigma^{\mathrm{DPS+SPS}}_{\mathrm{tot}} = \sigma^{\mathrm{SPS}} - \sigma_{1v1,\mathrm{pt}} + \sigma^{\mathrm{DPS}}_{1v1} + \sigma_{\mathrm{tw4}} - \sigma_{1v2,\mathrm{pt}} + \sigma^{\mathrm{DPS}}_{1v2}. \tag{2.82}$$

The detailed comparison between the approach of Diehl, Gaunt and Schönwald and the approaches of [195], [197], [198] and [199] was given in [200]. In the rest of this section, we shall briefly sketch some key-points we will need in the other parts of this thesis. Therefore, we will not discuss the comparison between the approach of Diehl, Gaunt and Schönwald and the approach of Manohar and Waalewijn since this discussion would be dedicated to the formal aspects of the DPS theory but not to its phenomenological applications. Instead, we will concentrate on the aspects of the formalism of [200] essential for the DPS phenomenology and their connection to the aforementioned publications of Blok *et al.* [195] and of Ryskin and Snigirev [197], [198].

First of all, the scale choice $\nu \sim Q$ implies that the term $\sigma_{\mathrm{tw4}} - \sigma_{1v2,\mathrm{pt}}$ does not acquire a large $\log(Q/\nu)$. Therefore, within the leading log approximation one can drop it. The twist-four contributions were not considered in the paper of Blok *et al.* and in the paper of Ryskin and Snigirev which then are also valid only within the leading logarithmic approximation[14]. Therefore, at this

[14]It was explicitly stated in the paper of Blok *et al.* [195].

accuracy level one can write

$$\sigma_{\rm tot}^{\rm DPS+SPS} = \sigma^{\rm SPS} - \sigma_{1v1,\rm pt} + \sigma_{1v1}^{\rm DPS} + \sigma_{1v2}^{\rm DPS}. \tag{2.83}$$

The next important point is a question of modelling of the two-parton distribution functions. In the papers of Blok *et al.* [195], [158] and papers of Ryskin and Snigirev [197], [198] the separation into "intrinsic" "$2v2$" and "perturbative" "$1v1$" parts was used. As we have noticed before, the approach of Diehl *et al.*, unlike the approaches of Blok *et al.* [196] and of Ryskin and Snigirev [197], [198], does not require such separation of gPDFs. However, due to the absence of gPDFs extracted out of the experimental data, the phenomenological modelling of gPDFs with splitting into "$2v2$" and "$1v2$" pieces is unavoidable. Namely, in Ref. [200] Diehl *et al.*, in order to provide numerical illustrations to their approach, used

$$\Gamma(x_1, x_2, \boldsymbol{b}, Q_1^2, Q_2^2) = \Gamma^{2v2}(x_1, x_2, \boldsymbol{b}, Q_1^2, Q_2^2) + \Gamma^{1v2}(x_1, x_2, \boldsymbol{b}, Q_1^2, Q_2^2), \tag{2.84}$$

where Γ^{2v2} and Γ^{1v2} follow homogeneous dDGLAP evolution equations *separately*. The detailed analysis performed in [200] demonstrated that at the leading log accuracy level the treatment of "$1v2$" DPS contribution within the approach of Diehl *et al.* is consistent within the approach of Blok *et al.* and of Ryskin and Snigirev. The treatment of "$1v1$" DPS contributions, however, leads to different results. Namely, it was shown that the evolution of gPDFs within the framework of [200] may enhance the term $\sigma_{1v1}^{\rm DPS} - \sigma_{1v1,\rm pt}$ which would lead to the disagreement with the approach of Blok *et al.* where the "$1v1$" DPS contribution was neglected. If such enhancement does not take place, the approach of Diehl *et al.* agrees with the approach of Blok *et al.* at the leading log accuracy level. Additionally, it was shown that the the upper cutoff for the $d^2\boldsymbol{k}$ integration for the "$1v1$" terms in the approach of Ryskin and Snigirev does not solve the double counting problem between the "$1v2$" DPS contribution and the one-loop SPS contribution.

At the moment there is no detailed phenomenological studies within the framework of [200]. However, in Ref. [200] Diehl *et al.* demonstrated how their method works using *regularized double parton luminosities* ($\mathcal{L}_{\rm DPS}^{\rm Reg}$) defined as

$$\mathcal{L}_{a_1a_2b_1b_2}(x_1, x_2, \bar{x}_1, \bar{x}_2, Q_1^2, Q_2^2, \nu) = \int d^2\boldsymbol{b}\, \Phi^2\left(|\boldsymbol{b}|\nu\right) \Gamma_{a_1a_2}(x_1, x_2, \boldsymbol{b}, Q_1^2, Q_2^2)\, \Gamma_{b_1b_2}(\bar{x}_1, \bar{x}_2, \boldsymbol{b}, Q_1^2, Q_2^2), \tag{2.85}$$

where Q_1, Q_2 are factorization scales and Φ is a certain cutoff function with properties as discussed above. In their study Diehl *et al.* used the phenomenological ansatz given by Eq. 2.84 with equal factorization scales $Q_1^2 = Q_2^2 = Q_2^2$. The "intrinsic" "2v2" part of $\Gamma(x_1, x_2, \boldsymbol{b}, Q^2)$ at the starting value of the evolution scale Q_0 was chosen to be equal to

$$\Gamma_{a_1a_2,}^{2v2}(x_1, x_2, \boldsymbol{b}, Q_0^2) = \frac{1}{4\pi h_{a_1a_2}} \exp\left[\frac{-\boldsymbol{b}^2}{4h_{a_1a_2}}\right] f_{a_1}(x_1, Q_0^2) f_{a_2}(x_2, Q_0^2) \times \tag{2.86}$$

$$\times \left(1 - x_1 - x_2\right)^2 \left(1 - x_1\right)^{-2} \left(1 - x_2\right)^{-2}, \tag{2.87}$$

where $f_a(x, Q^2)$ are standard collinear MSTW2008 LO PDFs [298] and the phase space factor

$$\left(1 - x_1 - x_2\right)^2 \left(1 - x_1\right)^{-2} \left(1 - x_2\right)^{-2} \tag{2.88}$$

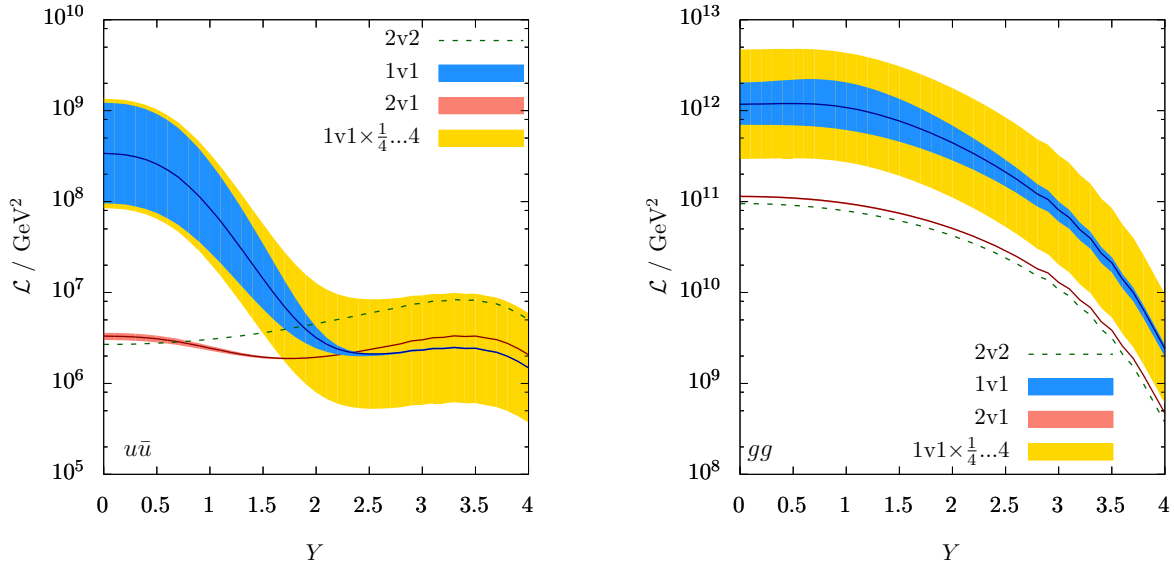

Figure 2.11: Double parton scattering luminosities $\mathcal{L}_{a_1a_2b_1b_2}$ for the production of two systems with $Q_1 = Q_2 = 80\,\text{GeV}$ at $\sqrt{S} = 14\,\text{TeV}$, one with rapidity Y and the other with rapidity $-Y$. The parton combinations $a_1a_2b_1b_2$ are $u\bar{u}\bar{u}u + \bar{u}uu\bar{u}$ (a) and $gggg$ (b). The plot is taken from [200].

ensures a smooth damping of $\Gamma^{2v2}_{a_1a_2}(x_1, x_2, \boldsymbol{b}, Q^2)$ at the border of the unphysical region where $x_1 + x_2 > 1$ [173]. The parameter $h_{a_1a_2}$ effectively provides the maximal distance between partons in the transverse plane. In the absence of partonic correlations it should be of the order of the proton size. However, the experimental studies of DPS suggest a value at least two times smaller, see Fig. 2.3. Moreover, its value can be different for various parton species and even demonstrate the x-dependence, see [149] - [160]. In the study of Diehl *et al.* $h_{a_1a_2}$ was chosen to be of the form $h_{a_1a_2} = h_{a_1} + h_{a_2}$ with $h_g = 2.33\,\text{GeV}^{-2}$ and $h_q = h_{\bar{q}} = 3.53\,\text{GeV}^{-2}$ which was inspired by the model of partonic correlations proposed in [159]. The initial condition for the "splitting" "$1v2$" part of $\Gamma(x_1, x_2, \boldsymbol{b}, Q^2)$ was taken in the form

$$\Gamma^{1v2}_{a_1a_2}(x_1, x_2, \boldsymbol{b}, Q^2_{0b}) = \frac{1}{\pi \boldsymbol{b}^2} \exp\left[\frac{-\boldsymbol{b}^2}{4h_{a_1a_2}}\right] \frac{f_{a_0}(x_1 + x_2, Q^2_{0b})}{x_1 + x_2} \times \tag{2.89}$$

$$\times \frac{\alpha_s(Q^2_{0b})}{2\pi} P_{a_0 \to a_1a_2}\left(\frac{x_1}{x_1 + x_2}\right), \tag{2.90}$$

where Q^2_{0b} is a starting evolution scale for $\Gamma^{1v2}_{a_1a_2}$.

In Fig. 2.11 we show one of the results from [200] where the regularized double parton luminosities for productions of two well-separated in rapidity systems were studied. The phenomenological ansatz in Eq. 2.84 allows to separate "$2v2$", "$1v2$" and "$1v1$" DPS luminosities which are plotted in Fig. 2.11 for two particular sets of parton species: $u\bar{u}\bar{u}u + \bar{u}uu\bar{u}$ in Fig. 2.11 a), and $gggg$ in Fig. 2.11 b). The dashed line in Fig. 2.11 corresponds to the "$2v2$" DPS luminosity evolved to $Q_1 = Q_2 = 80\,\text{GeV}$ and the solid lines in Fig. 2.11 correspond to "$1v2$" and "$1v1$" DPS luminosities evolved to $Q_1 = Q_2 = 80\,\text{GeV}$. The red and blue bands correspond to the variation of the cutoff parameter ν by a factor of 2 up and down. As we have discussed before, the "$1v1$" DPS luminosity,

unlike "$1v2$" DPS luminosity, depends on the value of the cutoff parameter ν quadratically. This dependence should lead to the wide bands due to the variation of μ. On the other hand, as it was argued in [200], the dependence on the cutoff parameter ν can be affected by the evolution effects. In order to estimate how the evolution effects impact this dependence in Fig. 2.11 Diehl *et al.* plotted a yellow band which corresponds to the variation of "$1v1$" DPS luminosity by the factor of 4 up and down. Therefore, in the case when evolution effects do not affect "$1v1$" DPS luminosity, the blue and yellow bands should coincide. By comparing the blue and yellow bands for "$1v1$" DPS contributions we see that dDGLAP evolution effects become important for "$1v1$" DPS luminosities at large values of rapidity separation. Another important effect shown in Fig. 2.11 is that "$1v2$" and "$1v1$" DPS luminosities tend to decrease with the increase of rapidity separation. Namely, we see that for the luminosities shown in Fig. 2.11 a) the "$2v2$" DPS luminosity dominates over "$1v2$" and "$1v1$" DPD luminosities at large values of rapidity separation. In Fig. 2.11 b) we also see that the difference between "$2v2$" DPS luminosity and "$1v1$" DPS luminosity becomes smaller towards to the large values of rapidity separation.

The approach of Diehl *et al.* opens a possibility to study DPS processes in a systematic way in all orders in perturbation theory. Recently first results on NLO DPS were obtained [177], [210]. However, its consistent implementation into Monte Carlo event generators and, therefore, its usage for realistic phenomenological analyses, still possesses a lot of challenging problems, though some progress towards to this goal was recently made [211]. We will come back to the discussion of some of these issues in Chapter 4 of this thesis.

2.6 General formalism of the DPS in proton-nucleus collisions

As it was mentioned in section 2.1 the first discussion of DPS in proton-nucleus collisions was given in one of the very first papers on DPS by Goebel *et al.* [114]. The authors of [114] predicted that in pA collisions, apart from the "standard" DPS contribution involving one incident proton and one nucleon, as shown in Fig. 2.12 a), a new DPS contribution involving one incident proton and two different nucleons is possible, see Fig. 2.12 b). Moreover, Goebel *et al.* have argued that both contributions should scale differently with a total number of nucleons A and that "... using targets with multiple nuclear composition, one can unambiguously separate two production mechanisms [DPS and SPS] experimentally.". However, for a long period of time the problem of DPS in pA collisions was staying outside of the research interest of the theoretical physicists. The study of the DPS phenomena in pA collisions was resumed in 2001 when Strikman and Treleani published the paper where the analytical expressions for a total DPS cross section in pA collisions was given for the first time and first quantitative predictions on scaling of two different DPS contributions were made [213]. As we have discussed in section 2.1, various studies of DPS performed at pp and $p\bar{p}$ colliders [133] - [134] suggest a presence of partonic correlations which leads to small values of the effective interaction area σ_{eff}. Unfortunately, a nature of correlations contributing to this effects is still debatable. One of the main problems is our disability to disentangle different sources of parton correlations in pp ($p\bar{p}$) collisions alone. In order to circumvent this issue, Strikman and Treleani proposed to study DPS processes in pA collisions [213] which would allow to separate *transverse* and *longitudinal* parton correlations according to the different A-dependence of corresponding contributions to the total DPS cross section. This idea got further developed in [215], [216] and

found some phenomenological applications in a series of papers [214] - [225].

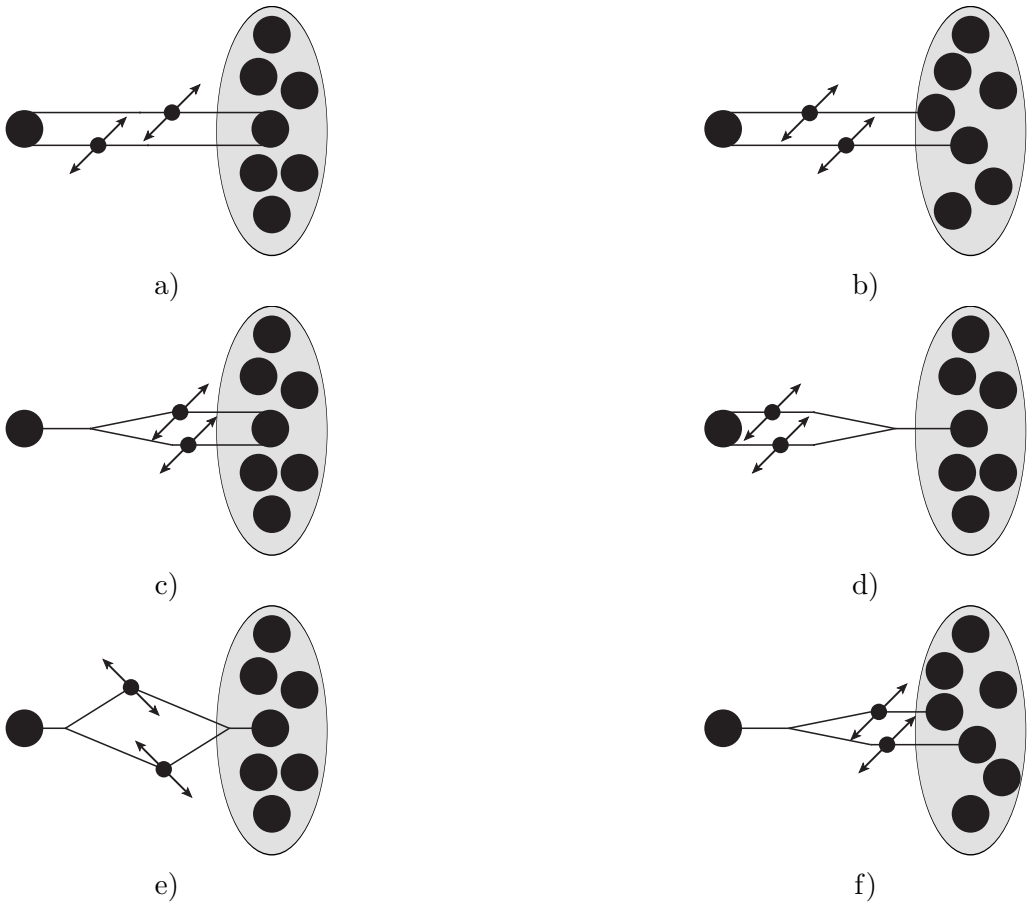

Figure 2.12: Schematic representation of different contributions to DPS in pA collisions assuming no cross talks between different nucleons.

However, in general, total DPS cross section in pA collisions is more complicated as discussed in [213] due to the various "splitting" contributions, see Fig. 2.12 c), d), e), f). In this section we will briefly sketch the results of [216] which correspond to current state-of-the-art of the description of DPS phenomena in pA collision. Let us start the discussion with the definition of the *generalized nuclear parton distribution functions* (gNPDFs)

$$\Gamma_{\rm A}(x_1, x_2, \boldsymbol{\delta}) = \Gamma_{\rm A}^{1v2,1N}\left(x_1, x_2, \boldsymbol{\delta}\right) + \Gamma_{\rm A}^{2v2,1N}\left(x_1, x_2, \boldsymbol{\delta}\right) + \Gamma_{\rm A}^{2N}\left(x_1, x_2, \boldsymbol{\delta}\right), \tag{2.91}$$

where the terms $\Gamma_{\rm A}^{1v2,1N}\left(x_1, x_2, \boldsymbol{\delta}\right)$ and $\Gamma_{\rm A}^{2v2,1N}\left(x_1, x_2, \boldsymbol{\delta}\right)$ correspond to the case where two partons with Bjorken variables x_1 and x_2 belong to the same nucleon. The first two terms on the RHS of Eq. 2.91 can be seen as a generalization of the ansatz of Blok *et al.* [195] to the case of gNPDFs. The gNPDF $\Gamma_{\rm A}^{2N}\left(x_1, x_2, \boldsymbol{\delta}\right)$ has no analogue among generalized proton PDFs and correspond to the case when two partons with Bjorken variables x_1 and x_2 belong to *two different* nucleons. The parameter $\boldsymbol{\delta}$ is a momentum transfer between initial and final state in the cut diagram in Fig. 2.13. It is the same quantity as the momentum transfer $\boldsymbol{r}$ between initial and final state in the cut diagram in Fig. 2.5, where we were using cut diagrams to write down 2-parton correlation function, see section 2.3. However, in this section we often take the Fourier transform of $\Gamma_{\rm A}(x_1, x_2, \boldsymbol{\delta})$. Therefore, in order not to confuse a momentum transfer $\boldsymbol{r}$ with the radius vector in position space, we change

the notation and use $\boldsymbol{\delta}$ instead of $\boldsymbol{r}$.

Since DPS cross sections includes a product of two gNPDFs, the ansatz in Eq. 2.91 give rise to six different DPS contributions shown in Fig. 2.12. Let us start our discussion with the DPS contributions involving only one nucleon as shown in 2.12 a), c) d) and e). In order to proceed further with a description of these processes one has to express $\Gamma_{\rm A}^{1N}$ in terms of gPDFs of a single nucleon. In this case the main formula reads

$$\Gamma_{\rm A}^{1N}\left(x_1,x_2,\boldsymbol{\delta}\right)=\int\frac{d\alpha}{\alpha}\,d^2\boldsymbol{p}\,\frac{1}{\alpha^2}\left[\Gamma_N^{1v2}\left(\frac{x_1}{\alpha},\frac{x_2}{\alpha},\boldsymbol{\delta}\right)+\Gamma_N^{2v2}\left(\frac{x_1}{\alpha},\frac{x_2}{\alpha},\boldsymbol{\delta}\right)\right]\,\rho_{\rm A}^{N}(\alpha,\boldsymbol{p}), \tag{2.92}$$

where $\rho_{\rm A}^{N}(\alpha,\boldsymbol{p})$ is the *light-cone nucleon density* of a nucleus introduced in [217] and defined as

$$\begin{aligned}\rho_{\rm A}^{N}(\alpha,\boldsymbol{p}) &= \int\prod_{i=1}^{\rm A}\frac{d\alpha_i}{\alpha_i}d^2\boldsymbol{p}_i\,\delta\left(1-\frac{\sum\alpha_i}{\rm A}\right)\,\delta\left(\sum_{i=1}^{\rm A}\boldsymbol{p}_i\right)\sum_{i=1}^{\rm A}\alpha_i\,\delta(\alpha-\alpha_i)\,\delta^2(\boldsymbol{p}-\boldsymbol{p}_i)\\ &\times\ \left|\psi\left(\alpha_1,...,\alpha_{\rm A},\boldsymbol{p}_1,...,\boldsymbol{p}_{\rm A}\right)\right|^2,\end{aligned} \tag{2.93}$$

where ψ is a wave function of a nucleus with A nucleons each carrying transverse momentum $\boldsymbol{p}_i$. The quantities α_i in Eq. 2.93 are defined as

$$\alpha_i={\rm A}\frac{p_i^+}{p_A^+}={\rm A}\frac{\sqrt{m_i^2+p_i^2}+p_{iz}}{\sqrt{m_{\rm A}^2+p_{\rm A}^2}+p_{{\rm A}z}}, \tag{2.94}$$

where p_i^+ and p_A^+ are "plus" components of the light-cone momenta of the i'th nucleon and the nucleus A, correspondingly[15]. The definition of α_i implies that $\alpha_i/{\rm A}$ is equal to the light-cone fraction of nucleus momentum carried by the i'th nucleon and that $\alpha_i\in[0,{\rm A}]$. It also implies that $\sum\limits_{i=1}^{\rm A}\alpha_i={\rm A}$. The light-cone nucleon density $\rho_{\rm A}^{N}(\alpha,\boldsymbol{p})$ obeys two important sum rules:

$$\int\limits_0^{\rm A}\rho_{\rm A}^{N}(\alpha,\boldsymbol{p})\,\frac{d\alpha}{\alpha}d^2\boldsymbol{p}={\rm A}, \tag{2.95}$$

$$\int\limits_0^{\rm A}\alpha\,\rho_{\rm A}^{N}(\alpha,\boldsymbol{p})\,\frac{d\alpha}{\alpha}d^2\boldsymbol{p}={\rm A}, \tag{2.96}$$

where Eq. 2.95 is called *baryon number sum rule* and Eq. 2.96 implies conservation of the "plus" components of the light-cone momenta, see Chapter 2.4.2 of [217]. Taking the difference between Eq. 2.96 and Eq. 2.95 we obtain an important expression

$$\int\limits_0^{\rm A}(\alpha-1)\,\rho_{\rm A}^{N}(\alpha,\boldsymbol{p})\,\frac{d\alpha}{\alpha}\,d^2\boldsymbol{p}=0. \tag{2.97}$$

In order to simplify Eq. 2.92 one has to make certain assumptions about α-dependence of Γ_N^{1v2} and Γ_N^{2v2}. As a first approximation one can assume that all nucleons are carrying the same amount of longitudinal light-cone momentum of a nucleus which implies $p_i^+=p_{\rm A}^+/{\rm A}$ or $\alpha_i=1\,\forall i$. Obviously, the motion of nucleons inside a nucleus implies that values of α_i are distributed around unity with a

[15] For the definition of the light-cone variables see Appendix C.

certain dispersion. However, if we assume that dispersion effects due to the motion of nucleons are small, then Γ_N^{1v2} and Γ_N^{2v2} are peaked around value $\alpha = 1$ and hence we can expand the integrand in Eq. 2.92 in powers of $(\alpha - 1)$. In order to do that we substitute $\alpha = 1 + (\alpha - 1)$ in Eq. 2.92 which yields

$$\Gamma_{\rm A}^{1N}\left(x_1, x_2, \boldsymbol{\delta}\right) = \int \frac{d\alpha}{\alpha}\, d^2\boldsymbol{p}\, \frac{1}{\left(1 + (\alpha - 1)\right)^2} \left[\Gamma_N\left(\frac{x_1}{1 + (\alpha - 1)}, \frac{x_2}{1 + (\alpha - 1)}, \boldsymbol{\delta}\right)\right] \rho_{\rm A}^N(\alpha, \boldsymbol{p}), \tag{2.98}$$

where we have denoted

$$\Gamma_N\left(\frac{x_1}{\alpha}, \frac{x_2}{\alpha}, \boldsymbol{\delta}\right) = \Gamma_N^{1v2}\left(\frac{x_1}{\alpha}, \frac{x_2}{\alpha}, \boldsymbol{\delta}\right) + \Gamma_N^{2v2}\left(\frac{x_1}{\alpha}, \frac{x_2}{\alpha}, \boldsymbol{\delta}\right). \tag{2.99}$$

Now we can expand Γ_N^{1v2} and Γ_N^{2v2} in powers of $(\alpha - 1)$. As it was argued in the paper of Blok *et al.* [216] the factor $1/\alpha^2$ in Eq. 2.92 ensures invariance of the quantity $\Gamma_N(x_1/\alpha, x_2/\alpha)/\alpha^2$ under boosts in the longitudinal direction and, therefore, has to be expanded together with Γ_N. Expanding $\Gamma_N(x_1/\alpha, x_2/\alpha)/\alpha^2$ in powers of $(\alpha - 1)$ we write Eq. 2.98 as

$$\begin{aligned}
\Gamma_{\rm A}^{1N}\left(x_1, x_2, \boldsymbol{\delta}\right) &= \int \frac{d\alpha}{\alpha}\, d^2\boldsymbol{p}\, \Gamma_N\left(x_1, x_2, \boldsymbol{\delta}\right)\, \rho_{\rm A}^N(\alpha, \boldsymbol{p}) + \\
&+ \mathcal{O}\left(\int \frac{d\alpha}{\alpha}\, d^2\boldsymbol{p}\, (1 - \alpha)\, \rho_{\rm A}^N(\alpha, \boldsymbol{p})\right) + \\
&+ \mathcal{O}\left(\int \frac{d\alpha}{\alpha}\, d^2\boldsymbol{p}\, (1 - \alpha)^2\, \rho_{\rm A}^N(\alpha, \boldsymbol{p})\right) + \text{higher order terms.}
\end{aligned} \tag{2.100}$$

By applying Eq. 2.97 to Eq. 2.100 we see that up to the terms of the order of $(\alpha - 1)^2$

$$\Gamma_{\rm A}^{1N}\left(x_1, x_2, \boldsymbol{\delta}\right) \approx {\rm A}\, \Gamma_N\left(x_1, x_2, \boldsymbol{\delta}\right) \left(1 + \mathcal{O}\left(\int \frac{d\alpha}{\alpha}\, d^2\boldsymbol{p}\, (1 - \alpha)^2 \rho_{\rm A}^N(\alpha, \boldsymbol{p})\right)\right), \tag{2.101}$$

where we have used Eq. 2.95 to write

$$\begin{aligned}
&\int \frac{d\alpha}{\alpha}\, d^2\boldsymbol{p}\, \Gamma_N\left(x_1, x_2, \boldsymbol{\delta}\right)\, \rho_{\rm A}^N(\alpha, \boldsymbol{p}) = \\
&= \Gamma_N\left(x_1, x_2, \boldsymbol{\delta}\right) \int \frac{d\alpha}{\alpha}\, d^2\boldsymbol{p}\, \rho_{\rm A}^N(\alpha, \boldsymbol{p}) = {\rm A}\, \Gamma_N\left(x_1, x_2, \boldsymbol{\delta}\right).
\end{aligned} \tag{2.102}$$

Therefore, for the processes shown in Fig. 2.12 a), c), d) and e) the gNPDF $\Gamma_{\rm A}^{1N}\left(x_1, x_2, \boldsymbol{\delta}\right)$, up to the terms of the order $\mathcal{O}(\alpha - 1)^2$, is given by ${\rm A}\, \Gamma_N\left(x_1, x_2, \boldsymbol{\delta}\right)$ which allows to write the total DPS cross section in pA collisions for the in Fig. 2.12 a), c), d) and e) as

$$\begin{aligned}
\sigma_{\rm DPS}^{\rm pA} &= {\rm A} \sum_{a_1, a_2, b_1, b_2} \int \prod_{i=1}^{4} dx_i\, \frac{d^2\boldsymbol{\delta}}{(2\pi)^2}\, \Gamma_{a_1, a_2/p}(x_1, x_2, \boldsymbol{\delta})\, \Gamma_{b_1, b_2/N}(x_3, x_4, -\boldsymbol{\delta}) \times \\
&\times \hat{\sigma}_{a_1\, b_1 \to A}\, \hat{\sigma}_{a_2\, b_2 \to B}.
\end{aligned} \tag{2.103}$$

We define the Fourier transform of $\Gamma(x_1, x_2, \boldsymbol{\delta})$ as

$$\Gamma(x_1, x_2, \boldsymbol{b}) = \int d^2\boldsymbol{b}\, e^{-i\boldsymbol{b}\boldsymbol{\delta}}\, \Gamma(x_1, x_2, \boldsymbol{\delta}). \tag{2.104}$$

Now, using Eq. 2.104, we can write Eq. 2.103 as

$$\sigma_{\rm DPS}^{\rm pA} = {\rm A} \sum_{a_1,a_2,b_1,b_2} \int \prod_{i=1}^{4} dx_i \, d^2\boldsymbol{b} \, \Gamma_{a_1,a_2/p}(x_1,x_2,\boldsymbol{b}) \, \Gamma_{b_1,b_2/N}(x_3,x_4,\boldsymbol{b}) \times \\ \times \hat{\sigma}_{a_1\, b_1 \to A} \, \hat{\sigma}_{a_2\, b_2 \to B}. \tag{2.105}$$

which, assuming that one can factorize $\boldsymbol{\delta}$-dependence as $\Gamma_{b_1,b_2/N}(x_3,x_4,\boldsymbol{b}) \approx D_{b_1,b_2/N}(x_3,x_4)F(\boldsymbol{b})$ and that $D_{b_1,b_2/N}(x_3,x_4) \approx D_{b_1,b_2/p}(x_3,x_4)$, yields

$$\sigma_{\rm DPS}^{\rm pA} \approx {\rm A}\sigma_{\rm DPS}^{\rm pp}, \tag{2.106}$$

where $\sigma_{\rm DPS}^{\rm pp}$ is a DPS cross section for pp collisions which includes "$2v2$", "$1v2$" and "$1v1$" DPS contributions shown in Fig. 2.7.

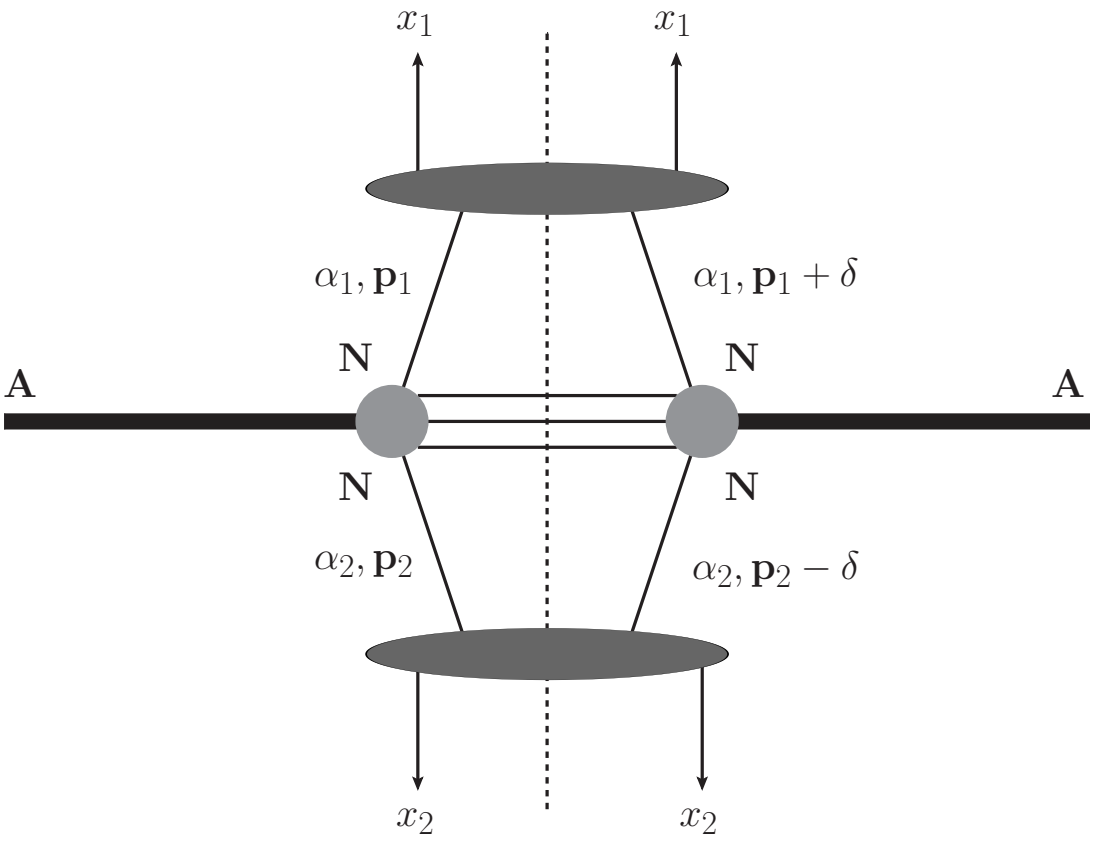

Figure 2.13: Schematic representation of the $\Gamma_{\rm A}^{2N}$ contribution to the gNPDFs. Here, two partons are drawn from two different nucleons with light-cone momentum fractions α_1, α_2 and transverse momenta $\boldsymbol{p}_1$, $\boldsymbol{p}_2$.

Now let us sketch the derivation of the total cross section for the processes given in Fig. 2.12 b) and f) as it was done in [216]. The corresponding gNPDF can be expressed in terms of the nuclear

light cone wave function $\psi_{\rm A}$ of the A-nucleon system

$$\begin{aligned}\Gamma_{\rm A}^{2N}\left(x_1,x_2,\boldsymbol{\delta}\right) &= {\rm A}({\rm A}-1)\int\prod_{i=1}^{\rm A}\frac{d\alpha_i}{\alpha_i}\,d^2\boldsymbol{p}_i\,\delta\left(\sum_i\alpha_i-{\rm A}\right)\delta^2\left(\sum_i\boldsymbol{p}_i\right)\times\\ &\times\ \psi_{\rm A}^*\left(\alpha_1,\alpha_2,...,\boldsymbol{p}_1,\boldsymbol{p}_2,...\right)\psi_{\rm A}\left(\alpha_1,\alpha_2,...,\boldsymbol{p}_1+\boldsymbol{\delta},\boldsymbol{p}_2-\boldsymbol{\delta},...\right)\times\\ &\times\ f_N\left(x_1/\alpha_1,\boldsymbol{\delta}\right)f_N\left(x_2/\alpha_2,-\boldsymbol{\delta}\right),\end{aligned}\tag{2.107}$$

where ${\rm A}({\rm A}-1)$ is a number of different nucleon permutations, index $i=1,2$ labels two active nucleons, $\boldsymbol{\delta}$ is a momentum transfer between them and f_N are *generalized nucleon single parton distribution functions*, see Fig. 2.13. Since the sign of the momentum transfer $\boldsymbol{\delta}$ is arbitrary, Γ^{2N} cannot depend on it. Therefore, $\Gamma_{\rm A}^{2N}\left(x_1,x_2,\boldsymbol{\delta}\right)=\Gamma_{\rm A}^{2N}\left(x_1,x_2,-\boldsymbol{\delta}\right)$ which implies

$$\begin{aligned}\Gamma_{\rm A}^{2N}\left(x_1,x_2,\boldsymbol{\delta}\right) &= \Gamma_{\rm A}^{2N}\left(x_1,x_2,-\boldsymbol{\delta}\right)=\\ &= {\rm A}({\rm A}-1)\int\prod_{i=1}^{\rm A}\frac{d\alpha_i}{\alpha_i}\,d^2\boldsymbol{p}_i\,\delta\left(\sum_i\alpha_i-{\rm A}\right)\delta^2\left(\sum_i\boldsymbol{p}_i\right)\times\\ &\times\ \psi_{\rm A}^*\left(\alpha_1,\alpha_2,...,\boldsymbol{p}_1,\boldsymbol{p}_2,...\right)\psi_{\rm A}\left(\alpha_1,\alpha_2,...,\boldsymbol{p}_1-\boldsymbol{\delta},\boldsymbol{p}_2+\boldsymbol{\delta},...\right)\times\\ &\times\ f_N\left(x_1/\alpha_1,-\boldsymbol{\delta}\right)f_N\left(x_2/\alpha_2,\boldsymbol{\delta}\right).\end{aligned}\tag{2.108}$$

Because the integration over transverse momenta is symmetric in Eq. 2.108 we can replace $\boldsymbol{p}_i\to-\boldsymbol{p}_i$. However, the nucleus wave function ψ_A should not change if we inverse transverse momenta of all nucleons, therefore

$$\begin{aligned}&\psi_{\rm A}\left(\alpha_1,\alpha_2,...,-\boldsymbol{p}_1-\boldsymbol{\delta},-\boldsymbol{p}_2+\boldsymbol{\delta},...\right)=\\ &=\psi_{\rm A}\left(\alpha_1,\alpha_2,...,-(\boldsymbol{p}_1+\boldsymbol{\delta}),-(\boldsymbol{p}_2-\boldsymbol{\delta}),...\right)=\\ &=\psi_{\rm A}\left(\alpha_1,\alpha_2,...,+(\boldsymbol{p}_1+\boldsymbol{\delta}),+(\boldsymbol{p}_2-\boldsymbol{\delta}),...\right),\end{aligned}\tag{2.109}$$

which allows to write Eq. 2.108 as

$$\begin{aligned}\Gamma_{\rm A}^{2N}\left(x_1,x_2,-\boldsymbol{\delta}\right) &= {\rm A}({\rm A}-1)\int\prod_{i=1}^{\rm A}\frac{d\alpha_i}{\alpha_i}\,d^2\boldsymbol{p}_i\,\delta\left(\sum_i\alpha_i-{\rm A}\right)\delta^2\left(\sum_i\boldsymbol{p}_i\right)\times\\ &\times\ \psi_{\rm A}^*\left(\alpha_1,\alpha_2,...,\boldsymbol{p}_1,\boldsymbol{p}_2,...\right)\psi_{\rm A}\left(\alpha_1,\alpha_2,...,\boldsymbol{p}_1+\boldsymbol{\delta},\boldsymbol{p}_2-\boldsymbol{\delta},...,+\right)\times\\ &\times\ f_N\left(x_1/\alpha_1,-\boldsymbol{\delta}\right)f_N\left(x_2/\alpha_2,\boldsymbol{\delta}\right).\end{aligned}\tag{2.110}$$

By comparing Eq. 2.107 and Eq. 2.110 we see that condition $\Gamma_{\rm A}^{2N}\left(x_1,x_2,\boldsymbol{\delta}\right)=\Gamma_{\rm A}^{2N}\left(x_1,x_2,-\boldsymbol{\delta}\right)$ is satisfied if

$$f_N\left(x_1/\alpha_1,\boldsymbol{\delta}\right) = f_N\left(x_1/\alpha_1,-\boldsymbol{\delta}\right),\tag{2.111}$$

$$f_N\left(x_2/\alpha_2,-\boldsymbol{\delta}\right) = f_N\left(x_2/\alpha_2,\boldsymbol{\delta}\right),\tag{2.112}$$

which implies that f_N can depend only on absolute value of $\boldsymbol{\delta}$. Therefore, we write Eq. 2.107 as

$$\begin{aligned}\Gamma_{\mathrm{A}}^{2N}\left(x_1,x_2,\boldsymbol{\delta}\right) &= \mathrm{A}(\mathrm{A}-1)\int\prod_{i=1}^{\mathrm{A}}\frac{d\alpha_i}{\alpha_i}\,d^2\boldsymbol{p}_i\,\delta\left(\sum_i\alpha_i-\mathrm{A}\right)\delta^2\left(\sum_i\boldsymbol{p}_i\right)\times\\ &\times\ \psi_{\mathrm{A}}^{*}\left(\alpha_1,\alpha_2,\boldsymbol{p}_1,\boldsymbol{p}_2,...\right)\psi_{\mathrm{A}}\left(\alpha_1,\alpha_2,\boldsymbol{p}_1+\boldsymbol{\delta},\boldsymbol{p}_2-\boldsymbol{\delta},...\right)\times\\ &\times\ f_N\left(x_1/\alpha_1,|\boldsymbol{\delta}|\right)f_N\left(x_2/\alpha_2,|\boldsymbol{\delta}|\right). \end{aligned}\tag{2.113}$$

Expanding in powers of (α_i-1) in Eq. 2.107, similarly to the case of Γ_A^{1N}, we obtain

$$\Gamma_{\mathrm{A}}^{2N}\left(x_1,x_2,\boldsymbol{\delta}\right) = \mathrm{A}(\mathrm{A}-1)\,f_N\left(x_1,|\boldsymbol{\delta}|\right)\,f_N\left(x_2,|\boldsymbol{\delta}|\right)\,F_{\mathrm{A}}^{2N}(\boldsymbol{\delta},-\boldsymbol{\delta}),\tag{2.114}$$

where

$$\begin{aligned}F_{\mathrm{A}}^{2N}(\boldsymbol{\delta},-\boldsymbol{\delta}) &= \int\prod_{i=1}^{\mathrm{A}}\frac{d\alpha_i}{\alpha_i}\,d^2\boldsymbol{p}_i\,\delta\left(\sum_i\alpha_i-\mathrm{A}\right)\delta^2\left(\sum_i\boldsymbol{p}_i\right)\psi_{\mathrm{A}}^{*}\left(\alpha_1,\alpha_2,\boldsymbol{p}_1,\boldsymbol{p}_2,...\right)\times\\ &\times\ \psi_{\mathrm{A}}\left(\alpha_1,\alpha_2,\boldsymbol{p}_1+\boldsymbol{\delta},\boldsymbol{p}_2-\boldsymbol{\delta},...\right). \end{aligned}\tag{2.115}$$

In the nucleus rest frame in the non-relativistic limit one can set $\alpha_i = 1 + p_{z,i}/m_N$ [217] and thus

$$\begin{aligned}F_{\mathrm{A}}^{NR,2N}(\boldsymbol{\delta},-\boldsymbol{\delta}) &= \int\prod_{i=1}^{\mathrm{A}}d^3p_i\,\delta^3\left(\sum_{i=1}^{\mathrm{A}}p_i\right)\psi_{\mathrm{A}}^{*}\left(\alpha_1,\alpha_2,p_1,p_2,...\right)\times\\ &\times\ \psi_{\mathrm{A}}\left(\alpha_1,\alpha_2,p_1+\boldsymbol{\delta},p_2-\boldsymbol{\delta},...\right), \end{aligned}\tag{2.116}$$

where p_i is a *three-momentum* of the i'th nucleon.

In order to perform further steps we have to specify a form of a nuclear wave function ψ_{A}. If we consider a nucleus as a superposition of independent nucleons, then we can write ψ_{A} as a product of independent nucleon wave functions ψ_N and neglect the kinematic constraint $\delta^3\left(\sum_i p_i\right)$ which gives

$$\begin{aligned}F_{\mathrm{A}}^{NR,2N}(\boldsymbol{\delta},-\boldsymbol{\delta}) &= \int\prod_{i=1}^{i=\mathrm{A}}d^3p_i\,\psi_N^{*}\left(p_1\right)\psi_N^{*}\left(p_2\right)\psi_N^{*}\left(p_3\right)\ldots\times\\ &\times\ \psi_N\left(p_1+\boldsymbol{\delta}\right)\psi_N\left(p_2-\boldsymbol{\delta}\right)\psi_N\left(p_3\right)\ldots\ . \end{aligned}\tag{2.117}$$

Equation 2.117 can be simplified by means of the Fourier transform. We define the Fourier transform of a single nucleon wave function ψ_N as

$$\psi_N(p) = \frac{1}{(2\pi)^{3/2}}\int d^3r\,\psi_N(r)\,e^{-ipr}.\tag{2.118}$$

By substituting Eq. 2.118 into Eq. 2.117 we can write for the functions $\psi_N(p_i)$ with $i \geq 3$

$$\begin{aligned}\int d^3p_i\,\psi_N^{*}(p_i)\psi_N(p_i) &= \frac{1}{(2\pi)^3}\int d^3p_i\,d^3r_i d^3r_i'\,\psi_N^{*}(r_i)\,\psi_N(r_i')\,e^{-ip(r_i-r_i')} =\\ &= \int d^3r_i\,|\psi_N(r_i)|^2 = \frac{1}{\mathrm{A}}\int d^3r_i\,\rho_{\mathrm{A}}(r_i) = 1, \end{aligned}\tag{2.119}$$

where $\rho_{\rm A}(r) = {\rm A}|\psi_N(r)|^2$ is a *single nucleon density function* normalized such that

$$\int d^3r\, \rho_{\rm A}(\boldsymbol{r}) = {\rm A}. \tag{2.120}$$

Therefore, after taking the Fourier transform for all single nucleon wave functions with $i \geq 3$, we are left over with

$$F_{\rm A}^{NR,2N}(\boldsymbol{\delta}, -\boldsymbol{\delta}) \;=\; \int d^3p_1\, d^3p_2\, \psi_N^*(p_1)\, \psi_N^*(p_2)\, \psi_N(p_1+\boldsymbol{\delta})\, \psi_N(p_2-\boldsymbol{\delta}), \tag{2.121}$$

which can be written as

$$\begin{aligned} F_{\rm A}^{NR,2N}(\boldsymbol{\delta}, -\boldsymbol{\delta}) &= \left[\frac{1}{\rm A}\int d^3r\, \rho_{\rm A}(r) e^{-i\boldsymbol{\delta}\boldsymbol{r}}\right]\left[\frac{1}{\rm A}\int d^3r\, \rho_{\rm A}(r) e^{+i\boldsymbol{\delta}\boldsymbol{r}}\right] = \\ &= \left|\frac{1}{\rm A}\int d^3r\, \rho_{\rm A}(r) e^{-i\boldsymbol{\delta}\boldsymbol{r}}\right|^2 \equiv |F_{\rm A}(\boldsymbol{\delta})|^2, \end{aligned} \tag{2.122}$$

where $F_{\rm A}(\boldsymbol{\delta})$ is the *single nucleon form-factor*.

Using Eq. 2.122 one can write Eq. 2.114 as

$$\Gamma_{\rm A}^{2N}(x_1, x_2, \boldsymbol{\delta}) \approx {\rm A}({\rm A}-1)\, f_N(x_1, |\boldsymbol{\delta}|)\, f_N(x_2, |\boldsymbol{\delta}|)\, |F_{\rm A}(\boldsymbol{\delta})|^2. \tag{2.123}$$

It is handy to express the single nucleon form factor in terms of the nuclear thickness function ${\rm T_A}$ which is defined as a single nucleon density function $\rho_{\rm A}(r)$ integrated over a longitudinal coordinate

$${\rm T_A}(\boldsymbol{s}) = \int dz\, \rho_{\rm A}(\boldsymbol{s}, z), \tag{2.124}$$

which gives

$$F_{\rm A}(\boldsymbol{\delta}) = \frac{1}{\rm A}\int d^2\boldsymbol{s}\, {\rm T_A}(\boldsymbol{s})\, e^{-i\boldsymbol{\delta}\boldsymbol{s}}, \tag{2.125}$$

where we used $\boldsymbol{\delta}\boldsymbol{r} = \boldsymbol{\delta}\boldsymbol{s}$.

Now we can write down corresponding cross sections for processes involving two independent nucleons. Consider, for example, the process shown in Fig. 2.12 b). The total DPS cross section for this process is given by the following integral

$$\begin{aligned} \sigma_{\rm DPS}^{\rm pA} &= \frac{1}{(2\pi)^2}\sum_{a_1,a_2,b_1,b_2}\int\prod_{i=1}^{2} dx_i\, d^2\boldsymbol{\delta}\, \Gamma_{a_1,a_2/p}^{2v2}(x_1, x_2, \boldsymbol{\delta})\, \Gamma_{b_1,b_2/{\rm A}}^{2N}(x_3, x_4, \boldsymbol{\delta}) \times \\ &\times\; \hat{\sigma}_{a_1\, b_1\to A}\, \hat{\sigma}_{a_2\, b_2\to B}, \end{aligned} \tag{2.126}$$

or approximately

$$\begin{aligned} \sigma_{\rm DPS}^{\rm pA} &\approx \frac{{\rm A}({\rm A}-1)}{(2\pi)^2}\sum_{a_1,a_2,b_1,b_2}\int\prod_{i=1}^{2} dx_i\, d^2\boldsymbol{\delta}\; \Gamma_{a_1,a_2/p}^{2v2}(x_1, x_2, \boldsymbol{\delta}) \times \\ &\times\; f_{b_1/N}(x_1, |\boldsymbol{\delta}|)\; f_{b_2/N}(x_2, |\boldsymbol{\delta}|)\; |F_{\rm A}(\boldsymbol{\delta})|^2\, \hat{\sigma}_{a_1\, b_1\to A}\, \hat{\sigma}_{a_2\, b_2\to B}. \end{aligned} \tag{2.127}$$

In order to perform further steps one has to know the $\boldsymbol{\delta}$-dependence of Γ_p^{2v2} and f_N. One can estimate a size of $|\boldsymbol{\delta}|$ by evaluating $|F_{\rm A}(\boldsymbol{\delta})|^2$ for a Gaussian parametrization of a nuclear mater density which yields

$$|F_{\rm A}(\boldsymbol{\delta})|^2 \approx e^{-\frac{1}{3}\boldsymbol{\delta}^2 R_{\rm A}^2}, \tag{2.128}$$

where $R_{\rm A}$ is a radius of a nucleus [216]. It allows to conclude that most of the contribution to a corresponding total cross section is suppressed for large values of $|\boldsymbol{\delta}|$ and thus

$$\boldsymbol{\delta}^2 < \mathcal{O}(3/R_{\rm A}^2), \tag{2.129}$$

which means that for large nuclei one can neglect the $\boldsymbol{\delta}$-dependence of f_N and Γ_p^{2v2} and, therefore, one can write

$$\Gamma^{2v2}_{a_1,a_2/p}(x_1,x_2,\boldsymbol{\delta}) \approx D^{2v2}_{a_1,a_2/p}(x_1,x_2), \tag{2.130}$$

$$\Gamma^{2N}_{\rm A}(x_1,x_2,\boldsymbol{\delta}) \approx {\rm A}({\rm A}-1)\, f_N(x_1)\, f_N(x_2)\, |F_{\rm A}(\boldsymbol{\delta})|^2 . \tag{2.131}$$

where f_N is a nucleon collinear single parton distribution function. One should not confuse the dPDFs $D^{2v2}(x_1,x_2)$ in Eq. 2.130 with dPDFs $D(x_1,x_2)$ in Eq. 2.13 since $D^{2v2}(x_1,x_2)$ account only for "$2v2$" DPS processes as it shown in Fig. 2.7 a) whereas $D(x_1,x_2)$ account for "$2v2$" and "$1v2$" DPS processes as it is shown in Fig. 2.7 b) and c). The reason for this is a division of dPDFs into "$2v2$" "intrinsic" part and into "$1v2$" "perturbative" part in the approach of Blok *et al.* as in Eq. 2.84 and Eq. 2.91.

Using Eq. 2.130 and Eq. 2.131 one can write Eq. 2.127 as

$$\begin{aligned}\sigma^{\rm pA}_{\rm DPS} &\approx {\rm A}({\rm A}-1)\sum_{a_1,a_2,b_1,b_2}\int\prod_{i=1}^{4} dx_i\, D^{2v2}_{a_1,a_2/p}(x_1,x_2) f_{b_1/N}(x_3)\, f_{b_2/N}(x_4)\,\times \\ &\times \hat{\sigma}_{a_1\,b_1\to A}\,\hat{\sigma}_{a_2\,b_2\to B}\int\frac{d^2\boldsymbol{\delta}}{(2\pi)^2}\,|F_{\rm A}(\boldsymbol{\delta})|^2 .\end{aligned} \tag{2.132}$$

The integral over $\boldsymbol{\delta}$ yields

$$\int\frac{d^2\boldsymbol{\delta}}{(2\pi)^2}\,|F_{\rm A}(\boldsymbol{\delta})|^2 = \frac{1}{{\rm A}^2}\int\frac{d^2\boldsymbol{\delta}}{(2\pi)^2} d^2\boldsymbol{s}\, d^2\boldsymbol{s}'\, e^{-i\boldsymbol{\delta}(\boldsymbol{s}-\boldsymbol{s}')}\,{\rm T}_{\rm A}(\boldsymbol{s})\,{\rm T}_{\rm A}(\boldsymbol{s}') = \frac{1}{{\rm A}^2}\int d^2\boldsymbol{s}\,{\rm T}^2_{\rm A}(\boldsymbol{s}), \tag{2.133}$$

which allows to write Eq. 2.132 as

$$\begin{aligned}\sigma^{\rm pA}_{\rm DPS} &\approx \frac{({\rm A}-1)}{\rm A}\sum_{a_1,a_2,b_1,b_2}\int\prod_{i=4}^{4} dx_i\, D^{2v2}_{a_1,a_2/p}(x_1,x_2) f_{b_1/N}(x_3)\, f_{b_2/N}(x_4)\,\times \\ &\times \hat{\sigma}_{a_1\,b_1\to A}\,\hat{\sigma}_{a_2\,b_2\to B}\int d^2\boldsymbol{s}\,{\rm T}^2_{\rm A}(\boldsymbol{s}).\end{aligned} \tag{2.134}$$

Using approximate relation for the radius of the nucleus $R_{\rm A} \approx {\rm A}^{1/3}$ and the constraint for $\boldsymbol{\delta}^2$ as in Eq. 2.129 one can find how Eq. 2.134 scales with A. Namely, Eq. 2.129 yields $\boldsymbol{\delta}^2 < \mathcal{O}(3/R_{\rm A}^2) \sim {\rm A}^{-2/3}$. If we now approximate $F_{\rm A}(\boldsymbol{\delta})$ by the step function with support $\boldsymbol{\delta}^2 < \mathcal{O}(3/R_{\rm A}^2)$ we can estimate the

size of the integral $\int \frac{d^2\boldsymbol{\delta}}{(2\pi)^2} |F_{\rm A}(\boldsymbol{\delta})|^2$ which yields

$$\int \frac{d^2\boldsymbol{\delta}}{(2\pi)^2} |F_{\rm A}(\boldsymbol{\delta})|^2 = \int d^2\boldsymbol{s}\, {\rm T}_{\rm A}^2(\boldsymbol{s}) \approx {\rm A}^{4/3}. \tag{2.135}$$

We see that the total cross sections for the DPS process shown in Fig. 2.12 b) scales approximately as $A^{4/3}$ contrary to the cross section for the DPS processes shown in Fig. 2.12 a), c) and d) which scales approximately as A.

The last contribution we have to discuss in shown in Fig. 2.12 f). This process involves "$1v2$" splitting which we discussed at the beginning of this section. For the study of the process shown in Fig. 2.12 f) Blok *et al.* applied the formalism already developed in [195] to describe "$1v2$" DPS contributions in pp collisions. In particular it follows that expression for the process in Fig. 2.12 f) is given by Eq. 2.134 but with proton dPDF $D^{2v2}(x_1, x_2)$ replaced by $D^{1v2}(x_1, x_2)$ which describes "$1v2$" splitting. This result follows from the splitting of the proton dPDFs into "intrinsic" part which is in charge for "$2v2$" DPS processes and "perturbative" part which is charge for the "$1v2$" DPS processes, see Eq. 2.71. In [158] Blok *et al* using the parametrization of $F_{\rm A}(\boldsymbol{\delta})$ as in Eq. 2.74 and the formalism of [195] have demonstrated that the "$1v2$" DPS contribution in pp collisions is getting enhanced in comparison to "$2v2$" DPS contribution. A similar study was performed for the pA collisions. However, in [216] Blok *et al.* found that for the large nuclei with $A \gg 1$ the relative weight of the DPS process in Fig. 2.12 f) taken with respect to the DPS processes shown in Fig. 2.12 b) is smaller as the corresponding relative weight in pp collisions. Namely, the numerical estimate given in [216] for $A \gg 1$ yields

$$\left(\frac{\sigma^{\rm pA}_{f,DPS}}{\sigma^{\rm pA}_{b,DPS}}\right) \Big/ \left(\frac{\sigma^{\rm pp}_{1v2,DPS}}{\sigma^{\rm pp}_{2v2,DPS}}\right) = {\rm const(A)} \sim \frac{1}{5}, \tag{2.136}$$

where $\sigma^{\rm pp}_{1v2,DPS}$ and $\sigma^{\rm pp}_{2v2,DPS}$ are $1v2$ and $2v2$ DPS contributions in pp collisions, correspondingly.

Now let us summarize most relevant results of [216]:

- The total cross section for the processes shown in Fig. 2.12 a), c), d) and e) is given by Eq. 2.106.
- The total cross section for the process shown in Fig. 2.12 b) is given by Eq. 2.134.
- The total cross section for the process shown in Fig. 2.12 f) is given by Eq. 2.134 where "$2v2$" dPDF is replaced by "$1v2$" dPDF.
- The total cross section for the process shown in Fig. 2.12 e) is suppressed for the production of two back-to-back di-jet pairs.
- The relative contribution of the DPS process shown in Fig. 2.12 f) taken with respect to the contribution from the DPS process shown in Fig. 2.12 b) in pA collisions for heavy nuclei is about five times smaller as in pp collisions.

We will discuss some phenomenological applications of this formalism in Chapter 5 and Chapter 7.

Chapter 3

Basic Monte Carlo algorithms

In this chapter we briefly discuss some algorithms essential to write a simple Monte Carlo event generator. Namely, we discuss the generation of unweighted events and the generation of colour charges in the *leading colour approximation* using the LO di-jet production as an example. Later, in Chapter 4 we will apply the methods discussed in this section to the four-jet LO DPS production. A pedagogical introduction to the addressed topics can be found, for example, in [74] and [78]-[80].

3.1 Generation of unweighted events

Let us assume that we have a distribution function $f(x)$ which gives a probability to find a certain quantity in the range between x and $x + \Delta x$. Additionally, let us assume that we have to generate events according to $f(x)$. This task can be accomplished in several different ways. One of the simplest algorithms is a generation of *weighted events*. The idea is to generate x uniformly in a given range, say between 0 and 1, and to evaluate $f(x)$ for each value of x. This will provide us a set of x-values which we denote as $\{x_i\}$ and a set of associated weights $\{\omega_i = f(x_i)\}$ which we can use to produce a weighted distribution of "events" $\{x_i\}$. However, the work with weighted events may be inconvenient. For example, it can be very inefficient to work with events with small weights and, more importantly, events coming from a real data samples are always unweighted. One can circumvent this obstacle by using a reweighting procedure called *hit-or-miss* algorithm[1]. It can be seen as a sequence of the following steps:

1. Generate a set of x-values $\{x_i\}$ according to the uniform probability distribution.
2. For each $x_i \in \{x_i\}$, evaluate corresponding weights according to $\omega_i = f(x_i)$, resulting in a set of weights $\{\omega_i\}$.
3. Find in $\{\omega_i\}$ the maximal value $\omega_{\max}$.
4. For each generated $x_i \in \{x_i\}$ evaluate the ratio $\omega_i/\omega_{\max} \equiv f(x_i)/f_{max}$ and compare it to a random number generated in the range $R \in (0, 1)$. If $R < f(x_i)/f_{max}$ keep the event, otherwise remove it from the sample $\{x_i\}$.

After performing this procedure one will get a set of unweighted events $\{x_i\}$ where events which have higher weights before unweighting will appear more frequently. Therefore, one can build a

[1] This approach is also sometimes called a *rejection sampling* or *von Neumann rejection algorithm*.

frequency distribution for the sample $\{x_i\}$ which will give us a distribution of events according to the distribution function $f(x)$.

The aforementioned procedure, however, has a potential flaw. Namely, in practice, one usually determines $\omega_{\max}$ approximately at the certain accuracy level. It means that sometimes one can generate events with weight bigger than $\omega_{\max}$ which will imply $\omega/\omega_{\max} > 1$. Such events, obviously, will *always* satisfy the condition $R < \omega_i/\omega_{\max}$. After the unweighting procedure all events which had a weight $\omega < \omega_{\max}$ have the same weight which is equal to one. However, the events with $\omega > \omega_{\max}$ after the unweighting procedure will have the weight *bigger than one*. Therefore, one has always make sure that the maximal weight $\omega_{\max}$ is determined precise enough to exclude the influence of the aforementioned effect on the generation procedure.

3.2 Generation of $2 \to 2$ LO QCD processes

Now let us discuss how the hit-or-miss algorithm can be applied to the generation of the LO $2 \to 2$ QCD processes. The master formula for the total di-jet cross section is given by

$$\sigma_{\text{di-jet}} = \sum_{a,b,c,d} \sigma^{a\,b\to c\,d}_{\text{di-jet}} = \sum_{a,b,c,d} \int dx_a dx_b d\hat{t}\, f_{a/h_A}(x_a, Q^2) f_{b/h_B}(x_b, Q^2)\, \frac{d\hat{\sigma}}{d\hat{t}}\,(a\,b \to c\,d)\,, \tag{3.1}$$

where f_{a/h_A} (f_{b/h_B}) is a collinear PDF of a hadron of a type h_A (h_B) and $d\hat{\sigma}/d\hat{t}$ is a partonic cross section for the process $a\,b \to c\,d$.

As we see, the set of variables $x_a, x_b, \hat{t}$ completely determines a di-jet total cross section. However, for many practical purposes, it is more convenient to use a differential cross section expressed in terms of measurable quantities such as rapidity and transverse momentum, see Chapter 17 of [5]. By changing the integration variables from $x_a, x_b, \hat{t}$ to $y_c, y_d, p_\perp$ we can write Eq. 3.1 as

$$\begin{aligned} \sigma_{\text{di-jet}} &= \sum_{a,b,c,d} \sigma^{a\,b\to c\,d}_{\text{di-jet}} = \\ &= \sum_{a,b,c,d} \int dy_c dy_d dp_\perp\, \frac{2p_\perp \hat{s}}{S}\, f_{a/h_A}(x_a, Q^2) f_{b/h_B}(x_b, Q^2)\, \frac{d\hat{\sigma}}{d\hat{t}}\,(a\,b \to c\,d)\,, \end{aligned} \tag{3.2}$$

where y_c and y_d are the values of rapidities of final state partons in the *center of mass frame of colliding hadrons* h_A and h_B and $p_\perp$ is an absolute value of transverse momentum of the final state particles, $\sqrt{\hat{s}}/2$ is a collision energy of initial state partons and $\sqrt{S}/2$ is a collision energy of hadrons. The corresponding differential cross sections

$$\frac{d^3\sigma^{a\,b\to c\,d}_{\text{di-jet}}}{dy_c dy_d dp_\perp} = f_{a/h_A}(x_a, Q^2) f_{b/h_B}(x_b, Q^2)\, \frac{2p_\perp \hat{s}}{S}\, \frac{d\hat{\sigma}}{d\hat{t}}\,(a\,b \to c\,d) \tag{3.3}$$

gives a probability to produce two final state partons c and d with $y_c \in [y_c, y_c + dy_c]$, $y_d \in [y_d, y_d + dy_d]$ and $p_\perp \in [p_\perp, p_\perp + dp_\perp]$. The analytical expressions for the partonic $2 \to 2$ LO QCD cross sections as functions of the Mandelstam variables $\hat{s}, \hat{t}, \hat{u}$ are given in Appendix D. The connection between

the set of variables $\{y_a, y_b, p_\perp\}$ with $\{x_a, x_b, \hat{s}, \hat{t}, \hat{u}\}$ is given by

$$x_a = \frac{2p_\perp}{\sqrt{S}} \cosh y_* \, e^{Y}, \tag{3.4}$$

$$x_b = \frac{2p_\perp}{\sqrt{S}} \cosh y_* \, e^{-Y}, \tag{3.5}$$

$$\hat{s} = 4p_\perp^2 \cosh^2 y_*, \tag{3.6}$$

$$\hat{t} = -2p_\perp^2 \cosh y_* e^{-y_*}, \tag{3.7}$$

where

$$y_* = y_c - y_d, \tag{3.8}$$

$$Y = \frac{1}{2}(y_c + y_d), \tag{3.9}$$

see Chapter 17 of [5].

Using the differential cross section given by Eq. 3.3 one can generate di-jet events for the process $a\,b \to c\,d$ according to the hit-or-miss algorithm. The generation cycle will look like this:

1. Explore the $2 \to 2$ phase space and find the phase space point $\{y_b, y_c, p_\perp\}$ which has the maximal weight $\omega_{max}(y_c, y_d, p_\perp) \equiv \max\left(d^3\sigma^{a\,b\to c\,d}_{\mathrm{di-jet}}/dy_c\,dy_b\,dp_\perp\right)$.

2. Generate uniformly $\{y_c, y_d, p_\perp\}$ in a certain range and for each combination of y_c y_d and $p_\perp$ find the corresponding weight $\omega_i(y_c, y_d, p_\perp) \equiv d^3\sigma^{a\,b\to c\,d}_{\mathrm{di-jet}}/dy_c\,dy_b\,dp_\perp$.

3. For each weight ω_i find the ratio $\omega_i(y_c^i, y_d^i, p_\perp^i)/\omega_{max}(y_c, y_d, p_\perp)$ and accept or reject a given event according to the hit-or-miss method.

4. For each accepted combination $\{y_c^i, y_d^i, p_\perp^i\}$ evaluate components of four-momenta of particles in the initial and final state according to

$$p_a^\mu = (x_a E_A,\, 0,\, 0,\, x_a E_A)\,, \tag{3.10}$$

$$p_b^\mu = (x_b E_B,\, 0,\, 0,\, -x_b E_B)\,, \tag{3.11}$$

$$p_c^\mu = (p_\perp \sinh y_c,\, p_\perp \cos\phi,\, p_\perp \sin\phi,\, p_\perp \cosh y_c)\,, \tag{3.12}$$

$$p_d^\mu = (p_\perp \sinh y_d,\, -p_\perp \cos\phi,\, -p_\perp \sin\phi,\, p_\perp \cosh y_d)\,, \tag{3.13}$$

   where the value of the azimuthal angle ϕ has to be generated with the uniform probability in the interval $[0, 2\pi]$.

One important comment has to be added to the considerations above, namely that the hard cross sections from Appendix D are averaged over spin and colour indices which means that the generated events will not carry any information about spin and colour of produced particles. For many purposes this turns out to be sufficient enough. However, if one wants to add *parton showering* (PS) processes on top of partonic events one has to generate colours of produced particles as well. In the next section we will describe a Monte Carlo algorithm to accomplish this task.

3.3 Generation of QCD events in the leading colour approximation

In this section we will discuss the original Lund Monte Carlo algorithm proposed by Bengtsson [94] which allows to generate colour charges of the initial and final state partons. The generation of the colour charges is required to take into account so called *colour coherence effects* [97], [93] since the *radiation function* W_{mn} of the "colour dipole" is proportional to the product of two *colour charge operators* Q_m, Q_n [98]. The colour charge operators are defined such that the colour charge operator squared gives $\mathrm{Q}_n^2 = C_F$, if n corresponds to a quark and $\mathrm{Q}_n^2 = C_A$, if n corresponds to a gluon, and, four colour singlets $\mathrm{Q}_n^2 = 0$. The constants C_F and C_A are called *quadratic Casimir operators* and are defined as

$$t_N^i t_N^i = C_F, \tag{3.14}$$

$$f^{ikl} f^{jkl} = C_A \delta^{ij}, \tag{3.15}$$

where t_N^i are SU(3) group generators in so called *fundamental representation* and f^{ijk} are so called SU(3) *group structure constants*, see Appendix A.

As an example to illustrate Bengtsson's algorithm let us consider a quark-quark scattering process $qq \to qq$. At the leading order a corresponding amplitude is given by a sum of two diagrams each containing one intermediate gluon, see Fig. 3.1. According to the Feynman rules given in Fig. 1.1, each diagram will contain a product of two SU(3) generators $(t)_b^a\,(t)_d^c$, where indices a, b, c, d correspond to the colours of initial and final state quarks. Consider, for example, a $\hat{t}$-channel of the $qq \to qq$ process. Using the *colour flow basis* of QCD one can show that the product of two SU(3) generators $(t)_b^a\,(t)_d^c$ can be written as[2]

$$(t)_c^a\,(t)_d^b = T_R \left(\delta_d^a \delta_c^b - \frac{1}{N_c} \delta_c^a \delta_d^b \right), \tag{3.16}$$

where N_c is a number of colours in QCD, T_R is defined in Appendix A and a graphical representation of this equation is given in Fig. 3.2. The colour structure of the QCD amplitudes can be drastically simplified in the large-N_c approximation proposed by 't Hooft [99]. According to this approach, one works in the limit $N_c \to \infty$ which allows to neglect the term proportional to $1/N_c$ in Eq. 3.16. The resulting colour flow topologies for the $\hat{t}$- and $\hat{u}$-channel matrix elements squared are shown in Fig. 3.3.

Note that in the large-N_c limit the interference term between $\hat{t}$- and $\hat{u}$-channels becomes subleading in comparison to the $\hat{t}$- and $\hat{u}$-channel matrix elements squared. In order to demonstrate it let us write the $\hat{t}$- and $\hat{u}$-channel amplitudes in the the large-N_c limit as

$$\mathcal{M}_{c,d}^{a,b}(\hat{t}) = \mathcal{C}_{c,d}^{a,b}\,\mathrm{M}(\hat{t}) \overset{large\,N_c}{\approx} \delta_d^a \delta_c^b\,\mathrm{M}(\hat{t}), \tag{3.17}$$

$$\mathcal{M}_{c,d}^{a,b}(\hat{u}) = \mathcal{C}_{d,c}^{a,b}\,\mathrm{M}(\hat{u}) \overset{large\,N_c}{\approx} \delta_c^a \delta_d^b\,\mathrm{M}(\hat{u}), \tag{3.18}$$

where $\mathcal{C}$ is the part of the amplitude $\mathcal{M}$ which carries information about the colours of initial and

[2] For the formulation of the QCD in the colour flow basis see [95], [96].

Figure 3.1: Diagrams contributing to the $qq \to qq$. a) $\hat{t}$-channel gluon exchange. b) $\hat{u}$-channel gluon exchange.

final state quarks. The matrix elements squared summed over all possible combinations of colours are given by

$$\sum_{a,b,c,d} |\mathcal{M}^{a,b}_{c,d}(\hat{t})|^2 \overset{large\,N_c}{\approx} \sum_{a,b,c,d} \delta^a_d \delta^b_c \, |\mathrm{M}(\hat{t})|^2 = N_c^2 \, |\mathrm{M}(\hat{t})|^2, \tag{3.19}$$

$$\sum_{a,b,c,d} |\mathcal{M}^{a,b}_{c,d}(\hat{u})|^2 \overset{large\,N_c}{\approx} \sum_{a,b,c,d} \delta^a_c \delta^b_d \, |\mathrm{M}(\hat{u})|^2 = N_c^2 \, |\mathrm{M}(\hat{u})|^2. \tag{3.20}$$

We see that in the large-N_c limit both $\hat{t}$- and $\hat{u}$-channel contributions being summed over all possible colour combinations are proportional to N_c^2. However, for the interference term we get

$$\sum_{a,b,c,d} \mathcal{M}^{a,b}_{c,d}(\hat{t}) \overline{\mathcal{M}}^{a,b}_{c,d}(\hat{u}) \overset{large\,N_c}{\approx} \sum_{a,b,c,d} \delta^a_d \delta^b_c \, \delta^a_c \delta^b_d \, \mathrm{M}(\hat{t}) \overline{\mathrm{M}}(\hat{u}) = N_c \, \mathrm{M}(\hat{t}) \overline{\mathrm{M}}(\hat{u}). \tag{3.21}$$

Therefore, the interference terms for the $qq \to qq$ process in the large-N_c limit gives a subleading contribution and thus can be neglected[3]. The colour flow topologies in the large-N_c limit for the $qq \to qq$ process are given in Fig. 3.3.

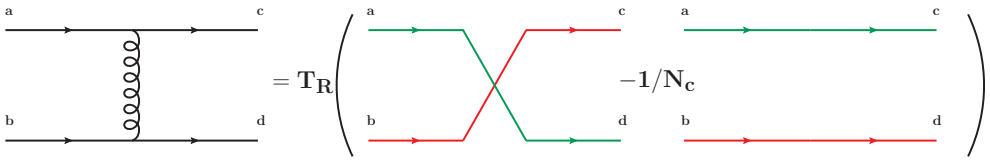

Figure 3.2: The colour flow decomposition for the $\hat{t}$-channel amplitude of the $qq \to qq$ process.

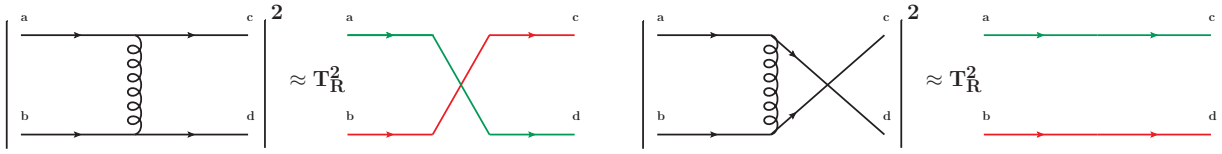

Figure 3.3: Large-N_c approximation for the process $qq \to qq$. a) $\hat{t}$-channel approximation. b) $\hat{u}$-channel approximation.

Now we can describe how the original Lund Monte Carlo colour assignment algorithm works

[3]For the other $2 \to 2$ LO QCD processes, see [94].

[94]. Since in the large-N_c limit we neglect the interference terms, the total cross section is given by a sum of two terms

$$\sigma \approx \sigma_T + \sigma_U, \tag{3.22}$$

where

$$\begin{aligned} \sigma_T &\sim \frac{\hat{s}^2 + \hat{u}^2}{\hat{t}^2}, \\ \sigma_U &\sim \frac{\hat{s}^2 + \hat{t}^2}{\hat{u}^2}. \end{aligned} \tag{3.23}$$

The colour assignment algorithm then is given by the following steps:

1. For each generated event evaluate a ratio $\sigma_T/(\sigma_T + \sigma_U)$.
2. Generate a random number $R \in [0, 1]$ according to the uniform probability distribution.
3. If condition $R < \sigma_T/(\sigma_T + \sigma_U)$ holds, select a colour topology shown in Fig. 3.3 a), otherwise select a colour topology shown in Fig. 3.3 b).

As a certain topology was selected, one stores the information about it according to the *Les-Houches Event File* (LHEF) standard[4] [81]. In this notation, each colour line is defined by two numbers: in the case of quarks, first number labels the colour line and the second number is always set to zero (and *vice versa* for antiquarks) and in the case of gluons both number are non-zero (since gluon carries two colour charges). The connection between the LHEF notation and the colour flow topologies in Fig. 3.3 is shown in Fig. 3.4. In the LHEF notation each colour flow line is labelled by an integer number. Depending on the version the LHEF standard the numbering of the colour flow lines start either from 101 (LHEF standard version 1) or from 501 (LHEF standard version 3). Different numbers are used to distinguish different colour lines. For example, for the process $qq \to qq$ we have only two different colour flow lines which are labelled by 501 and 502, correspondingly, as shown in Fig. 3.4. In the LHEF notation the correspondence between particles in different channels of a given process and corresponding colour flow topologies is described by two colour indices, see Fig. 3.5. For example, the connection between the $\hat{t}$-channel for the process $qq \to qq$ and the corresponding colour flow topology shown in Fig. 3.4 a) is given by $q\,(501\ 0)\ \ q\,(502\ 0) \xrightarrow{\hat{t}-channel} q\,(502\ 0)\ \ q\,(501\ 0)$. In case of quarks the first number in parenthesis is given by the number of the colour flow line associated with a given quark and the second number is always equal to zero. In case of antiquarks one has to "swap" both numbers. For example, for the $\hat{t}$-channel of the $\bar{q}\bar{q} \to \bar{q}\bar{q}$ process we have $\bar{q}\,(0\ 501)\ \ \bar{q}\,(0\ 502) \xrightarrow{\hat{t}-channel} \bar{q}\,(0\ 502)\ \ \bar{q}\,(0\ 501)$. For the gluons both integers are non-zero since in the large-N_c approximation the colour-flow of gluon is described by two colour lines. The connection between the $\hat{u}$-channel for the process $qq \to qq$ and the colour flow topology in Fig. 3.4 b) is given by $q\,(501\ 0)\ \ q\,(502\ 0) \xrightarrow{\hat{u}-channel} q\,(501\ 0)\ \ q\,(502\ 0)$. By comparing the assignment of the colour indices for the $\hat{t}$- and $\hat{u}$-channels of the $qq \to qq$ process we see that the numbers of the colour flow lines were swapped for the final state quarks. This interchange of indices is required by consistent treatment of the $\hat{t}$- and $\hat{u}$-channels since, $\hat{t}$- and

[4] In the following we will also refer to the files with events written according to the LHEF standard as to *Les-Houches Event* (LHE) files.

$\hat{u}$-channel diagrams are related to each other though the interchange of the final state legs which, in turn, leads to the interchange of the colour flow lines, see Fig. 3.3.

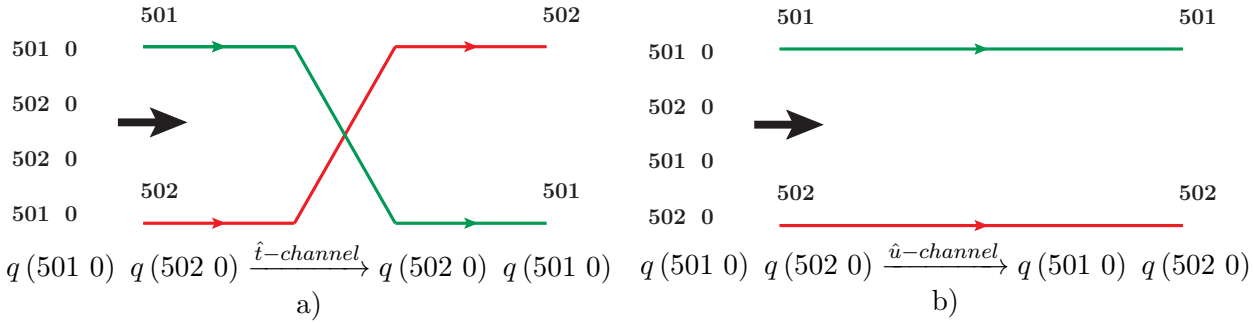

Figure 3.4: Representation of colour topologies from Fig. 3.3 in the LHEF notation. a) The $\hat{t}$-channel topology. b) The $\hat{u}$-channel topology.

For our DPS simulations in Chapter 4 and Chapter 5 we will use the original Lund Monte Carlo algorithm [94] as implemented into the `Pythia` event generator [255] - [257][5]. The usage of the same colour generation algorithm as in the `Pythia` code allows to combine our DPS simulations with the *initial state radiation* (ISR) and *final state radiation* (FSR) of `Pythia`. Later in Chapter 4.9 we will discuss the modifications to the `Pythia` code and to the LHEF standard necessary to read and "shower" the DPS events from the LHE files.

Finally, before closing this section, we shall notice that the large-N_c approximation is consistent with most standard ISR [92],[93] and FSR [85] - [91] algorithms since both large-N_c approximation and parton showering neglect the interference effects[6].

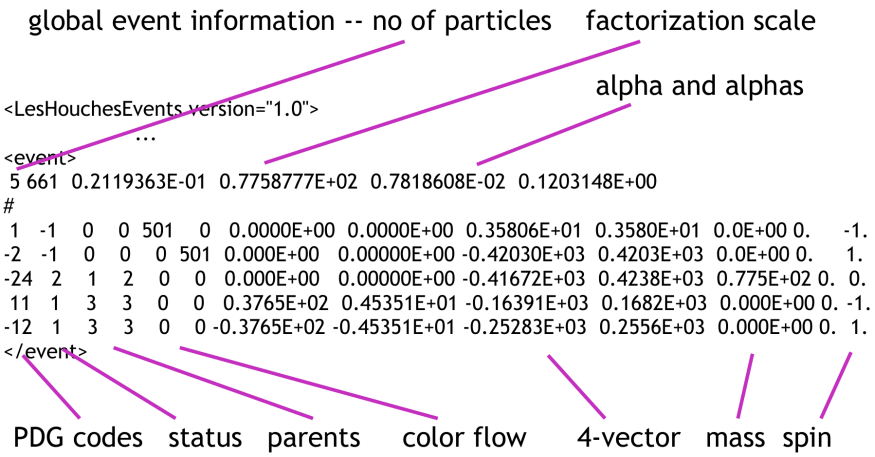

Figure 3.5: An event in the LHEF notation, from [79].

[5] A reader interested in the realization of the colour generation should also look into the description of the methods of the class `SigmaQCD` of the `Pythia` 8 code [83].

[6] For the improved parton shower algorithms see [100] - [103].

Chapter 4

Four-jet DPS production in proton-proton collisions

4.1 Introduction

Over decades the four-jet DPS production remains one the most intensively studied DPS production channels. The first theoretical study of the four-jet DPS production was made by Paver and Treleani [116], two years later after the pioneering paper on the double Drell-Yan production published by Goebel, Halzen and Scott [114]. In Ref. [116] Paver and Treleani founded main concepts of the DPS phenomenology. In particular, they provided a modern expression for the total DPS cross section, introduced transverse dependent generalized double parton distribution functions $\Gamma_{a_1,a_2/h_A}(x_1, x_2, \boldsymbol{b})$ and proposed a widely used factorization ansatz $\Gamma_{a_1,a_2/h_A}(x_1, x_2, \boldsymbol{b}) \approx f_{a_1/h_A}(x_1)\, f_{a_2/h_A}(x_2)\, F(\boldsymbol{b})$. Subsequently Paver and Treleani [119] performed the first phenomenological study of the four-jet DPS production within the DPS formalism developed in [116]. It was demonstrated that the four-jet DPS events could be observed at the Sp$\bar{\text{p}}$S and Tevatron colliders operating at that time. Furthermore, it was argued that four-jet events produced via DPS mechanism will have configurations distinctive from those produced via the standard SPS mechanism. This study was followed by two theoretical publications [121], [122] where it was proposed how to discriminate between SPS and DPS events and most of nowadays commonly used DPS-sensitive variables were introduced.

The aforementioned research motivated experimental studies of DPS phenomena and in 1986 the AFS collaboration performed the first pioneering measurements of the four-jet DPS production at $\sqrt{S} = 63$ GeV collision energy and determined $\sigma_{eff} = 5\,\text{mb}$ [128]. Unfortunately, neither statistical nor systematic uncertainties were provided. One of the main technical difficulties at that time was the correct estimation of the SPS background which is inextricably connected with correct extraction of the DPS signal. After the ASF measurements the study of the four-jet DPS production continued in both experimental and theoretical communities. In 1988 Mangano provided a new phenomenological study of the four-jet DPS production where the SPS background was estimated within an improved theoretical framework [127]. In 1991 the UA2 collaboration measured a DPS production in the four-jet final state at $\sqrt{S} = 630$ GeV collision energy [129]. This time only a lower error boundary was provided. Finally, in 1993 the CDF collaboration came up with the first convincing measurements of the four-jet DPS production at $\sqrt{S} = 1.8$ TeV collision energy [130]. Later, in 2013 and 2016 the CMS [108] and the ATLAS [145] collaborations measured the four-jet

DPS production at $\sqrt{S} = 7$ TeV collision energy.

References [128], [129], [130], [108], [145] list all currently available experimental studies of the four-jet DPS production in pp and p$\bar{\text{p}}$ collisions. Whereas in [128], [129], [130], [145] the main research goal was an extraction of the value of σ_{eff}, see Fig. 2.2 and Fig. 2.3, in [108] the main accent was put on studies of various DPS-sensitive distributions.

These experimental measurements were accompanied by several phenomenological studies. Namely, in 2009 Berger *et al.* [229] published a paper with a study of the impact of ISR and FSR effects on the four-jet DPS production where DPS events were constructed out of two sets of di-jet events simulated at NLO accuracy level with included PS effects. In the same year Domedy *et al.* [152] considered different models of correlations between Bjorken variables and the transverse distance between partons $\boldsymbol{b}$ in a generalized parton distribution function $\Gamma_{a_1,a_2/h_A}(x_1, x_2, \boldsymbol{b})$ and demonstrated that correlations of this type can lead to a scale-dependent σ_{eff}. A similar study was performed by Blok *et al.* [158]. It was demonstrated that the correlations of partons due to the "1v2" DPS contribution, see Fig. 2.7 b), can explain the measured value of σ_{eff}, see Fig. 2.2 and Fig. 2.3. In 2015 Maciuła and Szczurek proposed new jet cuts to increase the DPS contribution to the four-jet production and identified phase-space corners where the DPS exceeds the SPS contribution [230]. In particular, it was shown that under certain conditions the DPS contribution may reach up to 90% of the total four-jet cross section. A similar study of four-jet DPS production within the k_T-factorization approach was performed in [231], [232] and within the leading-logarithmic BFKL formalism [244] - [249] in [233].

We also should mention that concurrently to the aforementioned studies of four-jet DPS production development of Monte Carlo DPS and MPI models was significant advanced, see [258] - [263], [265], [266] and [268]. In particular, the MPI model of the `Pythia` event generator evolved from the very first MPI model proposed by Sjöstrand in mid-eighties of the past century [258] up to the very sophisticated modern model of `Pythia` 8 [258] - [263]. Among many other features, this model accounts for the momentum and number conservation and therefore takes into account partonic correlations in the longitudinal momentum and flavour. Additionally, there exist `Pythia` tunes for various DPS production processes [162], [163]. In particular, the tune for the four-jet DPS production [162] accounts for dynamical changes of σ_{eff} due to the longitudinal partonic correlations.

The studies of DPS by Domedy *et al.* [152] and Blok *et al.* [158] were dedicated to the connection between the values of σ_{eff} and the longitudinal partonic correlations. The DPS productions in the paper of Berger *et al.* were constructed by overlaying simulations of the SPS di-jet events which does not allow to study partonic correlations. In this chapter we present our simulations of four-jet DPS production and perform comparison between DPS and SPS contributions to the four-jet cross section. Additionally, we discuss various technical aspects of DPS simulations, such as factorization scale dependence, the role of different partial contributions to the four-jet DPS production and their impact on four-jet simulations. We also study the impact of longitudinal partonic correlations due to the dDGLAP evolution of dPDFs and identify regions of the DPS phase space where the dDGLAP evolution effects give rise to significant changes in differential DPS distributions. In section 4.9 we discuss an extension of the Les-Houches version = "1" standard and modifications to the `Pythia 8` code required to read and "shower" DPS events from Les-Houches files. This will make it possible to

combine our DPS simulations with the ISR and FSR simulations of `Pythia`. We also present checks of these modifications. Finally, in section 4.10 and section 4.11 we discuss problems of existing DPS parton shower algorithms as well as some recent achievements in their development. Furthermore, we present a study of the impact of initial and final state radiation on our DPS simulations.

4.2 Phenomenology of double parton scattering

We begin with a description of the main ingredients used to simulate four-jet DPS production. As a starting point to generate DPS events, we assume factorization of $\Gamma_{i,j/p}(x_1, x_2, \boldsymbol{b})$ into a product of longitudinal and transverse dependent pieces $\Gamma_{i,j/p}(x_1, x_2, \boldsymbol{b}) \approx D_{i,j/p}(x_1, x_2)\, F(\boldsymbol{b})$. Using this substitution one can write a total DPS cross section for pp collisions as

$$\begin{aligned}\sigma_{AB}^{\mathrm{DPS}} &= \frac{1}{1+\delta_{AB}} \frac{1}{\sigma_{eff}} \sum_{a_1,a_2,b_1,b_2} \int \prod_{i=1}^{4} dx_i\, D_{a_1,a_2}(x_1, x_2, Q_1^2, Q_2^2)\, D_{b_1,b_2}(x_3, x_4, Q_1^2, Q_2^2) \times \\ &\times \hat{\sigma}_{a_1\, b_1 \to A}\, \hat{\sigma}_{a_2\, b_2 \to B}, \end{aligned} \tag{4.1}$$

where the prefactor $1/(1+\delta_{AB})$ was used to reflect the fact that, in case of production of two indistinguishable finals states A and B, one has to divide a total DPS cross section by 2. Assuming no partonic correlations in x-space one can substitute $D_{a_1,a_2}(x_1, x_2, Q_1^2, Q_2^2) \approx f_{a_1}(x_1, Q_1^2) f_{a_2}(x_2, Q_2^2)$ in Eq. 4.1 which gives us the "pocket formula of DPS"

$$\sigma_{AB}^{\mathrm{DPS}} = \frac{1}{1+\delta_{AB}} \sum_{a_1,a_2,b_1,b_2} \frac{\sigma_{a_1\, b_1 \to A}\, \sigma_{a_2\, b_2 \to B}}{\sigma_{eff}}. \tag{4.2}$$

Such factorization, however, violates momentum and number (flavour) dPDF sum rules given by Eq. 2.17 - 2.20. The momentum conservation can be restored in a trivial way by multiplying a factorized product of PDFs by an appropriate cutoff function, for example

$$D_{a_1,a_2}(x_1, x_2, Q_1^2, Q_2^2) \approx f_{a_1}(x_1, Q_1^2)\, f_{a_2}(x_2, Q_2^2)\, \theta(1 - x_1 - x_2), \tag{4.3}$$

where $\theta(1 - x_1 - x_2)$ excludes unphysical region where $x_1 + x_2 > 1$. The number conservation, however, cannot be restored in a trivial way. Nevertheless, Eq. 4.3 is still commonly used for a phenomenological modelling of DPS. In this thesis we will refer to the dPDFs approximated according to Eq. 4.3 as to "naive" dPDFs and will use them as a baseline in comparison against more realistic GS09 dPDFs. We also should notice that "naive" dPDFs, as in Eq. 4.3, do not allow to reduce Eq. 4.1 to the "pocket formula" Eq. 2.11. Instead, by substituting Eq. 4.3 into Eq. 4.1, we get

$$\begin{aligned}\sigma_{AB}^{\mathrm{DPS}} &= \frac{1}{1+\delta_{AB}} \frac{1}{\sigma_{eff}} \sum_{a_1,a_2,b_1,b_2} \int \prod_{i=1}^{4} dx_i\, f_{a_1}(x_1, Q_1^2)\, f_{b_1}(x_3, Q_1^2)\, \hat{\sigma}_{a_1,b_1 \to A} \times \\ &\times f_{a_2}(x_2, Q_2^2)\, f_{b_2}(x_4, Q_2^2)\, \hat{\sigma}_{a_2,b_2 \to B}\, \theta(1 - x_1 - x_2)\, \theta(1 - x_3 - x_4). \end{aligned} \tag{4.4}$$

In the following we will use Eq. 4.1 with GS09 dPDFs [173] and Eq. 4.4 for the Monte Carlo generation of DPS events according to the *hit-or-miss* algorithm we have described in Chapter 3.

In order to find the total DPS cross section we also use Eq. 4.1 and Eq. 4.4. The partonic $2 \to 2$ QCD cross sections are calculated at LO accuracy level and given in Appendix D. In order to generate colour charges of the produced partons we use the original Lund Monte Carlo colour flow algorithm [94] which is also used in the `Pythia` event generator. A numerical integration is performed by means of the integration routines from GSL library [294]. In particular, we use the VEGAS algorithm of Lepage [295] which is based on importance sampling. As we have discussed in Chapter 3.1, it is essential to find a phase space point which gives a highest value of the DPS weight $\omega_{\rm max}^{\rm DPS}$ to avoid generation of events with weights bigger than one. Since during the Monte Carlo integration VEGAS performs a scan of the available DPS phase space in order to find regions which give the biggest contribution to the total DPS cross section, we combine in our code the search of $\omega_{\rm max}^{\rm DPS}$ with the evaluation of $\sigma_{AB}^{\rm DPS}$. Namely, we compare a weight ω_i of a generated phase space point against a weight ω_{i-1} of a previously generated phase space point and if condition $\omega_i \geq \omega_{i-1}$ is satisfied then we set $\omega_{\rm max}^{\rm DPS} = \omega_i$. When VEGAS finishes the scan of the DPS phase space we get a value of $\omega_{\rm max}^{\rm DPS}$ evaluated at the accuracy level high enough to avoid the problem events with the weights bigger than one, see Chapter 3.1.

After performing the aforementioned procedure for each subprocess contributing to $pp \xrightarrow{\rm DPS} 4j$ we end up with the array of maximal weights for each partial contribution and corresponding total cross sections. After that, the *hit-or-miss* algorithm is used to generate a desired number of unweighted DPS events. A corresponding number of DPS events for each subprocess $N_{\rm sub}^{\rm DPS}$ is obtained from the ratio

$$\frac{N_{\rm sub}^{\rm DPS}}{N_{\rm tot}^{\rm DPS}} = \frac{\sigma_{\rm sub}^{\rm DPS}}{\sigma_{\rm tot}^{\rm DPS}}, \tag{4.5}$$

where $N_{\rm tot}^{\rm DPS}$, $\sigma_{\rm sub}^{\rm DPS}$ and $\sigma_{\rm tot}^{\rm DPS}$ are the total number of DPS events, the total DPS cross section for a given subprocess and the total DPS cross section for the $pp \xrightarrow{\rm DPS} 4j$ process correspondingly. The generation of events for each subprocess runs until a number of generated events reach $N_{\rm sub}^{\rm DPS}$.

In our analysis we use two different models of dPDFs. As a base line we use "naive" dPDFs, as in Eq. 4.3, constructed out of MSTW2008 LO PDFs [298]. In order to estimate the impact of partonic correlations in x-space we use unequal scale GS09 dPDFs [173], [174] which were designed as the double parton counterparts of the MSTW2008 LO PDFs. In our program we also use the LHAPDF6 library [296] in order to work with MSTW2008 grids and the interpolation routine for GS09 dPDFs [297].

The last ingredient for the four-jet DPS phenomenology we have to discuss before presenting results is the symmetry factor $1/(1+\delta_{AB})$ in Eq. 4.1 and Eq. 4.4. In the available publications on four-jet DPS production it is sometimes used in a slightly different context which may lead to a possible confusion. We will start the discussion from the origin of the $1/2$ factor in the experimental parametrization of the DPS cross section and in the MPI model of `Pythia`. Then we will discuss the origin of the $1/2$ factor in the theoretical and phenomenological studies of DPS and argue that all approaches give equivalent results.

The "pocket formula of DPS", Eq. 2.11, used to extract the value of σ_{eff} in the four-jet

production processes [128], [129], [130], [145] is given by

$$\sigma^{\rm DPS}_{four-jet} = \frac{1}{2}\frac{\sigma^2_{di-jet}}{\sigma_{eff}}, \tag{4.6}$$

where σ^2_{di-jet} is a total di-jet cross section . This ansatz is inspired by the first Monte Carlo model of MPI developed by Sjöstrand in 1985 [258]. The model of [258] is based upon Poissonian statistics[1]. Within this framework a probability of an MPI event with n interactions to happen is given by

$$P_n = \frac{\langle n\rangle e^{-\langle n\rangle}}{n!}, \tag{4.7}$$

where $\langle n\rangle$ is an average number of interactions in the MPI event given by the ratio $\langle n\rangle = \sigma_n/\sigma_{\rm ND}$ where σ_n is the total cross section for n hard or semi-hard interactions and $\sigma_{\rm ND}$ is the total nondiffractive cross section. Assuming σ_n to be much smaller than $\sigma_{\rm ND}$ one can approximate $\exp(-\langle n\rangle) \approx 1$ and thus

$$P_n \approx \frac{\langle n\rangle}{n!}. \tag{4.8}$$

Therefore, a probability of an MPI event with one interaction to happen is $P_1 = \sigma_1/\sigma_{\rm ND}$. Using Eq. 4.8 iteratively one can express probabilities $P_2, \dots P_n$ in terms of P_1. For example,

$$P_2 = \frac{\sigma_2}{\sigma_{\rm ND}} = \frac{1}{2!}P_1^2 = \frac{1}{2}\left(\frac{\sigma_1}{\sigma_{\rm ND}}\right)^2. \tag{4.9}$$

As we see, within this approach the factor $1/2$ emerges due to $n!$ in the denominator of the Poisson distribution and the connection between MPI model of `Pythia` and the pocket formula of DPS is given by

$$\sigma_2 = \frac{\sigma_{\rm ND}}{2}\left(\frac{\sigma_1}{\sigma_{\rm ND}}\right)^2\frac{\sigma_{\rm ND}}{\sigma_{eff}} = \frac{1}{2}\frac{\sigma_1^2}{\sigma_{eff}}, \tag{4.10}$$

where $\sigma_{\rm ND}/\sigma_{eff}$ gauges the deviation from the Poisson distribution, see [260].

The parametrization of the DPS cross section in Eq. 4.10 coincides with the expression for the four-jet DPS cross section in Eq. 4.6. The factor $1/2$ in Eq. 4.6 and Eq. 4.10 also can be seen as a symmetry factor which one has to introduce for two *indistinguishable* di-jet production processes. Since in the experimental measurements of the four-jet DPS production one does not distinguish between di-jets produced by different partons all di-jet production processes are indistinguishable and thus the factor $1/2$ is always present in Eq. 4.6. In the MPI model of `Pythia` different di-jet production processes in general are not equivalent since they have different $2 \to 2$ cross sections and, therefore, different probabilities to be generated. In order to illustrate it let us assume that there are two different processes A and B which contribute to the MPI production. In this case

$$P_1 = \frac{\sigma_{1A}}{\sigma_{\rm ND}} + \frac{\sigma_{1B}}{\sigma_{\rm ND}} \tag{4.11}$$

[1]More precisely, upon Poissonian statistics with modifications necessary for correct description of charged multiplicity distribution and energy-momentum conservation. The review of the state-of-the-art of the MPI modelling is given in [263].

and, therefore,

$$\frac{\sigma_{2AB}}{\sigma_{\rm ND}} = \frac{1}{2}\left(\frac{\sigma_{1A}}{\sigma_{\rm ND}} + \frac{\sigma_{1B}}{\sigma_{\rm ND}}\right)^2 = \frac{1}{2}\left(\frac{\sigma_{1A}}{\sigma_{\rm ND}}\right)^2 + \frac{1}{2}\left(\frac{\sigma_{1B}}{\sigma_{\rm ND}}\right)^2 + \frac{\sigma_{1A}\,\sigma_{1B}}{\sigma^2_{\rm ND}}. \tag{4.12}$$

By multiplying Eq. 4.12 by $\sigma_{\rm ND}$ we get

$$\sigma_{2AB} = \frac{1}{2}\frac{\sigma^2_{1A}}{\sigma_{\rm ND}} + \frac{1}{2}\frac{\sigma^2_{1B}}{\sigma_{\rm ND}} + \frac{\sigma_{1A}\,\sigma_{1B}}{\sigma_{\rm ND}} = \frac{1}{2\sigma_{\rm ND}}\sum_{a,b=\{A,B\}}\sigma_a\,\sigma_b. \tag{4.13}$$

As we have mentioned before, the ratio $\sigma_{\rm ND}/\sigma_{eff}$ gauges the deviation from the Poisson distribution. Therefore, in the same way as in Eq. 4.10, in order to account for the deviation from the Poisson distribution, we can multiply the RHS of Eq. 4.13 by $\sigma_{\rm ND}/\sigma_{eff}$ yielding

$$\sigma_{2AB} = \frac{1}{2}\frac{\sigma^2_{1A}}{\sigma_{eff}} + \frac{1}{2}\frac{\sigma^2_{1B}}{\sigma_{eff}} + \frac{\sigma_{1A}\,\sigma_{1B}}{\sigma_{eff}} = \frac{1}{2\sigma_{eff}}\sum_{a,b=\{A,B\}}\sigma_a\,\sigma_b. \tag{4.14}$$

Now let us describe the origin of the factor 1/2 in theoretical and phenomenological studies of DPS. In the pioneering paper of Paver and Treleani [116] the distribution of partons in a transverse plane of a proton $F(\boldsymbol{b})$ was postulated to have a Gaussian form

$$F(\boldsymbol{b}) = \frac{1}{\pi R^2}\exp\left(-|\boldsymbol{b}|^2/R^2\right), \tag{4.15}$$

where R is the proton radius. Substituting this ansatz into Eq. 2.7 we get

$$\begin{aligned}\sigma^{\rm DPS}_{AB} &= \frac{1}{\pi^2 R^4}\int d^2b\, e^{-2|\boldsymbol{b}|^2/R^2}\left(\sum_{a_1,a_2,b_1,b_2}\int\prod_{i=1}^{4}dx_i\,[\ldots]\right) = \\ &= \frac{1}{2\pi R^2}\sum_{a_1,a_2,b_1,b_2}\int\prod_{i=1}^{4}dx_i\,[\ldots]\,.\end{aligned} \tag{4.16}$$

If we now neglect correlations in x-space we can write Eq. 4.16 as

$$\sigma^{\rm DPS}_{AB} = \frac{1}{2\pi R^2}\sum_{a_1,a_2,b_1,b_2}\sigma_{a_1b_1\to A}\,\sigma_{a_2b_2\to B}. \tag{4.17}$$

If we denote $\tilde{\sigma}_{eff} = \pi R^2$, we would get

$$\sigma^{\rm DPS}_{AB} = \frac{1}{2\tilde{\sigma}_{eff}}\sum_{a_1,a_2,b_1,b_2}\sigma_{a_1b_1\to A}\,\sigma_{a_2b_2\to B}, \tag{4.18}$$

which formally coincides with Eq. 4.14. However, the value of $\tilde{\sigma}_{eff}$ in Eq. 4.18 and the value of σ_{eff} in Eq. 4.14 will not coincide. In fact, the definition of σ_{eff} in Eq. 2.6 tells us that the factor 2 in the denominator of Eq. 4.18 has to be absorbed into the definition of σ_{eff} since $\sigma_{eff} = \left[\int d^2b\,F^2(\boldsymbol{b})\right]^{-1} = 2\pi R^2 = 2\tilde{\sigma}_{eff}$. Therefore, we see that Eq. 4.18 and Eq. 4.14 disagree between each other. However, as it was shown in [192], [193] the correct quantum treatment of the DPS cross section requires a symmetry factor 1/2! in case of a DPS production of *two*

indistinguishable final states[2]. Therefore, the correct expression reads

$$\sigma_{AB}^{\rm DPS} = \frac{1}{1+\delta_{AB}}\frac{1}{\sigma_{eff}}\sum_{a_1,a_2,b_1,b_2}\sigma_{a_1b_1\to A}^{di-jet}\,\sigma_{a_2b_2\to B}^{di-jet}, \tag{4.19}$$

where σ_{eff} is defined as in Eq. 2.6 and A and B are two final states produced in the first and the second hard interactions correspondingly. In the following we will refer to such approach to the symmetry factor 1/2 as to the quantum mechanical approach. It may seem that the treatment of the symmetry factor 1/2 as in Eq. 4.14 and Eq. 4.19 may lead to different results. However, it is not the case. For example, consider a DPS process involving $(gg \to gg)$ and $(q\bar{q} \to gg)$ processes. According to the Poissonian approach we get

$$\sigma_{AB}^{\rm DPS} = \frac{1}{2}\frac{1}{\sigma_{eff}}\left[\sigma_{gg\to gg}\,\sigma_{q\bar{q}\to gg} + \sigma_{q\bar{q}\to gg}\,\sigma_{gg\to gg}\right] = \frac{1}{\sigma_{eff}}\,\sigma_{gg\to gg}\,\sigma_{q\bar{q}\to gg}. \tag{4.20}$$

One would get the same expression according to the quantum mechanical approach. Namely, we get

$$\begin{aligned}\sigma_{AB}^{\rm DPS} &= \frac{1}{2}\frac{1}{\sigma_{eff}}\int\prod_{i=1}^{4}dx_i\,D_{gq}(x_1,x_2)\,D_{g\bar{q}}(x_3,x_4)\,\hat{\sigma}_{gg\to gg}(x_1,x_3)\,\hat{\sigma}_{q\bar{q}\to gg}(x_2,x_4) + \\ &+ \frac{1}{2}\frac{1}{\sigma_{eff}}\int\prod_{i=1}^{4}dx_i\,D_{qg}(x_1,x_2)\,D_{\bar{q}g}(x_3,x_4)\,\hat{\sigma}_{q\bar{q}\to gg}(x_1,x_3)\,\hat{\sigma}_{gg\to gg}(x_2,x_4) = \\ &= \frac{1}{\sigma_{eff}}\,\sigma_{gg\to gg}\,\sigma_{q\bar{q}\to gg}.\end{aligned} \tag{4.21}$$

Consider now the production of two *distinguishable* final states. For example, consider the DPS process involving $(gg \to gg)$ and $(gg \to q\bar{q})$. In this case the Poissonian approach yields

$$\sigma_{AB}^{\rm DPS} = \frac{1}{\sigma_{eff}}\,\sigma_{gg\to gg}\,\sigma_{gg\to q\bar{q}}, \tag{4.22}$$

and the quantum mechanical approach gives

$$\begin{aligned}\sigma_{AB}^{\rm DPS} &= \frac{1}{\sigma_{eff}}\int\prod_{i=1}^{4}dx_i\,D_{gg}(x_1,x_2)\,D_{gg}(x_3,x_4)\,\hat{\sigma}_{gg\to gg}(x_1,x_3)\,\hat{\sigma}_{gg\to q\bar{q}}(x_2,x_4) = \\ &= \frac{1}{\sigma_{eff}}\,\sigma_{gg\to gg}\,\sigma_{gg\to q\bar{q}},\end{aligned} \tag{4.23}$$

which again is the same us in Eq. 4.22. Similar checks can be performed for the other combinations of LO $2 \to 2$ processes.

Therefore, we can conclude that both Poissonian and quantum mechanical approaches give the same symmetry factor 1/2 for the four-jet DPS cross sections. We also have argued that the symmetry factor in some early papers on the four-jet DPS production was missed which together with the usage of the the Gaussian parametrization of the transverse plane distribution function

[2]To our knowledge, the first publication where it was *explicitly* stated that production of two indistinguishable final state partons in di-jet production processes $a_1b_1 \to A$ and $a_2b_2 \to B$ requires an additional symmetry factor was the paper of Treleani and Strikman [213]. The detailed derivation and a generalization for multiple hard scattering was given in papers of Diehl *et al.* [192], [193]. Earlier theoretical publications on DPS were motivating the presence of the factor 1/2 due to the Gaussian parametrization $F(\boldsymbol{b})$ which gives an incorrect expression for σ_{eff} as in Eq. 4.18.

$F(\boldsymbol{b})$ in Eq. 4.15 and interpretation of the σ_{eff} as a transverse area of proton could lead to the wrong estimate $\sigma_{eff} = \pi R^2$ instead of the correct $\sigma_{eff} = 2\pi R^2$.

In Chapter 3 and this section we have provided all necessary ingredients for the simulations of the four-jet DPS production. In the rest of this chapter we present our results on four-jet DPS production in pp collisions.

4.3 DPS-sensitive variables

It was noticed a long time ago that DPS and SPS events tend to occupy different regions of a four-jet phase space [119]. For example, this can be seen from the asymptotic behaviour of the LO $2 \to 2$ cross sections in Eq. 4.1 and Eq. 4.4. The LO $2 \to 2$ QCD processes at the low values of $p_\perp$ are dominated by the $\hat{t}$-channel gluon exchange which behaves like $1/\hat{t}^2 \sim 1/p_\perp^4$, see [263]. Therefore, at low $p_\perp$ values the LO DPS cross section will approximately behave like $\sim 1/p_\perp^8$. This behaviour leads to infra-red divergences for soft particle production in MPI models and has to be regularized according to a certain regularization scheme[3]. For example, one can impose a sharp cutoff on $p_\perp$ approximately at $\Lambda_{QCD} \approx 1 - 2$ GeV. This regularization is unavoidable for the MPI modelling where transverse momentum of produced partons is typically low. However, if we consider a four-jet DPS production of four *hard* jets, this infra-red divergence will be naturally regularized by corresponding cuts on transverse momenta of produced jets. Nevertheless, as we will see, the scaling behaviour $\sim 1/p_\perp^8$ will lead to the significant enhancement of a DPS cross section even for jets with relatively large values of the transverse momenta ($p_\perp \approx 20 - 35$ GeV). Moreover, the usage of the LO $2 \to 2$ matrix elements for the event generation automatically implies that the di-jets produced in a given DPS event will be well balanced in transverse momentum and well separated in rapidity, see Fig. 4.1. All these features of four-jet DPS events allow to introduce a set of so called *DPS-sensitive variables* one can use to discriminate between DPS and SPS events as it was first proposed in [119]. In Appendix E we list some of these variables used in different experimental analysis of four-jet production.

We will start our analysis of the four-jet DPS production in a relatively simple setup, without parton shower effects. In this case the di-jets generated according to Eq. 4.1 and Eq. 4.4 will be *exactly* balanced in transverse momentum drastically reducing the number of DPS-sensitive variables. Nevertheless, we will show that even without taking the parton shower effects into account one can draw important conclusions on behaviour of DPS differential distributions. At this stage we consider the DPS distributions in terms of a leading jet $p_\perp$ and a maximal rapidity separation $\Delta Y \equiv \max|y_i - y_j|$ of produced jets. Adding the ISR and FSR effects will, obviously, introduce some distortion to our parton level simulations. On the other hand, incorporation of ISR and FSR effects in the simulations will allow us to include additional DPS-sensitive variables into the analysis and make the simulations more realistic. In sections 4.9 - 4.11 we will demonstrate how DPS events produced with our own DPS code can be fed to the `Pythia` 8 event generator and show the impact of initial and final state radiation on the parton level simulations. Additionally, we will discuss some open problems and perspectives of modelling of the ISR in DPS processes.

[3] For the details see [263].

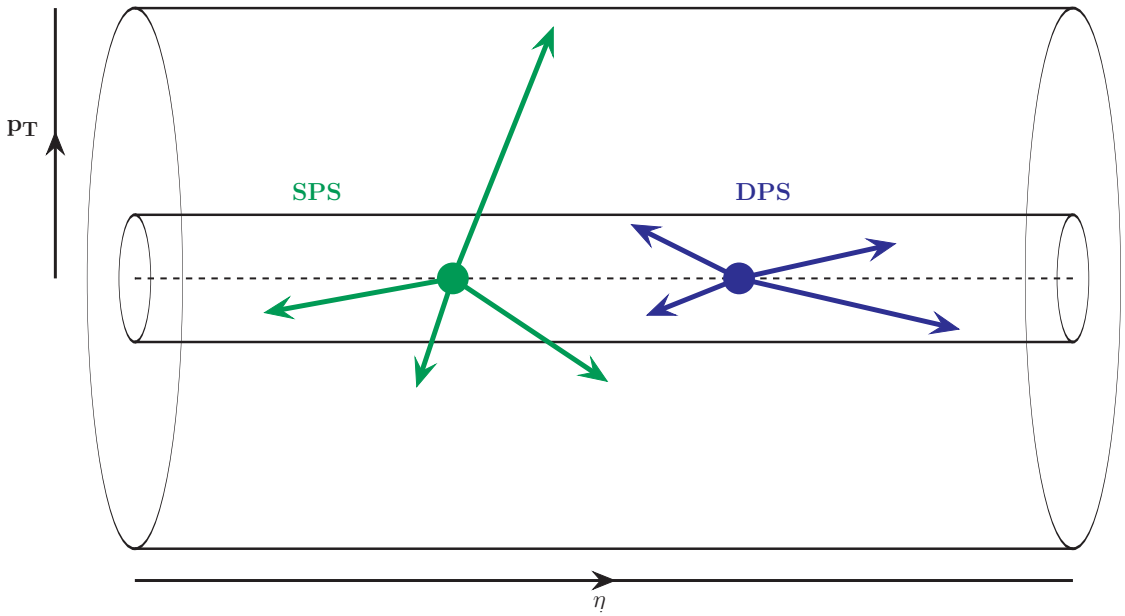

Figure 4.1: Schematic picture of the SPS and DPS events in the rapidity-transverse momentum coordinates.

4.4 Contributions to a four-jet DPS production

The LO QCD $2 \to 2$ partonic cross sections used in our simulations are listed in Appendix D. For N_f different flavours the generation of di-jet events with the LO QCD $2 \to 2$ partonic cross sections in Appendix D involves

$$\begin{aligned} N_{\mathrm{di-jet}} &= 1 + 2N_f + 2N_f(2N_f - 1) + N_f + N_f + 2N_f + N_f + N_f(N_f - 1) = \\ &= 5N_f^2 + 4N_f + 1 \end{aligned} \tag{4.24}$$

different $2 \to 2$ processes. Therefore, for $N_f = 4$ we have $N_{\mathrm{di-jet}} = 97$. It implies that the for four-jet DPS production we have $N_{4\mathrm{j}}^{\mathrm{DPS}} = \left(N_{\mathrm{di-jet}}^2 - N_{\mathrm{di-jet}}\right)/2 = 4656$ different DPS processes. As described in section 4.2, our code uses VEGAS algorithm to scan the DPS phase-space to find the maximal DPS weight and to evaluate the corresponding DPS cross section. Therefore, a complete four-jet DPS simulations requires evaluation of 4656 integrals according to Eq. 4.1 or Eq. 4.4 which is a time consuming procedure. However, not all of these DPS processes will contribute to the four-jet DPS production at the same rate. In order to illustrate it we draw 8×8 "chess like" colour plot where colour of each square corresponds to the contribution to the four-jet DPS production of all allowed flavour combinations for a given combination of two LO QCD $2 \to 2$ partonic cross sections. For example, the second square on the diagonal in Fig. 4.2 corresponds to the DPS contribution

$$\sum_i \left(q_i\, g \to q_i\, g\right) \otimes \left(q_i\, g \to q_i\, g\right), \tag{4.25}$$

where i runs over all flavours under consideration. It is known that the complete four-jet SPS production process $pp \xrightarrow{\mathrm{SPS}} 4j$ can be well approximated by production of two jets and two gluons as $pp \xrightarrow{\mathrm{SPS}} 2j + 2g$. For example, this approximation to the four-jet SPS production is used in the

ALPGEN event generator [253]. By comparing contributions of different squares to the four-jet DPS cross section in Fig. 4.2 we see that it is reasonable to approximate the four-jet DPS production $pp \xrightarrow{\text{DPS}} 4j$ by $pp \xrightarrow{\text{DPS}} 2j + 2g$, where $j = g, d, u, c, s, \bar{d}, \bar{u}, \bar{c}, \bar{s}$. Similar, though not exactly the same approximation of four-jet DPS production was used in [232].

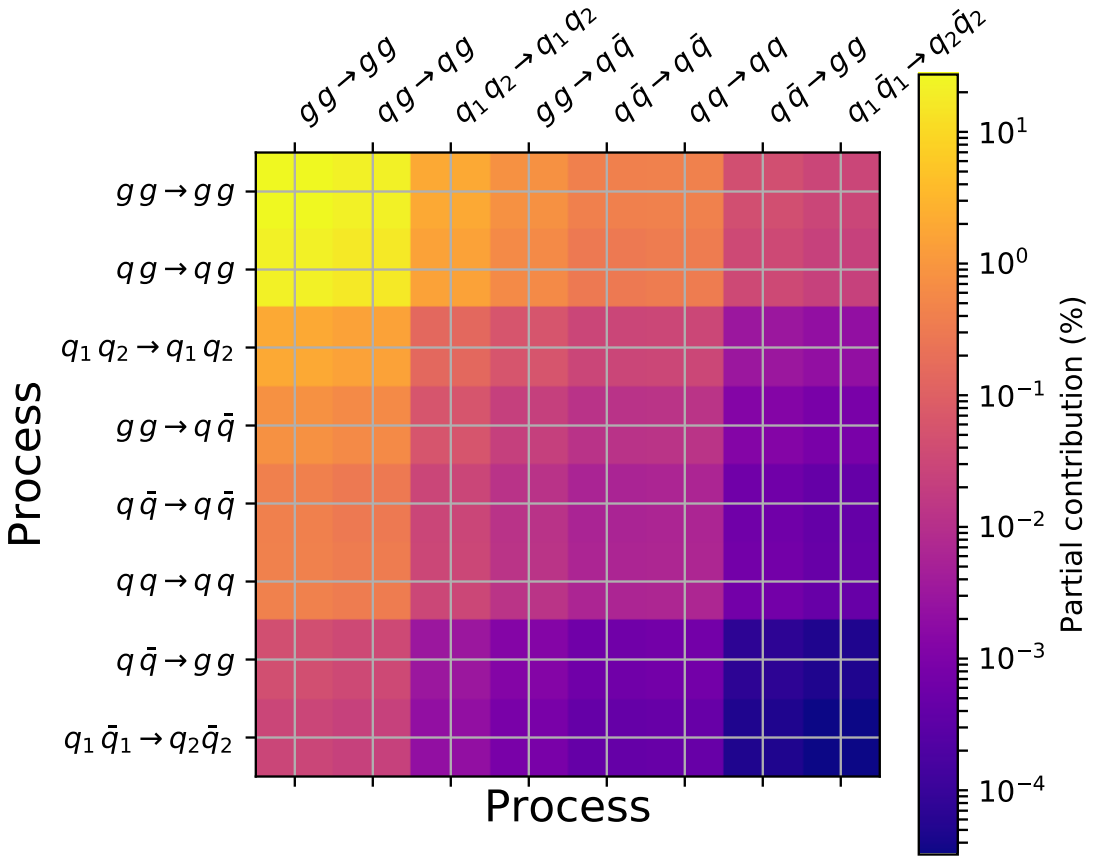

Figure 4.2: Partial contributions of different combinations of LO QCD $2 \to 2$ processes to the total DPS cross section evaluated for $\sqrt{S} = 7$ TeV, $p_{\perp}^{jet} \in [35, 100]$ GeV, $y^{jet} \in [-4.7, 4.7]$. Here we have used "naive" dPDFs constructed out of MSTW2008 LO PDFs. Factorization and renormalization scales are equal to $Q_1 = p_{1\perp}$, $Q_2 = p_{2\perp}$, where $p_{1\perp}$ and $p_{2\perp}$ are equal to the absolute values of the jet transverse momentum in the first and the second hard processes correspondingly.

In Table 4.1 we present our computation of the total DPS cross section for $pp \xrightarrow{\text{DPS}} 2j + 2g$ and $pp \xrightarrow{\text{DPS}} 4j$ processes for four different sets of cuts from [234]. As we can see, about 95% of the total four-jet DPS cross section is contained in the DPS cross section for $pp \xrightarrow{\text{DPS}} 2j + 2g$ process which is also in agreement with approximation from [232]. Nevertheless, one has to consider this approximation carefully while working with differential distributions of DPS events. Obviously, one expects that distributions obtained for $pp \xrightarrow{\text{DPS}} 4j$ process will show more activity then the distribution obtained for $pp \xrightarrow{\text{DPS}} 2j+2g$ process. However, it does not mean that one will get exactly the same increase for all regions of the DPS phase space. In Fig. 4.3 we present our simulations for $pp \xrightarrow{\text{DPS}} 4j$ and for $pp \xrightarrow{\text{DPS}} 2j + 2g$ processes. We see that in some regions of the DPS phase space the difference between distributions obtained for all possible DPS four-jet production processes and the distributions obtained only for DPS processes contributing to production of two jets and two gluons may reach $\sim 30\%$ level. The biggest disagreement occurs for events produced at high

values of $\Delta Y = \max|y_i - y_j|$, see the lower panel in Fig. 4.3. Since, according to Eq. 3.4 and Eq. 3.5, a sum of rapidities in a given di-jet event is equal to $y_1 + y_2 = \log(x_1/x_2)$, a high value of $\Delta Y = \max|y_i - y_j|$ will correspond to two di-jet events each initiated by one low-x and one high-x parton. It means that the contribution from the quark production processes which we discarded by replacing four-jet DPS production $pp \xrightarrow{\text{DPS}} 4j$ by $pp \xrightarrow{\text{DPS}} 2j+2g$ becomes more and more important as we move towards the high-ΔY region. Moreover, as we will show later in this thesis, the tail of the ΔY distribution demonstrates a strong dependence on different models of dPDFs and, as a consequence, on different models of longitudinal partonic correlations. Therefore, in our simulations we will use a complete set of four-jet DPS production processes to make sure that the correlation effects are not affected by approximation $pp \xrightarrow{\text{DPS}} 4j \approx 2j + 2g$.

Cuts and collision energy	σ_{DPS} for $pp \xrightarrow{\text{DPS}} 2j+2g$ process	σ_{DPS} for $pp \xrightarrow{\text{DPS}} 4j$ process	$\sigma^{4j}_{\text{DPS}}/\sigma^{2j2g}_{\text{DPS}}$
$\sqrt{S} = 7$ TeV, $\lvert y\rvert < 4.7$, $p_\perp \in [35, 100]$ GeV	42.45	45.45	1.07
$\sqrt{S} = 7$ TeV, $\lvert y\rvert < 4.7$, $p_\perp \in [20, 100]$ GeV	3726.48	3912.27	1.05
$\sqrt{S} = 13$ TeV, $\lvert y\rvert < 4.7$, $p_\perp \in [35, 100]$ GeV	330.53	347.13	1.05
$\sqrt{S} = 13$ TeV, $\lvert y\rvert < 4.7$, $p_\perp \in [20, 100]$ GeV	22109.18	22898.68	1.04

Table 4.1: Comparison between DPS cross sections evaluated for $pp \xrightarrow{\text{DPS}} 2j + 2g$ and $pp \xrightarrow{\text{DPS}} 4j$ processes. All cross sections are given in nb. Same dPDFs and scale choices as we used to produce Fig. 4.2.

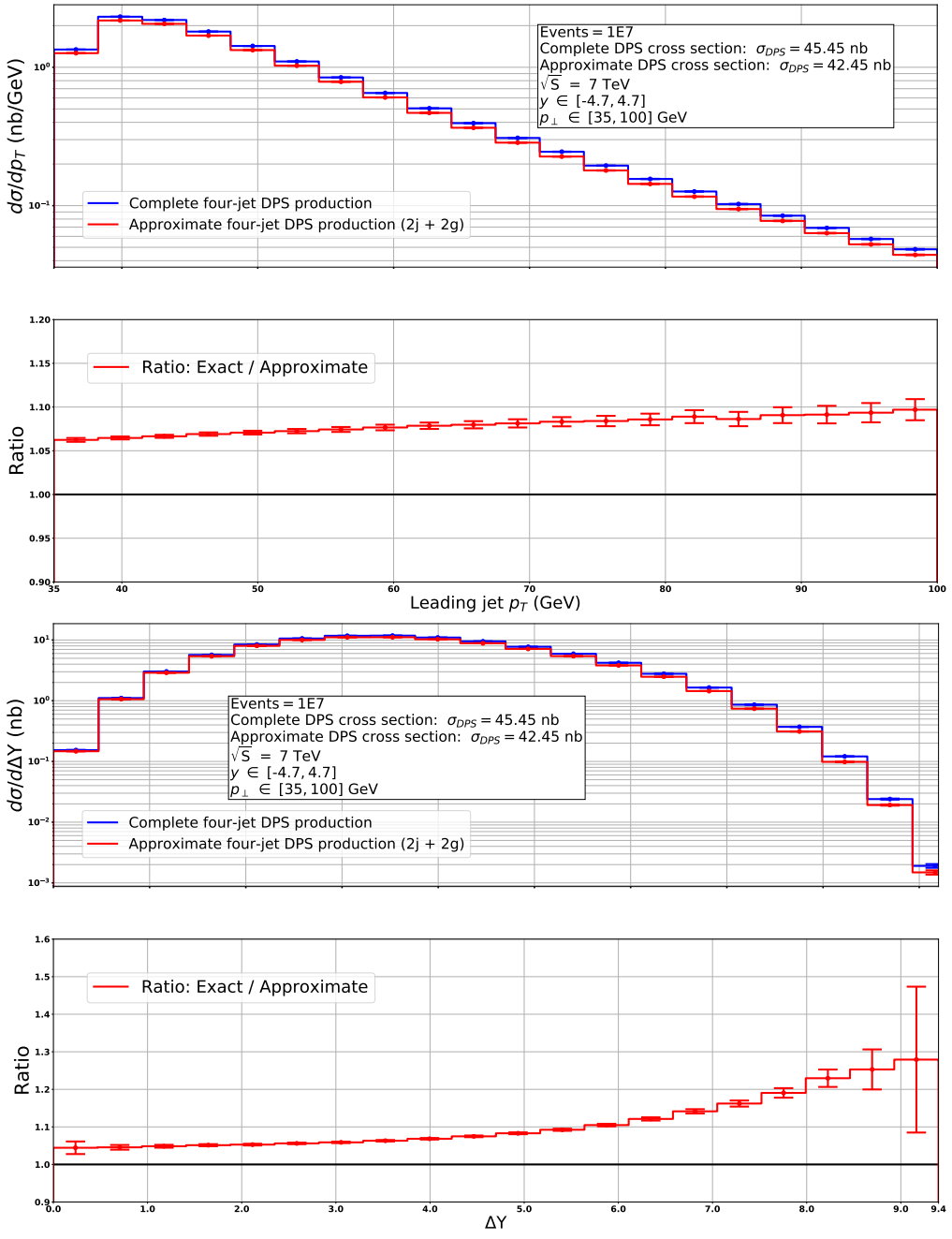

Figure 4.3: Upper panel: leading jet $p_\perp$ distributions simulated for $pp \xrightarrow{\text{DPS}} 4j$ and for $pp \xrightarrow{\text{DPS}} 2j{+}2g$ processes. Lower panel: $\Delta\text{Y} = \max|y_i - y_j|$ distributions simulated for $pp \xrightarrow{\text{DPS}} 4j$ and for $pp \xrightarrow{\text{DPS}} 2j + 2g$ processes. Here we have used "naive" dPDFs constructed out of MSTW2008 LO PDFs. Factorization and renormalization scales are equal to $Q_1 = p_{1\perp}$, $Q_2 = p_{2\perp}$, where $p_{1\perp}$ and $p_{2\perp}$ are equal to the absolute values of the jet transverse momentum in the first and the second hard processes correspondingly. Statistical errors are given by $\sigma_{\text{DPS}}\sqrt{N_{\text{bin}}}/N_{\text{tot}}$ where N_{bin} is a number of events in a given bin, σ_{DPS} is a corresponding DPS cross section and N_{tot} is total number of bin entries for a given histogram.

4.5 Scale dependence of the DPS cross section

Another important issue we have to discuss before presenting our simulation of the four-jet DPS production is the choice of the scales Q_1, Q_2 for the di-jet production processes[4]. In practice, for the DPS processes one selects the same values of Q_1, Q_2 as for the SPS processes. However, to the best of our knowledge, there are no studies which could decisively favor a particular scale choice for a particular DPS process. In our DPS studies we will compare our simulations against simulations made with the MadGraph 5 [254] and the `Pythia` 8 [256] event generators and thus we stick to the scale choices implemented into these two programs. Among the MadGraph options we will use either a sum of the transverse masses $Q = \sum_{i=1}^{2} \sqrt{m_i^2 + p_{\perp,i}^2}$ or the sum of the transverse masses divided by two. Among the `Pythia` options we will use either the geometric or the the arithmetic mean of the squared transverse masses of the two outgoing particles: $Q = \sqrt{(m_1^2 + p_{\perp,1}^2)(m_2^2 + p_{\perp,2}^2)}$ and $Q = \frac{1}{2}\sqrt{(m_1^2 + p_{\perp,1}^2)} + \frac{1}{2}\sqrt{(m_2^2 + p_{\perp,2}^2)}$. For the production of massless particles all the aforementioned scale choices reduce either to a transverse momentum of a jet $Q = p_\perp$ or to its doubled value $Q = 2p_\perp$, where $p_\perp$ is the absolute value of the transverse momentum of a jet in a di-jet event. In Table 4.5 we show how the total DPS cross sections depends on different scale choices. In addition to $Q = p_\perp$ and $Q = 2p_\perp$ options we add the partonic energy $Q = \sqrt{\hat{s}}$ option for illustrative purposes[5].

Cuts and collision energy	$Q_{1,2}^2 = p_{1,2\perp}^2$	$Q_{1,2}^2 = 4p_{1,2\perp}^2$	$Q_{1,2}^2 = \hat{s}_{1,2}$
$\sqrt{S} = 7$ TeV, $\lvert y\rvert < 4.7$, $p_\perp \in [35, 100]$ GeV	44.80	27.59	20.93
$\sqrt{S} = 7$ TeV, $\lvert y\rvert < 4.7$, $p_\perp \in [20, 100]$ GeV	3869.74	2529.62	1908.45
$\sqrt{S} = 13$ TeV, $\lvert y\rvert < 4.7$, $p_\perp \in [35, 100]$ GeV	343.47	229.751	177.173
$\sqrt{S} = 13$ TeV, $\lvert y\rvert < 4.7$, $p_\perp \in [20, 100]$ GeV	22729.2	16309.1	12696

Table 4.2: Dependence of the total DPS cross section for $pp \xrightarrow{\text{DPS}} 4j$ on different scale choices. All cross sections are given in nb. Here we have used "naive" dPDFs constructed out of MSTW2008 LO PDFs.

We see that the value of a total DPS cross section demonstrates a high sensitivity to the scale choice. The computation of the DPS cross section at the *next-to-leading order* (NLO) accuracy level could improve the situation and reduce the scale dependence. Unfortunately, a computation of the DPS processes at NLO accuracy level is a highly non-trivial task. Recently, the $1 \to 2$ splitting functions required for the NLO DPS computations were calculated for the first time [210]. However, the complete NLO DPS computations are yet to be done and hence the LO DPS computations still remain the only available option for the DPS modelling[6]. Nevertheless, as we will see later in

[4] In our simulations we always set renormalization and factorization scales to the same value.

[5] The $Q = \sqrt{\hat{s}}$ option is typically used for processes dominated by the $\hat{s}$-channel exchange. Since, as we have argued in Chapter 4.3, the LO QCD $2 \to 2$ processes at low $p_\perp$ are dominated by the $\hat{t}$-channel exchange we will not use this option in our simulations.

[6] In section 4.11 we discuss how one can improve LO DPS simulations by adding PS effects.

this thesis, the LO DPS computations still allow to make important conclusions, in particular, to identify the configurations of jets sensitive to partonic correlations in longitudinal momentum and flavour.

4.6 Impact of GS09 dPDFs

In Chapter 2.2 we have described the system of dDGLAP evolution equations and properties of its solutions called double parton distribution functions $D_{a_1,a_2}(x_1, x_2, Q_1^2, Q_2^2)$. These objects carry information about partonic correlations in x-space, which implies $D_{a_1,a_2}(x_1, x_2, Q_1^2, Q_2^2) \neq f_{a_1}(x_1, Q_1^2)\, f_{a_2}(x_2, Q_2^2)$, and approximately account for momentum and number conservation set by GS sum rules, Eq. 2.17 - 2.20. In our analysis we will use DPS distributions generated according to Eq. 4.4 as a baseline for the comparison against DPS distributions generated according to Eq. 4.1. In order to generate DPS events according to Eq. 4.1 we use GS09 set with 300 grid points. For the generation of events according to Eq. 4.4 we use central values of MSWT2009 LO PDF set. In our analysis we consider four different quark flavours: d, u, s and c which are treated as massless particles. We evaluate factorization scale for the first and the second hard interactions in a given DPS process according to $Q = \frac{1}{2}\sqrt{(m_1^2 + p_{\perp,1}^2)} + \frac{1}{2}\sqrt{(m_2^2 + p_{\perp,2}^2)}$. Since we consider LO production of massless particles this expression reduces to $Q = p_{\perp,i}$ where $p_{\perp,i}$ is an absolute value of a transverse momentum of a jet in a di-jet event.

Our results are given in Fig. 4.4 - Fig. 4.7. We see that the leading jet $p_\perp$ distributions for the DPS events generated with GS09 dPDFs differ by about 10% from the distributions of DPS events generated with "naive" dPDFs. The situation changes for the distributions in terms of $\Delta Y = \max|y_i - y_j|$ where the difference between both approaches may reach about 80% level at high values of ΔY, see Fig. 4.4.

Let us consider the ΔY DPS distributions in more details. The distributions in Fig. 4.4 - Fig. 4.7 were simulated for two different sets of $p_\perp$ cuts ($p_\perp \in [35, 100]$ GeV and $p_\perp \in [20, 100]$) and for two different collision energies ($\sqrt{S} = 7$ TeV and $\sqrt{S} = 13$ TeV). We see that if we change $p_\perp$ cuts from $p_\perp \in [35, 100]$ GeV to $p_\perp \in [20, 100]$ GeV while keeping the value of $\sqrt{S}$ fixed then we decrease the difference between the ΔY DPS distributions generated with "naive" and GS09 dPDFs. Namely, we see that the ratio between DPS distributions generated with "naive" and GS09 dPDFs at high values of ΔY stays closer to unity if we require $p_\perp \in [20, 100]$ GeV, compare the ΔY distribution in Fig. 4.4 with the ΔY distribution in Fig. 4.5 and the ΔY distribution in Fig. 4.6 with the ΔY distribution in Fig. 4.7. We also observe the same behaviour of the ratio between the ΔY DPS distributions generated with "naive" and GS09 dPDFs if we decrease the value of the collision energy while keeping $p_\perp$-cuts fixed, compare the ΔY distribution in Fig. 4.4 with the ΔY distribution in Fig. 4.6 and the ΔY distribution in Fig. 4.5 with the ΔY distribution in Fig. 4.7.

As we have argued in section 4.4, the DPS event with high value of ΔY consists of two di-jet production processes each involving one low-x and one high-x parton. However, at high values of x the impact of the valence quark distributions becomes important. The GS sum rules given by Eq. 2.18 - 2.20 preserve the conservation of the number of the valence quarks and therefore impose correlations in flavour which should manifest themselves at high values of x. Since "naive" dPDFs do not obey Eq. 2.18 - 2.20 we expect flavour correlations to contribute to the difference between ΔY DPS distributions generated with "naive" and GS09 dPDFs at high values of ΔY. The presence of

flavour correlations at high values of x can explain the observed behaviour of the difference between ΔY DPS distributions generated with "naive" and GS09 dPDFs at high values of ΔY. Namely, the connection between Bjorken variables, rapidities, collision energy and transverse momentum in a given di-jet event is given by Eq. 3.4 - 3.5. We see that the value of x is proportional to the ratio $2p_\perp/\sqrt{S}$. Therefore, for the fixed rapidities one can decrease the value of x either by increasing the value of the collision energy $\sqrt{S}$ or by decreasing the absolute value of the transverse momentum $p_\perp$. It means that by choosing lower value of the minimal $p_\perp$-cut or by increasing the collision energy we decrease values of Bjorken variables for a given di-jet event and hence move out of the valence region which should decrease the role of the flavour correlations and reduce the discrepancy between ΔY distributions generated with "naive" and GS09 dPDFs.

However, we shall stress that there are two possible contributions to the observed difference between ΔY distributions generated with "naive" and GS09 dPDFs. Namely, the effects due to the correlations induced by the GS sum rules Eq. 2.17 - 2.20 and the effects due to the dDGLAP evolution. Since "naive" dPDFs neither obey GS sum rules nor satisfy dDGLAP evolution equation both types of effects can contribute to the difference between the DPS distributions generated with "naive" and GS09 dPDFs. The comparison between DPS distributions generated with "naive" and GS09 dPDFs only does not allow to separate effects due to the dDGLAP evolution and due to the flavour correlations induced by GS sum rules. However, apart from GS09 and "naive" models of dPDFs there is another commonly used approach to model dPDFs, implemented in the `Pythia` event generator. This model does not account for dDGLAP evolution effects but accounts for momentum and number conservation of partons and, partially, for "1v2" effects, as described in [260]. In Chapter 6 of this thesis we will provide a detailed comparison between the GS09 and the `Pythia` approaches to model dPDFs, perform a phenomenological study of the four-jet DPS production similar to the one performed in this section and discuss the role of the flavour correlations.

Before closing this section several important comments have to be made. First of all, as it was discussed in Chapter 2.5, a realistic DPS process would include various splitting DPS contributions, see Fig. 2.7. Due to the splitting term on the RHS of the dDGLAP evolution equations, Eq. 2.13, the DPS simulations with GS09 dPDFs effectively include "1v2" and "1v1" splitting contributions schematically shown in Fig. 2.7 b) and c). However, as it was shown in [193], [194] the way "1v2" and "1v1" DPS contributions are modelled by inhomogeneous dDGLAP evolution equations, Eq. 2.13, is not consistent with the field-theoretical formulation of DPS. The consistent framework to model "1v2" and "1v1" contributions without double counting between DPS and SPS and without UV-divergences at small values of the transverse separation parameter $\boldsymbol{b}$ [193], [194] was proposed by Diehl, Gaunt and Schönwald in [200] (DGS approach). However, a detailed phenomenological analysis of the four-jet DPS production within the DGS framework is yet to be done. The study of the double parton luminosities performed in [200] suggests that "1v2" and "1v1" contributions are suppressed at large values of rapidity separation for $\mathcal{L}_{u\bar{u}u\bar{u}}$ DPS luminosity and enhanced for $\mathcal{L}_{gggg}$ as it is shown in Fig. 2.11. Clearly a more detailed phenomenological study within the DGS framework is needed to find the impact of the "1v1" and "1v2" DPS contributions on four-jet production processes. The comparative study of the four-jet DPS production within both GS09 and DGS approach could, therefore, find the importance of the "1v1" and "1v2" DPS contributions for the phenomenology of the four-jet DPS production processes. We suggest that our computations

can be used as a baseline for such comparisons.

Finally, we also should argue that apart from a correct treatment of "1v2" and "1v1" contributions one should also account for spin and colour partonic correlations in DPS events. In 1988 Mekhfi and Artru [208] demonstrated that such correlations should be Sudakov suppressed. However, in 2011 Diehl and Shäfer shown that colour interference effects become important for valence quarks [192]. Moreover, as it was demonstrated in [187], [159] and [209] the spin correlations may have a serious impact on the DPS distributions especially at large values of Bjorken-x. Therefore, we conclude that the experimental studies of the DPS distributions at large values of ΔY can potentially give access to the various partonic correlations and provide a deeper insight into the dynamics of the proton's constituents.

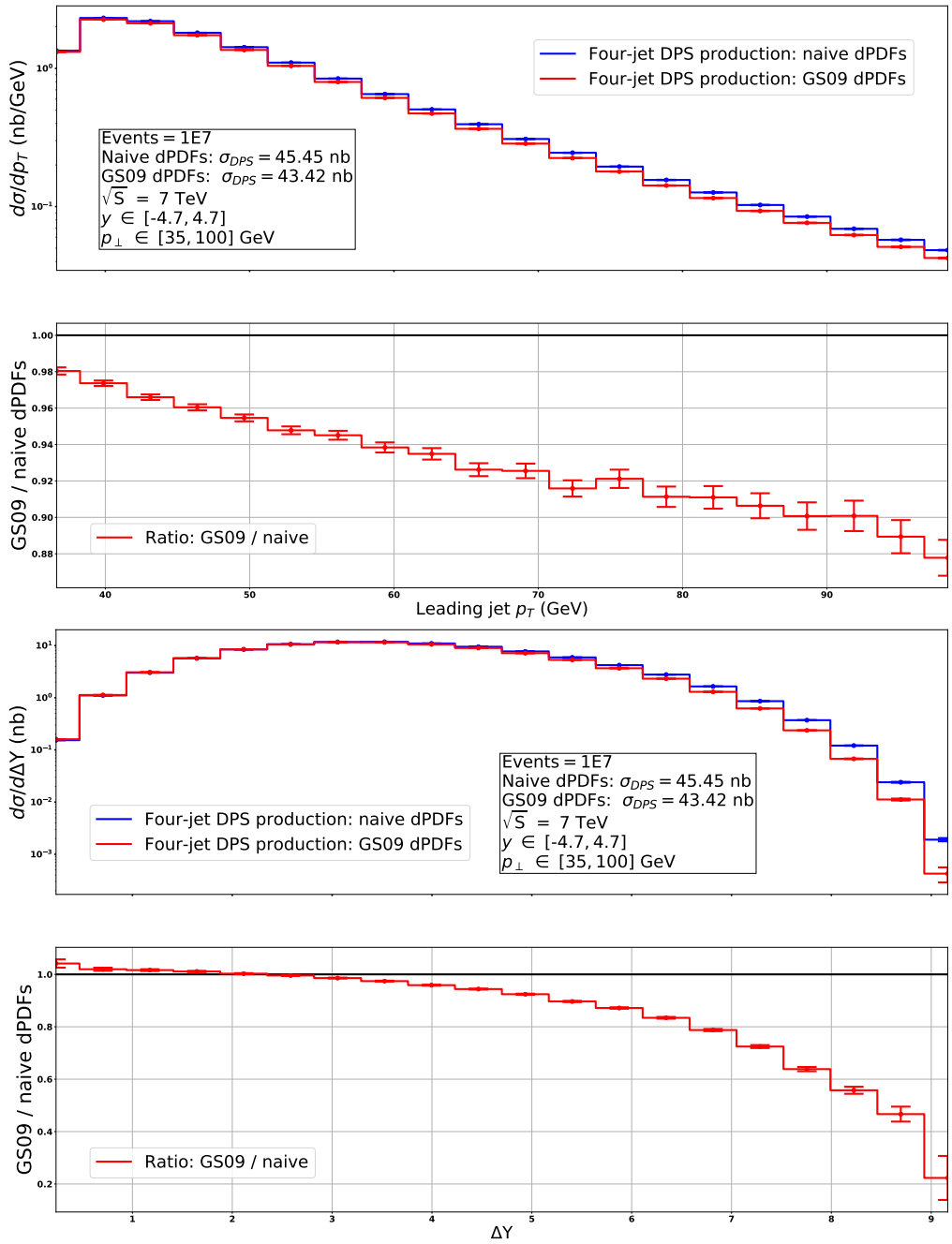

Figure 4.4: Upper panel: comparison between leading jet $p_\perp$ distributions for four-jet DPS events produced with GS09 dPDFs and "naive" dPDFs. Lower panel: comparison between $\Delta Y = \max|y_i - y_j|$ distributions for four-jet DPS events produced with GS09 dPDFs and "naive" dPDFs. Collision energy is equal to $\sqrt{S} = 7\,\text{TeV}$, $p_\perp \in [35, 100]$ GeV, $|y| < 4.7$. Factorization and renormalization scales are equal to $Q_1 = p_{1\perp}$, $Q_2 = p_{2\perp}$, where $p_{1\perp}$ and $p_{2\perp}$ are equal to the absolute value of a jet transverse momentum in a first and second hard processes in a given DPS event. Statistical errors are given by $\sigma_{\text{DPS}}\sqrt{N_{\text{bin}}}/N_{\text{tot}}$ where N_{bin} is a number of events in a given bin, σ_{DPS} is a corresponding DPS cross section and N_{tot} is total number of bin entries for a given histogram.

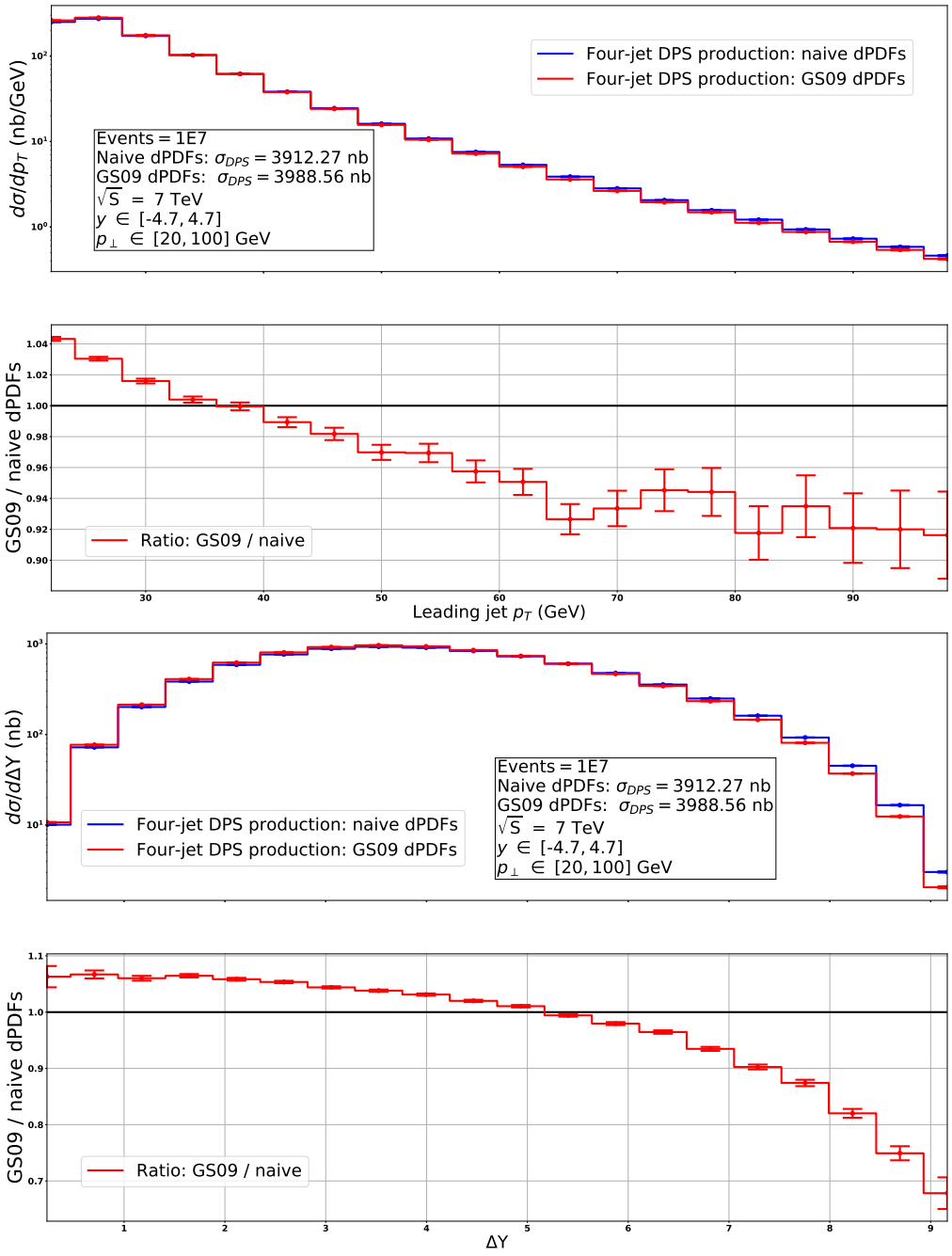

Figure 4.5: Upper panel: comparison between leading jet $p_\perp$ distributions for four-jet DPS events produced with GS09 dPDFs and "naive" dPDFs. Lower panel: comparison between $\Delta Y = \max|y_i - y_j|$ distributions for four-jet DPS events produced with GS09 dPDFs and "naive" dPDFs. Collision energy is equal to $\sqrt{S} = 7\,\text{TeV}$, $p_\perp \in [20, 100]$ GeV, $|y| < 4.7$. Factorization and renormalization scales are equal to $Q_1 = p_{1\perp}$, $Q_2 = p_{2\perp}$, where $p_{1\perp}$ and $p_{2\perp}$ are equal to the absolute value of a jet transverse momentum in a first and second hard processes in a given DPS event. Statistical errors are given by $\sigma_{\text{DPS}}\sqrt{N_{\text{bin}}}/N_{\text{tot}}$ where N_{bin} is a number of events in a given bin, σ_{DPS} is a corresponding DPS cross section and N_{tot} is total number of bin entries for a given histogram.

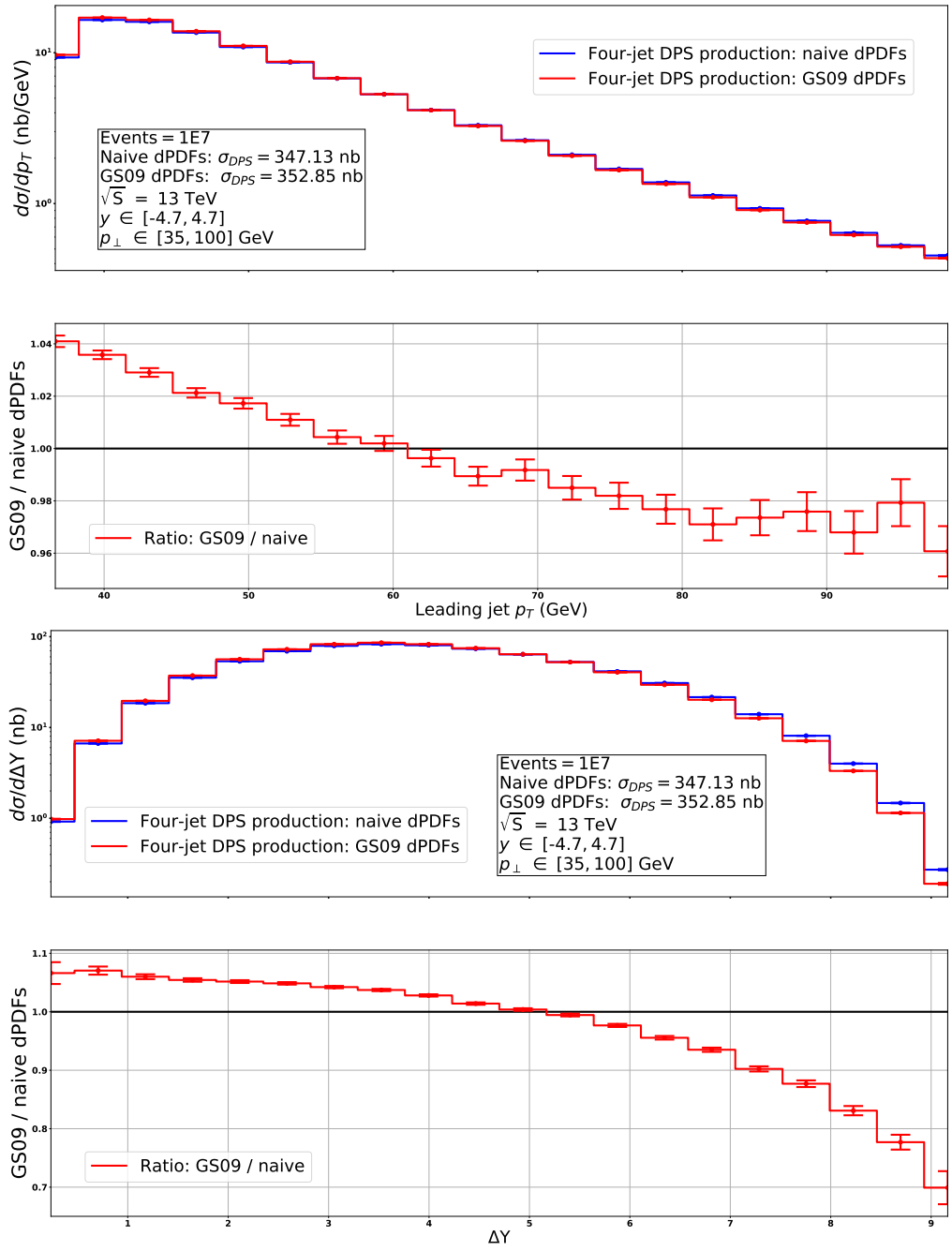

Figure 4.6: Upper panel: comparison between leading jet $p_\perp$ distributions for four-jet DPS events produced with GS09 dPDFs and "naive" dPDFs. Lower panel: comparison between $\Delta Y = \max|y_i - y_j|$ distributions for four-jet DPS events produced with GS09 dPDFs and "naive" dPDFs. Collision energy is equal to $\sqrt{S} = 13\,\text{TeV}$, $p_\perp \in [35, 100]$ GeV, $|y| < 4.7$. Factorization and renormalization scales are equal to $Q_1 = p_{1\perp}$, $Q_2 = p_{2\perp}$, where $p_{1\perp}$ and $p_{2\perp}$ are equal to the absolute value of a jet transverse momentum in a first and second hard processes in a given DPS event. Statistical errors are given by $\sigma_{\text{DPS}}\sqrt{N_{\text{bin}}}/N_{\text{tot}}$ where N_{bin} is a number of events in a given bin, σ_{DPS} is a corresponding DPS cross section and N_{tot} is total number of bin entries for a given histogram.

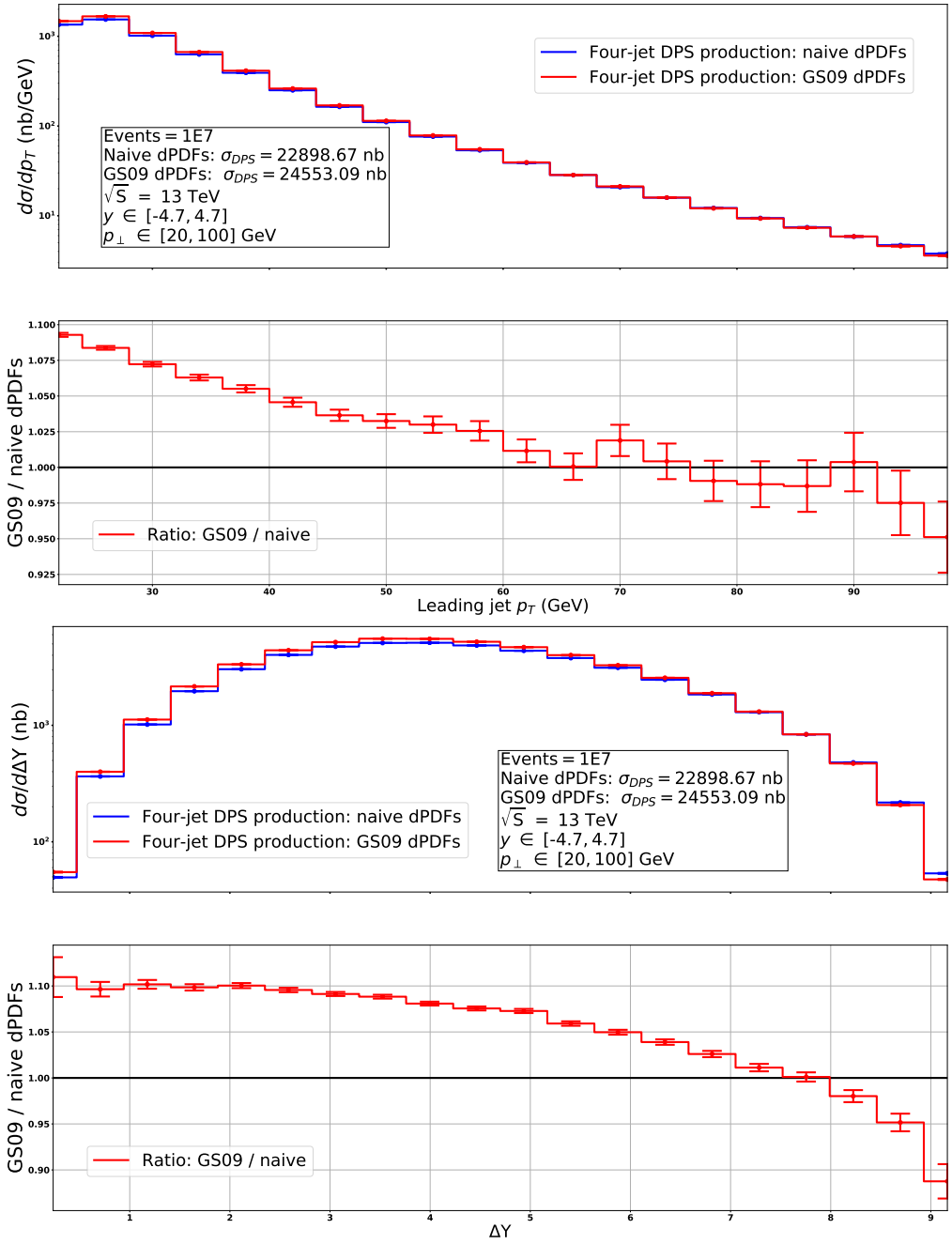

Figure 4.7: Upper panel: comparison between leading jet $p_\perp$ distributions for four-jet DPS events produced with GS09 dPDFs and "naive" dPDFs. Lower panel: comparison between $\Delta Y = \max|y_i - y_j|$ distributions for four-jet DPS events produced with GS09 dPDFs and "naive" dPDFs. Collision energy is equal to $\sqrt{S} = 13\,\text{TeV}$, $p_\perp \in [20, 100]$ GeV, $|y| < 4.7$. Factorization and renormalization scales are equal to $Q_1 = p_{1\perp}$, $Q_2 = p_{2\perp}$, where $p_{1\perp}$ and $p_{2\perp}$ are equal to the absolute value of a jet transverse momentum in a first and second hard processes in a given DPS event. Statistical errors are given by $\sigma_{\text{DPS}}\sqrt{N_{\text{bin}}}/N_{\text{tot}}$ where N_{bin} is a number of events in a given bin, σ_{DPS} is a corresponding DPS cross section and N_{tot} is total number of bin entries for a given histogram.

4.7 Simulation of the SPS background

In this section we discuss the way we simulate production of four-jet SPS events for the comparison against four-jet DPS events generated with our code. Namely, we discuss the generation of four-jet SPS events with the MadGraph [254] and the ALPGEN [253] event generators. Both codes use LO matrix elements to generate events. However, NLO corrections may significantly affect LO results. The total cross section for the four-jet SPS production at NLO accuracy level was at the first time was evaluated by Bern *et al.* [250] in 2011. The study of Bern *et al.* demonstrated that the total four-jet SPS cross section evaluated at NLO accuracy level is about two times smaller than the total four-jet SPS cross section evaluated at LO accuracy level. One year later Badger *et al.* [251] confirmed results of [250] and, in addition to the total four-jet SPS cross section, provided differential distributions. Moreover, Badger *et al.* found that the ratio between differential NLO and LO distributions demonstrates a mild dependence on rapidities and transverse momenta of produced jets[7] and is approximately equal to 0.5, see Fig. 4.8. In practice it is handy to encapsulate the impact of NLO corrections into a so called K-*factor* defined as a ratio of an NLO cross section (NLO distribution) to a LO cross section (LO distribution). Therefore, in the following, in order to account for the NLO effects in our SPS simulations we will multiply our LO SPS distributions by $\mathrm{K}_{\mathrm{NLO}}^{\mathrm{SPS}} = 0.5$. In Fig. 4.9 we compare $p_\perp$-distributions of jets generated with the ALPGEN event generator against the data measured by the CMS collaboration [108]. We see that the LO SPS distributions without $\mathrm{K}_{\mathrm{NLO}}^{\mathrm{SPS}}$, in general, provide to much activity, especially for high $p_\perp$-bins, and that multiplication of the differential distributions by $\mathrm{K}_{\mathrm{NLO}}^{\mathrm{SPS}} = 0.5$ leads to a fairly well description of data[8]. However, as we have argued in section 4.5, in the case of the four-jet DPS production the impact of NLO corrections on LO DPS distributions is unknown due to the absence of NLO DPS computations. Therefore, we do not use K-factors in our DPS simulations.

In the next section we present our study of the interplay between DPS and SPS contributions to the four-jet production. Typically in experimental measurements of the four-jet production one imposes different $p_\perp$ cuts on produced jets. For example, the jet distributions shown in Fig. 4.9 were measured for the following $p_\perp$-cuts: $p_{1,2\perp} > 50$ GeV and $p_{3,4\perp} > 50$ GeV where $p_{i\perp}$ is a transverse momentum of the i'th jet. However, as it was shown by Maciuła and Szczurek in [230], the DPS contribution to the four-jet production is suppressed for this set of $p_\perp$-cuts. In order to increase the strength of the DPS signal Maciuła and Szczurek proposed a new set of cuts where *all four jets* are required to have transverse momenta in the same $p_\perp$ interval. Since the four-jet SPS production typically results in one high-$p_\perp$ jet and three jets with softer transverse momenta these cuts should suppress the SPS contribution to the four-jet production. Contrary to the SPS case the DPS contribution to the four-jet production gives two di-jet pairs with approximately the same values of transverse momenta, see Fig. 4.1. Therefore, we will simulate the four-jet production for two combinations of $p_\perp$-cuts ($p_\perp \in [35, 100]$ GeV and $p_\perp \in [20, 100]$ GeV) and two different collision energies ($\sqrt{S} = 7$ TeV and $\sqrt{S} = 13$ TeV) as listed in Table 4.3.

Finally, before closing this section, we shall note that in the ALPGEN event generator the four-jet SPS production $pp \xrightarrow{\mathrm{SPS}} 4j$ is approximated by production of two jets and two gluons

[7] We shall note that differential distributions in [251] were simulated without parton shower effects. To combine NLO matrix elements with parton shower generators is a non-trivial task and, to the best of our knowledge, current state-of-the-art is a three-jet production at NLO combined with parton shower generators, see [252].

[8] The same value of $\mathrm{K}_{\mathrm{NLO}}^{\mathrm{SPS}}$ was used in the study of Maciuła and Szczurek [230].

as $pp \xrightarrow{\text{SPS}} 2j + 2g$. In order to estimate the error due to this approximation in Fig. 4.10 we compare distributions of events for $pp \xrightarrow{\text{SPS}} 4j$ and $pp \xrightarrow{\text{SPS}} 2j + 2g$ processes[9]. We see that the difference between total cross sections for the complete SPS four-jet production $\sigma^{4j}_{\text{SPS}} = 137.74$ and the approximate one $\sigma^{2j+2g}_{\text{SPS}} = 130.92$ is about 5%. We also shall note that the leading jet $p_\perp$ and ΔY distributions generated according to $pp \xrightarrow{\text{SPS}} 2j + 2g$ and $pp \xrightarrow{\text{SPS}} 4j$ processes differ by rather a constant quantity for the whole range of binning, see Fig. 4.10. This behaviour of the SPS distributions differs from the behaviour of corresponding DPS distributions where the difference between leading jet $p_\perp$ distributions generated according to $pp \xrightarrow{\text{DPS}} 2j + 2g$ and $pp \xrightarrow{\text{DPS}} 4j$ processes may reach 10% level and the difference between ΔY distributions generated according to $pp \xrightarrow{\text{DPS}} 2j + 2g$ and $pp \xrightarrow{\text{DPS}} 4j$ processes may reach 30% level, see Fig. 4.3. In order to be consistent with our four-jet DPS simulations, in the following we will simulate the four-jet SPS production for the complete four-jet final state.

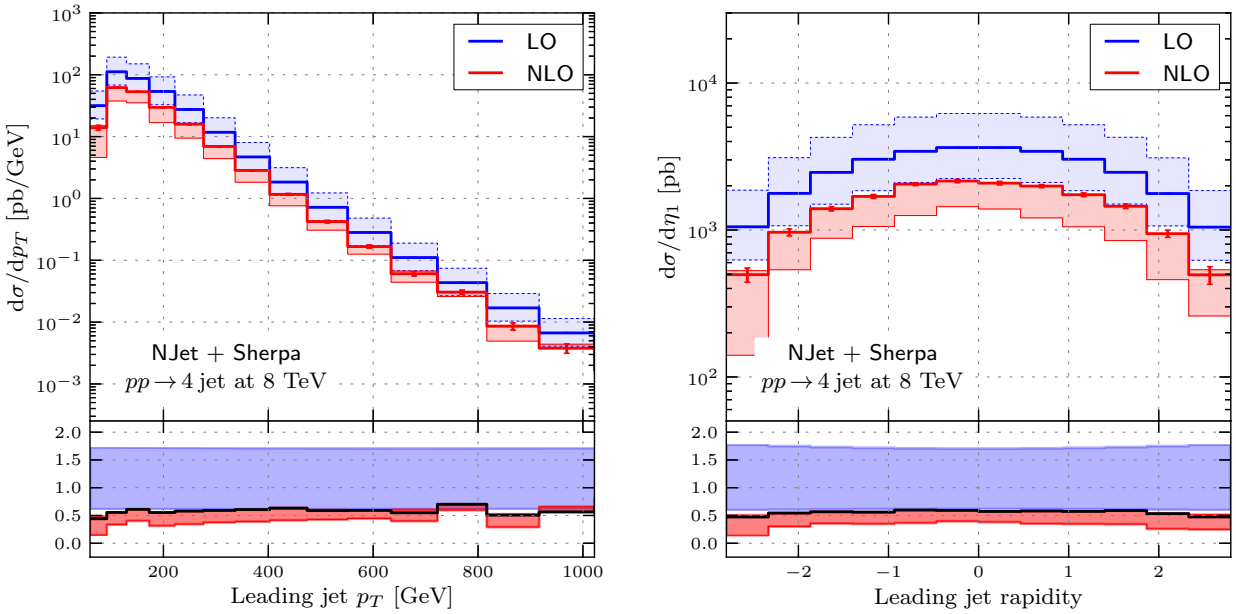

Figure 4.8: Comparison between LO and NLO four-jet SPS distributions. Fixed order in perturbation theory. Left panel: leading jet $p_\perp$ distribution. Right panel: leading jet rapidity distributions. The plot is taken from [251].

[9]Since with ALPGEN one can generate four-jet events only according to the approximate process $pp \xrightarrow{\text{SPS}} 2j + 2g$ we use MadGraph event generator to generate SPS events according to $pp \xrightarrow{\text{SPS}} 4j$ and $pp \xrightarrow{\text{SPS}} 2j + 2g$ processes.

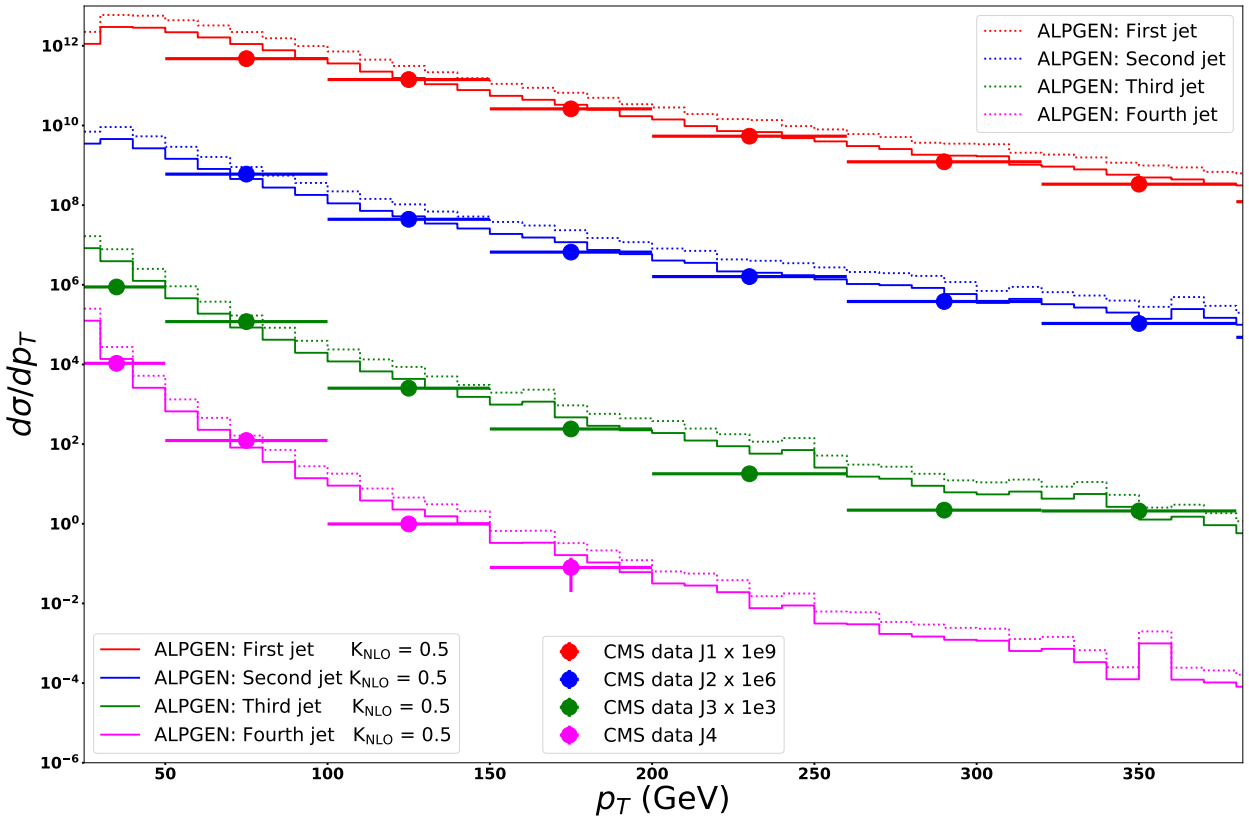

Figure 4.9: Comparison between ALPGEN and the CMS data [108] measured at $\sqrt{S} = 7$ TeV for the following cuts: $p_{1,2\perp} > 50$ GeV, $p_{3,4\perp} > 20$ and $|y| < 4.7$. In the ALPGEN simulations the factorization and renormalization scales are set to the average transverse momenta of the final state produced jets (`iqopt` = 2), the minimal value of the transverse momentum of a jet (`ptjmin`) is 20 GeV, the minimal distance between jets (`rjmin`) is set to 0.5. The collision energy $\sqrt{S} = 7$ TeV. The CTEQ6L1 PDF set [109].

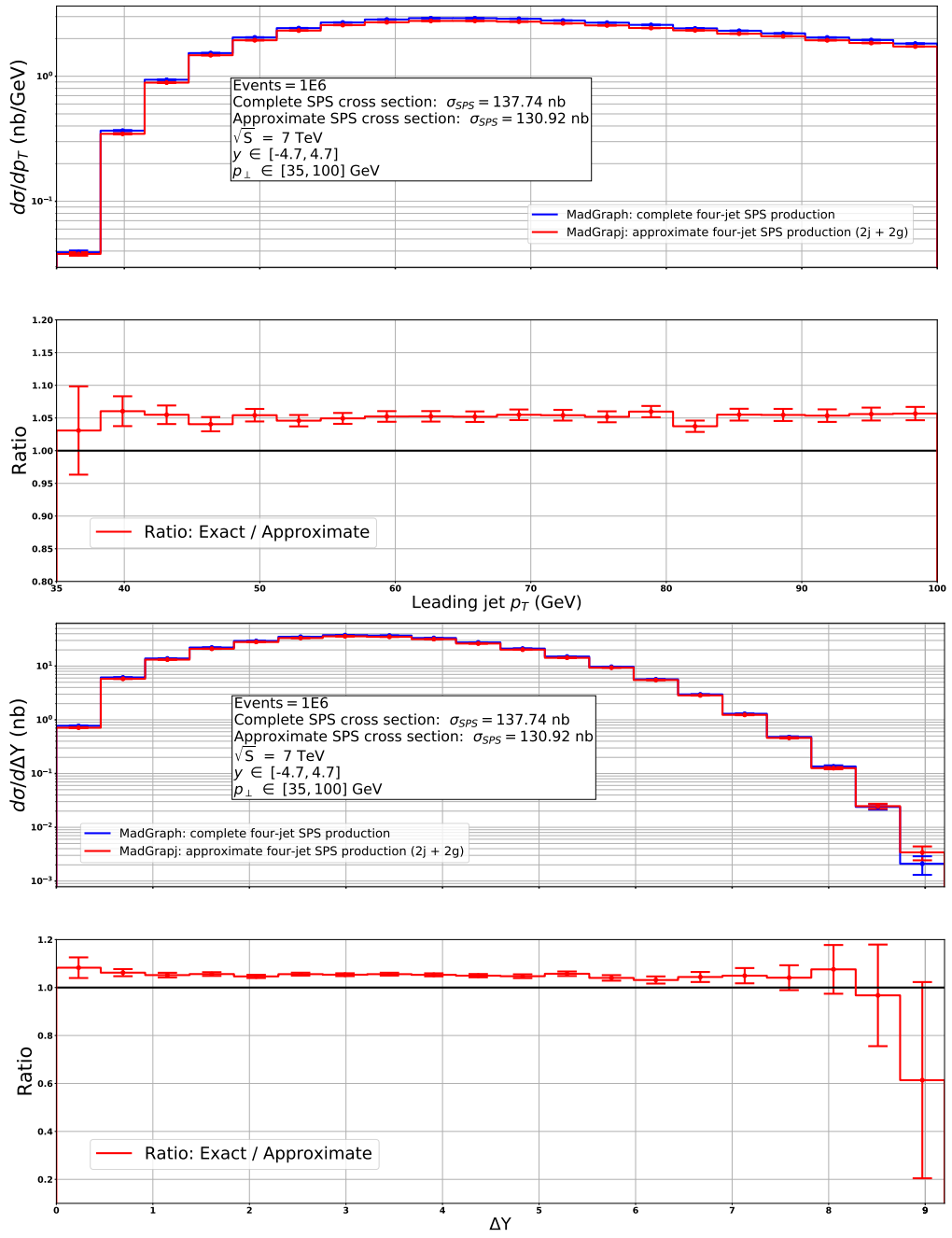

Figure 4.10: Comparison between distributions for the $pp \xrightarrow{\text{SPS}} 2j + 2g$, $pp \xrightarrow{\text{SPS}} 4j$ processes generated with the MadGraph event generator. MSTW2008 LO PDFs. Both factorization and renormalization scales are set to $Q = \frac{1}{2}\sum_{i=1}^{4}\sqrt{p_{\perp,i}^2}$. Only first 4 flavours (considered as massless). We use the following cuts: $p_{i\perp} \in [35, 100]$ GeV, $|y_i| < 4.7$, minimal distance between final state partons `drjj` is set to 0.5. Upper panel:distribution in terms of the leading jet $p_\perp$. Lower panel: distribution in terms of the maximal rapidity difference $\Delta Y = \max|y_i - y_j|$. Statistical errors are given by $\sigma_{\text{DPS}}\sqrt{N_{\text{bin}}}/N_{\text{tot}}$ where N_{bin} is a number of events in a given bin, σ_{DPS} is a corresponding DPS cross section and N_{tot} is total number of bin entries for a given histogram.

4.8 Four-jet DPS production versus four-jet SPS production

In this section we compare our four-jet DPS simulations against four-jet SPS simulations performed with the MadGraph code [254]. The LO matrix elements for the four-jet SPS production are known to be IR-divergent in case of production of soft and collinear final state particles and hence require certain regularization procedure. In the MadGraph code the LO four-jet SPS matrix elements are regularized by imposing a cut on a minimal allowed distance $\Delta R = \sqrt{(\phi_i - \phi_j)^2 + (\eta_i - \eta_j)^2}$ between final state particles which is controlled by the value of the parameter `drjj`. In our four-jet SPS simulations we set `drjj` $= 0.5$. In order to approximately account for NLO effects in our four-jet SPS simulations we use $\mathrm{K}_{\mathrm{NLO}}^{\mathrm{SPS}} = 0.5$ as we have argued in the previous section.

In Table 4.3 we list DPS and SPS contributions to the four-jet cross section for two different collision energies and two different sets of $p_\perp$-cuts. We see that the fraction of the DPS cross section in the total (DPS + SPS) four-jet cross section increases if the collision energy $\sqrt{S}$ grows or if the transverse momenta of all four jets become softer. We also see that the fraction of DPS cross section in total four-jet cross section may reach almost 80% for production of four jets with $p_\perp \in [20, 100]$ GeV at $\sqrt{S} = 13$ TeV. This enhancement is due to the increase in collision energy and the presence of $p_\perp$-cuts we use. The growth of the collision energy with fixed hard scale Q allows to probe lower values of Bjorken-x which, in turn, increases the total cross section due to the increase of parton densities. The $p_\perp$-cuts we use lead to suppression of the SPS cross section since the typical configuration of four-jet events produced via SPS mechanism is given by one hard jet and three softer jets, see Fig. 4.1. Contrary to the the SPS case the DPS production leads to two pairs of di-jets with approximately the same values of transverse momenta which implies that the aforementioned $p_\perp$-cuts do not lead to a strong suppression of the DPS at low values of transverse momenta of produced di-jets. Moreover, because the $\hat{t}$-channel of the LO di-jet cross sections becomes proportional to $\sim 1/p_\perp^4$ as the absolute value of the transverse momentum $p_\perp$ decreases, the DPS cross section, in turn, increases as the low $p_\perp$-cut becomes softer. The difference in the value of the DPS and SPS cross sections, obviously, has to also manifest itself in differential distributions. In Fig. 4.11 - Fig. 4.14 we present our simulations for the four-jet DPS and SPS production. In Fig. 4.11 we compare the leading jet $p_\perp$ and ΔY distributions for four-jets produced via DPS and SPS mechanisms at $\sqrt{S} = 7$ TeV and $p_\perp \in [35, 100]$ GeV. We see that DPS distribution dominate over the SPS distribution for the small values of transverse momentum of the leading jet, as shown in the upper plot of Fig. 4.11, and for the large values of the maximal rapidity separation $\Delta\mathrm{Y} > 6$, as shown in the lower plot of Fig. 4.11. These effects become stronger if one decreases the value of the low $p_\perp$-cut. In Fig. 4.12 we show leading jet $p_\perp$ and ΔY DPS and SPS distributions for four jets with $p_\perp \in [20, 100]$ GeV at $\sqrt{S} = 7$ TeV. We see that the difference between leading jet $p_\perp$ DPS and SPS distributions becomes stronger at small values of transverse momenta and that the ΔY DPS distribution now dominates over corresponding SPS distribution starting from $\Delta\mathrm{Y} > 4$. The growth of collision energy, in turn, leads to the increase of the DPS cross section and to the enhancement of the effects we discussed, compare Fig. 4.11 with Fig. 4.13 and Fig. 4.12 with Fig. 4.14. We also shall note that the ΔY DPS distribution generated for $p_\perp \in [20, 100]$ at $\sqrt{S} = 13$ TeV dominates over the corresponding SPS distribution over the whole range of binning, see the lower plot of Fig. 4.14.

Our results agree with the results of Maciuła and Szczurek [230] at qualitative level. Namely,

in Ref. [230] the DPS contribution to the total (DPS + SPS) cross section for the four-jet production at $\sqrt{S} = 7$ TeV and $p_\perp \in [35, 100]$ GeV was found to be equal to 42% (our result is 40%). The contribution of DPS to the total (DPS + SPS) cross section for the four jet production at $\sqrt{S} = 7$ TeV and $p_\perp \in [20, 100]$ GeV in Ref. [230] was found to be equal to 70% (our result is 68%). The comparison between ΔY distributions given in Fig. 4.11 and Fig. 4.12 and corresponding distributions from [230] is given in Fig. 4.15. We see that the four-jet ΔY distributions given in Fig. 4.11 and Fig. 4.12 demonstrate the same behaviour as the distributions from [230]. Unfortunately, in Ref. [230] many important details of DPS and SPS simulations, *e. g.* choice of factorization and renormalizetion scales, choice of PDFs *etc.*, were not provided which makes a quantitative comparison between our results and results given in [230] impossible. We also shall note that, as we have discussed in section 4.7, the approximation of the complete four-jet SPS production process $pp \xrightarrow{\text{SPS}} 4j$ by $pp \xrightarrow{\text{SPS}} 2j + 2g$ gives about 5% difference for the total cross sections. In Ref. [230] the ALPGEN event generator was used to simulate the four-jet SPS production which means that in [230] the SPS events were generated according to $pp \xrightarrow{\text{SPS}} 2j + 2g$ process. However, in our simulations we use complete four-jet SPS production $pp \xrightarrow{\text{SPS}} 4j$ as implemented in MadGraph event generator. This different approach to the generation of SPS events can partially explain the discrepancies between our results and results from [230]. For example, if we evaluate the DPS contribution to the four-jet production at $\sqrt{S} = 7$ TeV and $p_\perp \in [35, 100]$ GeV using the SPS cross section for the $pp \xrightarrow{\text{SPS}} 2j + 2g$ process we get

$$100 \times \frac{\sigma_{\text{DPS}}}{\sigma_{\text{DPS}} + \text{K}_{\text{NLO}}^{\text{SPS}} \sigma_{\text{SPS}}^{2j2g}} \approx 41\%, \tag{4.26}$$

where $\sigma_{\text{SPS}}^{2j2g} = 130.92$ nb is a total LO SPS cross section evaluated for the process $pp \xrightarrow{\text{SPS}} 2j + 2g$ at $\sqrt{S} = 7$ TeV and $p_\perp \in [35, 100]$ GeV, $\sigma_{\text{DPS}} = 45.35$ nb is a DPS cross section evaluated for the same cuts and collision energies and $\text{K}_{\text{NLO}}^{\text{SPS}} = 0.5$, as explained in section 4.7. Therefore, we see that if we switch from exact four-jet SPS production to the approximate one we get a better agreement with results given in [230].

Cuts and collision energy	σ_{SPS} for $pp \xrightarrow{\text{SPS}} 4j$ process	σ_{DPS} for $pp \xrightarrow{\text{DPS}} 4j$ process	$\sigma_{\text{DPS}} / (\sigma_{\text{DPS}} + \sigma_{\text{SPS}})$
$\sqrt{S} = 7$ TeV, $\lvert y\rvert < 4.7$, $p_\perp \in [35, 100]$ GeV	69.08	45.45	39.68 %
$\sqrt{S} = 7$ TeV, $\lvert y\rvert < 4.7$, $p_\perp \in [20, 100]$ GeV	1874.99	3912.27	67.60 %
$\sqrt{S} = 13$ TeV, $\lvert y\rvert < 4.7$, $p_\perp \in [35, 100]$ GeV	290.18	347.13	54.47 %
$\sqrt{S} = 13$ TeV, $\lvert y\rvert < 4.7$, $p_\perp \in [20, 100]$ GeV	6670.53	22898.67	77.44 %

Table 4.3: Comparison between the DPS cross sections evaluated for $pp \xrightarrow{\text{SPS}} 4j$ and $pp \xrightarrow{\text{DPS}} 4j$ processes. For the DPS computations we used "naive" dPDFs constructed out of MSTW2008 LO PDFs and for the SPS computations we used MSTW2008 LO PDFs. All cross sections are given in nb. The factorization and renormalization scales are set to: a) DPS $Q_{1,2} = |p_{\perp,1,2}|$, b) SPS $Q = \frac{1}{2}\sum_{i=1}^{4}\sqrt{p_{\perp,i}^2}$. The SPS cross sections are multiplied by $\text{K}_{\text{NLO}}^{\text{SPS}} = 0.5$.

We also shall note that in the simulations given in [230] the impact of parton shower effects was neglected. In sections 4.9 - 4.11 we discuss how one can improve the phenomenological study presented in this section by adding the ISR and FSR effects to our simulations.

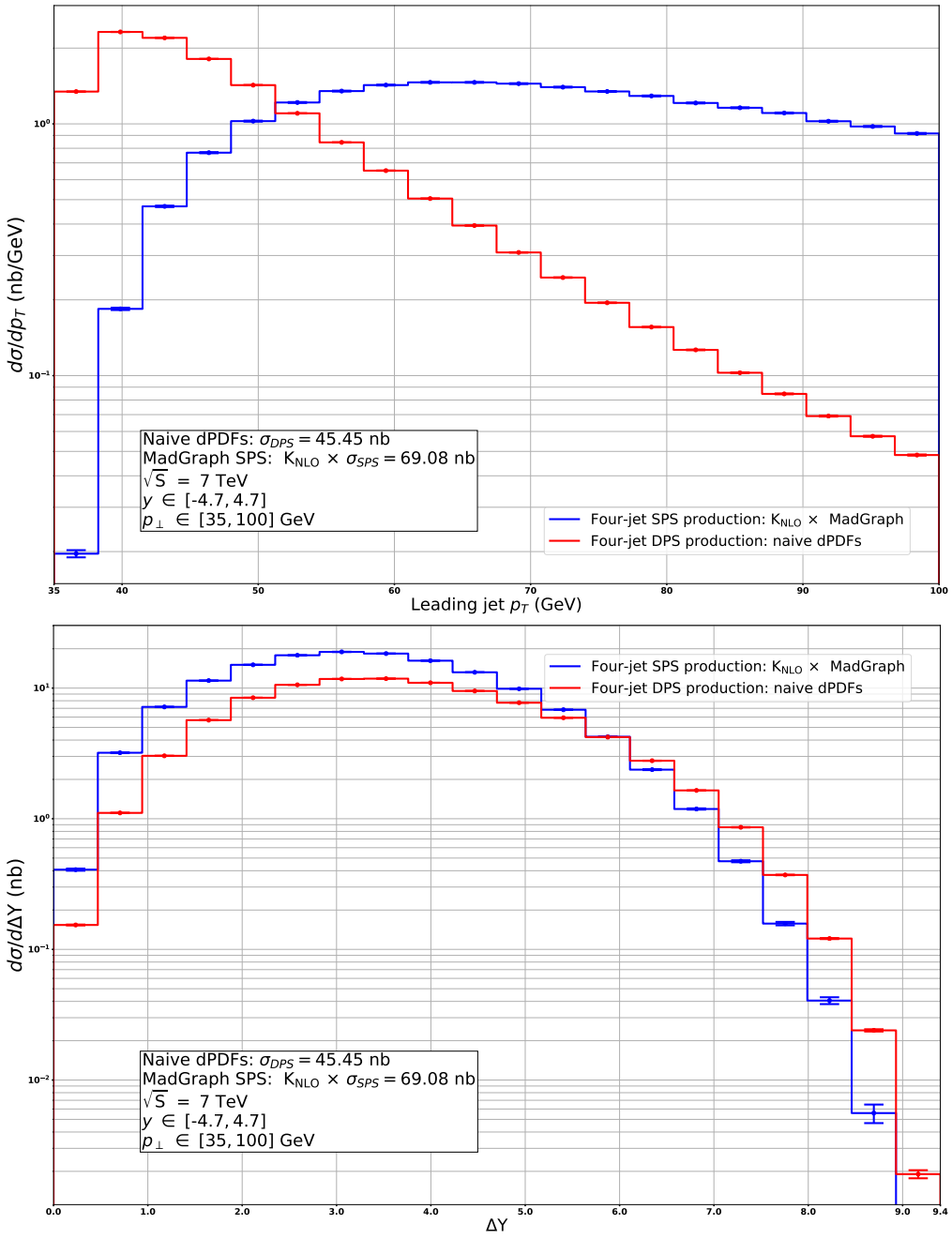

Figure 4.11: Upper panel: comparison between leading jet $p_\perp$ distributions for four-jet SPS and DPS events. Lower panel: comparison between $\Delta Y = \max|y_i - y_j|$ distributions for four-jet SPS and DPS events. Collision energy is equal to $\sqrt{S} = 7\,\text{TeV}$, $p_\perp \in [35, 100]$ GeV, $|y| < 4.7$. Factorization scales are equal to $Q_1 = p_{1\perp}$, $Q_2 = p_{2\perp}$, where $p_{1\perp}$ and $p_{2\perp}$ are equal to the absolute value of a jet transverse momentum in a first and second hard processes in a given DPS event. The SPS distributions were multiplied by $\text{K}_{\text{NLO}}^{\text{SPS}} = 0.5$. Statistical errors are given by $\sigma_{\text{DPS}}\sqrt{N_{\text{bin}}}/N_{\text{tot}}$ where N_{bin} is a number of events in a given bin, σ_{DPS} is a corresponding DPS cross section and N_{tot} is total number of bin entries for a given histogram.

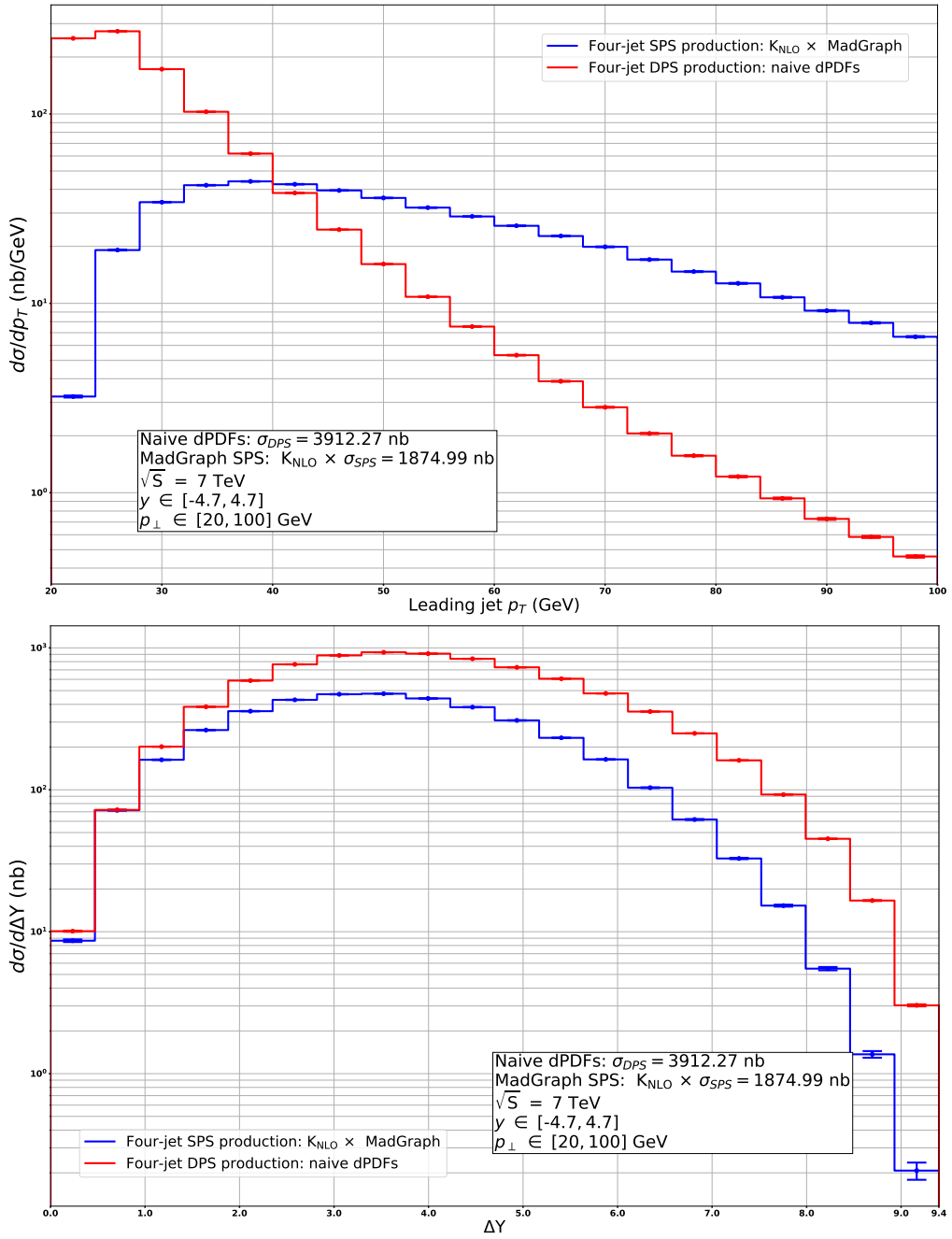

Figure 4.12: Upper panel: comparison between leading jet $p_\perp$ distributions for four-jet SPS and DPS events. Lower panel: comparison between $\Delta\mathrm{Y} = \max|y_i - y_j|$ distributions for four-jet SPS and DPS events. Collision energy is equal to $\sqrt{S} = 7\,\mathrm{TeV}$, $p_\perp \in [20, 100]$ GeV, $|y| < 4.7$. Factorization scales are equal to $Q_1 = p_{1\perp}$, $Q_2 = p_{2\perp}$, where $p_{1\perp}$ and $p_{2\perp}$ are equal to the absolute value of a jet transverse momentum in a first and second hard processes in a given DPS event. The SPS distributions were multiplied by $\mathrm{K}_{\mathrm{NLO}}^{\mathrm{SPS}} = 0.5$. Statistical errors are given by $\sigma_{\mathrm{DPS}}\sqrt{N_{\mathrm{bin}}}/N_{\mathrm{tot}}$ where N_{bin} is a number of events in a given bin, σ_{DPS} is a corresponding DPS cross section and N_{tot} is total number of bin entries for a given histogram.

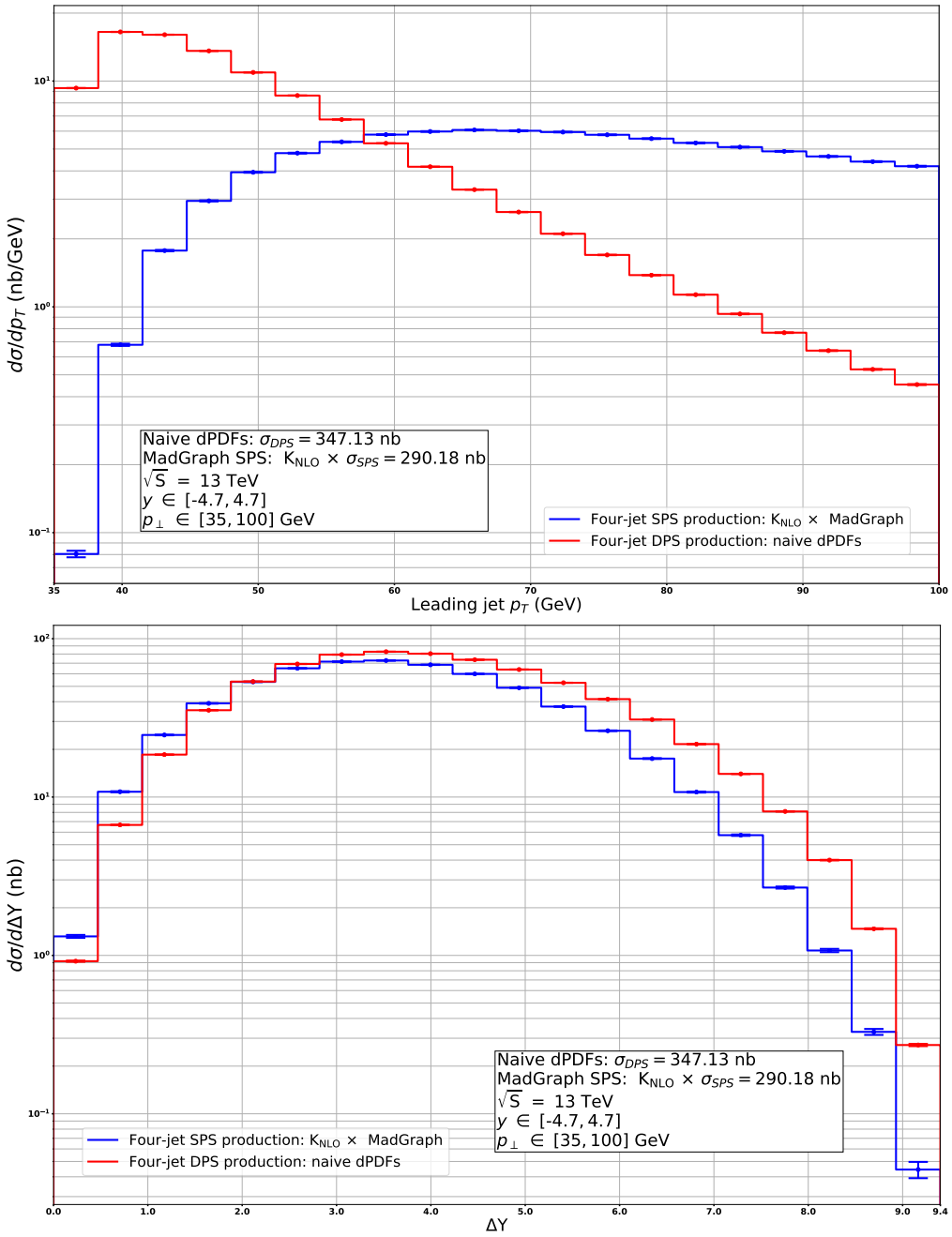

Figure 4.13: Upper panel: comparison between leading jet $p_\perp$ distributions for four-jet SPS and DPS events. Lower panel: comparison between $\Delta\mathrm{Y} = \max|y_i - y_j|$ distributions for four-jet SPS and DPS events. Collision energy is equal to $\sqrt{S} = 13\,\mathrm{TeV}$, $p_\perp \in [35, 100]$ GeV, $|y| < 4.7$. Factorization scales are equal to $Q_1 = p_{1\perp}$, $Q_2 = p_{2\perp}$, where $p_{1\perp}$ and $p_{2\perp}$ are equal to the absolute value of a jet transverse momentum in a first and second hard processes in a given DPS event. The SPS distributions were multiplied by $\mathrm{K}^{\mathrm{SPS}}_{\mathrm{NLO}} = 0.5$. Statistical errors are given by $\sigma_{\mathrm{DPS}}\sqrt{N_{\mathrm{bin}}}/N_{\mathrm{tot}}$ where N_{bin} is a number of events in a given bin, σ_{DPS} is a corresponding DPS cross section and N_{tot} is total number of bin entries for a given histogram.

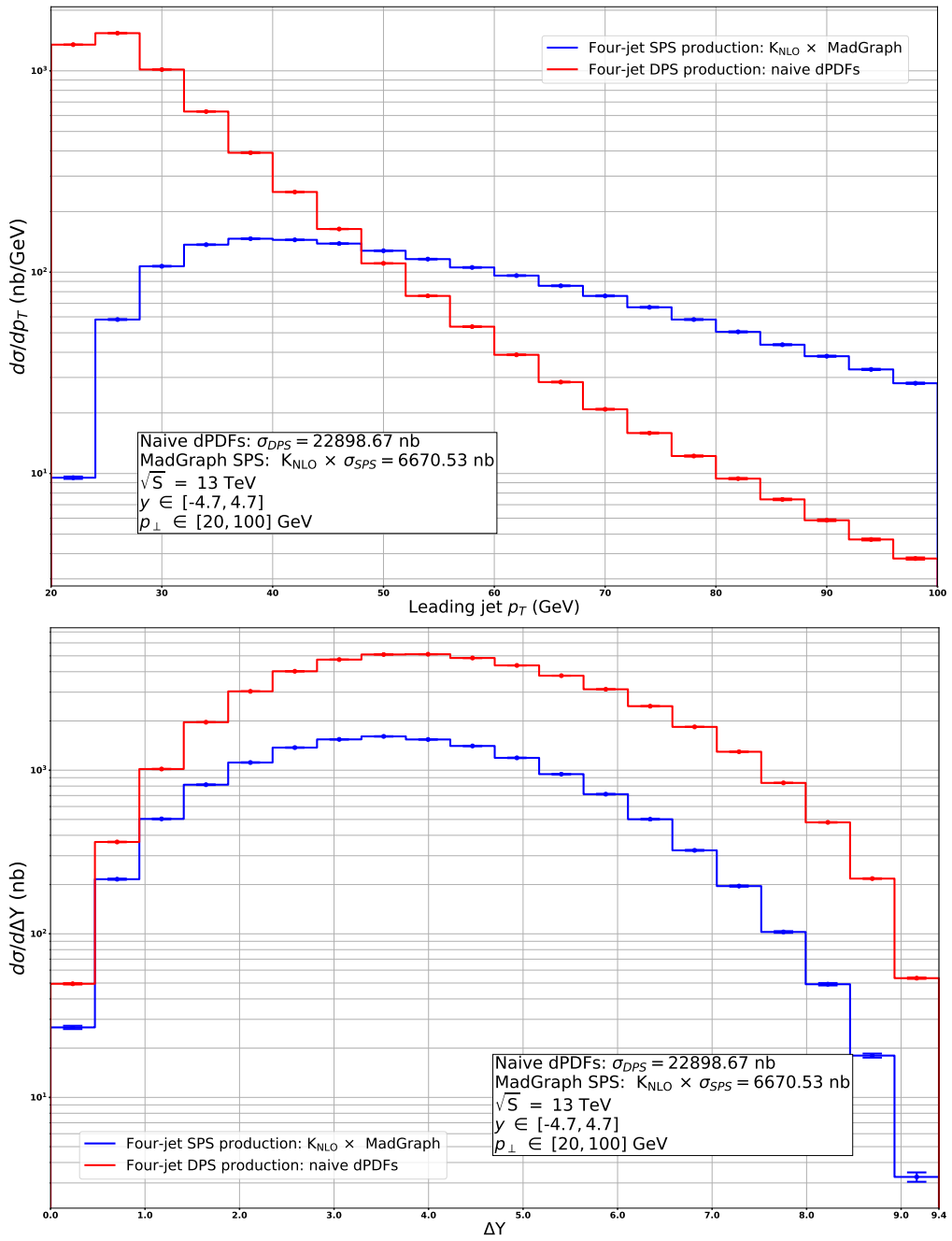

Figure 4.14: Upper panel: comparison between leading jet $p_\perp$ distributions for four-jet SPS and DPS events. Lower panel: comparison between $\Delta Y = \max|y_i - y_j|$ distributions for four-jet SPS and DPS events. Collision energy is equal to $\sqrt{S} = 13\,\text{TeV}$, $p_\perp \in [20, 100]$ GeV, $|y| < 4.7$. Factorization scales are equal to $Q_1 = p_{1\perp}$, $Q_2 = p_{2\perp}$, where $p_{1\perp}$ and $p_{2\perp}$ are equal to the absolute value of a jet transverse momentum in a first and second hard processes in a given DPS event. The SPS distributions were multiplied by $\text{K}_{\text{NLO}}^{\text{SPS}} = 0.5$. Statistical errors are given by $\sigma_{\text{DPS}}\sqrt{N_{\text{bin}}}/N_{\text{tot}}$ where N_{bin} is a number of events in a given bin, σ_{DPS} is a corresponding DPS cross section and N_{tot} is total number of bin entries for a given histogram.

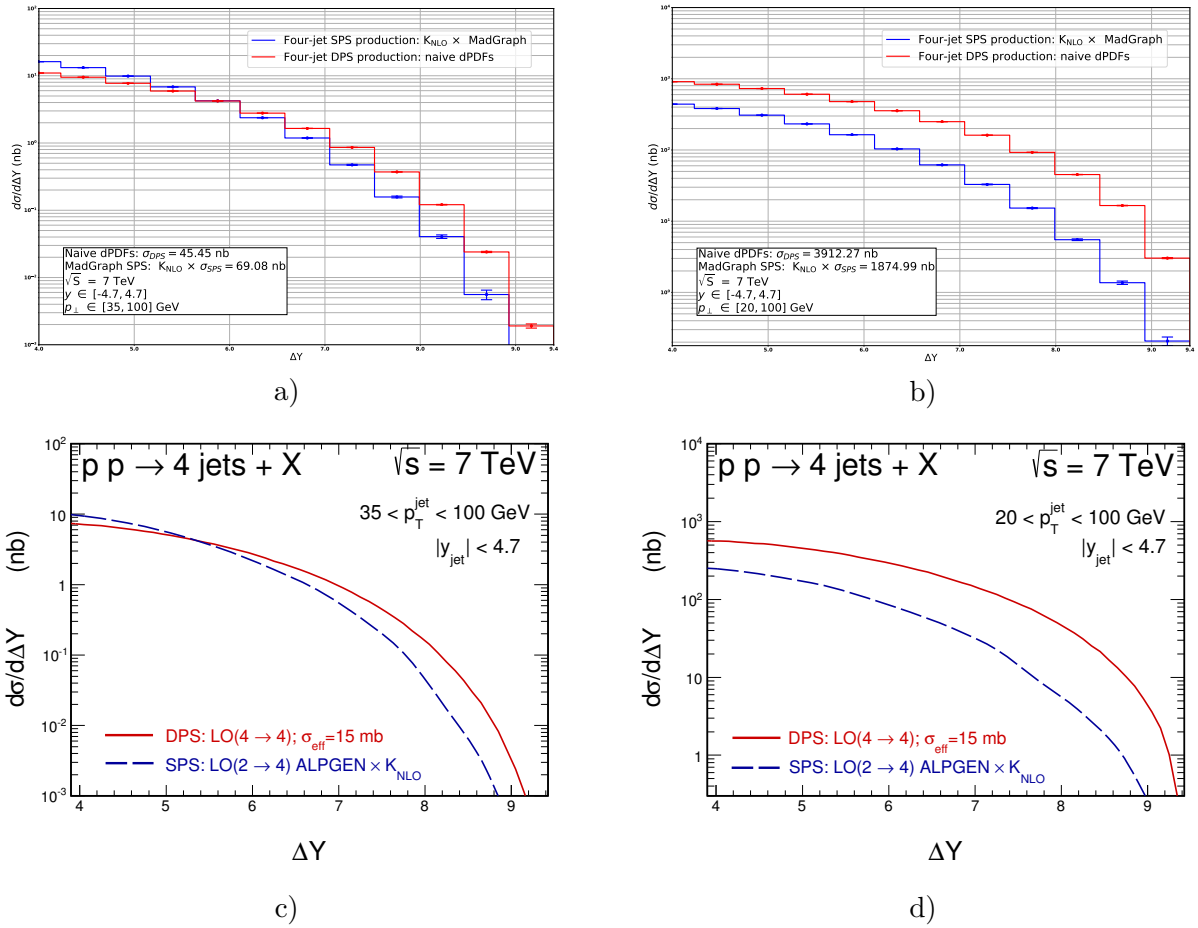

Figure 4.15: Comparison between our simulations of four-jet production via DPS and SPS mechanism against simulations performed in [230]. Our results are given by plots a) and b), the results from [230] are given by plots c) and d).

4.9 Pythia and "double" Les-Houches files

In section 4.6 and section 4.8 we have presented our parton-level simulations of the four-jet DPS production in pp collisions. We have identified regions of the DPS phase space where the difference between GS09 and "naive" dPDFs can significantly affect the ΔY differential distributions. We also have studied the interplay between DPS and SPS four-jet production in a way similar to the study of Maciuła and Szczurek [234]. However, in [234] the impact of the initial and final state radiation was neglected. Such approach leads to two important consequences. First of all it effectively reduces a set of DPS-sensitive observables to the transverse momenta of produced jets and the maximal rapidity difference ΔY. Since without initial and final state radiation effects we have to deal with production of a pair of di-jets with *exactly* back-to-back jets, the DPS-sensitive variables based upon $p_\perp$-momenta imbalance and angular correlations between produced jets cannot be applied in the DPS analysis. For example, the transverse momenta imbalance variable $\Delta_{ij} = \left|\boldsymbol{p}_i + \boldsymbol{p}_j\right| / \left(|\boldsymbol{p}_i| + |\boldsymbol{p}_j|\right)$ would always be equal to zero for exact back-to-back jets. Secondly, the initial and final state radiation may lead to a strong difference between distributions of partonic events and distributions of jets.

In this section we describe how one can combine our DPS code with the `Pythia` event generator, discuss modifications to the LHEF standard [81] and the `Pythia` code necessary to and ISR and FSR effects to our DPS stimulations. We also present technical checks of these modifications.

In the `Pythia` framework one can use its MPI model [258] - [262] to produce DPS events. However, according to the MPI model of `Pythia` all MPI events are strictly ordered in transverse momentum, see review [263]. It would imply that in a four-jet DPS event produced via MPI mechanism the jets produced via second hard interaction will "always" have transverse momenta smaller than jets produced via first hard interaction. This ordering in transverse momentum is necessary to combine MPI events with initial and final state radiation and to get a correct shape of charged multiplicity distributions, see [263]. However, it is not suitable for DPS modelling. Therefore, starting from `Pythia` version = "8" [256], [256] a possibility to *always* have two hard interactions was implemented. This mode can be activated by setting `SecondHard:generate = on` during the initialization of `Pythia`. The usage `SecondHard:generate = on` will imply that roughly half of the time the second hard process will appear with the transverse momentum higher than the first one. One can also combine `SecondHard:generate = on` with `PartonLevel:MPI = on` to add a sequence of MPI events on top of a generated DPS event[10].

We see that the combination of parton-level DPS events generated with our DPS code with the `Pythia` event generator in the DPS mode would allow to add ISR and FSR effects to our DPS simulations. Therefore, in order to do that, one would have to first generate LHE files with our DPS code and then supply them to `Pythia` to add ISR and FSR effects. However, this procedure requires the extension of the LHEF standard as well as some modifications to the files `Pythia.cc`, `ProcessContainer.cc` and `PartonLevel.cc` of the `Pythia` code version = "8.240". The modifications to the `Pythia` code and the LHEF standard are given in Appendix G.

After introducing the aforementioned modifications to the `Pythia` code and the LHEF standard one can read DPS events from the LHE files and add initial and final state radiation on top of them. We check the implementation in the following way: first we generate four-jet DPS

[10] In Chapter 6 we will discuss in more details the differences between DPS and MPI modelling in `Pythia`.

events at collision energy $\sqrt{S} = 13$ TeV with `Pythia` in the DPS mode using settings shown in Table 4.4. In our simulations we use MSTW2008 LO PDF set [298]. In order to speed up the generation procedure we restrict the phase space by setting `PhaseSpace:pTHatMin = 20` GeV and `PhaseSpace:pTHatMax = 40` GeV. This choice of $p_\perp$ cuts is not realistic, however, allows to collect high statistics necessary for our checks relatively quickly. In order to reconstruct jets we use the FastJet [220] core implemented into `Pythia` and the anti-k_t jet clustering algorithm [221] with jet parameters: $\eta_{\max} = 4.7$, $R = 0.8$ and $p_{\mathrm{T,\,jet\,min}} = 10$ GeV. After finishing the generation of events in the standalone mode we perform a check of the modifications given in Appendix G. These modifications affect only the parts of the code used to initialize `Pythia` while reading DPS events from the LHE files. Therefore, in order to check them, we first use `Pythia` to create the LHE files with the same number of DPS events as we generated in the standalone mode. After creating the LHE files we supply them to `Pythia` and perform the same simulation as in the standalone mode. If the DPS distributions produced with `Pythia` in the standalone mode coincide with the DPS distributions produced by supplying LHE files with DPS events to `Pythia`, then it means that the modifications listed in Appendix G work properly and that we can use modified `Pythia` to "shower" parton-level DPS events produced with our DPS code.

The results of the aforementioned comparison are given in Fig. 4.16 and Fig. 4.17. We see that the DPS distributions produced in the standalone mode and the DPS distributions produced out of LHE files with DPS events practically coincide (see the ratio plots below the histograms) which implies that with the aforementioned modifications `Pythia` can successfully read DPS events out of LHE files and "shower" them.

`Pythia` Master Switch	Value
`HardQCD:all`	`on`
`SecondHard:generate`	`on`
`SecondHard:TwoJets`	`on`
`PartonLevel:ISR`	`on`
`PartonLevel:FSR`	`on`
`PartonLevel:MPI`	`off`
`HadronLevel:all`	`off`

Table 4.4: Pythia settings we use to check that reading and showering of the DPS events from the LHE files was performed properly.

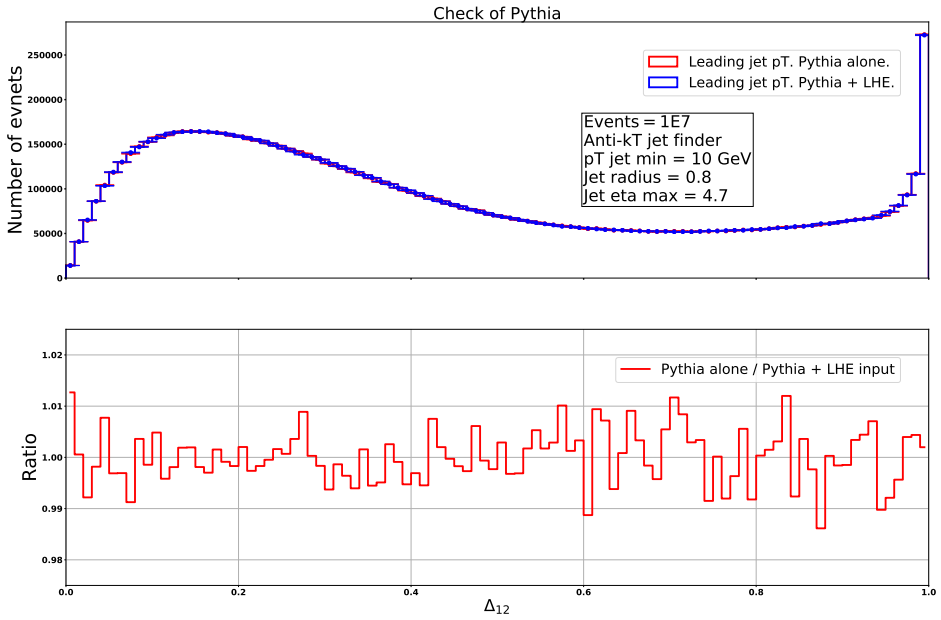

Figure 4.16: Check of the modifications of the Pythia's code. Here we compare four-jet DPS events produced with Pythia in a stand alone mode against DPS events produced out of the modified LHE files. Distribution in terms of the transverse momenta imbalance $\Delta_{12} = |\boldsymbol{p}_1 + \boldsymbol{p}_2| \,/\, (|\boldsymbol{p}_1| + |\boldsymbol{p}_2|)$ of two hardest jets.

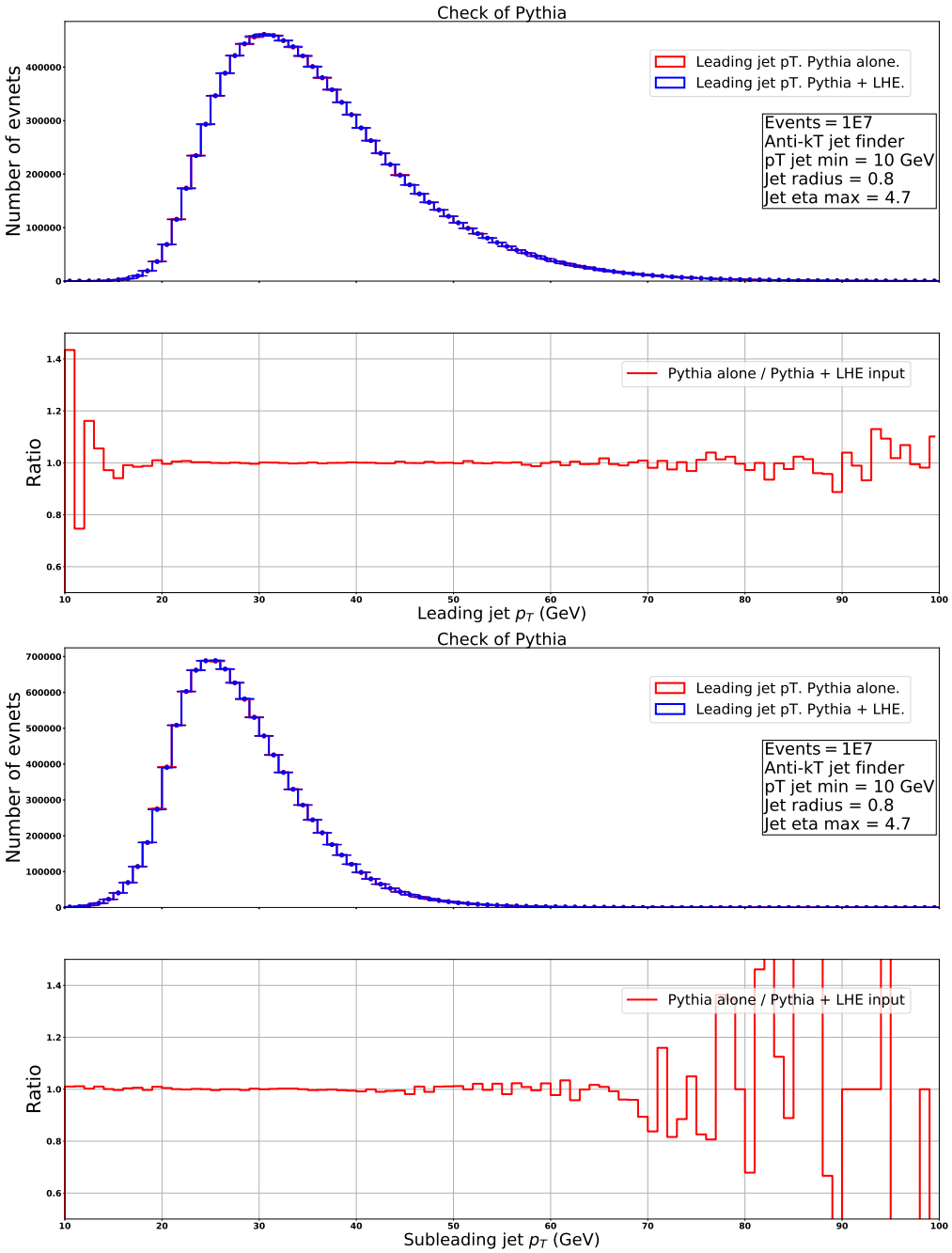

Figure 4.17: Check of the modifications of the `Pythia`'s code. Here we compare four-jet DPS events produced with `Pythia` in a stand alone mode against DPS events produced out of the modified LHE files. Upper panel: Leading jet $p_\perp$ distribution. Lower panel: Subleading jet $p_\perp$ distribution.

4.10 Technical aspects of the four-jet simulations.

In section 4.9 we have described modifications to the `Pythia` 8.240 code necessary to read DPS events from LHE files and to add initial and final state radiation effects on top of the DPS events. In section 4.11 we discuss how strongly initial and final state radiation affect results presented in section 4.8. However, before doing that we have to discuss some important technical aspects of four-jet DPS simulations. In the following we refer to the simulations presented in section 4.4, section 4.6 and section 4.7 as to *parton level simulations* and to the simulations presented below as to the the *jet level simulations*. We also call the events produced in the parton level simulations and the jet level simulations as *parton events* and *jet events* correspondingly.

First of all, it is know that LO di-jet cross sections become divergent when transverse momenta of the final state particles go to zero. Namely, at the low $p_\perp$-values the contribution due to the $\hat{t}$-channel exchange scales approximately as $\sim 1/p_\perp^4$. This divergent behaviour can be explained by the colour screening phenomenon: as the transverse momentum of the mediator in the $\hat{t}$-channel exchange becomes softer, its de Broglie wave-length becomes longer. This implies that at sufficiently small $p_\perp$-values the $\hat{t}$-channel mediator will not be able to resolve colour charges of the individual partons which indicates the failure of the interaction picture of point-like partons, see review [263]. Therefore, in order to be able to generate events, one has to regularize the low-$p_\perp$ divergence. In the MPI modelling of `Pythia` this is realized via a smooth damping around $p_\perp \approx 2$ GeV [259]. This low-$p_\perp$ damping is crucial for the MPI modelling, since the MPI processes typically lead to production of many low-$p_\perp$ particles. However, in the case of *hard* four-jet production the low-$p_\perp$ divergence can be eliminated by a sharp $p_\perp$ cut which we will call $p_\perp^{\rm reg}$. If one performs parton level simulations one can arrange partons generated at the fixed order in perturbation theory into jets. At this level of accuracy $p_\perp^{\rm reg}$ can be set to the minimal jet $p_\perp^{\rm min}$ cut as we have done in section 4.4, section 4.6 and section 4.7. However, if one wants to perform jet level simulations one cannot anymore associate $p_\perp^{\rm reg}$ cut with transverse momenta produced jets and its value has to be chosen such that it does not affect jet level simulations. In section 4.11 we present our simulations for the DPS production of four jets with transverse momenta in the range between 35 and 100 GeV. Therefore, we set $p_\perp^{\rm reg} = 20$ GeV. We also shall note that because we move from the parton level simulations to the jet level simulations the upper $p_\perp$ cut in the parton level simulations has to be removed. Instead, for the correct generation procedure, one has to perform first the parton level simulations with $p_\perp \in [p_\perp^{\rm reg}, \sqrt{S}/2]$, then supply the resulted LHE file to `Pythia`, simulate initial and final state radiation, reconstruct jets and only afterwards impose cuts on the transverse momenta of the resulting jets. However, the time needed to generate unweighted parton level events grows with the upper $p_\perp$ cut. The reason is that at the high-$p_\perp$ jet distributions are strongly suppressed which means that, according to the hit-or-miss algorithm described in Chapter 3.1, one needs more generation calls to generate high-$p_\perp$ events. However, one can make generation time shorter by imposing an additional high-$p_\perp$ cut in the parton level simulations which we call $p_\perp^{\rm max}$ cut. In this case one has to make sure that the both $p_\perp^{\rm reg}$ and $p_\perp^{\rm max}$ cuts in the parton level simulations do not affect the jet level simulations. The corresponding checks are shown in Fig. 4.18 where we compare the leading jet $p_\perp$ distribution for the jet level simulations performed by adding ISR and FSR effects to three different sets of parton events generated in the $p_\perp$-intervals $p_\perp \in [20, 150]$ GeV, $p_\perp \in [20, 200]$ GeV and $p_\perp \in [20, 250]$ GeV. We see that effects of the variation of the $p_\perp^{\rm max}$ cut

start to appear at the values $p_\perp \sim 150$ GeV and that the leading-jet $p_\perp$ distributions in the $p_\perp$ range between 35 and 100 GeV are not affected by the values of $p_\perp^{\max}$ cut. Therefore, for our jet level simulations we will use LHE files with DPS events with $p_\perp \in [20, 150]$ GeV and we will reject all reconstructed jets with $p_\perp$ outside of the interval between 35 and 100 GeV. Similar checks of "stability" with respect to $p_\perp^{\mathrm{reg}}$ and $p_\perp^{\max}$ cuts can be performed for other relevant DPS distributions, see Appendix I.

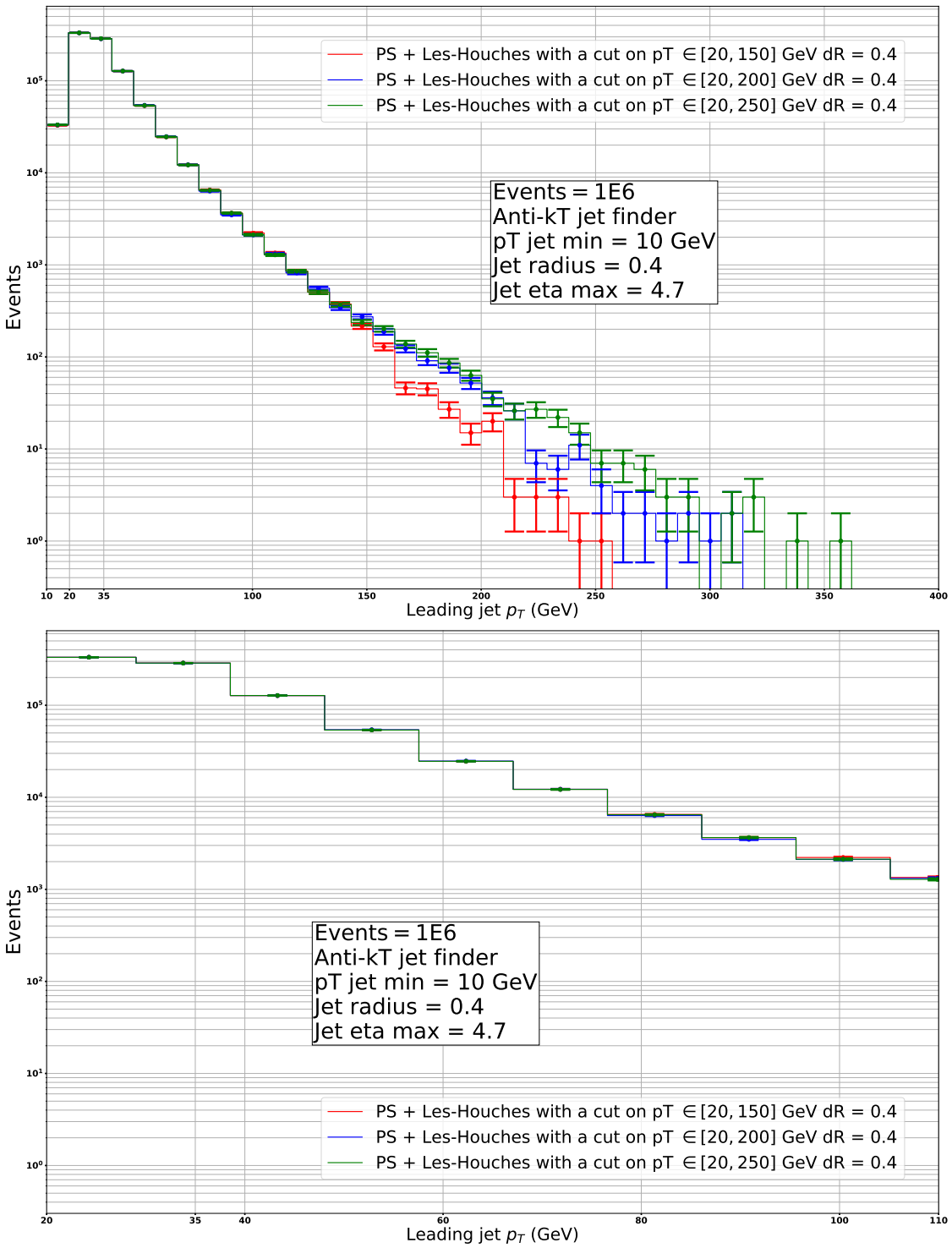

Figure 4.18: Test of stability of the leading jet $p_\perp$ distributions under the variation $p_\perp^{\max}$ cut. Four-jet DPS simulation performed for the collision energy $\sqrt{S} = 13\,\text{TeV}$ with naive dPDFs constructed out of MSTW2008 LO PDFs [298]. Factorization and renormalization scales are equal to $Q_1 = p_{1\perp}$, $Q_2 = p_{2\perp}$, where $p_{1\perp}$ and $p_{2\perp}$ are equal to the absolute value of a jet transverse momentum in a first and second hard processes in a given DPS event. Statistical errors are given by $\sqrt{N_{\text{bin}}}$ where N_{bin} is a number of events in a given bin. Upper panel: leading jet $p_\perp$ distribution of the jets produced by adding ISR and FSR effects to the parton level DPS simulations performed with $p_\perp^{\max} = 150$ GeV, $p_\perp^{\max} = 200$ GeV and $p_\perp^{\max} = 250$ GeV. Lower panel: same as in the upper panel but we show only $p_\perp$ interval between 20 and 110 GeV.

Finally, before discussing our jet level DPS simulations, we have to comment on the connection between ISR and the evolution of the dPDFs. A master equation for the ISR and FSR radiation reads

$$t\frac{\partial}{\partial t}\left(\frac{f_i(x,t)}{\Delta_i(t)}\right) = \frac{1}{\Delta_i(t)}\sum_j \int dz\, \frac{\alpha_s(t)}{2\pi}\, \tilde{P}_{i\to j}(z) f_j(x/z,t), \tag{4.27}$$

where $\tilde{P}_{j\to i}(z)$ are *unregularized* LO DGLAP splitting functions, $f_i(x,t)$ is a collinear PDF of a parton of a type i and $\Delta_i(t)$ is a Sudakov form-factor defined as

$$\Delta_i(t) \equiv \exp\left\{-\sum_j \int_{t_0}^{t} \frac{dt'}{t'} \int dz\, \frac{\alpha_s(t')}{2\pi}\, \tilde{P}_{j\to i}(z)\right\}. \tag{4.28}$$

A pedagogical introduction to the parton shower algorithms as well as the derivation of Eq. 4.27 and Eq. 4.28 can be found in [2], [78]. We do not provide here a detailed discussion of different parton shower algorithms which is beyond the scope of this thesis. Instead we briefly discuss the conceptual difference between ISR and FSR algorithms. Namely, in the Monte Carlo models of FSR [85] - [91] the probability $\mathcal{R}_{\rm FSR}$ that a parton in a cascade will evolve from a lower scale t_1 to the higher scale t_2 without resolvable branching is given by the ratio of two Sudakov form factors

$$\mathcal{R}_{\rm FSR} = \frac{\Delta(t_2)}{\Delta(t_1)}. \tag{4.29}$$

However, in the Monte Carlo models of ISR [92] - [93] the probability $\mathcal{R}_{\rm ISR}$ to evolve *backwards* from t_2 to t_1 depends not only on the ratio of Sudakov form factors but also one the ratio of PDFs. The corresponding expression is given by

$$\mathcal{R}_{\rm ISR} = \frac{\Delta(t_2)}{\Delta(t_1)}\,\frac{f(x,t_1)}{f(x,t_2)}. \tag{4.30}$$

The aforementioned difference in the definition of probabilities $\mathcal{R}_{\rm FSR}$ and $\mathcal{R}_{\rm ISR}$ implies that one has to introduce new schemes for the Monte Carlo models of ISR effects in DPS processes. The main obstacle here is the absence of sets of two-parton distribution functions obtained by the fit to the experimental data. Moreover, even if we had sets of generalized two-parton distributions obtained from the fit to the measured data we still would face the same problem in the modelling of MPI processes. Therefore, in order to evaluate $\mathcal{R}_{\rm ISR}$ for DPS processes one has to rely on some models of two-parton distributions. A possible option would the GS09 dPDFs set [173], [174]. However, the direct application of GS09 dPDFs to the ISR modelling is a non-trivial task due to the presence of "$1v2$" splitting term on the RHS of Eq. 2.13. Therefore, a correct backward evolution has to account for the "$1v2$" effects and for possible recombinations of two different ISR cascade into one single ISR cascade as schematically shown in Fig. 4.19. A correct handling of such ISR evolution processes in Monte Carlo event generators is a non-trivial task which still lacks a complete solution. Recently, first results on combining ISR evolution which accounts for "$1v2$" effects and the impact parameter depended distributions $\Gamma(x_1, x_2, \boldsymbol{b}, Q^2)$ from [200] were reported [211]. Since in our simulations we use the `Pythia` event generator the dPDFs for the ISR will be modelled according to the original

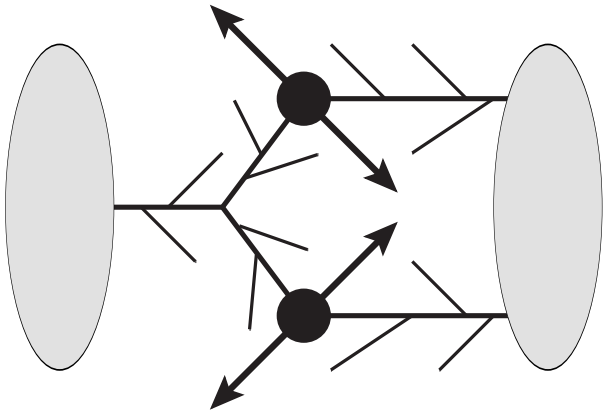

Figure 4.19: Schematic picture of the ISR in "1v2" DPS processes. Here thin lines represent emission of partons during the backward ISR evolution.

`Pythia`'s algorithm [260]. In Chapter 6 we will describe the way `Pythia` models dPDFs in more details. We will also provide a detailed comparison against GS09 approach. Here we shall just note that the dPDFs modelled by `Pythia` account for momentum and number conservation. Therefore, a combination of the DPS events produced with our code with the parton shower of `Pythia` can be seen as an approximation where FSR effects are modelled correctly, ISR effects are modelled approximately and the hard DPS process is modelled as in section 4.6 either with "naive" or GS09 dPDFs. We suggest that our results can be used as a baseline for comparison against recently reported results of [211]. Such combined study may help to estimate the relative impact of different effects which affect DPS, *e. g.* dDGLAP evolution effects, correlations in momentum and flavour and "1v2" splitting effects.

4.11 Impact of the initial and final state radiation

In this section we present our study of the impact of the ISR and FSR effects on our parton level DPS simulations. Let us consider first leading jet $p_\perp$ DPS distributions. We expect that the ISR and FSR effects will lead to an increase of activity for high-$p_\perp$ bins due to the redistribution of transverse momenta caused by the parton shower as schematically shown in Fig. 4.20 where the arrows represent redistribution of transverse momenta among different $p_\perp$-bins. More precisely, the jet reconstruction procedure leads to a redistribution of particles created by different evolution cascades. It implies that a certain number of the reconstructed leading jets acquire more transverse momenta due to the particles captured from other jets and approximately the same amount of the reconstructed leading jets loose some transverse momenta due to the particles which "escape" from the jet cone. If we had had a uniform $p_\perp$-distribution, then all bins, apart from those close to $p_\perp^{\rm reg}$ and $p_\perp^{\rm max}$, would have not been affected by the ISR and FSR effects. However, in each collision, it is less likely to produce high-$p_\perp$ particles than the low-$p_\perp$ ones. It means that the parton level $p_\perp$-distributions decrease as $p_\perp$ grows. Therefore, the redistribution of transverse momenta as shown in Fig. 4.20 will add more activity to the high-$p_\perp$ bins since the N'th $p_\perp$-bin will get more transverse momenta from the $(N-1)$'th $p_\perp$-bin than it will transmit to the $(N+1)$'th $p_\perp$-bin. Obviously, in $p_\perp$-bins close to the $p_\perp^{\rm reg}$-cut, the aforementioned redistribution of transverse momenta

provides *less* activity for the reconstructed jets. The reason is that the jet reconstruction can create some jets with $p_\perp$ smaller than $p_\perp^{\rm reg}$ which implies that some events will "leak" below the $p_\perp^{\rm reg}$-cut as shown in Fig. 4.18 where the jet reconstruction created some jets with $p_\perp = 10$ GeV which is below the regulating cut $p_\perp^{\rm reg} = 20$ GeV. It implies that for the $p_\perp$-bins close to $p_\perp^{\rm reg}$ the parton level $p_\perp$-distributions will exceed the jet level distributions. Such bins are affected by boundary effects and have to be excluded out of consideration.

In the upper plot of Fig. 4.21 we compare leading jet $p_\perp$ DPS distributions with and without parton shower effects. In order to perform this simulation we created first a Les-Houches file with DPS events and then supplied it to the `Pythia` event generator to add ISR and FSR effects to our parton-level DPS simulations. The modifications to the LHEF standard and `Pythia`'s code necessary for the aforementioned simulation are described in Appendix G and their checks are presented in section 4.9. The Les-Houches file contains DPS events generated at $\sqrt{S} = 13$ TeV with $p_\perp \in [20, 150]$ GeV and $|\eta| < 4.7$. In order to simulate ISR and FSR effects we use the `Pythia` setup as in Table 4.4. In order to reconstruct jets we use the FastJet [220] core implemented into `Pythia` and the anti-k_t jet clustering algorithm [221] with jet parameters: $\eta_{\rm max} = 4.7$, $R = 0.4$. and $p_{\rm T,\,jet\,min} = 10$ GeV. In order to exclude boundary effects due to the $p_\perp$-cuts imposed in our parton level simulations after the jet reconstruction we trigger on events with at least four-jets with $p_\perp \in [35, 100]$. We see that in comparison with the parton level simulations the simulations with the ISR and FSR effects lead to a higher activity for the high-$p_\perp$ bins, see the upper plot of Fig. 4.21. This result is in agreement with the dependence of the distributions of the reconstructed jets on the $p_\perp$-cuts imposed in the parton level simulations as shown in Fig. 4.18.

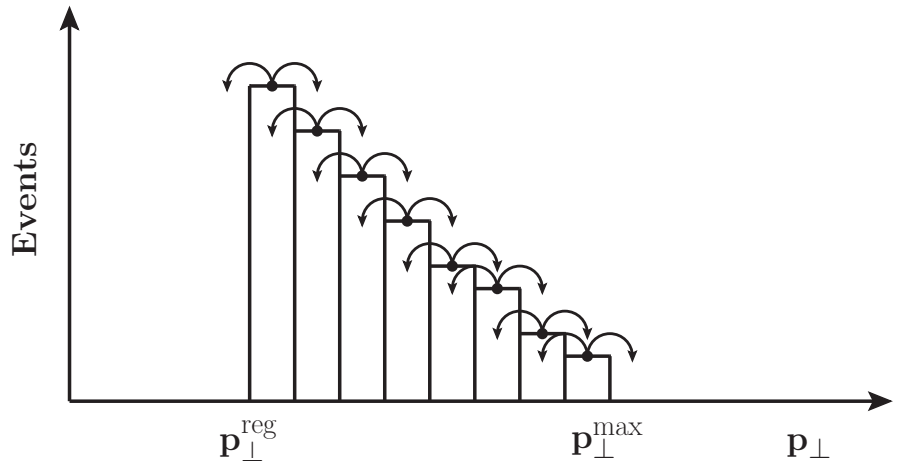

Figure 4.20: Schematic representation of the transverse momentum of jets due to the initial and final state radiation effects.

Now, if we consider the impact of the parton shower effects on the ΔY DPS distributions the situation changes as shown in the lower plot of Fig. 4.21. For this simulation we have used the same setup as for the simulations of the leading jet $p_\perp$ distributions we just discussed. We see that PS effects "bend down" the ΔY distribution at high values of ΔY. The reason is that the jet reconstruction procedure will lead to some deviation of the reconstructed jets from the collision axis which, in turn, leads to smaller rapidities and smaller values of ΔY.

After having discussed the impact of the ISR and FSR effects on leading jet $p_\perp$ and ΔY DPS

distributions we can study how the inclusion of the PS effects changes the results on comparison between DPS and SPS contributions to the four-jet production presented in section 4.8. In Fig. 4.22 we compare the leading jet $p_\perp$ distributions and ΔY distributions of the SPS and DSP events after parton showering. The SPS distributions were produced by supplying four-jet MadGraph events to the `Pythia` event generator without performing merging procedure. We see that the ISR and FSR effects do not spoil the separation between DPS and SPS events discussed in section 4.8, compare Fig. 4.22 with Fig. 4.13.

The extension of the LHEF standard and modifications to the `Pythia` code as described in Appendix G allow to study the interplay between DPS and SPS contribution for various differential distributions which cannot be modelled without PS effects. As an example, in Fig. 4.23 we show two such distributions, namely a distribution of the transverse momenta imbalance of two hardest jets Δ_{12} and a distribution in the azimuthal angle between two di-jet planes ΔS defined as

$$\Delta\mathrm{S} = \arccos\left(\frac{\boldsymbol{p}_1^{\mathrm{di-jet}} \times \boldsymbol{p}_2^{\mathrm{di-jet}}}{|\boldsymbol{p}_1^{\mathrm{di-jet}}||\boldsymbol{p}_2^{\mathrm{di-jet}}|}\right), \tag{4.31}$$

where $\boldsymbol{p}_1$ ($\boldsymbol{p}_2$) is a transverse momentum of the hard (soft) di-jet pair. In addition to the DPS distributions generated with "naive" dPDFs we also plot DPS distributions generated with GS09 dPDFs. We see that DPS dominates over SPS at small and high values of Δ_{12} and at high values of ΔS. The increase of the DPS distributions at small values of Δ_{12} and high values of ΔS is due to the production of two pairs of back-to-back di-jets which is more probable for DPS processes than for SPS processes. The increase of the DPS distributions at high values of Δ_{12} is a jet reconstruction effect. Namely, it means that the jet reconstruction resulted into two collinear jets with high transverse momenta and two softer jets. We also see that both Δ_{12} and ΔS distributions do not demonstrate dependence on the choice of the model of dPDFs strong enough to tell the impact of "naive" dPDFs from the impact of GS09 dPDFs. Therefore, we conclude that the most sensitive to GS09 dPDFs distributions is a distribution in terms of the maximal rapidity difference ΔY, see Fig. 4.13. Later in Chapter 6 we will study the impact of different models of dPDFs on ΔY distributions in more details.

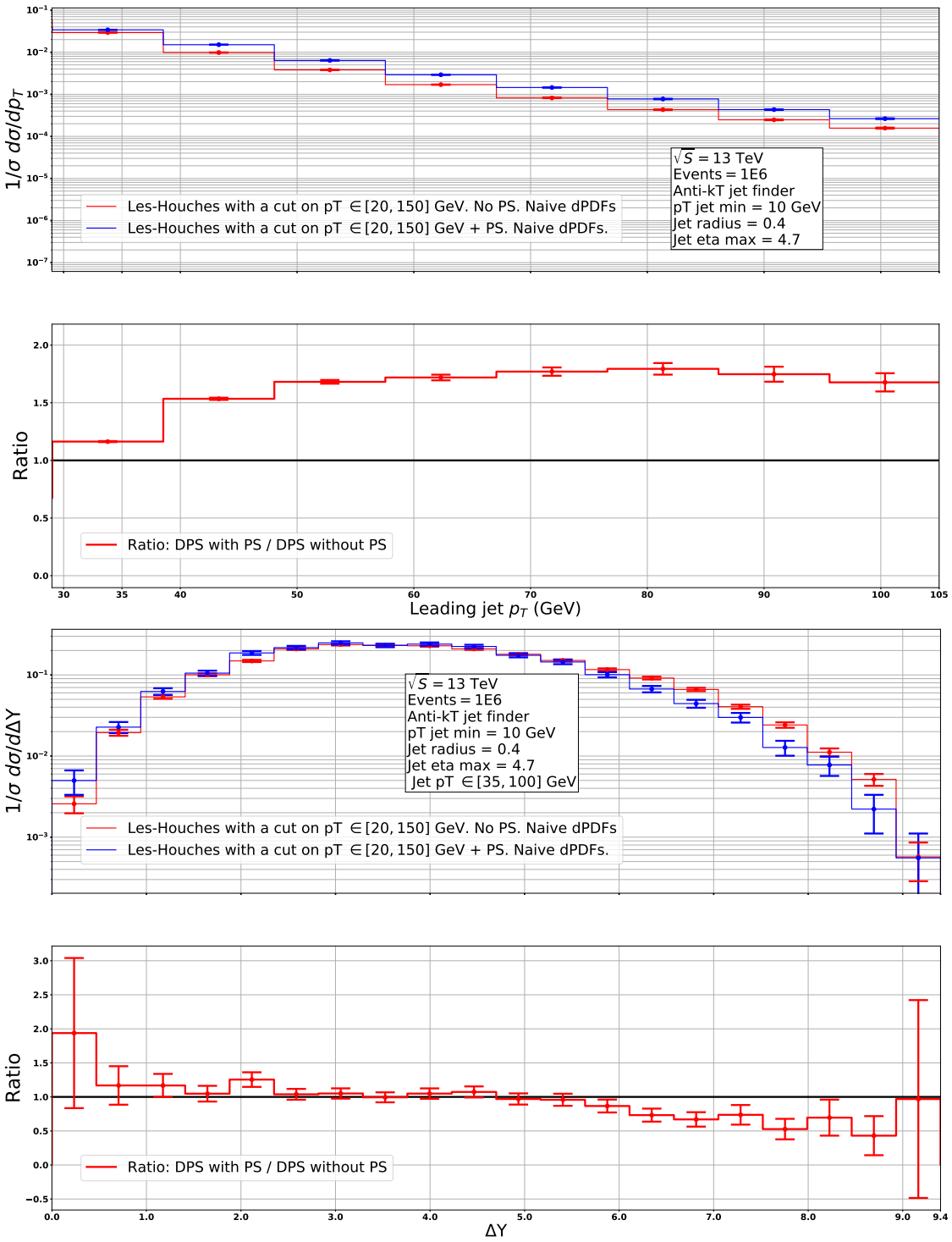

Figure 4.21: Impact of the parton shower on leading jet $p_\perp$ and ΔY DPS distributions. Four-jet DPS simulation performed for the collision energy $\sqrt{S} = 13$ TeV with "naive" dPDFs constructed out of MSTW2008 LO PDFs [298]. Factorization and renormalization scales are equal to $Q_1 = p_{1\perp}$, $Q_2 = p_{2\perp}$, where $p_{1\perp}$ and $p_{2\perp}$ are equal to the absolute value of a jet transverse momentum in a first and second hard processes in a given DPS event. Statistical errors are given by $\sigma_{\mathrm{DPS}}\sqrt{N_{\mathrm{bin}}}/N_{\mathrm{tot}}$ where N_{bin} is a number of events in a given bin, σ_{DPS} is a corresponding DPS cross section and N_{tot} is total number of bin entries for a given histogram. The parton level DPS simulations performed with $p_\perp^{\mathrm{reg}} = 20$ GeV and $p_\perp^{\mathrm{max}} = 150$ GeV.

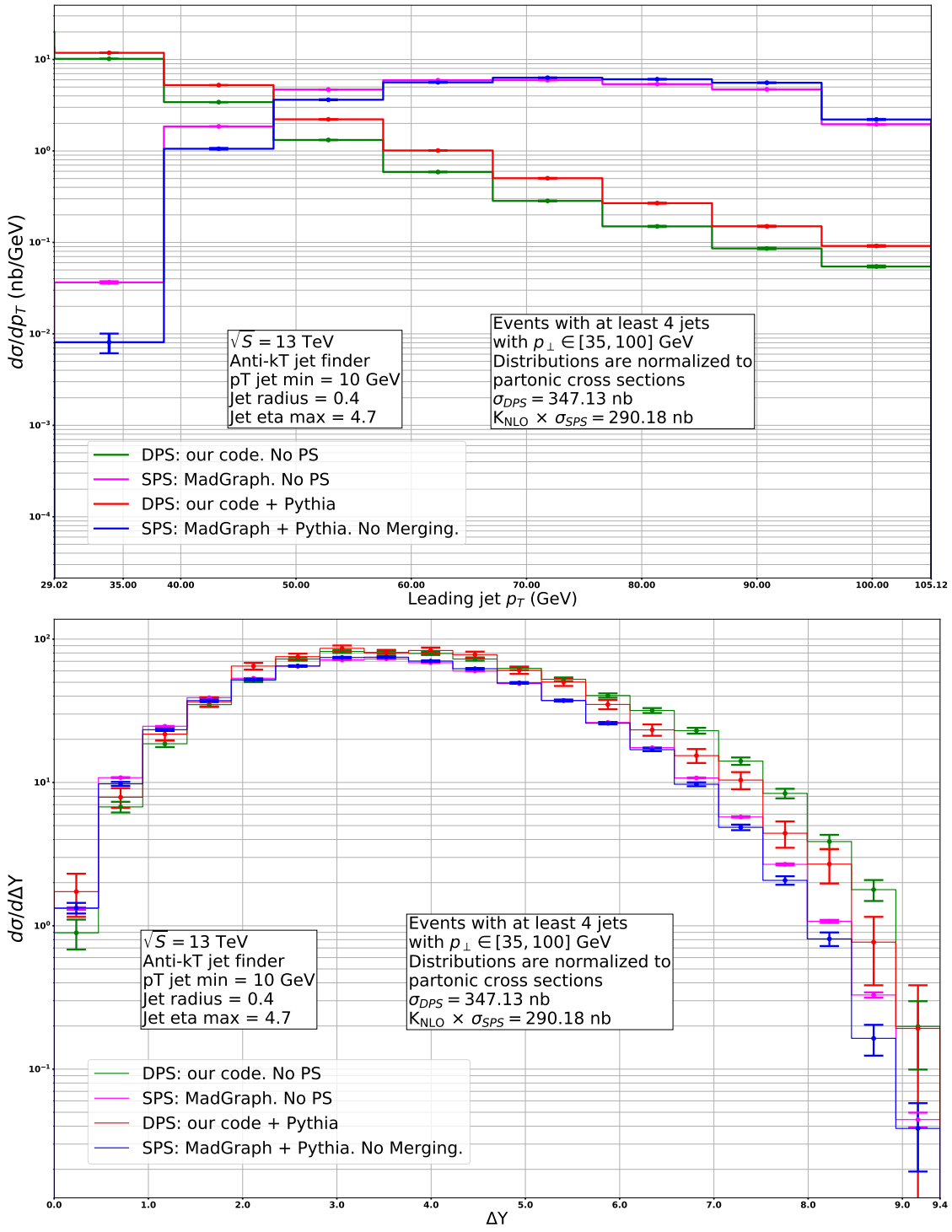

Figure 4.22: Upper panel: comparison between leading jet $p_\perp$ distributions for four-jet SPS and DPS events with and without PS effects. Lower panel: comparison between $\Delta Y = \max|y_i - y_j|$ distributions for four-jet SPS and DPS events with and without PS effects. Collision energy is equal to $\sqrt{S} = 13\,\text{TeV}$. We have selected events with at least four-jets with $p_\perp \in [35, 100]$ GeV and $|y| < 4.7$. Factorization and renormalization scales are equal to $Q_1 = p_{1\perp}$, $Q_2 = p_{2\perp}$, where $p_{1\perp}$ and $p_{2\perp}$ are equal to the absolute value of a jet transverse momentum in a first and second hard processes in a given DPS event. Statistical errors are given by $\sigma_{\text{DPS}}\sqrt{N_{\text{bin}}}/N_{\text{tot}}$ where N_{bin} is a number of events in a given bin, σ_{DPS} is a corresponding DPS cross section and N_{tot} is total number of bin entries for a given histogram. The SPS distributions were multiplied by $\text{K}_{\text{NLO}}^{\text{SPS}} = 0.5$.

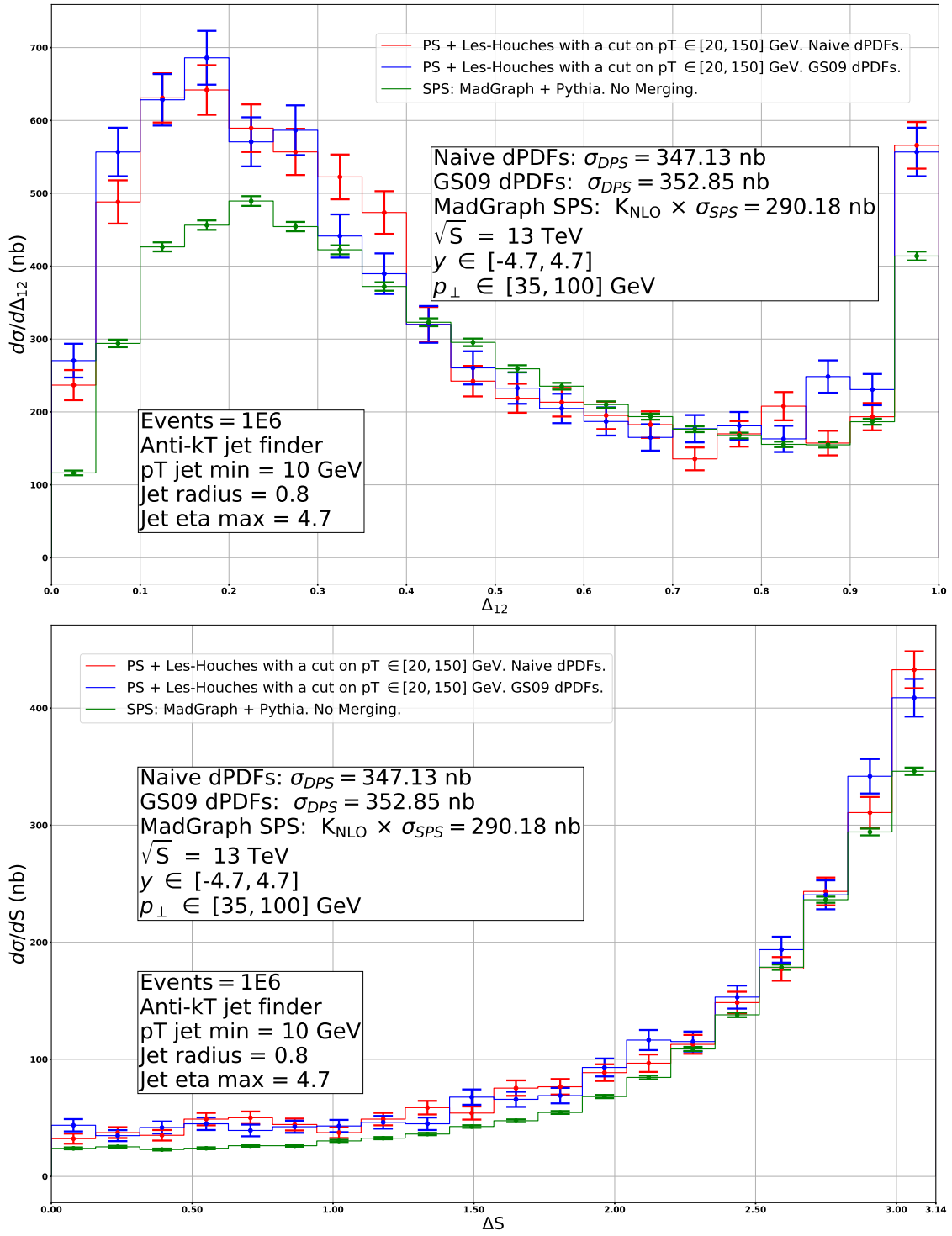

Figure 4.23: Comparison between Δ_{12} and ΔS distributions simulated with "naive" and GS09 dPDFs. Four-jet DPS simulation performed for the collision energy $\sqrt{S} = 13$ TeV with naive dPDFs constructed out of MSTW2008 LO PDFs [298]. Factorization and renormalization scales are equal to $Q_1 = p_{1\perp}$, $Q_2 = p_{2\perp}$, where $p_{1\perp}$ and $p_{2\perp}$ are equal to the absolute value of a jet transverse momentum in a first and second hard processes in a given DPS event. Statistical errors are given by $\sigma_{\rm DPS}\sqrt{N_{\rm bin}}/N_{\rm tot}$ where $N_{\rm bin}$ is a number of events in a given bin, $\sigma_{\rm DPS}$ is a corresponding DPS cross section and $N_{\rm tot}$ is total number of bin entries for a given histogram. The parton level DPS simulations performed with $p_\perp^{\rm reg} = 20$ GeV and $p_\perp^{\rm max} = 150$ GeV. Upper panel: transverse momenta imbalance Δ_{12} of two hardest jets. Lower panel: azimuthal angle between the two di-jet planes ΔS. The SPS distributions were multiplied by $\mathrm{K}_{\rm NLO}^{\rm SPS} = 0.5$.

4.12 Conclusions

In this chapter we have presented results of our phenomenological study of the four-jet DPS production in pp collisions. In particular, we have estimated the impact of the momentum and flavour correlations in the GS09 model on various differential DPS distributions. It was found that the distributions in terms of the maximal rapidity difference $\Delta Y = \max|y_i - y_j|$ produced with GS09 dPDFs significantly differ from the distributions produced with "naive" dPDFs at high values of ΔY. We also discussed how one can incorporate the ISR and FSR effects into our simulations and studied their impact on the various differential distributions, in particular on the leading jet $p_\perp$ and ΔY distributions. The inclusion of the ISR and FSR effects also made it possible to study the impact of the GS09 dPDFs on differential distributions in the DPS-sensitive variables. We have found that the variables based upon transverse momentum of produced jets, *e. g.* transverse momenta imbalance Δ_{ij}, demonstrate mild dependence on the choice of the model of dPDFs. Finally, we performed a comparison of the DPS and SPS distributions similar to the one performed by Maciuła and Szczurek in [234]. Our results agree with the results of [234] at qualitative level, however, we shall note that the absence of information in [234] about many important technical aspects of both DPS and SPS simulations make the exact comparison impossible. In our four-jet analysis we studied the impact of the ISR and FSR effects on our parton-level simulations and found that parton shower effects do not spoil the separation of the DPS and SPS events produced at low-$p_\perp$ or high-ΔY values as it was predicted in [234]. We also should stress that our approach to study the impact of ISR effects on our DPS simulations can be seen only as an approximations since it does not include a correct backward evolution for the "$1v2$" DPS processes. The first results on the modelling of the ISR for "$1v2$" DPS processes were recently reported [211]. The comparison between our DPS simulations and the results of [211] would help to estimate the error due to the approximate modelling of the ISR effects in our simulations.

The observed difference between ΔY distributions simulated with GS09 and "naive" dPDFs clearly requires more detailed investigation. Two potential sources of this difference are dDGLAP evolution effects and partonic correlations in flavour (number). In Chapter 6 we will demonstrate how one can approximately estimate the impact the flavour correlations by comparing the differential distributions produced with GS09 dPDFs against differential distributions produced with the dPDFs modelled by the `Pythia` event generator.

Finally, we argue that our study of the partonic correlations within the GS09 framework should be considered rather as a qualitative identification of the regions of the DPS phase space which can be interesting for further theoretical and experimental studies. Since many different models of partonic correlations [192], [187], [159] [209] predict important contributions at high values of the rapidity separation, the experimental study of the DPS events at high values of ΔY will be able to favour or disfavour some of these models and hence provide new information on the structure of proton.

Chapter 5

Four-jet DPS production in proton-nucleus collisions

5.1 Enhancement of the DPS in proton-nucleus collisions

Here we summarize first phenomenological studies of different DPS contributions to a total DPS cross section in pA collisions performed by Strikman and Treleani [213] and by Del Fabbro and Treleani [214]. Historically, these were the first papers where enhancement of a total DPS cross section was studied in detail. Later, the concepts established in [213], [214] got further developed by Blok *et al.* in [216]. In Ref. [213] Treleani and Strikman considered two different DPS processes, shown in Fig. 5.1 a), b). The process in Fig. 5.1 a) is a generalization of the "standard" "2v2" DPS process in pp collisions to pA collisions. The process shown in Fig. 5.1 b), however, is new and corresponds to the situation when the DPS occurs between one incident proton and *two different nucleons* which are located within the same impact-parameter distance. In this section we will give a short introduction to the formalism proposed by Treleani and Strikman in [213]. In the following we will refer to the DPS processes shown in Fig. 5.1 a), b) as DPS I and DPS II processes, correspondingly.

Since the DPS I and DPS II contributions involve different number of nucleons it is quite natural to expect a different dependence of the corresponding total cross sections on the atomic mass number A[1]. In 2001 Strikman and Treleani have published pioneering paper [213] where the expressions for the total cross sections for DPS I and DPS II processes were derived for the first time. Within their model a total DPS cross section for pA collisions, assuming no interference between DPS I and DPS II processes, is written as a sum of two terms

$$\sigma_{\mathrm{pA}}^{\mathrm{DPS}} = \sigma_{\mathrm{I}}^{\mathrm{DPS}} + \sigma_{\mathrm{II}}^{\mathrm{DPS}}, \tag{5.1}$$

where $\sigma_{\mathrm{I}}^{\mathrm{DPS}}$ is expressed, neglecting the difference between proton and neutron, in terms of a total

[1]To the best of our knowledge, a similar, but somewhat different, assumption was first made by C. Goebel, F. Halzen and D. M. Scott in 1980 [114]. Namely, it was postulated that total cross sections for DPS and "standard" QCD processes in pA collision will have a different A-dependence. However, no distinction between DPS I and DPS II contributions was made and corresponding expressions for total cross sections were not provided.

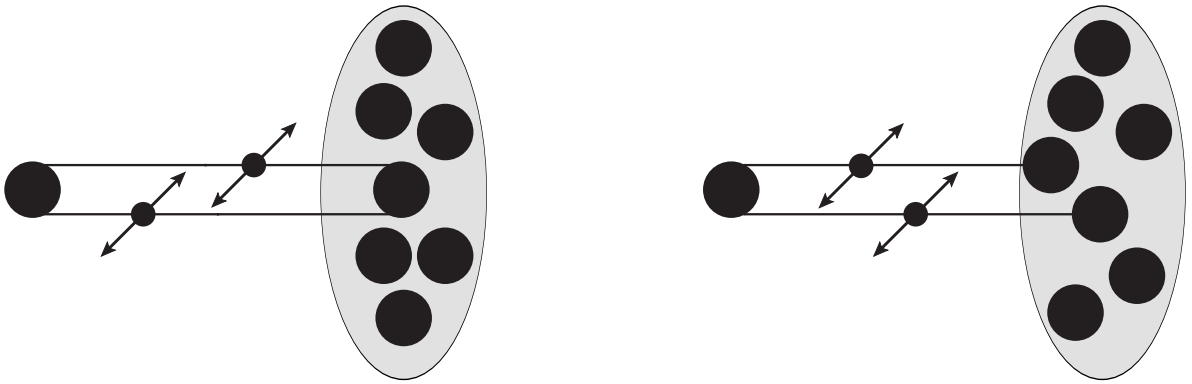

a) b)

Figure 5.1: Schematic representation of some possible DPS processes in pA collision: a) DPS occur between one incident proton and one nucleon. b) DPS occur between one incident proton and two different nucleons.

DPS cross section for pp collisions as

$$\sigma_{\mathrm{I}}^{\mathrm{DPS}} = \mathrm{A}\,\sigma_{\mathrm{pp}}^{\mathrm{DPS}} = \frac{\mathrm{A}}{1+\delta_{ab}}\frac{\sigma_a \sigma_b}{\sigma_{eff}}, \tag{5.2}$$

where σ_{eff} is an effective transverse interaction area of a proton. We use $1+\delta_{ab}$ in the denominator in order to reflect the fact that one has to divide the total cross section by 2 for production of two indistinguishable final states. We see that $\sigma_{\mathrm{I}}^{\mathrm{DPS}}$ scales simply as a total number of nucleons A. The DPS II contribution, however, scales differently. The expression for $\sigma_{\mathrm{II}}^{\mathrm{DPS}}$ was found to be equal to

$$\sigma_{\mathrm{II}}^{\mathrm{DPS}} = \frac{1}{1+\delta_{ab}}\frac{\mathrm{A}-1}{\mathrm{A}}\sigma_a\sigma_b \int d^2s\, \mathrm{T}_{\mathrm{A}}^2(\mathbf{s}) = \frac{1}{1+\delta_{ab}}\sigma_a\sigma_b\,\mathrm{F}_{\mathrm{pA}}, \tag{5.3}$$

where we defined

$$\mathrm{F}_{\mathrm{pA}} = \frac{\mathrm{A}-1}{\mathrm{A}} \int d^2s\, \mathrm{T}_{\mathrm{A}}^2(\mathbf{s}) \tag{5.4}$$

and the factor $(\mathrm{A}-1)/\mathrm{A}$ is a number of possible nucleon pairs $\mathrm{A}(\mathrm{A}-1)$ divided by the factor A^2 which comes from the normalization of single nucleon density functions[2], see Chapter 2.6 Eq. 2.107 and Eq. 2.125. The function T_{A} is defined as

$$\mathrm{T}_{\mathrm{A}}(\mathbf{s}) = \int dz\, \rho_{\mathrm{A}}(\mathbf{s}, z), \tag{5.5}$$

where $\rho_{\mathrm{A}}(r)$ obeys a standard normalization condition

$$\int d^3r\, \rho_{\mathrm{A}}(r) = \mathrm{A}. \tag{5.6}$$

Note that only the DPS I contribution depends on σ_{eff} which, in turn, is sensitive to the partonic correlations in a transverse plane of a hadron, see [215], [148] - [158] and the review [161].

[2]The factor $(A-1)/A$ was absent in the original publication of Strikman and Treleani [213]. It was also absent in the paper of Del Fabbro and Treleani [214] which followed [213]. To the best of our knowledge, this factor appears first in the paper of Frankfurt *et al.* [215] and a detailed derivation was later given in the paper of Blok *et al.* [216].

Combining the DPS I and DPS II contributions together one can write Eq. 5.1 as

$$\sigma_{\mathrm{pA}}^{\mathrm{DPS}} = \sigma_{\mathrm{pp}}^{\mathrm{DPS}} \left(\mathrm{A} + \sigma_{eff} \mathrm{F_{pA}}\right). \tag{5.7}$$

We see that within the approach of Strikman & Treleani one can express the difference between $\sigma_{\mathrm{pp}}^{\mathrm{DPS}}$ and $\sigma_{\mathrm{pA}}^{\mathrm{DPS}}$ solely in terms of a geometrical quantity $\mathrm{T_A}(\mathbf{s})$ which, in turn, depends on a distribution of matter in a given nucleus. In order to perform numerical evaluations with this formula one has to specify the nuclear matter density function ρ_A which we choose to have the shape of the Woods-Saxon potential[3]

$$\rho_{\mathrm{A}}(r) = \rho_0 \frac{1 + \omega \left(r/R_{\mathrm{A}}\right)^2}{1 + \exp\left[(r - R_{\mathrm{A}})/a\right]}, \tag{5.8}$$

where R_{A} is a nuclear radius, a is a length representing the "thickness" of the nuclear surface, ω describes deviation from a spherical form and a value of ρ_0 is fixed by the normalization condition in Eq. 5.6. In the case of a spherical nucleus the Woods-Saxon nuclear matter density function reduces to the Fermi distribution

$$\rho_{\mathrm{A}}(r) = \frac{\rho_0}{1 + \exp\left[(r - R_{\mathrm{A}})/a\right]}. \tag{5.9}$$

For our computations within Strikman & Treleani framework we use values of parameters in Eq. 5.9 as implemented in the GLISSANDO 2 code [219]. Namely, for nuclei with mass numbers in the range $4 \leq \mathrm{A} \leq 208$ we use Eq. 5.9 with

$$R_{\mathrm{A}} = \left[1.10\mathrm{A}^{1/3} - 0.656\mathrm{A}^{-1/3}\right] \text{ fm}, \; a = 0.459\,\text{fm}, \tag{5.10}$$

which corresponds to spherical nuclei with a nucleon-nucleon (NN) repulsion distance equal to $d = 0.9\,\text{fm}$ [219].

Now we can evaluate $\mathrm{A} + \sigma_{eff}\mathrm{F_{pA}}$. In order to do that we evaluate $\mathrm{F_{pA}}$ according to Eq. 5.4 using the parametrization of the nuclear matter density given by Eq. 5.9 and Eq. 5.10. The numerical integration in Eq. 5.4 is performed by means of the GSL [294] library. In order to illustrate the dependence of the total DPS cross section on σ_{eff} we vary σ_{eff} in between 10 mb and 20 mb which agrees with most experimental studies of the four-jet DPS production, see Fig. 2.3. In Fig. 5.2 we plot the ratio $\sigma_{\mathrm{pA}}^{\mathrm{DPS}}/\mathrm{A}\,\sigma_{\mathrm{pp}}^{\mathrm{DPS}} = 1 + \frac{1}{\mathrm{A}}\,\sigma_{eff}\mathrm{F_{pA}}$ as a function of A. In the absence of the second term in Eq. 5.1 this ratio would always be equal to unity. However, we see that a total DPS cross section for heavy nuclei in pA collisions is about 3A times bigger as the corresponding DPS cross section in pp case. We also see that the variation of σ_{eff} leads to significant changes in the behaviour of $\sigma_{\mathrm{pA}}^{\mathrm{DPS}}/\mathrm{A}\,\sigma_{\mathrm{pp}}^{\mathrm{DPS}}$. Such numerical estimates were first made in [213] and the enhancement $\sim$ 3A was later given in [214] - [223].

[3]More precisely, Woods and Saxon used complex potential with real and imaginary components written as in Eq. 5.9 but with different values of ρ_0. Such potential was used to compute the differential cross section for elastic scattering of protons by medium and heavy nuclei, see [218].

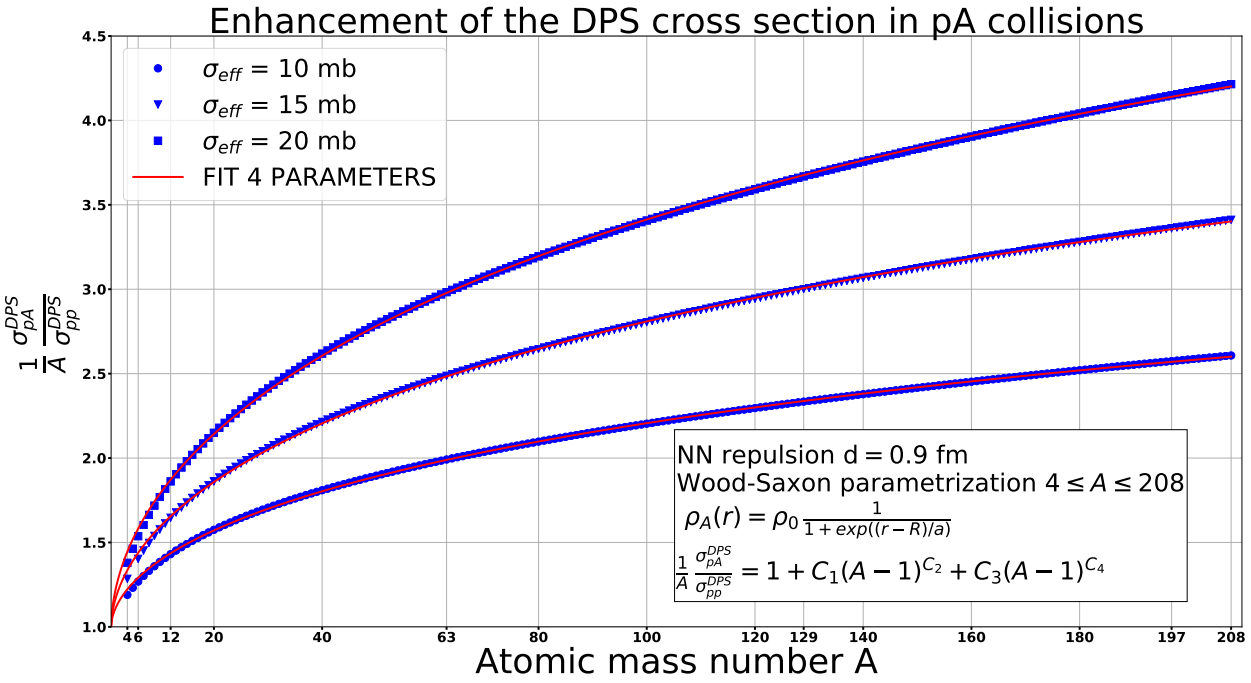

Figure 5.2: Enhancement of the $\sigma_{\mathrm{pA}}^{\mathrm{DPS}}$ with respect to $\sigma_{\mathrm{pp}}^{\mathrm{DPS}}$ normalized according to the atomic mass number A. Wood-Saxon (Fermi) form of the nuclear matter distribution $\rho_{\mathrm{A}}(r)$ with parameters taken from [219].

It is handy to approximate a behaviour of the DPS enhancement factor $\sigma_{\mathrm{pA}}^{\mathrm{DPS}}/\mathrm{A}\,\sigma_{\mathrm{pp}}^{\mathrm{DPS}}$ as

$$\frac{1}{\mathrm{A}}\frac{\sigma_{\mathrm{pA}}^{\mathrm{DPS}}}{\sigma_{\mathrm{pp}}^{\mathrm{DPS}}} = 1 + C_1(\mathrm{A}-1)^{C_2} + C_3(\mathrm{A}-1)^{C_4}, \tag{5.11}$$

where the second term was added to correctly describe enhancement for heavy nuclei and coefficients C_1-C_4 can be identified by a fitting Eq. 5.11 to our simulations, as it is shown in Fig. 5.2. This fitting may look somewhat superfluous, since computations within Strikman & Treleani approach are not time consuming, however, its advantage will become clear in Chapter 7 where we compare predictions of Strikman & Treleani model and Monte Carlo simulations performed with the `Pythia` event generator.

It is important to emphasize that, in principle, the different A-dependence of the two terms in Eq. 5.7 allows to distinguish between them experimentally, as it was proposed in [213]. Moreover, the DPS II contribution does not involve σ_{eff} and hence does not depend on the partonic correlations in the transverse plane of an incident proton. Therefore, a combined study of DPS processes in both pp and pA collisions can be used to disentangle different sources of partonic correlations and to answer the question if they are predominantly of longitudinal or transverse nature [213].

5.2 Generation of DPS events in pA collisions

Let us demonstrate how one can extend the analysis of the four-jet DPS production from Chapter 4 to the pA collision using the framework of Strikman & Treleani [213]. First of all we shall note that, in general, the two terms in Eq. 5.1 correspond to integration over different x-regions and thus a factorized form of a total DPS cross section given in Eq. 5.7 violates conservation of a longitudinal

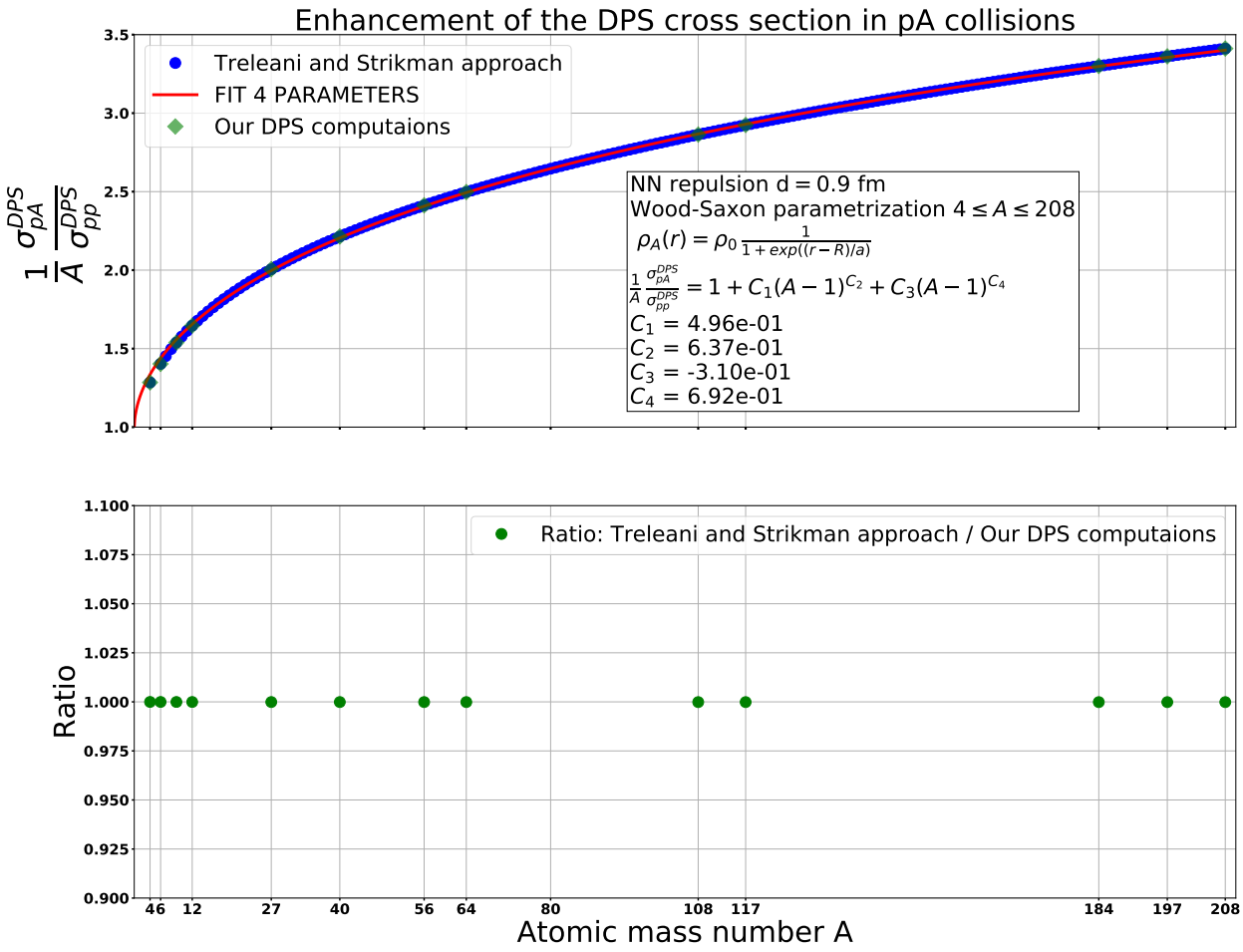

Figure 5.3: Enhancement of the $\sigma_{\rm pA}^{\rm DPS}$ with respect to $\sigma_{\rm pp}^{\rm DPS}$ normalized according to the atomic mass number A evaluated with Eq. 5.7 (blue dots) and Eq. 5.14, Eq. 5.15 (green diamonds). Wood-Saxon form of the nuclear matter distribution $\rho_A(r)$ with parameters taken from [219]. Collision energy $\sqrt{S_{NN}} = 5.02$ TeV, with cuts on final sate partons $p_\perp \in [35, 100]$ GeV and $|y_i| < 4.7$. Here we have used "naive" dPDFs constructed out of MSTW2008 LO PDFs.

momentum. It becomes clear if one writes down corresponding differential cross sections

$$\sigma_{\rm I}^{\rm DPS} = \frac{\rm A}{\sigma_{eff}} \sum_{a_1,a_2,b_1,b_2} \int \prod_{i=1}^{4} dx_i \, D_{a_1,a_2/p}(x_1,x_2) \, D_{b_1,b_2/p}(x_3,x_4) \, \hat{\sigma}_{a_1,b_1} \, \hat{\sigma}_{a_2,b_2}, \tag{5.12}$$

$$\sigma_{\rm II}^{\rm DPS} = {\rm F_{pA}} \sum_{a_1,a_2,b_1,b_2} \int \prod_{i=1}^{4} dx_i \, D_{a_1,a_2/p}(x_1,x_2) \, f_{b_1/p}(x_3) \, f_{b_2/p}(x_4) \, \hat{\sigma}_{a_1,b_1} \, \hat{\sigma}_{a_2,b_2}, \tag{5.13}$$

where $f_{i/p}(x_1)$ are standard collinear PDFs, $D_{i,j/p}(x_1,x_2)$ are dPDFs as in Eq. 4.1 and we have omitted factorization scale dependence for brevity's sake. Also, in order not to overload our notation, we omitted final state labels A and B for the partonic processes $a_1\, b_1 \to A$ and $a_2\, b_2 \to B$ as well as the corresponding symmetry factor $1/\left(1+\delta_{AB}\right)$. Assuming no correlations in x-space, Eq. 5.12

and Eq. 5.13 can be written as

$$\begin{aligned}\sigma_{\rm I}^{\rm DPS} &= \frac{\rm A}{\sigma_{eff}} \sum_{a_1,a_2,b_1,b_2} \int \prod_{i=1}^{4} dx_i \, f_{a_1/p}(x_1) \, f_{a_2/p}(x_2) \, f_{b_1/p}(x_3) \, f_{b_2/p}(x_4) \, \times \\ &\times \; \theta(1-x_1-x_2)\,\theta(1-x_3-x_4)\,\hat{\sigma}_{a_1,b_1}\,\hat{\sigma}_{a_2,b_2}, \qquad (5.14)\\ \sigma_{\rm II}^{\rm DPS} &= {\rm F_{pA}} \sum_{a_1,a_2,b_1,b_2} \int \prod_{i=1}^{4} dx_i \, f_{a_1/p}(x_1) \, f_{a_2/p}(x_2) \, f_{b_1/p}(x_3) \, f_{b_2/p}(x_4) \, \times \\ &\times \; \theta(1-x_1-x_2)\,\theta(x_3)\,\theta(x_4)\,\hat{\sigma}_{a_1,b_1}\,\hat{\sigma}_{a_2,b_2}. \qquad (5.15)\end{aligned}$$

We see that different kinematic constraints on Bjorken variables in Eq. 5.14 and Eq. 5.15 lead to different integration regions which does not let us to write a total DPS cross section as in Eq. 5.7. However, as it was argued in [213] the difference between two integrands in Eq. 5.14 and Eq. 5.15 should become relevant only for large x'es where dPDFs have relatively small values and, therefore, their impact on a total DPS cross section is negligible. In order to check it, in Fig. 5.3 we show a comparison between the enhancement factor $\sigma_{\rm pA}^{\rm DPS}/{\rm A}\,\sigma_{\rm pp}^{\rm DPS}$ evaluated with approximated expression as in Eq. 5.7 and the exact expressions given by Eq. 5.14 and Eq. 5.15. One can see that the difference between both approaches is negligible.

In order to estimate the difference between the differential distributions corresponding to the DPS I and DPS II contributions we have implemented Eq. 5.14 and Eq. 5.15 into the code we developed to study the four-jet DPS production in pp collisions. The factor ${\rm F_{pA}}$ in Eq. 5.15 is evaluated as described in section 5.1. For this check we study the ΔY DPS distributions since, as it was argued in Chapter 4, the DPS production of four jets at high values of ΔY involves two low-x and two high-x partons and, therefore, ΔY DPS distributions can be sensitive to the different kinematic constraints in Eq. 5.14 and Eq. 5.15. The results of our simulations are shown in Fig. 5.4 where we plot DPS I and DPS II ΔY distributions normalized to unity. We see that both DPS I and DPS II histograms have the same profiles within the statistical errors. It implies that even at very high accuracy one can use the relation between $\sigma_{\rm pA}^{\rm DPS}$ and $\sigma_{\rm pp}^{\rm DPS}$ proposed by Treleani and Strikman, Eq. 5.7, to relate four-jet DPS production in pp collisions and four-jet DPS production in pA collisions.

In Fig. 5.5 we show our DPS and SPS simulations of the four-jet DPS production in pPb collisions within the framework of Treleani and Strikman. We have used the same set of cuts as in Chapter 4. The SPS distributions for pPb collisions were obtained by multiplying corresponding pp SPS distribution by the atomic mass number of ^{208}Pb. The DPS distributions for pPb collisions were obtained by multiplying the corresponding pp DPS distributions by the enhancement factor as in Eq. 5.7. The simulations presented in Fig. 5.5 were performed in the center of mass of the proton-nucleon reference frame. In order to account for NLO effects in our SPS simulations we use ${\rm K_{NLO}^{SPS}} = 0.5$, see Chapter 4.8.

Let us compare DPS and SPS distributions generated for pp collisions at $\sqrt{S} = 7$ TeV shown in Fig. 4.11 against DPS and SPS distributions for pA collisions at $\sqrt{S} = 5.02$ TeV shown in Fig. 5.5. Both distributions were generated for jets with $p_\perp \in [35, 100]$ GeV and $|y| < 4.7$. We see that the fraction of DPS events in the total (DPS + SPS) four-jet cross section for pA collisions at $\sqrt{S} = 5.02$ TeV is equal to 62% against 40% for the pp collisions shown in Fig. 4.11 and Table 4.3. By comparing Fig. 4.11 and Fig. 5.5 we also see that DPS and SPS distributions are better separated

for the pA collisions at $\sqrt{S} = 5.02$ TeV than for pp collisions at $\sqrt{S} = 7$ TeV. These effects are due to the enhancement of the DPS cross section in pA collisions in Strikman & Treleani model. The enhancement factor for ^{208}Pb is almost 3.5A, as shown in Fig. 5.3, which strongly affects the ratio $\sigma_{\rm pA}^{\rm DPS} \Big/ \left(\sigma_{\rm pA}^{\rm SPS} + \sigma_{\rm pA}^{\rm DPS}\right)$ and leads to increase of the fraction of the DPS cross section.

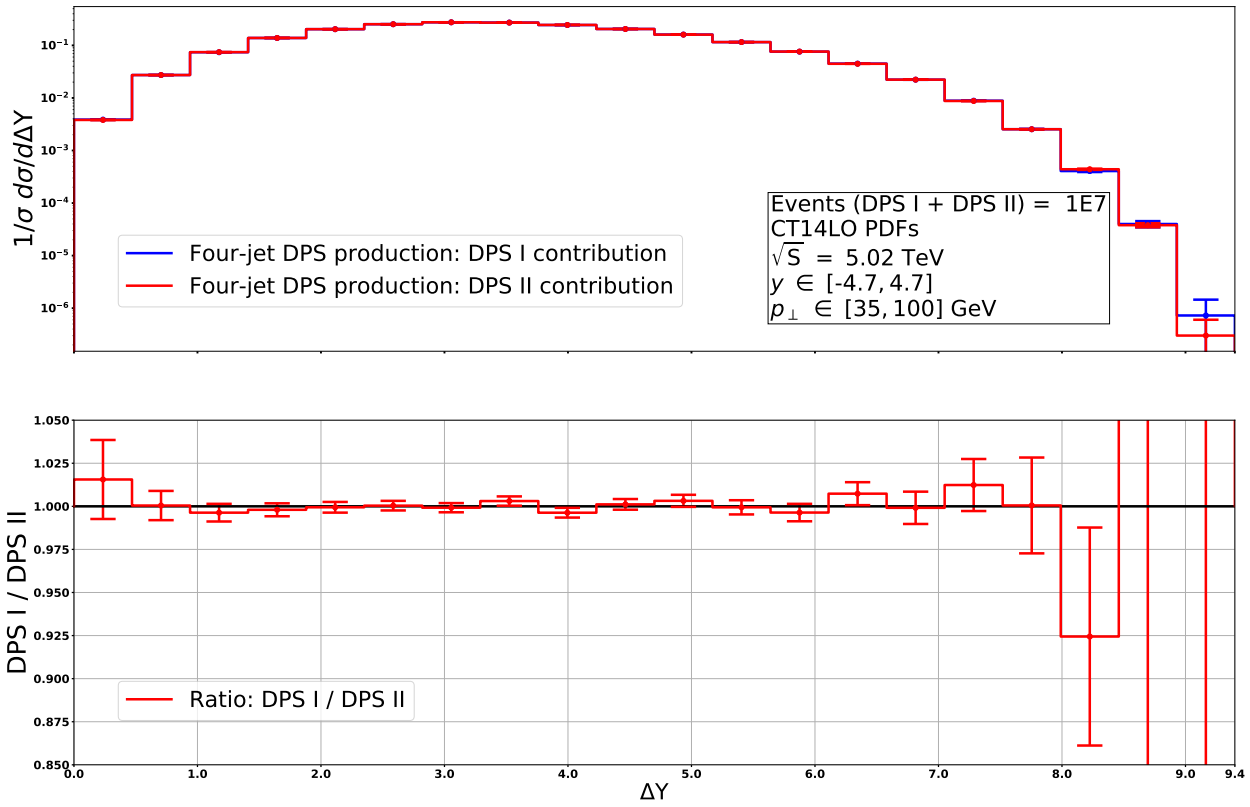

Figure 5.4: Comparison between distributions for the $\sigma_{\rm I}^{\rm DPS}$ and $\sigma_{\rm II}^{\rm DPS}$ contributions. Collision energy $\sqrt{S_{NN}} = 5.02$ TeV, with cuts on final sate partons $p_\perp \in [35, 100]$ GeV and $|y_i| < 4.7$. Here we have used naive dPDFs constructed out of CT14LO PDFs [299]. Factorization and renormalization scales are equal to $Q_1 = p_{1\perp}$, $Q_2 = p_{2\perp}$, where $p_{1\perp}$ and $p_{2\perp}$ are equal to the absolute value of a jet transverse momentum in a first and second hard processes in a given DPS event. Statistical errors are given by $\sigma_{\rm DPS}\sqrt{N_{\rm bin}}/N_{\rm tot}$ where $N_{\rm bin}$ is a number of events in a given bin, $\sigma_{\rm DPS}$ is a corresponding DPS cross section and $N_{\rm tot}$ is total number of bin entries for a given histogram. Simulated for ^{208}Pb nucleus. All distributions are normalized to unity.

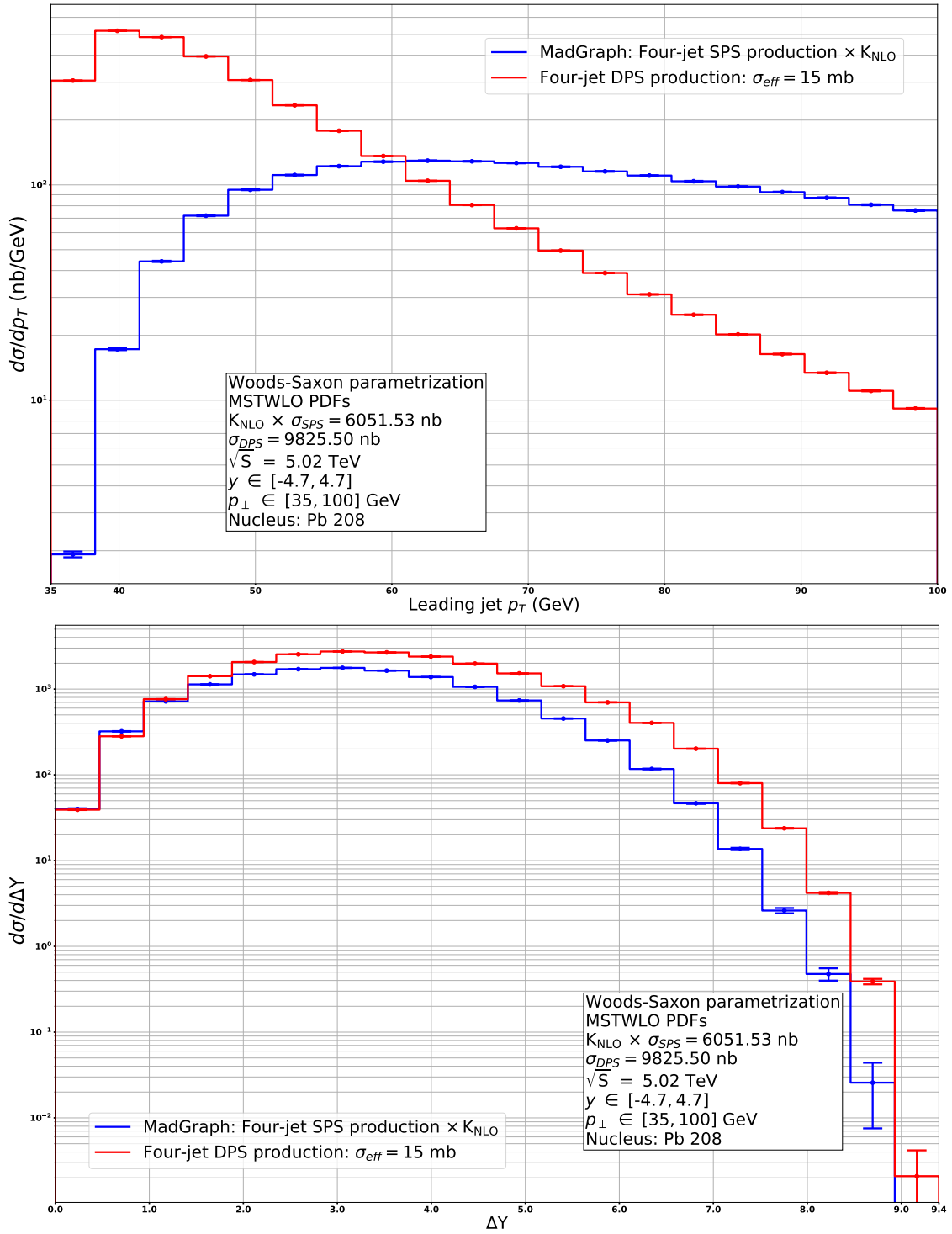

Figure 5.5: DPS in pA collisions within the framework of Treleani and Strikman. Upper panel: comparison between leading jet $p_\perp$ distributions for four-jet SPS and DPS events with included parton shower effects. Lower panel: comparison between $\Delta Y = \max|y_i - y_j|$ distributions for four-jet SPS and DPS events with included parton shower effects. Collision energy is equal to $\sqrt{S_{NN}} = 5.02\,\text{TeV}$. We have selected events with at least four-jets with $p_\perp \in [35, 100]$ GeV and $|y| < 4.7$. Factorization and renormalization scales are equal to $Q_1 = p_{1\perp}$, $Q_2 = p_{2\perp}$, where $p_{1\perp}$ and $p_{2\perp}$ are equal to the absolute value of a jet transverse momentum in a first and second hard processes in a given DPS event. Statistical errors are given by $\sigma_{\text{DPS}}\sqrt{N_{\text{bin}}}/N_{\text{tot}}$ where N_{bin} is a number of events in a given bin, σ_{DPS} is a corresponding DPS cross section and N_{tot} is total number of bin entries for a given histogram. The SPS distributions were multiplied by $\text{K}_{\text{NLO}}^{\text{SPS}} = 0.5$.

5.3 Impact of the nuclear PDFs

In section 5.2 we have discussed how one can extend the simulation of the four-jet DPS production from pp to pA collisions according to the framework of Strikman & Treleani [213]. However, in section 5.2, in order to simulate pA events according to Eq. 5.14 and Eq. 5.15, we have used standard proton PDFs. The *nuclear parton distribution functions* (nPDFs), in general, may strongly differ from proton PDFs due to the *cold nuclear matter* (CNM) effects. A common approach to parametrize these effects is to introduce so called *nuclear modification factors*

$$R_i^A(x, Q^2) = \frac{f_{i/A}(x, Q^2)}{f_{i/p}(x, Q^2)}. \tag{5.16}$$

The schematic dependence of the nuclear modification factor $R_i^A(x, Q^2)$ on the Bjorken-x is shown in Fig. 5.6.

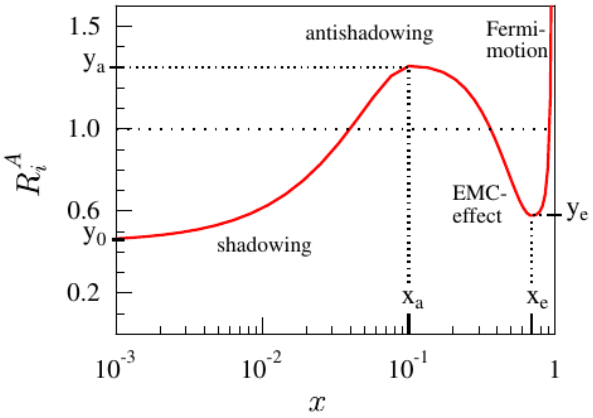

Figure 5.6: Schematic picture of the nuclear modification factor $R_i^A(x, Q^2)$ as a function of Bjorken-x, from [107].

In order to estimate the impact of the nPDFs on our DPS simulations one could, for example, use Eq. 5.14 and Eq. 5.15 with a certain set of nPDFs or reweight the DPS distributions for pp collisions with the nuclear modification factor as in Eq. 5.16. However, before doing that, several important comments need to be made.

For our simulations in section 5.2 as well as for simulations in Chapter 4 we were using LO PDFs together with LO partonic cross section as required by factorization theorem, see Chapter 1.4. Since nuclear PDFs are less constrained by experimental measurements than proton PDFs we would like to use a recent set of nuclear PDFs constrained by most of the available data[4] for which the associated proton PDFs are also available. The two most recent sets of nPDFs are CTEQ15 [300] and EPPS16 [301] NLO nPDFs. The comparison between both sets is shown in Fig. 5.7. We see that both sets within their uncertainties bands agree with each other. Therefore, in order to estimate the overall impact of nPDFs on our DPS simulations, we will work with one particular set of nPDFs which we choose to be CTEQ15 [300]. However, before presenting our simulations of DPS in pA collisions with CTEQ15 PDFs, we want to estimate the impact due to using of NLO PDFs with LO partonic cross sections on our analysis. In Table 5.1 we list the four-jet DPS cross sections

[4]The review of the state-of-the-art of nPDFs is given in [302].

evaluated with the "naive" dPDFs constructed as in Eq. 4.3 out of different sets of single PDFs. We see that the difference between the DPS cross sections evaluated with MSTW2008 [298] and CT14 [299] LO PDFs is about 95%. The strong difference between DPS cross section evaluated with different sets of LO PDFs is due to the fact that the LO gluon PDFs are not well constrained. As shown in Fig. 4.2 the main contribution to the total four-jet DPS cross section comes from the DPS processes involving $gg \to qq$ and $qg \to qg$ LO QCD processes which leads to strong discrepancies between predictions made with different LO sets[5]. We also see that the difference between the DPS cross sections evaluated with CT14 LO and CT14 NLO [299] PDFs is about 4%. Furthermore, we see that the difference between total DPS cross sections evaluated with CT14 NLO and CTEQ15 NLO proton PDFs is about 2%.

Since we are interested in impact of nPDFs on differential DPS distributions we also have to estimate the impact due to the usage of NLO PDFs with LO partonic cross sections on differential DPS distributions. In the upper panel of Fig. 5.8 we compare the distributions of the four-jet DPS events in terms of the maximal rapidity difference ΔY. We have generated DPS events according to Eq. 5.14 and Eq. 5.15 for three different "naive" dPDFs constructed out of CT14 LO, CT14 NLO and CT15 NLO (proton) PDFs according to Eq. 4.3. The simulations presented in Fig. 5.8 were performed in the center of mass of the proton-nucleon reference frame. We see that the difference between distributions generated with CT14 LO and CT14 NLO sets grows with the value of ΔY and can reach about 60% for large values of ΔY. We also see that the difference between DPS distributions generated with CT14 NLO and CTEQ15 NLO (proton) sets may reach about 20% difference for large values of ΔY. The statistical errors for the distribution shown in Fig. 5.8 were estimated separately for the distributions generated with Eq. 5.14 (DPS I distribution) and Eq. 5.15 (DPS II distribution) as $\sigma_{\mathrm{DPS}}\sqrt{N_{\mathrm{bin}}}/N_{\mathrm{tot}}$ where N_{bin} is a number of events in a given bin, σ_{DPS} is a corresponding cross section and N_{tot} is a total number of bin entries for a given histogram. The error δ_{DPS} for the combined distributions shown in Fig. 5.8 was estimated as

$$\delta_{\mathrm{DPS}} = \frac{\sigma^{\mathrm{pA}}_{\mathrm{DPS}}}{N^{\mathrm{pA}}_{\mathrm{tot}}}\sqrt{\left(\delta_{\mathrm{DPS\,I}}\right)^2 + \left(\delta_{\mathrm{DPS\,II}}\right)^2}, \tag{5.17}$$

where $\sigma^{\mathrm{pA}}_{\mathrm{DPS}}$ is a total DPS cross section (DPS I + DPS II) in pA collisions, $N^{\mathrm{pA}}_{\mathrm{tot}}$ is a total number of generated events, $\delta_{\mathrm{DPS\,I}}$ and $\delta_{\mathrm{DPS\,II}}$ are statistical errors for DPS I and DPS II distributions correspondingly.

[5]We shall stress that these discrepancies do not cancel results of our DPS simulations with LO PDFs since they were performed in a consistent way, as it is required by factorization theorem. However, the large uncertainties due to the badly constrained LO gluon PDFs clearly indicate necessity of consistent NLO DPS computations. Recently a significant progress in development of a consistent theoretical framework for NLO DPS computations was made, see [177], [200] and [210]. However, a phenomenological application of results from [177], [200] and [210] is yet to be done.

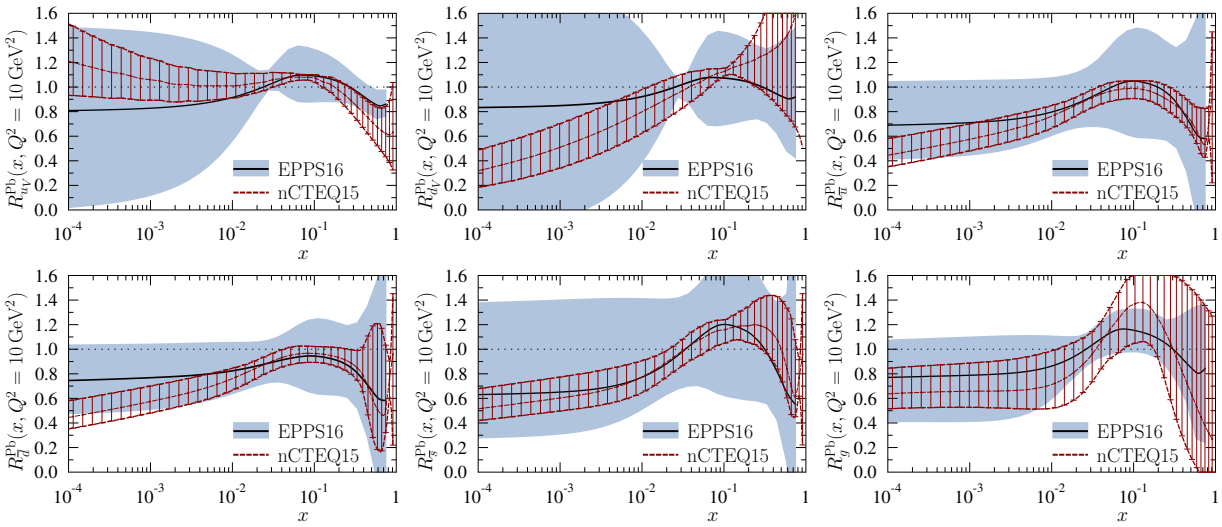

Figure 5.7: Nuclear modification factor $R_i^A(x, Q^2)$ as a function of Bjorken-x evaluated with CTEQ15 [300] and EPPS16 [301]. The plot is taken from [301].

PDF set	MSTW2008 LO	CT14 LO	CT14 NLO	CTEQ15 NLO (proton)
$\sigma_{\rm DPS}$ $\sqrt{S_{NN}} = 5.02\,\text{TeV}$ $Q_1 = p_{1\perp}$, $Q_2 = p_{2\perp}$ $p_\perp \in [35, 100]$ $\lvert y\rvert < 4.7$	9825.50 nb	5028.03 nb	5231.89 nb	5131.30 nb

Table 5.1: Total DPS cross sections for the four-jet DPS production in pA collisions evaluated with different LO and NLO PDFs according to the approach of Strikman & Treleani.

After studying the impact of the different sets of proton PDFs on the Monte Carlo simulations of the four-jet DPS production in the framework of Strikman & Treleani we estimate the overall impact of the CNM effects encapsulated in nPDFs. In order to do that we reweight the DPS generated with CTEQ15 NLO proton PDFs using the nuclear modification factor $R_i^A(x, Q^2)$ evaluated as the ratio of CTEQ 15 NLO nPDFs to the corresponding CTEQ 15 NLO proton PDFs. The results are given in the lower panel of Fig. 5.8. We see that the distributions generated with CTEQ15 NLO proton PDFs and the reweighted distributions demonstrate about 20% of difference at large values of ΔY. However, as we have discussed before, the difference between CT14 NLO and CTEQ15 (proton) NLO PDFs at the large values of ΔY is of the same order of magnitude, compare upper and lower plots in Fig. 5.8. Moreover, the comparison between DPS cross sections evaluated with proton and nuclear CTEQ15 PDFs shows about 2% difference which means that the impact of CTEQ15 nPDFs on the DPS cross section is the same as the impact due to the usage of different NLO PDFs, see Table 5.1. Therefore, we conclude that the impact of nuclear PDFs on our simulations of four-jet DPS production is very modest.

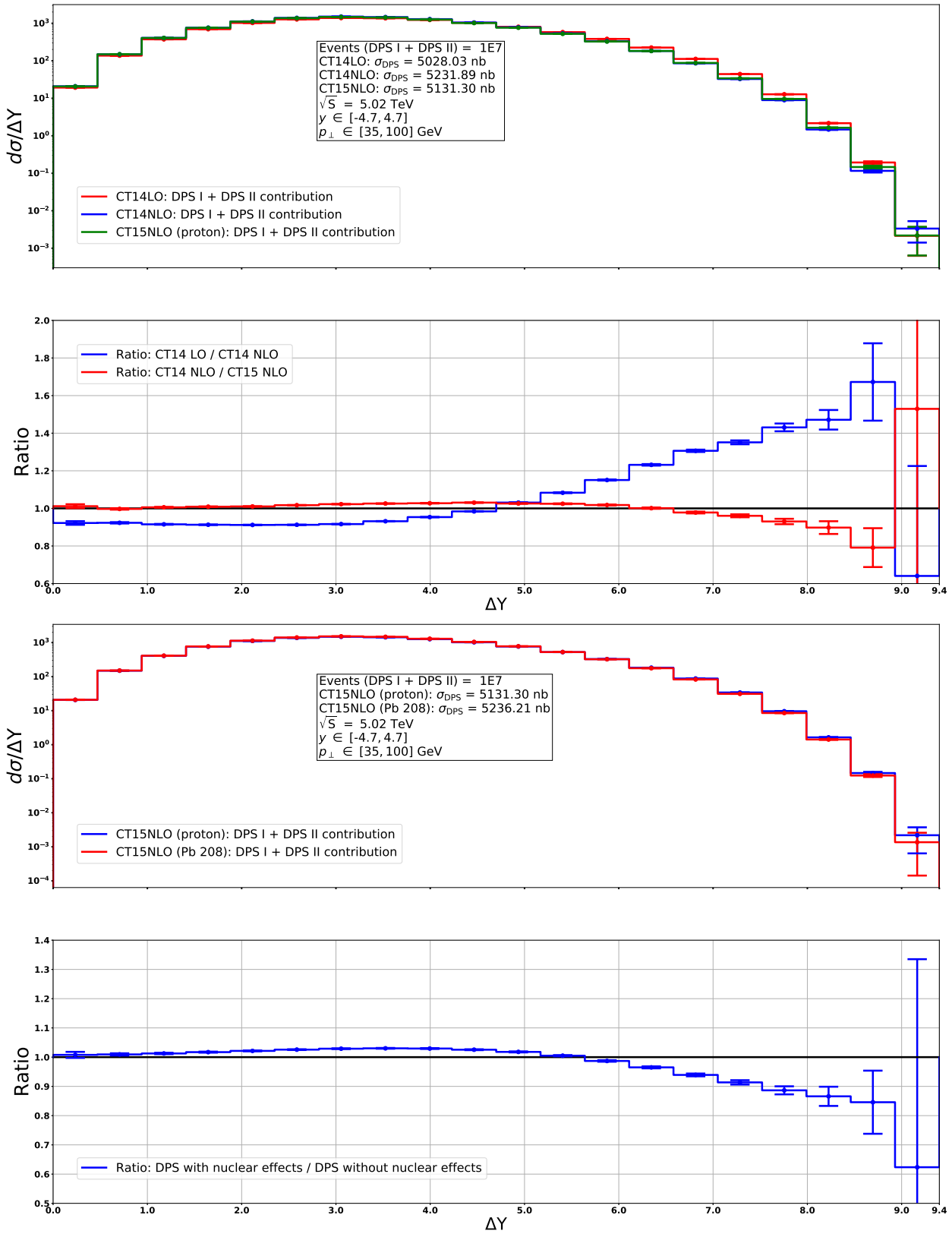

Figure 5.8: Upper panel: comparison between distributions for the DPS distributions evaluated with CT14LO [299], CT14NLO [299] and CT15NLO (proton) PDFs [300]. Lower panel: comparison between distributions for the DPS distributions evaluated with CT15NLO (proton) and CT15NLO (^{208}Pb) [300] PDFs. Collision energy $\sqrt{S_{NN}} = 5.02$ TeV, with cuts on the final sate partons $p_\perp \in [35, 100]$ GeV and $|y_i| < 4.7$. Evaluated for ^{208}Pb nucleus. Statistical errors are given by $\sigma_{\mathrm{DPS}}\sqrt{N_{\mathrm{bin}}}/N_{\mathrm{tot}}$ where N_{bin} is a number of events in a given bin, σ_{DPS} is a corresponding DPS cross section and N_{tot} is total number of bin entries for a given histogram.

5.4 Conclusions

In this chapter we have studied the four-jet DPS production in pA collision within the framework proposed by Strikman & Treleani [213]. We have demonstrated that effects due to the different kinematic constraints for the DPS I and DPS II processes are negligible for the total DPS cross sections and differential DPS distributions. Using the approach of Strikman & Treleani we have studied the interplay between the DPS signal and the SPS background for the leading jet $p_\perp$ and ΔY differential distributions for the jet cuts used in Chapter 4. These simulations were performed at $\sqrt{S_{NN}} = 5.02$ TeV collision energy which should lead to decrease of the fraction of the DPS events comparing to the pp collision energies we have considered in Chapter 4. Nevertheless, we demonstrated that the enhancement of the DPS cross section in pA collisions predicted in [213] compensates decrease of the fraction of the DPS due to decrease of collision energy. In fact, we found that the enhancement of the DPS cross section for the proton-lead collisions at $\sqrt{S_{NN}} = 5.02$ TeV leads to a better separation between the DPS and SPS contributions than the separation between DPS and SPS contributions to four-jet production in pp collisions at $\sqrt{S} = 7$ TeV.

Apart from the studies of the interplay between the DPS signal and the SPS background in pA collisions we also have estimated the overall impact of the CNM effects on the four-jet DPS production. The estimate of the impact of the shadowing effect on the DPS cross section within the framework of [303] was given in [213] and was found to be of the order of 10%. Our DPS simulations, however, include the overall impact of the CNM effects from the nPDFs and, therefore, a direct comparison between our simulations and results from [213] is not possible. We also argue that overall impact of the nPDFs on our DPS simulations is of a compatible size with the impact due to the usage of different PDF sets. Therefore, we conclude that the effects due to the nPDFs appear to be less relevant than other theoretical uncertainties.

Finally, we should note that among the phenomenological studies of DPS in pA (AA) collisions [222], [228], [224], [223], [225] the differential distributions of DPS events were discussed only in [222]. However, the phenomenological studies of DPS in pA collisions definitely require realistic Monte Carlo simulations. The simulations of DPS I and DPS II contributions as we have performed in this chapter can be combined with the ISR and FSR models of the `Pythia` event generator in the way we described in Chapter 4.9.

Chapter 6

Four-jet DPS production in proton-proton collisions within the Pythia's framework

6.1 Double parton scattering and multiple parton interactions in Pythia event generator

We will start with a brief sketch of a formalism being used in the `Pythia` event generator [255], [256] to model processes involving multiple parton interactions and, in particular, double parton scattering. Current approach of `Pythia` to MPI events has a long history of development starting from first models of MPI [258], [259] up to a very sophisticated model of `Pythia` 8 [260], [261], [262][1]. Here we will briefly sketch some particular features of the MPI model of `Pythia` essential for the understanding of our results. Namely, we will describe the way `Pythia` models *multiple parton distribution functions* (mPDFs) and, more specifically, dPDFs.

Before starting the description of the approach of `Pythia` let us note that, starting from `Pythia` version 8, a possibility to *always* have two hard interactions in a given event was added (flag `SecondHard:generate = on`). Moreover, this option allows to generate DPS events separately from MPIs (with a flag `PartonLevel:mpi = off`). Therefore, there are two options to produce DPS events with `Pythia` 8:

- With flags `SecondHard:generate = on` and `PartonLevel:mpi = off` which allows to collect a good statistics for a relatively small number of calls.
- With flags `PartonLevel:mpi = on` and `SecondHard:generate = off` which requires a large number of calls since the second interaction will always occur at sufficiently lower scale than the first one.

In this section we will not distinguish between both methods even though they are quite different in some aspects. Instead we will start with a description of some common concepts and discuss corresponding differences later in this chapter.

[1]The review of the development of MPI modelling in the `Pythia` event generator is given in [263].

A starting point is to generate the first hard $2 \to 2$ event according to

$$\frac{d\sigma}{dp_\perp^2} = \sum_{ijk} \int dx_1 dx_2 d\hat{t}\, f^i_{raw}(x_1, Q^2)\, f^j_{raw}(x_2, Q^2)\, \frac{d\sigma^k_{ij}}{d\hat{t}}\, \delta\left(p_\perp^2 - \frac{\hat{t}\hat{u}}{\hat{s}}\right), \tag{6.1}$$

where $f^i_{raw}(x_1, Q^2)$ and $f^j_{raw}(x_1, Q^2)$ are unmodified collinear PDFs.

After successful generation of the first hard event one has to generate other events due to the subsequent interactions. In order to do that, `Pythia` dynamically modifies $f^i_{raw}(x_1, Q^2)$ and $f^j_{raw}(x_2, Q^2)$ according to a history of all previous interactions in a given proton-proton collision. In the first model of MPI `Pythia` could only preserve an overall conservation of energy and momentum by reducing the value of Bjorken-x after each interaction according to

$$x'_i = \frac{x_i}{1 - \sum\limits_{j=1}^{i-1} x_j} < 1, \tag{6.2}$$

where x'_i is the value of Bjorken-x used for the i'th interaction. For example, if $i = 2$ we have

$$x'_2 = \frac{x_2}{1 - x_1} < 1, \tag{6.3}$$

which implies $x_1 + x_2 < 1$ and thus effectively we have generated an MPI (DPS) event with a dPDF being equal to

$$D^{ij}(x_1, x'_2, Q^2) = f^i_{raw}(x_1, Q^2)\, f^j_{raw}(x'_2, Q^2). \tag{6.4}$$

This approach, however, does not take into account changes in a quark content of a proton. For example, if one selects a "valence" u-quark in the first hard interaction then, effectively, one is left over with only one "valence" u-quark in a beam remnant. From the other side, if one probes a u-quark PDF at low-x it means that with a high probability it originates from a perturbative "$1v2$" splitting of a gluon into a quark-antiquark pair, which, in turn, implies that there is a leftover "companion" antiquark which has to be included into a beam remnant. The effects due to the "$1v2$" splitting, obviously, apply to all quark flavours. In Fig. 6.1 we sketch the MPI (DPS) "$1v2$" process involving perturbative $g \to c\,\bar{c}$ splitting. Namely, in Fig. 6.1 a) we show a "$1v2$" MPI (DPS) process where both c- and $\bar{c}$-quarks originate due to the perturbative $g \to c\,\bar{c}$ splitting and in Fig. 6.1 b) we show a "$1v2$" MPI (DPS) process where a c-quark originates due to a perturbative $g \to c\,\bar{c}$ splitting and a $\bar{c}$-quark originates from a "raw" $\bar{c}$ PDF.

In 2004 the MPI model of `Pythia` was significantly improved. In particular a possibility to handle the above-mentioned effects was added [260]. The starting point of the new approach is to split PDFs into valence and sea parts as

$$f(x, Q^2) = f_{val}(x, Q^2) + f_{sea}(x, Q^2), \tag{6.5}$$

where the flavour-antiflavour symmetry is assumed. By comparing the ratio $f_{sea}(x, Q^2)/f(x, Q^2)$ against a random number $R \in [0, 1]$ generated according to a uniform probability distribution one can decide in a probabilistic way if a generated quark is either a "valence" or a "sea" one. Then, for

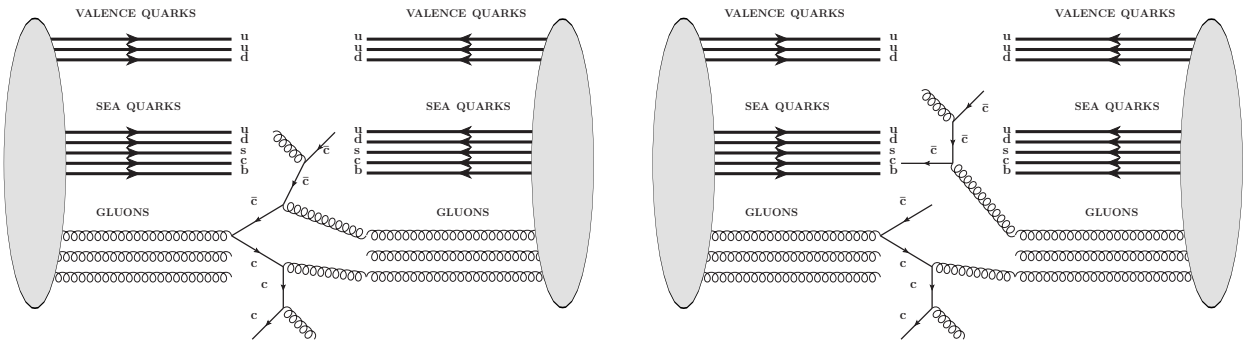

Figure 6.1: Two different possibilities to select an antiquark in a second interaction: a) a $\bar{c}$-quark comes from a perturbative "$1v2$" spiting process $g \to c\,\bar{c}$, b) a $\bar{c}$-quark comes from a "raw" $\bar{c}$ PDF.

example, if in the first interaction we have selected a valence quark of a flavour f with a distribution function $q_{fv0}(x, Q^2)$ then we have to modify its PDF according to

$$q_{fvn}(x, Q^2) = \frac{N_{fvn}}{N_{fv0}} \frac{1}{X} q_{fv0}(x/X, Q^2), \tag{6.6}$$

where N_{fv0} is an original number valence quarks of a flavour f and q_{fvn} and N_{fvn} are distribution and number of a valence quarks of the flavour f after n interactions correspondingly, $X = 1 - \sum_{i=1}^{n} x_i$ is a total momentum fraction already taken by previous interactions. One can see that modification in Eq. 6.6 changes the standard number rule

$$\int_0^1 dx\, q_{fv0}(x, Q^2) = N_{fv0} \tag{6.7}$$

to

$$\int_0^1 dx\, q_{fvn}(x, Q^2)\, \theta(X - x) = \frac{N_{fvn}}{N_{fv0}} \int_0^X \frac{dx}{X} q_{fv0}(x/X, Q^2) = N_{fvn}. \tag{6.8}$$

Equation 6.6 allows to account for changes in a number of valence quarks. However, it cannot be used in a straightforward way since a subtraction of a valence quark also removes an average momentum fraction carried by $q_{fvn}(x, Q^2)$

$$\langle x_{fvn}(Q^2)\rangle \equiv \frac{\int_0^X dx\, x\, q_{fvn}(x, Q^2)}{\int_0^X dx\, q_{fvn}(x, Q^2)} = X \int_0^1 dx\, x q_{fvn}(x, Q^2) = X \langle x_{fv0}(Q^2)\rangle, \tag{6.9}$$

which is in contradiction with the momentum rule

$$\int_0^X dx\, x \left(\sum_i q_{fn}(x, Q^2) + g_n(x, Q^2) \right) = X, \tag{6.10}$$

because Eq. 6.10 already accounts for removing a fraction of momentum $\sum_i^n x_i$. Therefore, removing an additional average momentum fraction $\langle x_{fv0}(Q^2)\rangle$ will lead to momentum violation. In general, $\langle x_{fv0}(Q^2)\rangle$ is a scale-dependent quantity which also can differ for various PDF sets. However, in order to facilitate a generation procedure, `Pythia` assumes a general functional form of this dependence

$$\langle x_{fv0}(Q^2)\rangle = \frac{A_f}{1 + B_f \log\left(\log\left(\max(Q^2, 1\,\mathrm{GeV})\,/\Lambda_{QCD}\right)\right.}, \tag{6.11}$$

where, neglecting the difference between various PDF sets, coefficient A_f and B_f are found from the fit to the CTEQ5L PDF set [269]. The quantity $\langle x_{fv0}(Q^2)\rangle$ is thus computed according to Eq. 6.11 and, in order to preserve Eq. 6.10, has to be compensated by a certain modification procedure of sea and gluon PDFs which we will describe later in this section. However, before doing that let us consider another important situation when a gluon splits perturbatively into a quark-antiquark pair as shown in Fig. 6.1. We will see that such processes may also lead to a violation of momentum conservation expressed by Eq. 6.10. Following the original notation of [260] we write

$$g \to q_s + q_c, \tag{6.12}$$

where we assume that a gluon is carrying a momentum fraction y, a sea quark q_s is carrying a momentum fraction x_s and its companion q_c, therefore, has a momentum fraction $x = y - x_s$. Then, according to [260], a PDF of a companion quark is

$$\begin{aligned} q_c(x, x_s) &= C \int_0^1 dz\, g(y)\, P_{g\to q_s q_c}(z)\, \delta(x_s - zy) = \\ &= C\, P_{g\to q_s q_c}(x_s/y) \frac{g(y)}{y} = \\ &= C\, P_{g\to q_s q_c}\left(\frac{x_s}{x_s + x}\right) \frac{g(x_s + x)}{x_s + x}, \end{aligned} \tag{6.13}$$

where $P_{g\to q_s q_c}\left(\frac{x_s}{x_s+x}\right) = \frac{1}{2}\left[z^2 + (1-z)^2\right]$ and C is a normalization constant which is fixed by

$$\int_0^{1-x_s} dx\, q_c(x, x_s) = 1. \tag{6.14}$$

Note that in this particular case a structure of the splitting term on the RHS of Eq. 6.13 coincide with a splitting term on the RHS of dDGLAP evolution equations, Eq. 2.13, up to a constant. One can easily show it using the relation between standard DGLAP splitting kernels and "$1v2$" splitting kernels in Eq. 2.14 which allows one to express $P^R_{g\to q}(z)$ via $P_{g\to q\bar{q}}(z)$ as

$$P^R_{g\to q}(z) = \sum_k P_{g\to qk}(z) = P_{g\to q\bar{q}}(z), \tag{6.15}$$

and since $P^R_{g\to q}(z) = P_{g\to q}(z)$ we have

$$P_{g\to q}(z) = P_{g\to q\bar{q}}(z) = \frac{1}{2}\left[z^2 + (1-z)^2\right]. \tag{6.16}$$

As a next simplifying step `Pythia` uses a following parametrization of a gluon distribution

$$g(x) \sim \frac{(1-x)^p}{x}, \tag{6.17}$$

where p is an integer by default set to 4. This parametrization allows to find an analytical expression for the normalization constant C and thus for the companion quark distribution $q_c(x, x_s)$. An example of a distribution of companion quarks is given in Fig. 6.2. Using Eq. 6.13 and Eq. 6.17

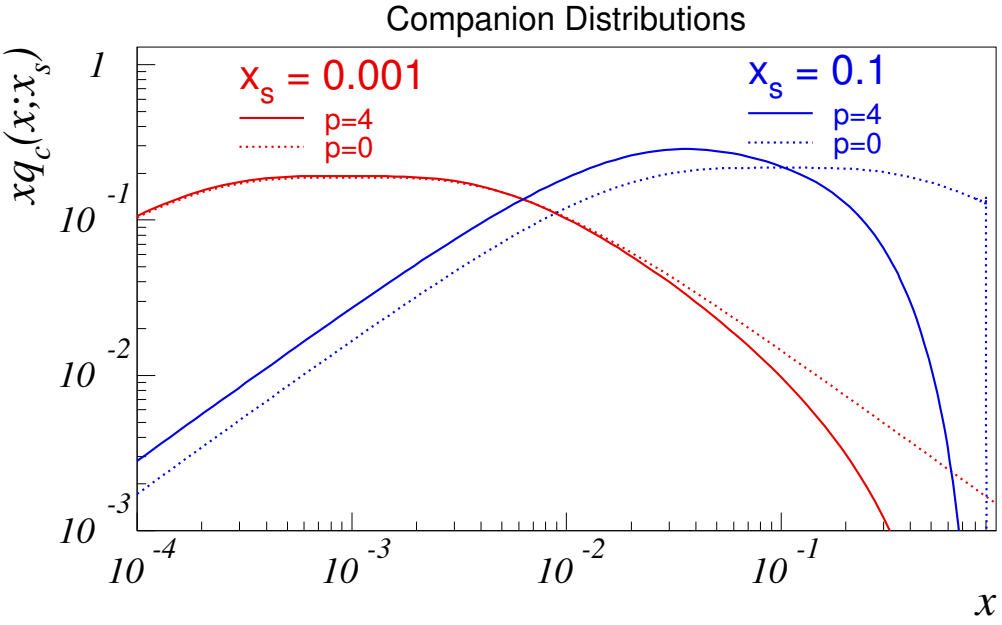

Figure 6.2: Companion quark distributions evaluated for different p and x_s, from [260].

one can analytically compute an average momentum fraction introduced by a companion quark to a beam remnant $\langle x_{cn}\rangle = X\langle x_{c0}(x_s)\rangle$ which we do not show here since it is a rather lengthy function of x_s, see [260].

Now we have seen that modification of a number of valence quarks and modification of a companion quark PDF leads to a negative contribution $X\langle x_{fv0}(Q^2)$ and a positive contribution $X\langle x_{c0}(x_s)\rangle$ to a total averaged momentum fraction. However, such contributions will violate the momentum rule given by Eq. 6.10. The way to circumvent this issue is to let sea and gluon distributions fluctuate in such a way that both contributions are compensated and the momentum rule is preserved together with the number rules

$$\int_0^X dx\, q_{fvn}(x, Q^2) = N_{fvn}, \tag{6.18}$$

$$\int_0^X dx\, q_{fc_jn}(x, x_j) = 1, \forall j. \tag{6.19}$$

In order to do that one changes the normalization of sea and gluon PDFs according to

$$q_{fs}(x,Q^2) \to a q_{fs}(x,Q^2), \tag{6.20}$$
$$g(x,Q^2) \to a g(x,Q^2), \tag{6.21}$$

which allows to rewrite the momentum rule as

$$\begin{aligned}
1 &= \frac{1}{X}\int_0^X dx\, x \left(\sum_f \left[q_{fvn}(x,Q^2) + \sum_j q_{fc_jn}(x,x_j) + a q_{fs}(x,Q^2) \right] + a g_n(x,Q^2) \right) = \\
&= \int_0^1 dx\, x \left(\sum_f \left[\frac{N_{fvn}}{N_{fv0}} q_{fv0}(x,Q^2) + \sum_j q_{fc_j0}(x,x_j) + a q_{fs0}(x,Q^2) \right] + a g_0(x,Q^2) \right) = \\
&= a + \sum_f \int_0^1 dx\, x \left[\left(\frac{N_{fvn}}{N_{fv0}} - a \right) q_{fv0}(x,Q^2) + \sum_j q_{fc_j0}(x,x_j) \right] = \\
&= a \left(1 - \sum_f N_{fv0} \langle x_{fv0} \rangle \right) + \sum_f N_{fvn} \langle x_{fv0} \rangle + \sum_{f,j} \langle x_{fc_j0} \rangle,
\end{aligned} \tag{6.22}$$

where $\langle x_{fv0} \rangle$ and $\langle x_{fc_j0} \rangle$ are average momentum fractions carried by valence and companion quarks before the first hard interaction. Equation 6.22 fixes a value of a normalization constant a and allows to express it as

$$a = \frac{1 - \sum\limits_f N_{fvn} \langle x_{fv0} \rangle - \sum\limits_{f,j} \langle x_{fc_j0} \rangle}{1 - \sum\limits_f N_{fv0} \langle x_{fv0} \rangle}. \tag{6.23}$$

Constrains set by Eq. 6.10, Eq. 6.18 and Eq. 6.19 and realized via Eq. 6.2, Eq. 6.6, Eq. 6.13, Eq. 6.20 and Eq. 6.21 are valid for all PDFs used to simulate n'th interaction and, therefore, can be seen as a generalization of standard sum rules. In the next section we will consider a particular case of DPS and compare the `Pythia`'s approach to dPDFs and sum rules against the approach of Gaunt and Stirling [173].

After performing the modification of PDFs `Pythia` generates events using *hit-or-miss* algorithm, see Chapter 3.1. Namely, it evaluates dPDFs for both hadrons such that

$$\begin{aligned}
D^{ij}(x_1,x_2,Q_1^2,Q_2^2) &= f^i_{raw}(x_1,Q_1^2)\, f^j_{mod}(x_2,Q_2^2), \\
D^{kl}(x_3,x_4,Q_1^2,Q_2^2) &= f^k_{raw}(x_3,Q_1^2)\, f^l_{mod}(x_4,Q_2^2).
\end{aligned} \tag{6.24}$$

As the next step it assigns to each event a weight w evaluated according to

$$\begin{aligned}
\omega &= \frac{f^i_{raw}(x_1,Q_1^2)\, f^j_{mod}(x_2,Q_2^2)\, f^k_{raw}(x_3,Q_1^2)\, f^l_{mod}(x_4,Q_2^2)}{f^i_{raw}(x_1,Q_1^2)\, f^j_{raw}(x_2,Q_2^2)\, f^k_{raw}(x_3,Q_1^2)\, f^l_{raw}(x_4,Q_2^2)} \\
&= \frac{f^j_{mod}(x_2,Q_2^2)\, f^l_{mod}(x_4,Q_2^2)}{f^j_{raw}(x_2,Q_2^2)\, f^l_{raw}(x_4,Q_2^2)},
\end{aligned} \tag{6.25}$$

where PDFs in the denominator have Bjorken variables satisfying longitudinal momentum conservation constraints $x_1 + x_2 < 1$ and $x_3 + x_4 < 1$. After producing a weighted event one compares its weight ω against a maximal weight ω_{max} allowed by the phase space of a given DPS process and according to the *hit-or-miss* algorithm decides either to keep or discard the given event. Later in this chapter we will discuss an improved version of this approach to the generation of DPS events available starting from `Pythia` version 8.240.

6.2 Sum rules: comparison between Pythia's and Gaunt & Stirling approaches

Having explored some key aspects of `Pythia`'s model of dPDFs, we can start to compare its predictions against predictions of the GS09 model. In this section we will check in detail how well both models of dPDFs satisfy the "double" sum rules given by Eq. 2.17 - Eq. 2.20 and discuss some differences and similarities between both `Pythia` and GS09 dPDFs.

In order to perform a comparison between both models it is convenient to write dPDFs in `Pythia`'s notation

$$D_p^{j_1 j_2}(x_1, x_2, Q_1^2, Q_2^2) = f_{raw}^{j_1}(x_1, Q_1^2) f_{mod}^{j_2}(x_2, Q_2^2), \tag{6.26}$$

where $f_{raw}^{j_1}(x_1, Q_1^2)$ is a standard collinear PDF being used for the first hard interaction and $f_{mod}^{j_2}(x_2, Q_2^2)$ is a PDF modified according to the first hard interaction and being used for the second one. In this section, for simplicity's sake, we will set $Q_1^2 = Q_2^2 = Q^2$. The rules set by Eq. 2.17 - Eq. 2.20 can be also written for the first parton (j_1, x_1) being fixed:

$$\sum_{j_2} \int_0^{1-x_1} dx_2\, x_2\, D_{j_1 j_2}(x_1, x_2, Q^2) = (1 - x_1)\, f_{j_1}(x_1, Q^2), \tag{6.27}$$

$$\int_0^{1-x_1} dx_2\, \left[D_{j_1 j_2}(x_1, x_2, Q^2) - D_{j_1 \bar{j_2}}(x_1, x_2, Q^2)\right] = N_{j_{2v}}\, f_{j_1}(x_1, Q^2), \text{ if } j_1 \neq j_2 \text{ or } \bar{j_2}, \tag{6.28}$$

$$\int_0^{1-x_1} dx_2\, \left[D_{j_1 j_2}(x_1, x_2, Q^2) - D_{j_1 \bar{j_2}}(x_1, x_2, Q^2)\right] = (N_{j_{2v}} - 1)\, f_{j_1}(x_1, Q^2), \text{ if } j_1 = j_2, \tag{6.29}$$

$$\int_0^{1-x_1} dx_2\, \left[D_{j_1 j_2}(x_1, x_2, Q^2) - D_{j_1 \bar{j_2}}(x_1, x_2, Q^2)\right] = (N_{j_{2v}} + 1)\, f_{j_1}(x_1, Q^2), \text{ if } j_1 = \bar{j_2}. \tag{6.30}$$

First of all, let us check how the ansatz given by Eq. 6.26 satisfies the momentum sum rule given by Eq. 6.27. By substituting Eq. 6.26 into Eq. 6.27 we get

$$\sum_{j_2} \int_0^{1-x_1} dx_2\, x_2\, f_{raw}^{j_1}(x_1, Q^2) f_{mod}^{j_2}(x_2, Q^2) = (1 - x_1)\, f_{raw}^{j_1}(x_1, Q^2), \tag{6.31}$$

or

$$\sum_{j_2} \int_0^{1-x_1} dx_2\, x_2\, f_{mod}^{j_2}(x_2, Q^2) = (1 - x_1). \tag{6.32}$$

Since j_2 in $\sum_{j_2}$ runs over all parton species one can write Eq. 6.32 as

$$\int_0^{1-x_1} dx_2\, x_2 \left(\sum_{j=q,\bar{q}} f_{mod}^{j}(x_2, Q^2) + f_{mod}^{g}(x_2, Q^2) \right) = (1 - x_1), \tag{6.33}$$

which is exactly equivalent to the momentum conservation constraint being used in `Pythia` as in

Eq. 6.10 with $n = 2$, $X = 1 - x_1$. Therefore, we see that dPDFs in GS09 and `Pythia` models satisfy the same momentum rule expressed by Eq. 2.17 and Eq. 6.10, correspondingly. Now let us check numerically how well both models satisfy momentum sum rule given by Eq. 6.27 and Eq. 6.33. In order to do that we write Eq. 6.27 and Eq. 6.33 in a schematic form as

$$x_1 f_{j_1}(x_1, Q^2) \quad + \int\limits_{\min(x_1)}^{1-x_1} dx_2\, x_2 \sum () = 1, \tag{6.34}$$

$$x_1 \quad + \int\limits_{\min(x_1)}^{1-x_1} dx_2\, x_2 \sum () = 1, \tag{6.35}$$

and check how well the LHS of Eq. 6.35 and Eq. 6.35 matches unity. We use Eq. 6.35 to check the momentum sum rule for GS09 dPDFs and Eq. 6.35 to check the momentum sum rules for the `Pythia` dPDFs. We set the lower integration boundary $\min(x_1)$ in Eq. 6.35 to 10^{-6} which is the lower x value of the GS09 grids we use. As we will see later in this section the grid limitations lead to the violation of the sum rules for the values of x_1 close to the lower grid boundary. In order to avoid these boundary effects for the checks of sum rules with `Pythia` dPDFs we will set the lower integration boundary in Eq. 6.35 to 10^{-8}.

In order to be able to perform numerical integration in Eq. 6.35 one has to be able to evaluate PDFs modified by `Pythia` $f^i_{mod}(x, Q^2)$ in the given integration range. Normally, it is not possible since the corresponding part of the MPI model is hidden from a standard `Pythia` user. However, it can be achieved by instantiation of objects which are members of the `BeamParticle` class as explained in Appendix H. For numerical integration we use CQUAD doubly-adaptive integration routine from GSL Scientific Library v2.4 [294]. In order to get values of single PDFs in Eq. 6.33 we use LHAPDF6 library [296] and MSTW LO PDF set [298]. In order to check how well GS09 dPDFs satisfy the momentum sum rule we use two grids with 300 and 600 grid points. The results of numerical checks are given in Table 6.1.

x_1	id_1	`Pythia`	GS09 300 grid points	GS09 600 grid points
1.0000e-06	1	9.9909e-01 ± 8.2e-04	8.9508e-01 ± 8.7e-04	8.9851e-01 ± 8.7e-04
5.0000e-06	1	9.9909e-01 ± 8.2e-04	9.9784e-01 ± 9.8e-04	9.9297e-01 ± 9.7e-04
2.5000e-05	1	9.9909e-01 ± 8.1e-04	1.0081e+00 ± 9.6e-04	1.0067e+00 ± 9.9e-04
1.2500e-04	1	9.9909e-01 ± 9.2e-04	1.0058e+00 ± 9.6e-04	1.0088e+00 ± 9.8e-04
6.2500e-04	1	9.9904e-01 ± 8.5e-04	1.0145e+00 ± 9.9e-04	1.0137e+00 ± 9.9e-04
3.1250e-03	1	9.9911e-01 ± 6.9e-03	1.0249e+00 ± 1.0e-03	1.0225e+00 ± 9.9e-04
1.5625e-02	1	9.9914e-01 ± 1.2e-01	1.0355e+00 ± 1.0e-03	1.0381e+00 ± 1.0e-04
7.8125e-02	1	1.0039e+00 ± 1.9e-01	1.0243e+00 ± 8.9e-04	1.0385e+00 ± 9.2e-04
3.9063e-01	1	1.0046e+00 ± 5.7e-04	1.0060e+00 ± 6.0e-04	1.0002e+00 ± 5.8e-04

Table 6.1: Test of the momentum sum rule, Eq. 6.27 and Eq. 6.33. Pythia and GS09 models of dPDFs. The factorization scales are set to 5 GeV.

We see that both approaches satisfy Eq. 6.27 and Eq. 6.33 rule at 1% accuracy level for most of the values of x_1. Relatively strong deviations from unity for GS09 dPDFs at low values of x_1 are

related to the low x integration limit which is 10^{-6} for the grids we use. The errors in Table 6.1 are given by an estimate of the absolute error (`abserr`) returned by the `gsl_integration_cquad` routine which we run with desired absolute (`epsabs`) and relative error (`epsrel`) limits set to 0 and 10^{-3} respectively. We see that the estimate of the absolute error for CQUAD method is usually smaller than 10^{-3}. However we observe `abserr` $\sim 10^{-1}$ for the check of Eq. 6.33 with `Pythia`'s dPDFs at $x_1 \sim 10^{-2}$. The reason is in the different treatment of valence and sea quarks within `Pythia`'s frameworks which makes numerical integration in this particular range of x complicated. We will discuss it in more detail later when we perform numerical checks of the number sum rules. For the moment let us note that one gets a better error estimate using the VEGAS algorithm [295] supplied with the GSL Library, see Table 6.2.

x_1	id_1	`Pythia` CQUAD integration	`Pythia` VEGAS integration
1.0000e-06	1	9.9909e-01 ± 8.2e-04	9.990794e-01 7.579513e-07
5.0000e-06	1	9.9909e-01 ± 8.2e-04	9.990747e-01 6.055986e-06
2.5000e-05	1	9.9909e-01 ± 8.1e-04	9.990668e-01 1.343860e-05
1.2500e-04	1	9.9909e-01 ± 9.2e-04	9.991279e-01 2.772772e-05
6.2500e-04	1	9.9904e-01 ± 8.5e-04	9.993865e-01 5.407137e-05
3.1250e-03	1	9.9911e-01 ± 6.9e-03	1.000161e+00 9.574375e-05
1.5625e-02	1	9.9914e-01 ± 1.2e-01	1.001569e+00 1.472444e-04
7.8125e-02	1	1.0039e+00 ± 1.9e-01	1.002877e+00 1.809566e-04
3.9063e-01	1	1.0046e+00 ± 5.7e-04	1.004329e+00 6.467959e-05

Table 6.2: Test of the momentum sum rule, Eq. 6.33, with different integration routines. Pythia model of dPDFs. Both factorization scales are set to 5 GeV.

Now let us switch attention to the number rules. It is convenient to express them in terms of a ratio

$$R_{j_1 j_2}(x_1, x_2, Q^2) = x_2 \, \frac{D_p^{j_1 j_2}(x_1, x_2, Q^2) - D_p^{j_1 \bar{j}_2}(x_1, x_2, Q^2)}{f_{raw}^{j_1}(x_1, Q^2)}. \tag{6.36}$$

The meaning of $R_{j_1 j_2}(x_1, x_2, Q^2)$ becomes clear if one neglects momentum and number conservation and substitute $D_p^{j_1 j_2}(x_1, x_2, Q^2) = f_{raw}^{j_1}(x_1, Q^2) f_{raw}^{j_2}(x_2, Q^2)$ in Eq. 6.36. The function $R_{j_1 j_2}(x_1, x_2, Q^2)$ then turns simply into a valence quark PDF multiplied by Bjorken-x:

$$R^{j_1 j_2}(x_1, x_2, Q^2) = x_2 \left[f_{raw}^{j_2}(x_2, Q^2) - f_{raw}^{\bar{j}_2}(x_2, Q^2) \right] = x_2 f_{Val}^{j_2}(x_2, Q^2). \tag{6.37}$$

Using $R_{j_1 j_2}(x_1, x_2, Q^2)$ one can write number sum rules in a compact form as

$$\begin{aligned}
&\int_0^{1-x_1} \frac{dx_2}{x_2} \, R_{j_1 j_2}(x_1, x_2, Q^2) = N_{j_{2v}}, \quad \text{if } j_1 \neq j_2 \text{ or } \bar{j}_2, \\
&\int_0^{1-x_1} \frac{dx_2}{x_2} \, R_{j_1 j_2}(x_1, x_2, Q^2) = (N_{j_{2v}} - 1), \quad \text{if } j_1 = j_2, \\
&\int_0^{1-x_1} \frac{dx_2}{x_2} \, R_{j_1 j_2}(x_1, x_2, Q^2) = (N_{j_{2v}} + 1), \quad \text{if } j_1 = \bar{j}_2.
\end{aligned} \tag{6.38}$$

Since $D_p^{j_1 j_2}(x_1, x_2, Q^2) = f_{raw}^{j_1}(x_1, Q^2) f_{mod}^{j_2}(x_2, Q^2)$ one can write $R_{j_1 j_2}(x_1, x_2, Q^2)$ as

$$\begin{aligned} R_{j_1 j_2}(x_1, x_2, Q^2) &= x_2 \frac{f_{raw}^{j_1}(x_1, Q^2) f_{mod}^{j_2}(x_2, Q^2) - f_{raw}^{j_1}(x_1, Q^2) f_{mod}^{\bar{j_2}}(x_2, Q^2)}{f_{raw}^{j_1}(x_1, Q^2)} \\ &= x_2 \left[f_{mod}^{j_2}(x_2, Q^2) - f_{mod}^{\bar{j_2}}(x_2, Q^2) \right] \end{aligned} \tag{6.39}$$

which allows to rewrite the number sum rules as

$$\begin{aligned} &\int_0^{1-x_1} \frac{dx_2}{x_2}\, x_2 \left[f_{mod}^{j_2}(x_2, Q^2) - f_{mod}^{\bar{j_2}}(x_2, Q^2) \right] = N_{j_{2v}} \quad j_1 \neq j_2 \text{ or } \bar{j_2}, \\ &\int_0^{1-x_1} \frac{dx_2}{x_2}\, x_2 \left[f_{mod}^{j_2}(x_2, Q^2) - f_{mod}^{\bar{j_2}}(x_2, Q^2) \right] = (N_{j_{2v}} - 1), \quad \text{if } j_1 = j_2, \\ &\int_0^{1-x_1} \frac{dx_2}{x_2}\, x_2 \left[f_{mod}^{j_2}(x_2, Q^2) - f_{mod}^{\bar{j_2}}(x_2, Q^2) \right] = (N_{j_{2v}} + 1), \quad \text{if } j_1 = \bar{j_2}, \end{aligned} \tag{6.40}$$

where one can consider the difference $f_{mod}^{j_2}(x_2, Q^2) - f_{mod}^{\bar{j_2}}(x_2, Q^2)$ as a PDF of a valence quark of a flavour j_2 modified according to the first hard interaction involving a parton of a flavour f_1.

We see that the number sum rules given in Eq. 6.38 and Eq. 6.40 formally coincide with number constraints used in `Pythia` as in Eq. 6.18 and Eq. 6.19. However, there is a significant difference between the ways Eq. 6.38 and Eq. 6.18 - 6.19 are satisfied in GS09 and `Pythia` models. Below we illustrate the difference between GS09 and `Pythia` dPDFs taking as an example $R_{\rm dd}(x_1, x_2, Q^2)$. In Fig. 6.3 we compare $R_{\rm dd}(x_1, x_2, Q^2)$ evaluated with `Pythia` and GS09 dPDFs against a valence d-quark PDF. One can see how "$1v2$" splitting leads to negative values of $R_{\rm dd}(x_1, x_2, Q^2)$. For example, if in the first interaction we select a d-quark at $x_1 = 10^{-6}$ it is probably a sea quark, which was created due to a perturbative "$1v2$" splitting of a gluon into a $d\bar{d}$ pair. Therefore, the remaining $\bar{d}$-quark has to be included into a "raw" $\bar{d}$-quark PDF which means that $f_{raw}^{\bar{d}}(x_2, Q^2) < f_{mod}^{\bar{d}}(x_2, Q^2)$ for $x_2 \sim 10^{-6}$. It implies that $R_{\rm dd}(x_1, x_2, Q^2)$ also becomes negative for $x_2 \sim 10^{-6}$. Moreover, negative value of $R_{\rm dd}(x_1, x_2, Q^2)$ at low x should be compensated by positive contribution at high x in order to preserve the number sum rule given by Eq. 6.41. One can see it in the upper panel in Fig. 6.3. In this case

$$\int_0^{1-x_1} \frac{dx_2}{x_2}\, R_{\rm dd}(x_1, x_2, Q^2) = N_{vd0} - 1 = 0. \tag{6.41}$$

The same holds if one selects a d-quark at higher values of x, see the middle and the lower panels in Fig. 6.3. In Tab. 6.3 we provide a numerical check of Eq. 6.41 with the QCDAD integration routine. We see that for $x_1 > 10^{-4}$ GS09 satisfies Eq. 6.41 at a percent level. The violation of Eq. 6.41 at low values of x_1 is a boundary effect due to the limitation of the GS09 grid, see Fig. 6.3. In case of the dPDFs modelled by `Pythia` Eq. 6.41 is violated for the values of x_1 approximately in between 10^{-3} and 10^{-2}. The reason for it is that `Pythia` treats valence and sea PDFs separately, as described in section 6.1. For each generation `Pythia` decides in a probabilistic way what type of

PDFs (sea or valence) to use to model dPDFs for a given event. Therefore, for the region where valence and sea PDFs overlap the dPDFs used in `Pythia` will become difficult to integrate. In the lower panel of Fig. 6.3 one sees first signs of these effect given by the kink of the $R^{j_1 j_2}(x_1, x_2, Q^2)$ function for the x_2 in between 10^{-4} and 10^{-3}. However, we argue that the integration algorithm which involves multiple evaluations of the integrand in Eq. 6.41 should demonstrate better results as the CQUAD algorithm since multiple evaluation of $R^{j_1 j_2}(x_1, x_2, Q^2)$ has to "washout" the kink structures due to the different treatment of the valence and sea PDFs in `Pythia` model. In order to illustrate that we compare results of numerical integration in Eq. 6.41 obtained with CQUAD algorithm against results obtained with the VEGAS algorithm, see Table 6.4. We see that the numerical integration in Eq. 6.41 performed with the VEGAS algorithm gives zero for the values of x_1 located in the "difficult" region between 10^{-3} and 10^{-2}. The numerical checks performed for the other sum rules give similar results.

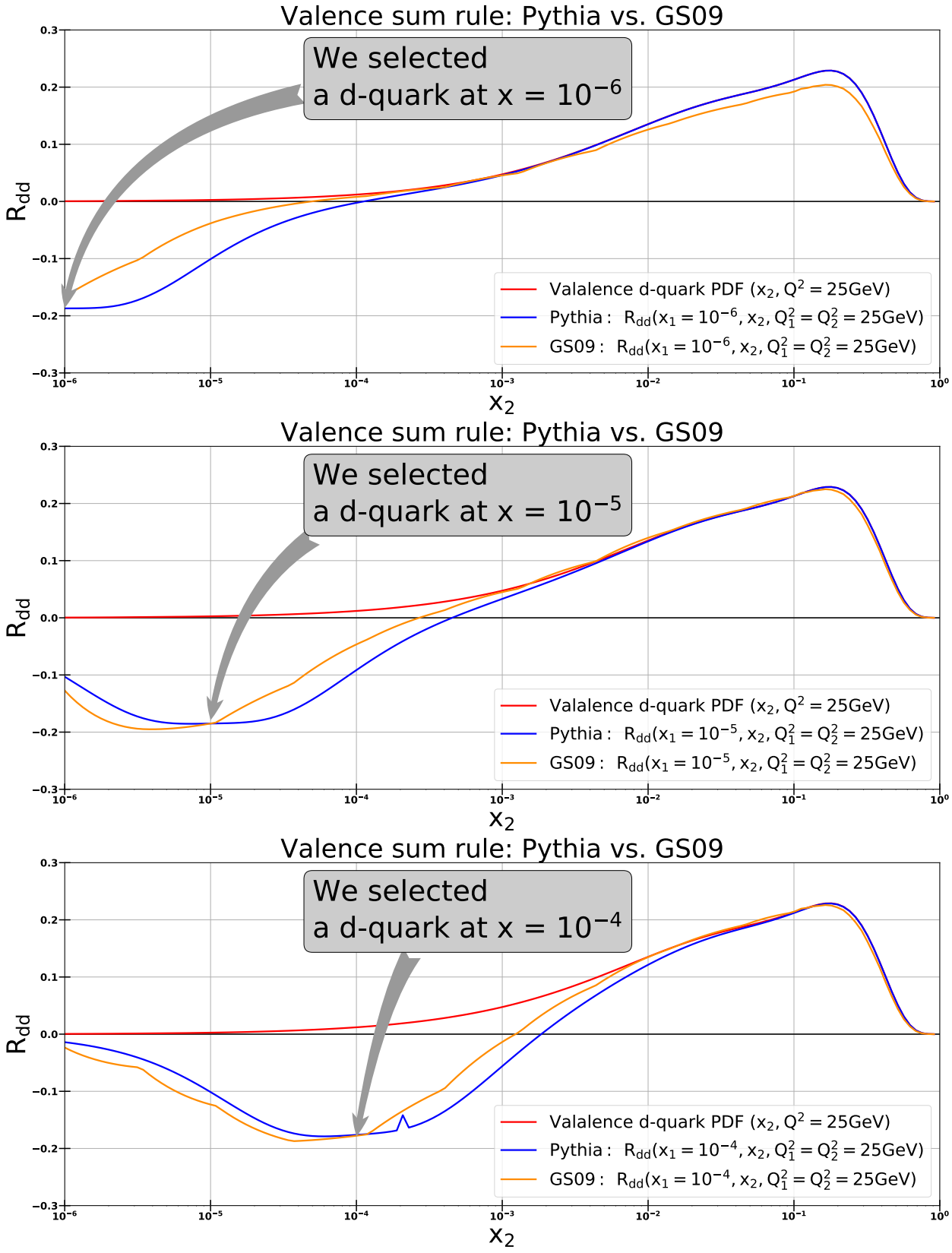

Figure 6.3: The modification of the valence d-quark PDF $R_{\mathrm{dd}}(x_1, x_2, Q^2)$ as a function of x_2 for $\mathrm{x}_1 = 10^{-6}, 10^{-5}, 10^{-4}$. Comparison between GS09 and `Pythia` dPDFs.

x_1	N_{d2v} `Pythia`	N_{d2v} GS09 300 grid points
1.0000e-06	1.4e-02 ± 1.3e-05	6.4e-01 ± 6.3e-04
5.0000e-06	1.9e-03 ± 1.8e-06	3.7e-01 ± 3.7e-04
2.5000e-05	-5.3e-04 ± 5.2e-07	1.5e-01 ± 1.4e-04
1.2500e-04	-1.0e-03 ± 1.0e-06	6.4e-02 ± 6.4e-05
6.2500e-04	-7.7e-04 ± 4.5e-02	4.8e-02 ± 4.8e-05
3.1250e-03	3.2e-01 ± 1.6e+01	3.6e-02 ± 3.6e-05
1.5625e-02	-1.9e-01 ± 4.1e+01	2.1e-02 ± 2.1e-05
7.8125e-02	-1.2e-01 ± 5.4e+01	7.8e-03 ± 7.7e-06
3.9063e-01	0.0e+00 ± 0.0e+00	2.9e-03 ± 2.9e-06

Table 6.3: Pythia: test of the second number sum rule for a d-quark, Eq. 6.29. Numerical integration with the CQUAD routine. We use red colour for the cells where the results of the numerical integration in Eq. 6.41 strongly deviate from zero.

x_1	N_{d2v} `Pythia` CQUAD integration	N_{d2v} `Pythia` VEGAS integration
1.0000e-06	1.4e-02 ± 1.3e-05	1.4e-02 ± 1.1e-04
5.0000e-06	1.9e-03 ± 1.8e-06	2.0e-03 ± 2.0e-04
2.5000e-05	-5.3e-04 ± 5.2e-07	-1.1e-02 ± 5.4e-03
1.2500e-04	-1.0e-03 ± 1.0e-06	-4.5e-03 ± 7.7e-03
6.2500e-04	-7.7e-04 ± 4.5e-02	-1.4e-02 ± 1.3e-02
3.1250e-03	3.2e-01 ± 1.6e+01	5.9e-03 ± 2.5e-02
1.5625e-02	-1.9e-01 ± 4.1e+01	-5.7e-03 ± 4.5e-02
7.8125e-02	-1.2e-01 ± 5.4e+01	-4.4e-03 ± 5.7e-02
3.9063e-01	0.0e+00 ± 0.0e+00	-1.7e-02 ± 2.5e-02

Table 6.4: Pythia: test of the second number sum rule for a d-quark, Eq. 6.29. Comparison between numerical integration with CQUAD and VEGAS routines. We use red colour for the cells where the results of the numerical integration in Eq. 6.41 strongly deviate from zero.

In this section we have demonstrated that both GS09 and `Pythia` dPDFs satisfy the same set of sum rules proposed by Gaunt and Stirling in [173]. A short summary on both models of dPDFs is given in Table 6.4. In the next section we will discuss how the differences between GS09 and `Pythia` dPDFs affects the differential DPS distributions.

Model of dPDFs	Pythia dPDFs	GS09 dPDFs
Different approaches to describe valence and sea partons	Yes	No
Double DGLAP evolution	No	Yes
Momentum sum rule	Yes	Yes
Number sum rules	Yes	Yes
Splitting term	Used for dynamical modification of sea PDFs. Up to a normalisation constant coincides with a splitting term in dDGLAP evolution equations, however accounts only for $g \to q\bar{q}$ splitting processes	Included in dDGLAP evolution. Accounts for all possible splitting processes

Table 6.4: Short summary of GS09 and `Pythia` models of dPDFs.

6.3 Four-jet DPS production: comparison between Pythia's and Gaunt & Stirling approaches

Since double parton distribution functions are unknown objects one has to use certain phenomenologically motivated assumptions to model them. The easiest way to model dPDFs is a so called "naive" approach where one replaces a dPDF by a product of two "single" collinear PDFs and a θ-function to preserve conservation of a longitudinal momentum

$$D_{j_1 j_2}(x_1, x_2, Q_1^2, Q_2^2) = f_{j_1}(x_1, Q_1^2)\, f_{j_2}(x_2, Q_2^2)\, \theta(1 - x_1 - x_2), \tag{6.42}$$

see Chapter 2.1. This approach neglects correlations in x-space and violates the number sum rules given by Eq. 2.18 - Eq. 2.20. Moreover, as it was shown in [164], [167] and [168], this ansatz does not satisfy dDGLAP evolution equations. Nevertheless, it is still quite commonly used in phenomenological studies of DPS. Here we will use it as a baseline for our comparisons against GS09 and `Pythia` models of dPDFs. In our analysis we will compare impact of different models of dPDFs on differential distributions of DPS events. Namely we will study distributions in terms of a leading jet $p_\perp$ and the maximal rapidity difference $\Delta \mathrm{Y} = \max|y_i - y_j|$. We require four jets produced in each DPS event to have $p_\perp \in [20, 100]$ GeV. We normalize all distributions such that the total area under each histogram is equal to the corresponding total cross section (given in nanobarns). These values are evaluated according to the following procedure: first one finds how the total `Pythia` DPS cross section changes after imposing cuts on produced partons. The new cross section $\sigma_{\mathrm{cut}}^{\mathrm{Pythia}}$ is related to the old one $\sigma_{\mathrm{tot}}^{\mathrm{Pythia}}$ as

$$\frac{\sigma_{\mathrm{tot}}^{\mathrm{Pythia}}}{\sigma_{\mathrm{cut}}^{\mathrm{Pythia}}} = \frac{\omega_{\mathrm{tot}}^{\mathrm{Pythia}}}{\omega_{\mathrm{cut}}^{\mathrm{Pythia}}}, \tag{6.43}$$

where $\omega_{\mathrm{tot}}^{\mathrm{Pythia}}$ is the total weight of all generated events and $\omega_{\mathrm{cut}}^{\mathrm{Pythia}}$ is the total weight of events that remain after cuts[2].

After evaluating $\sigma_{\mathrm{cut}}^{\mathrm{Pythia}}$ one has to find the impact of GS09 and "naive" dPDFs. In order to do that one modifies a weight of each `Pythia` event according to

$$\omega_i^{\mathrm{GS09}} = \omega_i^{\mathrm{Pythia}} \frac{D(x\mathrm{A}_1, x\mathrm{A}_2, Q_1^2, Q_2^2)\, D(x\mathrm{B}_1, x\mathrm{B}_2, Q_1^2, Q_2^2)}{f_{raw}(x\mathrm{A}_1, Q_1^2) f_{mod}(x\mathrm{A}_2, Q_2^2) f_{raw}(x\mathrm{B}_1, Q_1^2) f_{mod}(x\mathrm{B}_2, Q_2^2)}, \tag{6.44}$$

and

$$\begin{aligned} \omega_i^{\mathrm{Naive}} &= \omega_i^{\mathrm{Pythia}} \frac{f_{raw}(x\mathrm{A}_2, Q_2^2) f_{raw}(x\mathrm{B}_2, Q_2^2)}{f_{mod}(x\mathrm{A}_2, Q_2^2) f_{mod}(x\mathrm{B}_2, Q_2^2)} \times \\ &\times \theta(1 - x\mathrm{A}_1 - x\mathrm{A}_2)\, \theta(1 - x\mathrm{B}_1 - x\mathrm{B}_2), \end{aligned} \tag{6.45}$$

where $D(x\mathrm{A}_i, x\mathrm{A}_i, Q_1^2, Q_2^2)$ are GS09 dPDFs, $f_{raw}(x\mathrm{A}_i, Q_i^2)$ are standard PDFs used by `Pythia` to

[2] Usually `Pythia` generates unweighted events with weights equal to unity which implies that $\omega_{\mathrm{tot}}^{\mathrm{Pythia}}$ and $\omega_{\mathrm{cut}}^{\mathrm{Pythia}}$ are the total number of generated events $N_{\mathrm{tot}}^{\mathrm{Pythia}}$ and the total number of events remaining after imposing cuts $N_{\mathrm{cut}}^{\mathrm{Pythia}}$. However, there are several important cases when each event acquires a non-trivial weight, for example, in pA collisions. Therefore, in Eq. 6.43 we use $\omega_{\mathrm{tot}}^{\mathrm{Pythia}}$ and $\omega_{\mathrm{cut}}^{\mathrm{Pythia}}$ instead of $N_{\mathrm{tot}}^{\mathrm{Pythia}}$ and $N_{\mathrm{cut}}^{\mathrm{Pythia}}$. More details on event weights in `Pythia` can be found in [84].

describe the first hard interaction and $f_{mod}(x\mathrm{A}_i, Q_i^2)$ are PDFs modified by `Pythia` to describe the second hard interaction. Here we use the `Pythia`'s notation as shown in Fig. 6.5.

After reweighting histograms one evaluates the modified total weights of all events that pass through the cuts according to

$$\begin{aligned} \omega_{\rm cut}^{\rm GS09} &= \sum_i \omega_i^{\rm GS09}, \\ \omega_{\rm cut}^{\rm Naive} &= \sum_i \omega_i^{\rm Naive}, \end{aligned}$$

and then evaluates the corresponding total cross sections from

$$\begin{aligned} \frac{\omega_{\rm tot}^{\rm GS09}}{\omega_{\rm cut}^{\rm Pythia}} &= \frac{\sigma_{\rm tot}^{\rm GS09}}{\sigma_{\rm cut}^{\rm Pythia}}, \\ \frac{\omega_{\rm tot}^{\rm Naive}}{\omega_{\rm cut}^{\rm Pythia}} &= \frac{\sigma_{\rm tot}^{\rm Naive}}{\sigma_{\rm cut}^{\rm Pythia}}. \end{aligned}$$

We shall note that a standard `Pythia` user can access PDFs being used to simulate the first hard interaction but not the PDFs being used for all subsequent interactions and, therefore, cannot compute $\omega^{\rm GS09}$, $\omega^{\rm Pythia}$ and $\omega^{\rm Naive}$. In order to solve this problem we added new members to the `Event` class to store the information about the PDFs being used for the second interaction. We also added two new methods to set and to read the values of these new members. This additional information has to be written to the event record in the `ProcessLevel::nextOne(Event& process)` method of the `ProcessLevel` class after the successful generation of the second hard interaction. The information assigned in a such way is then accessible together with the other standard information stored in the event record and can be used to evaluate ω^{GS09}, $\omega^{\rm Pythia}$ and ω^{Naive} during the generation procedure.

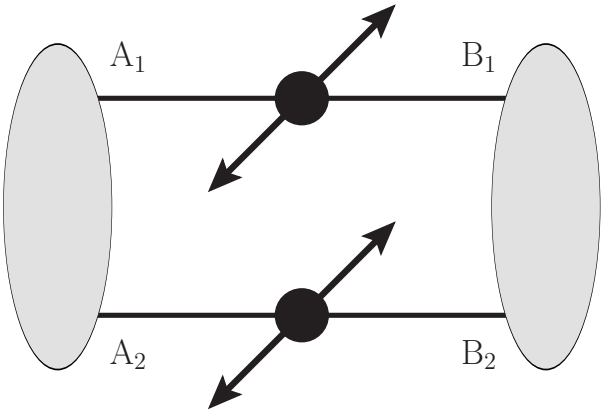

Figure 6.5: The notation being used in `Pythia`. All variables with A_1 and B_1 (A_2 and B_2) in their names correspond to the first (second) hard interaction.

The differential distributions for "naive", `Pythia` and GS09 dPDFs are given in Fig. 6.6 and Fig. 6.7. Before discussing our results we shall make several important comments. First of all, in order to produce DPS distributions in Fig. 6.6 and Fig. 6.7 we have set `SecondHard:generate = on` and `PartonLevel:mpi = off` in the `Pythia` setup. This combination of flags allows to always generate

events with only two hard interactions per one proton-proton collision. However, it implies that the total DPS cross section will be given by

$$\sigma_2 = \frac{\sigma_{\rm ND}}{2}\left(\frac{\sigma_1}{\sigma_{\rm ND}}\right)^2, \tag{6.46}$$

where $\sigma_{\rm ND}$ is the total nondiffractive cross section [260]. The connection between the "pocket formula" of DPS and Eq. 6.46 is given by

$$\sigma_2 = \frac{\sigma_{\rm ND}}{2}\left(\frac{\sigma_1}{\sigma_{\rm ND}}\right)^2 \frac{\sigma_{\rm ND}}{\sigma_{eff}} = \frac{1}{2}\frac{\sigma_1^2}{\sigma_{eff}}, \tag{6.47}$$

where $\sigma_{\rm ND}/\sigma_{eff}$ gauges the deviation from the Poissonian statistics [260]. The transition from Eq. 6.46 to Eq. 6.47 in `Pythia`, however, is performed only if the MPI modelling is switched on. Therefore, the parameter σ_{eff} does not enter into our DPS simulations performed with the aforementioned setup. It implies that the DPS cross sections in our simulations are evaluated according to Eq. 6.46 with $\sigma_{\rm ND}$ instead of σ_{eff}. However, since we are interested only in the relative difference between distributions of DPS events produced with different models of dPDFs, the aforementioned difference in the normalization of the DPS cross section does not affect our analysis. The complete setup we use is given in Table 6.5.

As we can see in Fig. 6.6 the DPS distributions in terms of the leading jet $p_\perp$ demonstrate a mild dependence on the the choice of the model of the dPDFs. The distributions in terms of the maximal rapidity difference ΔY, however, demonstrate a strong difference at the high values of ΔY. We also see that at high values of ΔY the difference between DPS distributions generated with GS09 and `Pythia` dPDFs is smaller than the difference between distributions generated with GS09 and "naive" dPDFs. Since, as we have discussed in section 6.2, both GS09 and `Pythia` models of dPDFs obey the same set of sum rules, we conclude that the constraints on dPDFs imposed by the sum rules play an important role at high values of ΔY. Moreover, since the model of `Pythia` does not account for the effects due to the double DGLAP evolution of dPDFs we conclude that the evolution effects and the effects induced by momentum and number sum rules in GS09 model are of comparable size at large values of ΔY.

Also by comparing ratios of `Pythia` distributions reweighted with GS09 and "naive" dPDFs in Fig 6.6 and Fig. 6.7 with the corresponding ratios in Fig. 4.5 and Fig. 4.7 we conclude that predictions made with our standalone DPS code agree at qualitative level with the predictions obtained with reweighted `Pythia` distributions. Namely, the ratio between `Pythia` distributions reweighted with GS09 and "naive" dPDFs in Fig 6.6 and Fig. 6.7 demonstrate the same dependence on the collision energy as the corresponding ratios in Fig. 4.5 and Fig. 4.7. However, we shall note that in this chapter we have used a default `Pythia` setup which implies that only first three flavours are considered as massless. Therefore, the four-jet DPS production in this chapter was simulated without taking contributions from charm quarks into account. We leave a detailed comparison between the `Pyhia` event generator and our standalone DPS code as well as the study of the role of different flavour contributions for the future work.

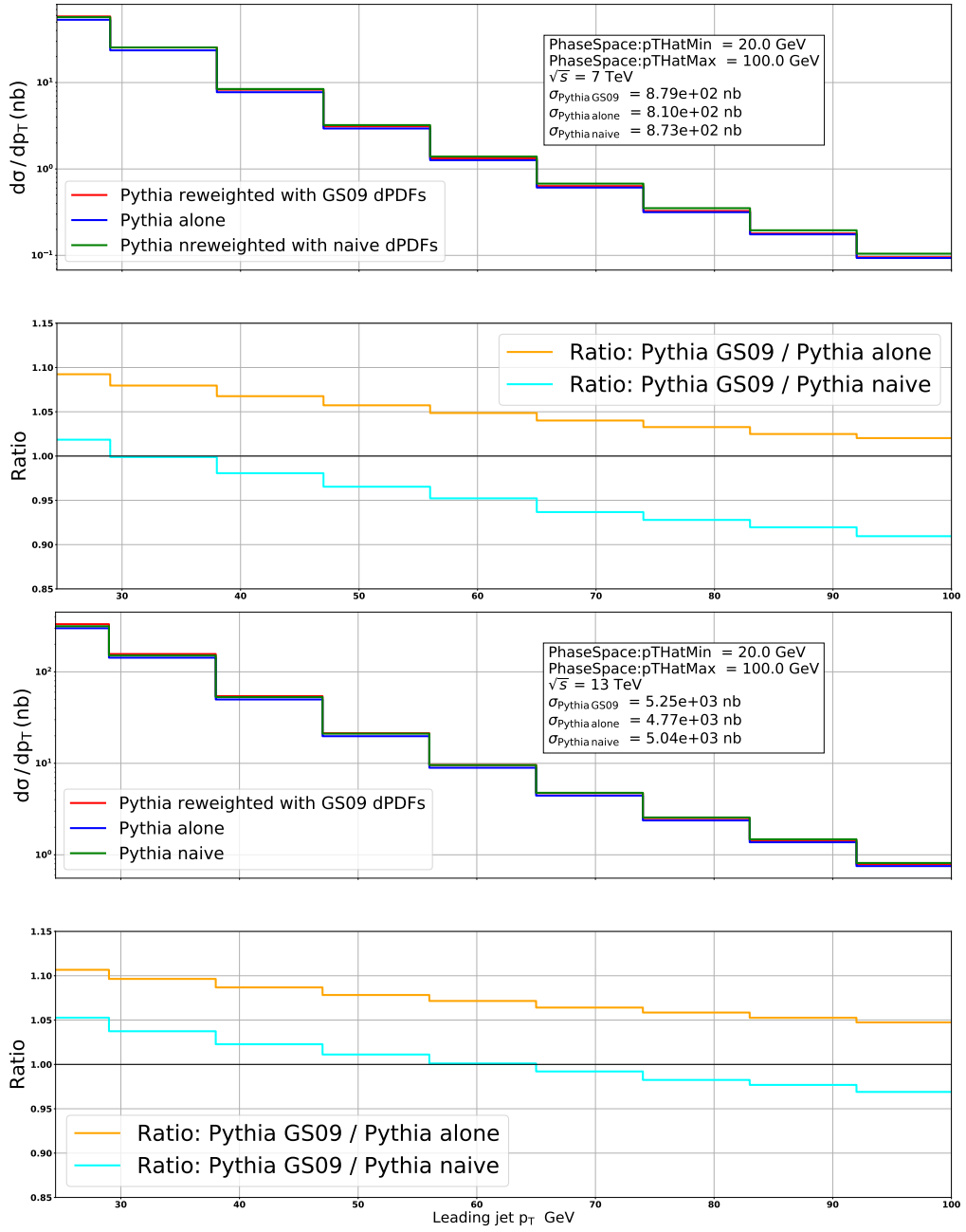

Figure 6.6: Comparison between leading jet $p_\perp$ DPS distributions generated with GS09, `Pythia` and "naive" dPDFs. Upper panel: $\sqrt{S} = 7$ TeV. Lower panel: $\sqrt{S} = 13$ TeV.

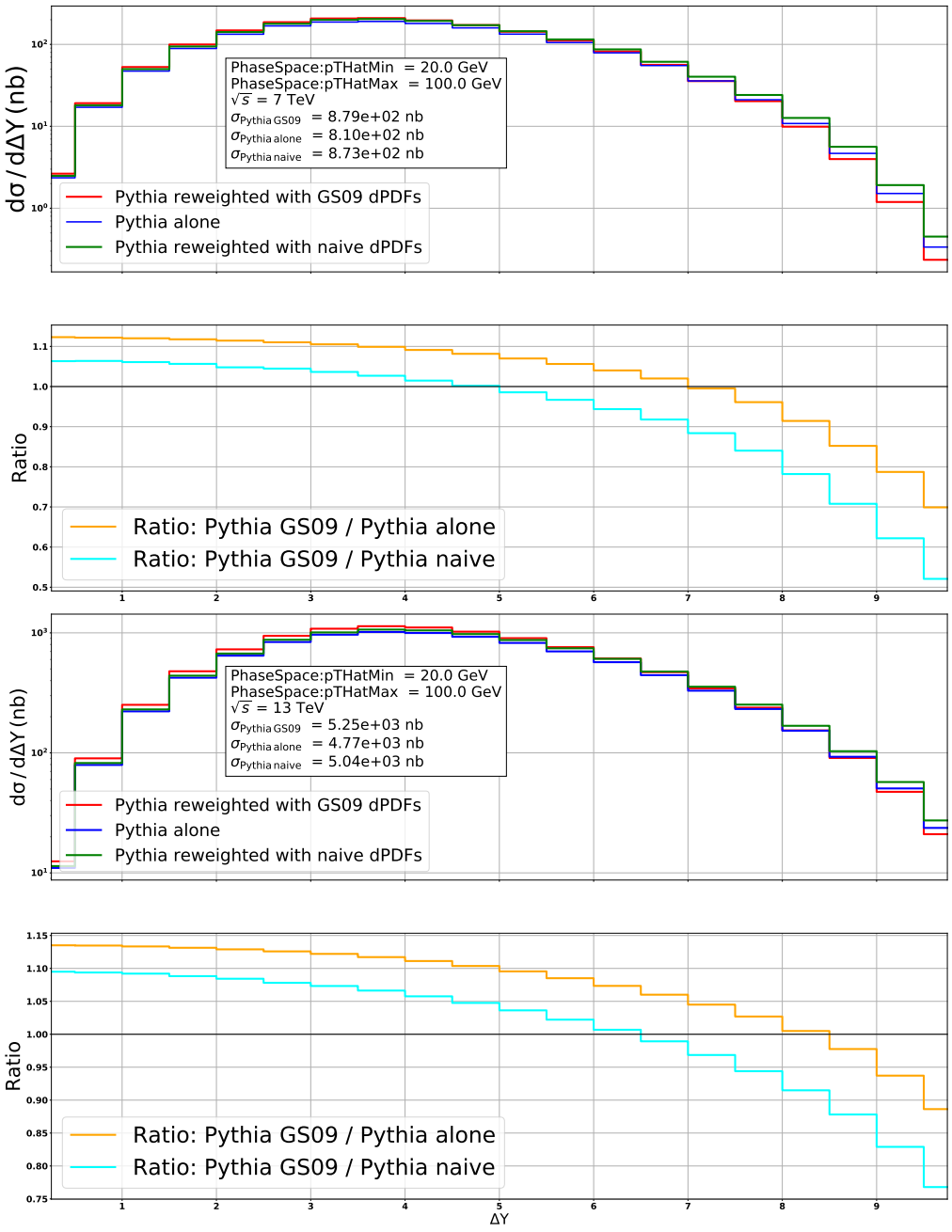

Figure 6.7: Comparison between leading jet $\Delta Y = \max|y_i - y_j|$ DPS distributions generated with GS09, `Pythia` and "naive" dPDFs. Upper panel: $\sqrt{S} = 7$ TeV. Lower panel: $\sqrt{S} = 13$ TeV.

6.4 Symmetrisation of dPDFs in the Pythia event generator

In the previous section we have not made a distinction between DPS and MPI models being used in the `Pythia` event generator. For example, in Chapter 6.1 we have described the way `Pythia` modifies PDFs in order to account for the momentum and number conservation in subsequent interactions, which applies both to MPI and DPS. Here, however, we will discuss some distinctive features of DPS and MPI models of `Pythia` as well as some recent modifications of DPS modelling.

The model of DPS used in `Pythia` has inherited its main concepts from the original `Pythia`'s model of MPI. This, in particular, implies that only PDFs used to generate the second hard interaction are modified in order to account for momentum and flavour conservation. This procedure, however, introduces asymmetry of the `Pythia`'s dPDFs and is in contradiction with the GS09 approach. This contradictions arise from the symmetry of dPDF under a simultaneous interchange of all its indices

$$D_{a_1,a_2}\left(x_1,x_2,Q_1^2,Q_2^2\right) = D_{a_2,a_1}\left(x_2,x_1,Q_2^2,Q_1^2\right), \tag{6.48}$$

which is simply a reflection of the fact that there is no ordering of hard interactions in DPS. However, dPDFs being used in `Pythia` do not posses such symmetry since

$$\begin{aligned} D_{a_1,a_2}\left(x_1,x_2,Q_1^2,Q_2^2\right) &\simeq f_{raw}(x_1,Q_1^2) f_{mod}(x_2,Q_2^2) \neq & (6.49)\\ &\neq f_{raw}(x_2,Q_2^2) f_{mod}(x_1,Q_1^2), & (6.50) \end{aligned}$$

and, therefore, within the `Pythia`'s framework

$$D_{a_1,a_2}\left(x_1,x_2,Q_1^2,Q_2^2\right) \neq D_{a_2,a_1}\left(x_2,x_1,Q_2^2,Q_1^2\right). \tag{6.51}$$

We illustrate this discrepancy by studying a distribution of the ratio between GS09 and `Pythia` DPS luminosities for a given event

$$\omega = \frac{D_{a_1,a_2}(x_1,x_2,Q_1^2,Q_2^2)\, D_{b_1,b_2}(x_3,x_4,Q_1^2,Q_2^2)}{f_{raw}^{a_1}(x_1,Q_1^2) f_{mod}^{a_2}(x_2,Q_2^2) f_{raw}^{b_1}(x_3,Q_1^2) f_{mod}^{b_2}(x_4,Q_2^2)}. \tag{6.52}$$

Since ω is a function of 10 variables, in order to facilitate our analysis, we consider production of two quarks of the same flavour and two gluons via $(q\,g \to q\,g) \otimes (q\,g \to q\,g)$ DPS process. Moreover, we consider only two different combinations of dPDFs, namely $D_{qq} \otimes D_{gg}$ and $D_{gg} \otimes D_{qq}$ which allows to express ω as

$$\omega = \frac{D_{qq}(x_1,x_2,Q_1^2,Q_2^2)\, D_{gg}(x_3,x_4,Q_1^2,Q_2^2)}{f_{raw}^{q}(x_1,Q_1^2) f_{mod}^{q}(x_2,Q_2^2) f_{raw}^{g}(x_3,Q_1^2) f_{mod}^{g}(x_4,Q_2^2)}. \tag{6.53}$$

We see that the numerator of Eq. 6.53 is symmetric under the simultaneous interchange $x_1 \leftrightarrow x_2$ and $Q_1^2 \leftrightarrow Q_2^2$. This, however, is not true for the denominator. Therefore ω depends on the ordering in x_1, x_2 and Q_1^2, Q_2^2. In order to illustrate it we consider four different permutations:

1. $x_1 > x_2$ and $Q_1 > Q_2$,
2. $x_1 < x_2$ and $Q_1 > Q_2$,
3. $x_1 > x_2$ and $Q_1 < Q_2$,

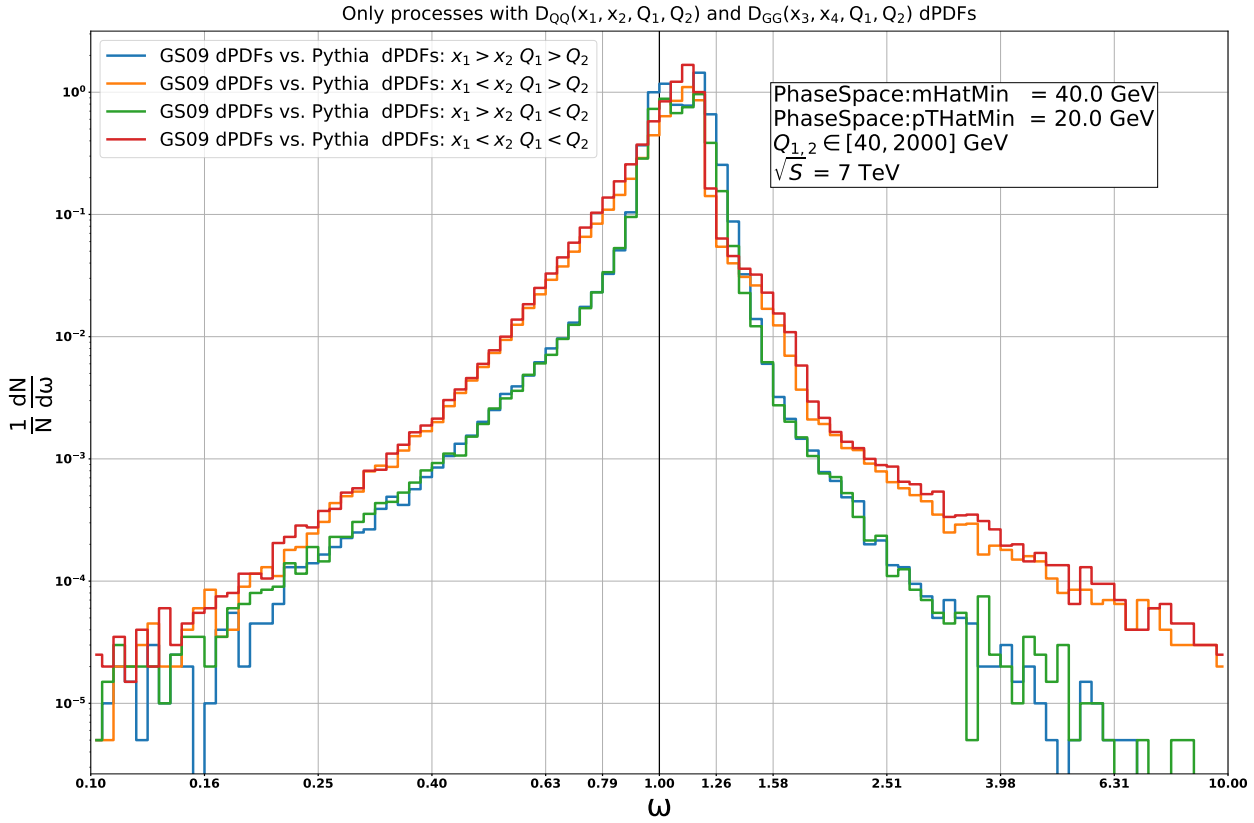

Figure 6.8: Distribution of the ratio of GS09 and `Pythia` DPS luminosities: old asymmetric approach available in `Pythia` releases with versions earlier than `8.240`.

4. $x_1 < x_2$ and $Q_1 < Q_2$.

In Fig. 6.8 we plot the distributions of ω for the aforementioned combinations of Bjorken variables and factorization scales. The distributions are normalized such that the total area under each histogram is equal to unity. We see that the maximum of each histogram is located close to unity which means that despite the significant conceptual differences between the GS09 and `Pythia` approaches both models give rather similar predictions. However, we also see that among four different histograms one can identify two separate subgroups, namely we see that distributions with $x_1 > x_2$, $Q_1 > Q_2$ and $x_1 > x_2$, $Q_1 < Q_2$ (blue and green histograms) coincide as well as distributions with $x_1 < x_2$, $Q_1 > Q_2$ and $x_1 < x_2$ and $Q_1 < Q_2$ (orange and red histograms). This implies that DPS events generated with `Pythia` do not demonstrate dependence on the ordering in factorization scales but instead depend on the ordering in Bjorken variables. The DPS model of `Pythia` has inherited this ordering from the `MPI` model of `Pythia` where such ordering is used to preserve conservation of the longitudinal momentum.

In the rest of the section we describe how to symmetrize dPDFs used to generate DPS events in the `Pythia` event generator. In Chapter 6.1 we have described how a standard *hit-or-miss* approach works in a context of generation of DPS events within `Pythia`'s framework. In particular, we have discussed the way `Pythia` produces weighted events at the first stage of the generation algorithm, see Eq. 6.25. The key idea of the improved approach is to replace an asymmetric product of two `Pythia`'s PDFs

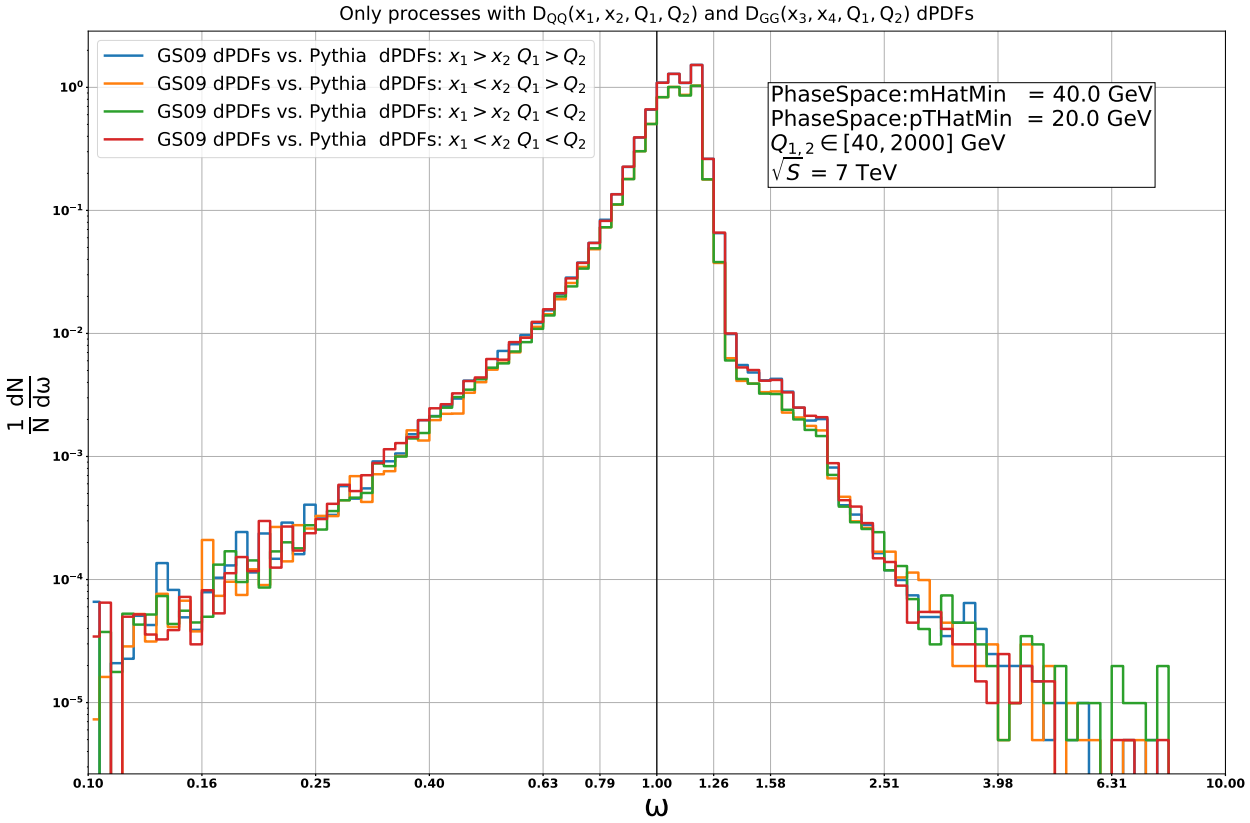

Figure 6.9: Distribution of the ratio of GS09 and `Pythia` DPS luminosities: new symmetric approach implemented in `Pythia 8.240`.

$D_{ij}^{Pythia}\left(x_1, x_2, Q_1^2, Q_2^2\right)\, D_{kl}^{Pythia}\left(x_3, x_4, Q_1^2, Q_2^2\right)$ by a symmetric one

$$\begin{aligned} & \frac{1}{2}\, f_{raw}^{i}(x_1, Q_1^2)\, f_{mod}^{j}(x_2, Q_2^2)\, f_{raw}^{k}(x_3, Q_1^2)\, f_{mod}^{l}(x_4, Q_2^2) + \\ + \quad & \frac{1}{2}\, f_{mod}^{i}(x_1, Q_1^2)\, f_{raw}^{j}(x_2, Q_2^2)\, f_{mod}^{k}(x_3, Q_1^2)\, f_{raw}^{l}(x_4, Q_2^2). \end{aligned} \tag{6.54}$$

After doing that one evaluates a symmetric DPS weight

$$\begin{aligned} \omega_{sym} \quad = \quad & \frac{1}{2}\, \frac{f_{raw}^{i}(x_1, Q_1^2)\, f_{mod}^{j}(x_2, Q_2^2)\, f_{raw}^{k}(x_3, Q_1^2)\, f_{mod}^{l}(x_4, Q_2^2)}{f_{raw}^{i}(x_1, Q_1^2)\, f_{raw}^{j}(x_2, Q_2^2)\, f_{raw}^{k}(x_3, Q_1^2)\, f_{raw}^{l}(x_4, Q_2^2)} + \\ + \quad & \frac{1}{2}\, \frac{f_{mod}^{i}(x_1, Q_1^2)\, f_{raw}^{j}(x_2, Q_2^2)\, f_{mod}^{k}(x_3, Q_1^2)\, f_{raw}^{l}(x_4, Q_2^2)}{f_{raw}^{i}(x_1, Q_1^2)\, f_{raw}^{j}(x_2, Q_2^2)\, f_{raw}^{k}(x_3, Q_1^2)\, f_{raw}^{l}(x_4, Q_2^2)} = \\ = \quad & \frac{1}{2}\, \left(\frac{f_{mod}^{j}(x_2, Q_2^2)\, f_{mod}^{l}(x_4, Q_2^2)}{f_{raw}^{j}(x_2, Q_2^2)\, f_{raw}^{l}(x_4, Q_2^2)} + \frac{f_{mod}^{i}(x_1, Q_1^2)\, f_{mod}^{k}(x_3, Q_1^2)}{f_{raw}^{i}(x_1, Q_1^2)\, f_{raw}^{k}(x_3, Q_1^2)} \right), \end{aligned} \tag{6.55}$$

where a conservation of the longitudinal momentum is implicitly assumed. Unlike the old DPS weight in Eq. 6.25 by construction the new weight ω_{sym} possesses the same symmetry under permutations $i \leftrightarrow j$, $x_1 \leftrightarrow x_2$, $Q_1 \leftrightarrow Q_2$ and $k \leftrightarrow l$, $x_3 \leftrightarrow x_4$, $Q_1 \leftrightarrow Q_2$ as GS09 dPDFs. After evaluation of ω_{sym} one performs the second step of the *hit-or-miss* algorithm to produce unweighted DPS events.

Now we can study the distribution of a ratio between GS09 DPS luminosities and symmetrized

`Pythia` DPS luminosities given by Eq. 6.54. The results are presented in Fig. 6.9. We see that the new distributions, contrary to the distributions shown in Fig. 6.8 have a narrower shape and demonstrate a symmetry under the simultaneous interchange of Bjorken variables and factorization scales.

We can study now how the effect of the symmetrization of the DPS weights. In order to do that we compare predictions of recently released `Pythia 8.240` which contains the improved model[3] of DPS against predictions of older release `Pythia 8.235`. Namely, we simulate the four-jet DPS production in pp collisions at $\sqrt{S} = 7\,\text{TeV}$ and $\sqrt{S} = 13\,\text{TeV}$. Similarly to our previous analysis we require all four jets to have a transverse momentum between 20 GeV and 100 GeV and we choose the factorization and renormalization scales to be equal to the geometric mean of the squared transverse masses of the two outgoing particles *i.e.* transverse momentum squared in the case of massless particles. The complete setup is given in Table 6.5. The results of the simulation are

PYTHIA SWITCH	VALUE
`Random:setSeed`	on
`HardQCD:all`	on
`SecondHard:generate`	on
`SecondHard:TwoJets`	on
`PartonLevel:isr`	off
`PartonLevel:fsr`	off
`PartonLevel:Remnants`	off
`Check:event`	off
`ColourReconnection:reconnect`	off
`PartonLevel:mpi`	off
`HadronLevel:all`	off

PYTHIA FLAG	VALUE
`HardQCD:nQuarkNew`	3
`PhaseSpace:pTHatMin`	20.0
`PhaseSpace:pTHatMax`	100.0
`Beams:idA`	2212
`Beams:idB`	2212
`Beams:frameType`	1
`Beams:eCM`	7, 13 TeV
`PDF:pSet`	MSTW2008lo68cl
`SigmaProcess:renormScale2`	2
`SigmaProcess:factorScale2`	2

Table 6.5: Pythia settings.

shown in Fig. 6.10. We see that the overall impact of the symmetrization of dPDFs is very modest and hardly exceeds 1% level. The small difference between both approaches can be explained by an exponential suppression of "tails" of distributions of ω as it is shown in Fig. 6.8 - 6.9.

[3]For the implementation see the `nextTwo` method of the `ProcessLevel` class.

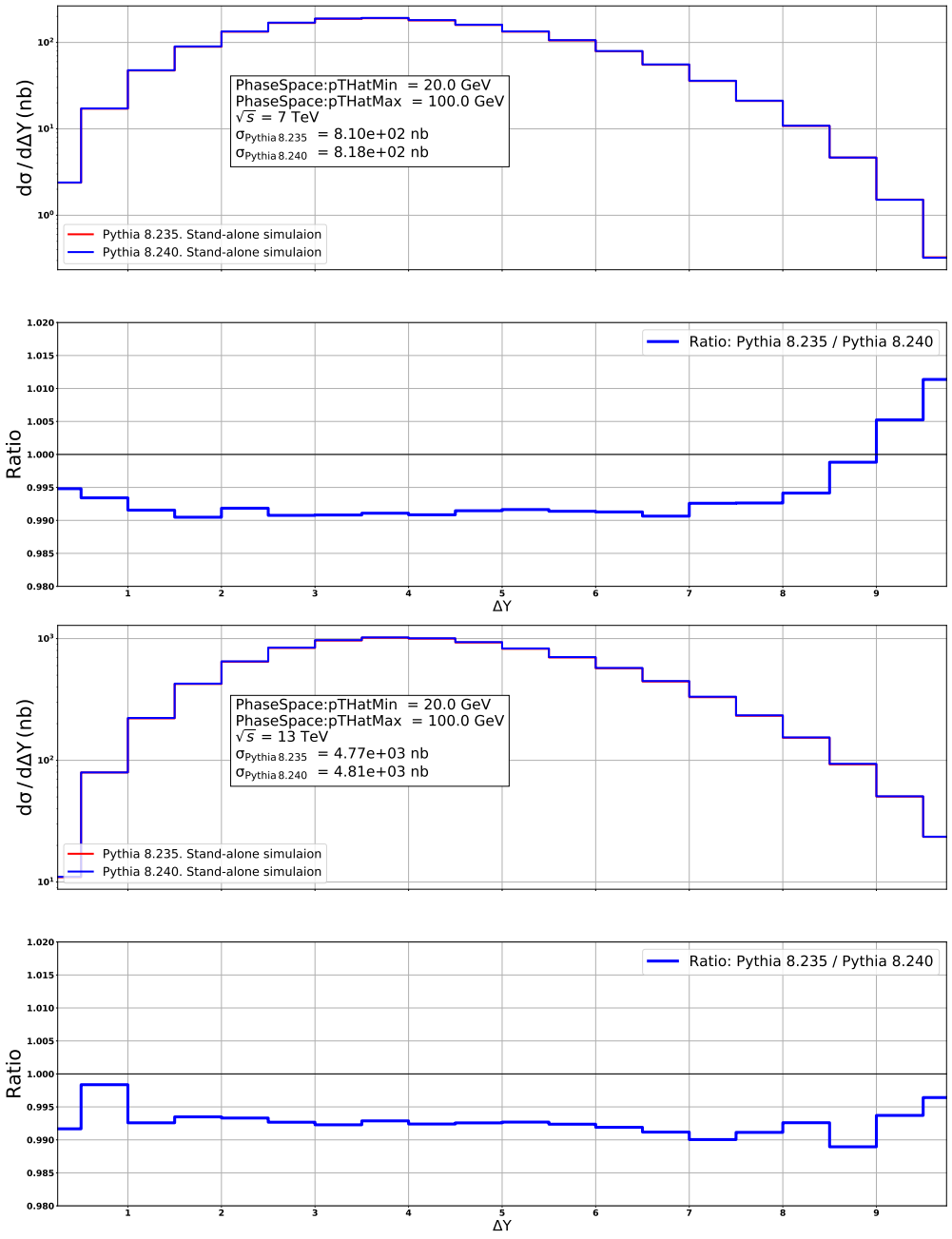

Figure 6.10: Four jet production at $\sqrt{S} = 7\,\text{TeV}$ and $\sqrt{S} = 13\,\text{TeV}$. Comparison between ΔY distributions simulated with `Pythia 8.240` and `Pythia 8.235`.

6.5 Conclusions

In this chapter we have provided a detailed comparison between GS09 model of dPDFs and the model of dPDFs by Sjöstrand and Skands [260] being used in the `Pythia` event generator [255] - [257]. We have demonstrated that both models of dPDFs obey the same set of sum rules proposed by Gaunt & Stirling in [173] (GS sum rules). The fundamental character of the GS sum rules was recently demonstrated in the paper of Diehl *et al.* [177] where it was shown that GS sum rules are preserved in QCD in all orders in perturbation theory. Since the GS sum rules state the conservation of momentum and number (flavour) of partons in the DPS processes they may induce the important partonic correlations especially at large values of $\Delta Y = \max|y_i - y_j|$ where one can probe valence quark distributions. In order to disentangle the evolution effects in GS09 model and the flavour and momentum correlations induced by the GS sum rules, we have studied the four-jet DPS production for three different models of dPDFs: GS09, Sjöstrand & Skands and "naive" dPDFs. Since the model of Sjöstrand & Skands preserves the GS sum rules but does not include the evolution effects due to the dDGLAP evolution equations the aforementioned comparison allows to study the impact of the GS sum rules separately. The comparison between ΔY DPS distributions generated with these three sets of dPDFs shows that at high values of ΔY the difference between distributions generated with GS09 and Sjöstrand & Skands dPDFs is smaller than the difference between distributions generated with GS09 and "naive" dPDFs. Therefore, we conclude that the correlations in momentum and flavour induced by the GS sum rules may have a sizeable impact on the DPS production of four well separated in rapidity jets. The weights used to generate DPS events in the `Pythia` event generator are evaluated according to the `Pythia` model of MPI [258] - [262]. Among the other things, it implies that the DPS weights are not symmetric under simultaneous interchange of the Bjorken variables, factorization scales and labels of the partons involved into the first and second hard interactions correspondingly. This ordering is dictated by the symmetry of the DPS processes under the interchange of the initial state partons. We have studied the impact of the symmetrization of the DPS weights on the four-jet DPS production and found it to be very modest. The symmetrized DPS weights are available in the `Pythia` event generator starting from the version 8.240.

Chapter 7

Four-jet DPS production in proton-nucleus collisions within the Pythia's framework

7.1 Introduction

While a significant progress in theoretical description of DPS in pA collisions have been achieved [213] - [216], a framework for realistic simulations of DPS in pA collisions is yet to be developed. In this chapter we compare predictions of the Strikman & Treleani model [213] against predictions of the `Angantyr` model of pA collisions [271], recently implemented in the `Pythia 8` event generator [255], [256].

7.2 The Angantyr model of pA collisions

Usually, the existing Monte Carlo event generators for pA collisions are more "special purpose" and mostly dedicated to studies of formation and evolution of the *Quark-Gluon Plasma*, *e.g.* EPOS-LHC [272], AMPT [273] and HIJING [274]. On the other side there are models postulating flow-like effects to have a non-thermal origin and, therefore, aiming to reproduce general features of pA (AA) collisions by adding a nuclear structure "on top" of existing pp models. One of such models called `Angantyr` [271], was recently implemented in the `Pythia` 8 event generator. It was inspired by the old Lund Fritiof model [275] and the DIPSY code [278] - [280] which models BFKL evolution of a gluon cascade via Mueller dipole approach [276], [277].

The production of final state particles in `Angantyr` is based upon `Pythia`'s models for *multiple parton interaction* (MPI) [258] - [262] and diffractive processes [282], [283] with certain modifications which we are going to discuss below.

First of all let us describe the way `Angantyr` treats production of particles in interactions involving one incident proton and a single nucleon as in Fig. 7.1 a). In this case one could expect that all MPI would be distributed according to a Poissonian distribution. This approach to MPI modelling, however, may lead to momentum violation and is in contradiction with KNO scaling [281] of charge multiplicity distributions, see review [263]. In order to solve this issues all MPI in `Pythia`

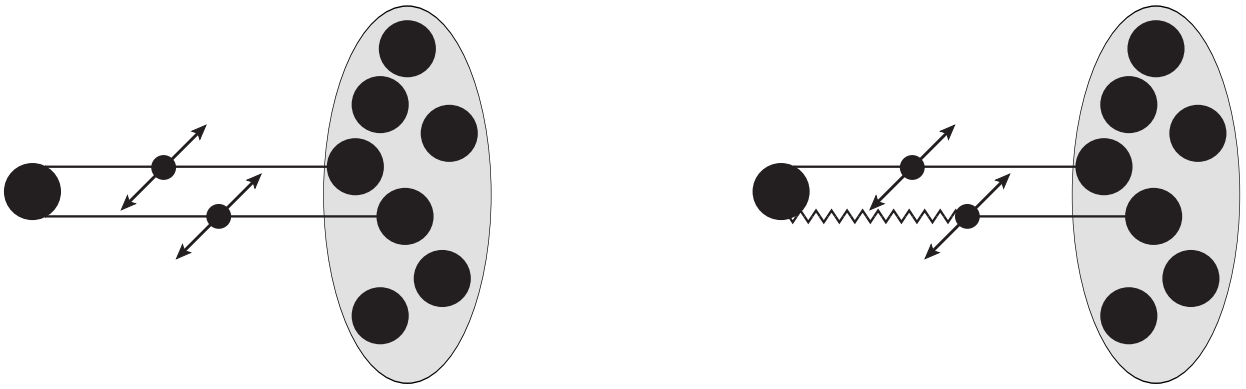

a) b)

Figure 7.1: A schematic representation of different contributions to DPS from Angantyr model. a) Two versus two contribution. b) One versus two contribution. A zigzag line stands for a hard pomeron exchange.

are ordered in transverse momentum as $\sqrt{s}/2 > p_{\perp 1} > p_{\perp 2} > \ldots > p_{\perp n} > p_{\perp \min}$. A probability of the first interaction to happen at a given transverse momentum $\frac{d\sigma}{dp_{\perp 1}}/\sigma_{\mathrm{ND}}^{\mathrm{pp}}(s)$ is multiplied by a Sudakow-like exponent

$$\frac{d\mathcal{P}}{dp_{\perp 1}} = \frac{1}{\sigma_{\mathrm{ND}}^{\mathrm{pp}}(s)} \frac{d\sigma}{dp_{\perp 1}} \exp\left(- \int_{p_{\perp 1}}^{\sqrt{s}/2} \frac{1}{\sigma_{\mathrm{ND}}^{\mathrm{pp}}(s)} \frac{d\sigma}{dp'_{\perp}} dp'_{\perp} \right), \tag{7.1}$$

which ensures that no other interactions will happen in $p_{\perp}$ range between $\sqrt{s}/2$ and $p_{\perp 1}$. Therefore, a probability for all subsequent interactions is given by

$$\frac{d\mathcal{P}}{dp_{\perp i}} = \frac{1}{\sigma_{\mathrm{ND}}^{\mathrm{pp}}(s)} \frac{d\sigma}{dp_{\perp i}} \exp\left(- \int_{p_{\perp i}}^{p_{\perp i-1}} \frac{1}{\sigma_{\mathrm{ND}}^{\mathrm{pp}}(s)} \frac{d\sigma}{dp'_{\perp}} dp'_{\perp} \right), \tag{7.2}$$

which ensures the aforementioned ordering. In addition to this, the MPI model of `Pythia` accounts for momentum and number conservation which implies that PDFs used for the second interaction (as well as for all subsequent interactions) will be "squeezed" and reweighted according to a history of all previous interactions such that momentum and number conservation is preserved, see [260] and Chapter 6.1. We shall also note that σ_{eff} does not enter explicitly in this model. More specifically a ratio $\sigma_{\mathrm{ND}}^{\mathrm{pp}}(s)/\sigma_{eff}$ describes a deviation of a distribution of MPIs from a Poissonian distribution, see Chapter 4.2. However, it implies that direct comparison between predictions of `Angantyr` and DPS model of Strikman and Treleani is not possible since the corresponding value of parameter σ_{eff} is unknown. We will come back to this issue later in section 7.3.

Description of processes involving one incoming proton and *two different* nucleons is somewhat more sophisticated. In principle one would want to implement the same contribution as shown in Fig. 5.1 b). However, in practice, incorporation of such processes in `Angantyr`'s framework leads to serious technical difficulties. It is possible to circumvent these issues by mimicking the second interaction in Fig. 5.1 a) via pomeron-nucleon collision as shown in Fig. 7.1 b). In order to be consistent with the terminology of the original `Angantyr` paper [271] in the following we refer to

the processes shown in Fig. 5.1 as to double absorptive processes. In order to simulate double absorptive process from Fig. 5.1 b), `Angantyr` will first simulate a single absorptive process by using a standard model of pp collisions and then simulate a second absorptive process *as it was* produced through a single diffractive excitation. All subsequent interactions will be produced by using standard pp or pomeron-proton MPI models taking into account momentum conservation but neglecting a number conservation as in old MPI model of `Pythia` [259].

There are several ways to produce diffractive events in `Pythia` 8. The `Angantyr` model is based upon a model of *soft* diffraction in `Pythia`. For high-mass diffraction `Pythia` uses Ingelman and Schlein model where pomeron is considered as a hadronic state [284]. Within this approach `Pythia` treats a proton-pomeron collision as a normal non-diffractive hadron-hadron collision using standard MPI, ISR and FSR models. Therefore, a corresponding differential $2 \to 2$ cross section is given by

$$d\sigma_{ij}^{\mathrm{p}\mathbb{P}} = \frac{dx_{\mathbb{P}}}{x_{\mathbb{P}}} \frac{dx_1}{x_1} \frac{d\beta}{\beta} F\left(x_{\mathbb{P}}\right) x_1 f_{i/p}(x_1, Q^2)\, \beta f_{j/\mathbb{P}}(\beta, Q^2)\, d\hat{\sigma}_{ij}, \tag{7.3}$$

where $x_{\mathbb{P}}$ is a fraction of the target proton momentum taken by the pomeron, β is a fraction of the pomeron's momentum taken by the parton j and x_1 is a fraction of pomeron's momentum taken by parton i. A diffractive mass M_X^2 is therefore given by $M_X^2 = x_{\mathbb{P}} s$. In the `Angantyr` model a pomeron flux $F\left(x_{\mathbb{P}}\right)$ is postulated to be a constant which implies a flat distribution in $\log\left(M_X^2\right)$. A hard cross section $\hat{\sigma}_{ij}$ on the RHS of Eq. 7.3 is a standard *leading order* (LO) $2 \to 2$ cross section which is known to be divergent for low $p_\perp$ values. In this case `Pythia` imposes a smooth cut-off on $\hat{\sigma}_{ij}$ according to

$$\frac{d\hat{\sigma}_{ij}}{dp_\perp^2} \propto \frac{\alpha_s^2(p_\perp^2)}{p_\perp^4} \to \frac{\alpha_s^2(p_\perp^2 + p_{\perp 0}^2)}{(p_\perp^2 + p_{\perp 0}^2)^2}, \tag{7.4}$$

where $p_{\perp 0}$ is a soft regulator which depends either on diffractive mass (for diffractive processes) or on collision energy (for standard pp processes). Nevertheless, even after a regularization of $\hat{\sigma}_{ij}$ as in Eq. 7.4, an integrated partonic cross section may exceed a total non-diffractive proton-pomeron cross section for a given diffractive mass M_X. In the MPI model of `Pythia` it is interpreted as a possibility to have several sub-scatterings in each collision with an average number

$$\langle N_{sc}^{\mathrm{p}\mathbb{P}}\left(M_X^2\right)\rangle = \frac{1}{\sigma_{\mathrm{ND}}^{\mathrm{p}\mathbb{P}}\left(M_X\right)} \int \frac{dx_1}{x_1} \frac{d\beta}{\beta} dp_\perp^2 \sum_{ij} x_1 f_{i/p}(x_1, Q^2)\, \beta f_{j/\mathbb{P}}(\beta, Q^2) \frac{d\hat{\sigma}_{ij}}{dp_\perp^2}. \tag{7.5}$$

However, as it was pointed out in [270], a modelling of single absorptive events via *single diffractive* (SD) events results in too low activity in pA collisions. In principle, one can solve this problem either by tuning the value of $\sigma_{\mathrm{ND}}^{\mathrm{p}\mathbb{P}}\left(M_X\right)$ in Eq. 7.5 or by changing pomeron PDFs. By comparing a distribution $d\langle N_{sc}^{\mathrm{p}\mathbb{P}}\rangle/dy$ for SD events

$$\begin{aligned} \frac{d\langle N_{sc}^{\mathrm{p}\mathbb{P}}\rangle}{dy} &= \frac{1}{\sigma_{\mathrm{ND}}^{\mathrm{p}\mathbb{P}}\left(M_X^2\right)} \int \frac{dx_1}{x_1} \frac{d\beta}{\beta} dp_\perp^2 \sum_{ij} x_1 f_{i/p}(x_1, Q^2)\, \beta f_{j/\mathbb{P}}(\beta, Q^2) \times \\ &\times \frac{d\hat{\sigma}_{ij}}{dp_\perp^2} \delta\left(y - \frac{1}{2}\log\frac{x_1}{\beta x_{\mathbb{P}}}\right), \end{aligned} \tag{7.6}$$

against a corresponding distribution for standard non-diffractive pp events

$$\frac{d\langle N_{sc}^{\rm pp}\rangle}{dy} = \frac{1}{\sigma_{\rm ND}^{\rm pp}(s)} \int \frac{dx_1}{x_1}\frac{dx_2}{x_2} dp_\perp^2 \sum_{ij} x_1 f_{i/p}(x_1,Q^2)\, x_2 f_{j/p}(x_2,Q^2) \times \\ \times \frac{d\hat{\sigma}_{ij}}{dp_\perp^2}\delta\left(y - \frac{1}{2}\log\frac{x_1}{x_2}\right), \tag{7.7}$$

we see that if in Eq. 7.6 we set $\beta f_{j/\mathbb{P},Q^2} \to x_{\mathbb{P}}\beta f_{j/p}\left(x_{\mathbb{P}}\beta, Q^2\right)$, $\sigma_{\rm ND}^{\rm p\mathbb{P}}(M_X) \to \sigma_{\rm ND}^{\rm pp}(s)$ we will get an expression very similar to Eq. 7.7. In addition to this, a soft regulator $p_{\perp 0}$ in Eq. 7.4 now depends on a collision energy $p_{\perp 0}\left(M_X^2\right) \to p_{\perp 0}(s)$.

Validity of this approach was studied in detail in [271]. In particular it was shown that Eq. 7.6 with aforementioned modification provides an overall fair description of experimental data, see, for example, Fig. 7.2. However, all `Angantyr` checks in [271] were related to MPI-sensitive distributions. *e. g.* a charged multiplicity distribution. Indeed, such distributions are known to be very sensitive to a number of semi-hard and soft sub-collisions in a given event, see, for example, review [263]. Therefore, correct predictions of shapes of such distributions can be seen as a validation of both MPI and `Angantyr` models. In the next section of this chapter we will switch our attention from MPI to DPS processes and perform another check of the `Angantyr` model. Namely, we will study how well it can reproduce predictions of Strikman and Treleani for DPS production of four *hard* jets in pA collisions.

7.3 Predictions of Pythia

In section 7.2 we have described the `Angantyr` model of pA collisions implemented in `Pythia` event generator. Originally this model was not designed to study DPS in pA collisions. However, as we discussed in section 7.2, the `Angantyr` model accounts for interactions which occur not only between an incident proton and a single nucleon but also for processes which occur between an incident proton and *two different nucleons*, as schematically shown in Fig. 7.1. These interactions are realized via the MPI model and the model of diffractive interactions of `Pythia` with modifications described in section 7.3. In the MPI model of `Pythia` all interactions are strictly ordered in transverse momentum which implies that second interaction always will be softer than the first one. It means that production of DPS events in MPI model is suppressed. Nevertheless, for the number of generation calls large enough one can collect a sufficiently large DPS statistics by generating MPI events. It means that, in principle, one can use the `Angantyr` model to simulate DPS events in pA collisions. In Chapter 5 we discussed the application of Strikman & Treleani model of DPS in pA collisions [213] to four-jet DPS production. Now, we investigate how well the `Angantyr` model can reproduce predictions obtained within Strikman & Treleani framework.

However, before starting to compare predictions of `Pythia` against Strikman & Treleani model several important comments have to be made. First of all, as we already mentioned in Chapter 6, all MPI produced in a given event are strictly ordered in $p_\perp$. This ordering, however, is in contradiction with Strikman & Treleani model where a second process can have with equal probability a hard scale either smaller or bigger than a hard scale of the first one. One should also keep in mind that, in order to derive Eq. 5.7, Strikman and Treleani neglected partonic correlations in x-space and

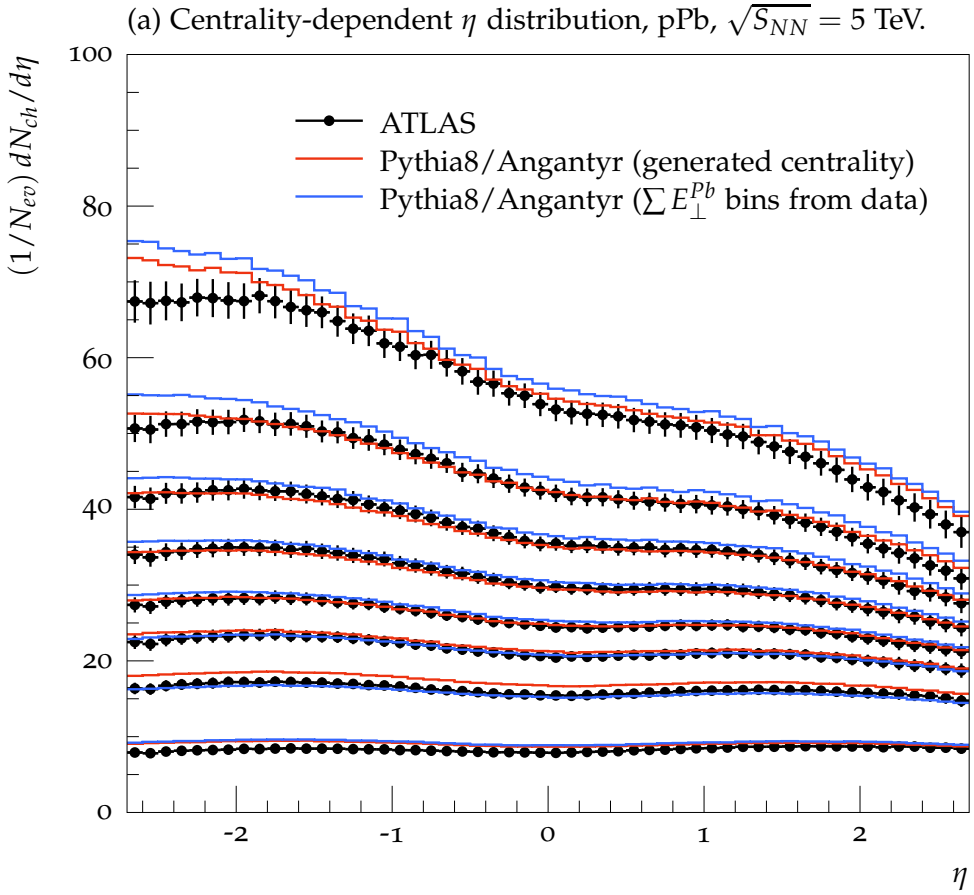

Figure 7.2: Comparison between the average charged multiplicity as a function of pseudo rapidity in percentile bins of centrality for pPb collisions at $\sqrt{s_{NN}} = 5$ TeV. Here the data from ATLAS [289] is compared to results from `Angantyr`, from [271].

assumed that both DPS I and DPS II contributions populate the same phase space region. As we have demonstrated in Chapter 5.2, the error due to this phase space approximation is completely negligible, see Fig. 5.3 and Fig. 5.4. Effects due to the correlations in x-space, nevertheless, may have a sizeable impact, see [216] and [171]-[173]. We also should keep in mind that `Pythia`'s approach to momentum and number conservation effectively means presence of non-trivial x-space partonic correlations in the MPI model. In the original paper of Strikman & Treleani the isospin invariance between all nucleons was assumed. However, the `Angantyr` model distinguish between protons and neutrons for signal processes (first hard interaction) and assumes the isospin invariance for the minimum bias processes (sequential MPI generated after the first hard interaction). Finally, we need to stress that the parameter σ_{eff} does not enter explicitly into MPI model of `Pythia`. Therefore, in order to compare the predictions of Strikman & Treleani model against predictions of `Angantyr` model one has to find the value of σ_{eff} in Strikman & Treleani model by fitting its predictions to the prediction of `Angantyr`.

Now, after describing all the important differences between both approaches, let us study how the DPS enhancement factor $\sigma_{\mathrm{pA}}^{\mathrm{DPS}}/\mathrm{A}\,\sigma_{\mathrm{pp}}^{\mathrm{DPS}}$ depends on a total number of nucleons A in the `Angantyr` model. Due to the aforementioned ordering of MPI one will need to perform a high number of generation calls in order to collect a good statistics for a four-jet DPS production, since a second

MPI will most of the time occur at too low scale to be considered as a hard interaction[1]. Therefore, we evaluate $\sigma_{\mathrm{pA}}^{\mathrm{DPS}}$ according to a following algorithm:

- find a total weight $w_{\mathrm{pA}}^{\mathrm{tot}}$ for all events produced in pA collisions and a corresponding total cross section $\sigma_{\mathrm{pA}}^{\mathrm{tot}}$.
- Find a total weight $w_{\mathrm{pA}}^{\mathrm{DPS}}$ of all events which satisfy a given set of cuts.
- Find a total DPS cross section in pA collisions $\sigma_{\mathrm{pA}}^{\mathrm{DPS}}$ from the ratio

$$\frac{\sigma_{\mathrm{pA}}^{\mathrm{DPS}}}{\sigma_{\mathrm{pA}}^{\mathrm{tot}}} = \frac{w_{\mathrm{pA}}^{\mathrm{DPS}}}{w_{\mathrm{pA}}^{\mathrm{tot}}}.$$

- Repeat the same for pp collisions. Find a corresponding total DPS cross section $\sigma_{\mathrm{pp}}^{\mathrm{DPS}}$.
- Evaluate $\sigma_{\mathrm{pA}}^{\mathrm{DPS}}/\mathrm{A}\sigma_{\mathrm{pp}}^{\mathrm{DPS}}$.

In principle, `Pythia` allows users to implement any isotope with given values of Z and N. Eight nuclei: ^{4}He, ^{6}Li, ^{12}C ,^{16}O, ^{63}Cu, ^{129}Xe, ^{197}Au and ^{208}Pb are available by default. Since a computation of a total DPS cross section according to the aforementioned algorithm can take tens of hours (depending on a chosen nucleus and a system performance), we decided to work only with already implemented nuclei and use the fit in Eq. 5.11 for better visualisation of our results and for comparison against Strikman & Treleani model.

Our results for $\sigma_{\mathrm{pA}}^{\mathrm{DPS}}/\mathrm{A}\sigma_{\mathrm{pp}}^{\mathrm{DPS}}$ are given in Table 7.2. In our simulations we were triggering on events with *at least* four jets with $p_{\perp} > 20$ GeV. We have also performed a stability check by varying a parameter `SDTries` which is a number of attempts to construct kinematics for double absorptive processes as in Fig. 7.1 b). By comparing values of $\sigma_{\mathrm{pA}}^{\mathrm{DPS}}/\mathrm{A}\sigma_{\mathrm{pp}}^{\mathrm{DPS}}$ evaluated at different values of `SDTries` parameter, we see that fluctuations of $\sigma_{\mathrm{pA}}^{\mathrm{DPS}}/\mathrm{A}\sigma_{\mathrm{pp}}^{\mathrm{DPS}}$ do not exceed a few percent level, see Table 7.1

A comparison against Strikman & Treleani model is given in Fig. 7.3 and Table 7.2. The `Pythia` setup we have used is given in Table 7.3 and Table 7.4. In order to compare our results against Strikman & Treleani model we have tuned σ_{eff} in order to get an agreement in the value of the DPS enhancement factor $\sigma_{\mathrm{pA}}^{\mathrm{DPS}}/\mathrm{A}\sigma_{\mathrm{pp}}^{\mathrm{DPS}}$ for ^{208}Pb. We see that by choosing $\sigma_{eff} = 11\,\mathrm{mb}$ we can get a satisfactory agreement between both models not only for ^{208}Pb but also for other for heavy isotopes: ^{63}Cu, ^{129}Xe and ^{197}Au.

It could be very tempting to interpret `Angantyr` simulations as a fake data and to use main formula of Strikman & Treleani model, Eq. 5.7, for a fitting procedure to extract a value of σ_{eff} out of `Angantyr` simulations. However, due to the aforementioned differences between both models such procedure will not be correct. Also, as it was shown by Blok *et al.* [216], a treatment of DPS for light nuclei differs from a treatment of DPS for heavy nuclei due to the presence of additional DPS contributions, as shown in Fig 2.12 c) and d), which become less important for large values of A, see [216] and Chapter 2.6. Whereas the MPI model of `Pythia` partially accounts[2] for processes

[1] `Pythia` 8 allows to generate *always* two hard interactions in a given event by setting `SecondHard:generate = on`. However, usage of this flag together with `Angantyr` is not supported and will lead to wrong results.

[2] Namely, it accounts only for a gluon splitting of a type $g \to q\bar{q}$, for details see [260].

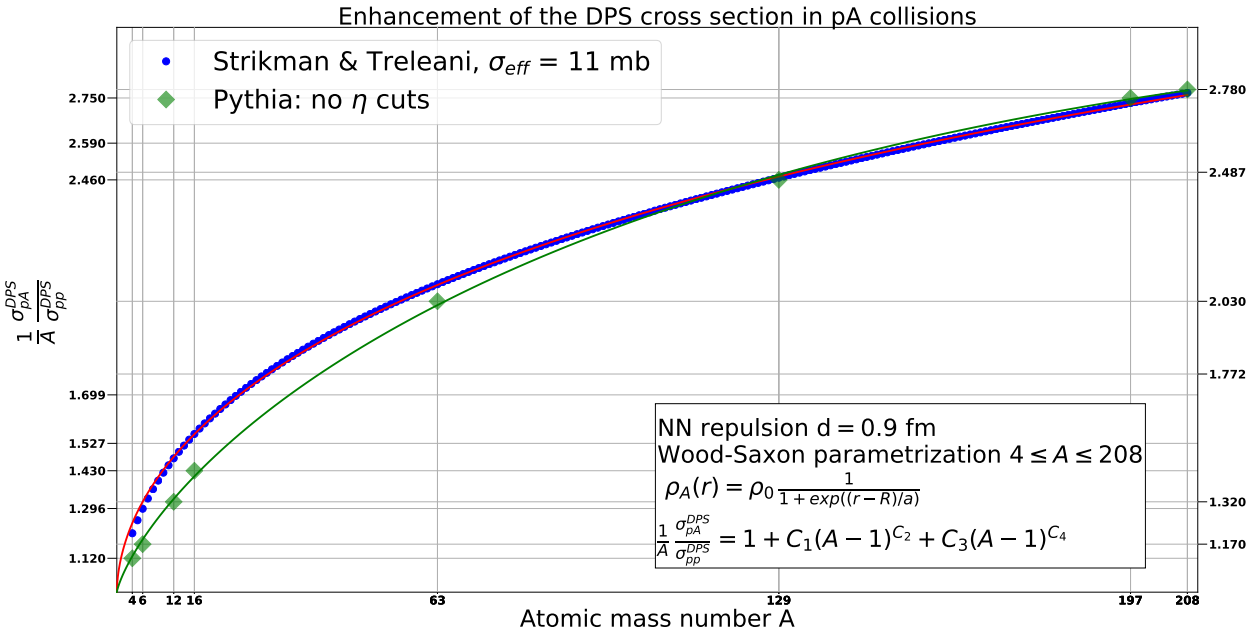

Figure 7.3: A DPS enhancement factor $\sigma_{\mathrm{pA}}^{\mathrm{DPS}}/\mathrm{A}\,\sigma_{\mathrm{pp}}^{\mathrm{DPS}}$. Comparison between theoretical predictions of Strikman and Treleani [213] and `Pythia`'s (`Angantyr`) simulations.

shown in Fig 2.12 c) and d), incorporation of such terms in the Strikman & Treleani framework is a non-trivial task, see [200] and [202].

Nucleus	Angantyr SDTries = 1	Angantyr SDTries = 2
^{4}He	1.12	1.12e+00
^{6}Li	1.17	1.18e+00
^{12}C	1.32	1.34e+00
^{16}O	1.43	1.43e+00
^{63}Cu	2.03	2.03e+00
^{129}Xe	2.46	2.43e+00
^{197}Au	2.75	2.75e+00
^{208}Pb	2.78	2.83e+00

Table 7.1: Predictions for enhancement factor for DPS in pA collisions at $\sqrt{S} = 5012$ GeV (10^6 Pythia calls).

Nucleus	Angantyr SDTries = 1	Strikman & Treleani
^{4}He	1.12	1.21
^{6}Li	1.17	1.30
^{12}C	1.32	1.47
^{16}O	1.43	1.56
^{63}Cu	2.03	2.09
^{129}Xe	2.46	2.51
^{197}Au	2.75	2.73
^{208}Pb	2.78	2.77

Table 7.2: Predictions for enhancement factor $\sigma_{\rm pA}^{\rm DPS}/{\rm A}\sigma_{\rm pp}^{\rm DPS}$ at $\sqrt{S} = 5012$ GeV (10^6 Pythia calls). In Strikman & Treleani model we set $\sigma_{eff} = 11\,{\rm mb}$.

`Pythia` Master Switch	Value
`Random:setSeed`	`on`
`HardQCD:all`	`on`
`PartonLevel:mpi`	`on`
`PartonLevel:Remnants`	`on`
`Check:event`	`on`
`PartonLevel:isr`	`off`
`PartonLevel:fsr`	`off`
`ColourReconnection:reconnect`	`off`
`HadronLevel:all`	`off`

Table 7.3: Values of the master switches of Pythia we use in our pA simulations.

`Pythia` Flag	Value
`Beams:idA`	2212
`Beams:idB`	1000020040 (as an example for ^{4}He)
`Beams:eA`	4000 GeV
`Beams:eB`	1570 GeV
`Beams:frameType`	2
`PDF:pSet`	LHAPDF6:MSTW2008lo68cl
`PhaseSpace:pTHatMin`	20.0 GeV
`SigmaProcess:renormScale2`	2
`SigmaProcess:factorScale2`	2

Table 7.4: Pythia beam parameters, scales, PDFs and cuts we use in our pA simulations.

7.4 Impact of rapidity cuts

In the simulations in section 7.3 we were triggering on events with at least four jets with $p_\perp > 20$ GeV without imposing any cuts on their rapidities. However, it is known that activity in pA collisions depends on rapidity of produced particles in a non-trivial way. Namely, as it was observed by the first time by Busza *et al.* [288], the charged multiplicity distribution $dN_{ch}/d\eta$ in pA collisions grows for the negative values of η (assuming that the nucleus A is located in the negative direction of the η-axis), see Fig. 7.2. There are several explanation of this phenomenon. Originally the growth of activity in the charged multiplicity distributions was explained by the original non-perturbative "wounded nucleon model" [285] - [287]. The `Angantyr` model of pA collisions can be seen as a perturbative version of the "wounded nucleon model" which includes which includes MPI produced according to Eq. 7.6 with modifications described in section 7.2. As shown in Fig. 7.2 the `Angantyr` model correctly describes the aforementioned enhancement. Since the particle production in `Angantyr` relies on the MPI model of the `Pythia` event generator the charged multiplicity distribution should be correlated with production of (mini-)jets. More precisely, the growth of charged multiplicity

$dN_{ch}/d\eta$ for negative η values in `Angantyr` model is inextricably connected with growth of a number of sub-scatterings in a given event, see Eq. 7.6 and Eq. 7.7. Therefore, it is natural to assume that in the `Angantyr` model probability to generate an event of a DPS II type will depend on η in a way similar to a $dN_{ch}/d\eta$ distribution. In order to check this we evaluate $\sigma_{\rm pA}^{\rm DPS}/{\rm A}\sigma_{\rm pp}^{\rm DPS}$ for events with at least four jets with $p_\perp$>20 GeV and at least one jet with a pseudo rapidity value smaller[3] than a certain value η_{cut}. Obviously, additional η cuts will reduce the total DPS cross section in pp and pA collisions. Nevertheless, one could expect that the total DPS cross section in the pA case will decrease much slower than corresponding one in the pp case. As a consequence, the enhancement factor $\sigma_{\rm pA}^{\rm DPS}/{\rm A}\sigma_{\rm pp}^{\rm DPS}$ will grow since in the `Angantyr` model probability to generate a processes of DPS II type will grow for small negative values of η.

The results are presented in Fig. 7.4. In order to study how the DPS enhancement factor $\sigma_{\rm pA}^{\rm DPS}/{\rm A}\sigma_{\rm pp}^{\rm DPS}$ depends on rapidity cuts we have used the same set up as before but with additional cuts $\eta_{cut} = -1$, $\eta_{cut} = -2$ and $\eta_{cut} = -3$. We see that indeed the ratio $\sigma_{\rm pA}^{\rm DPS}/{\rm A}\sigma_{\rm pp}^{\rm DPS}$ demonstrates a strong dependence on the value of η_{cut}. The experimental verification of the growth of the DPS enhancement factor $\sigma_{\rm pA}^{\rm DPS}/{\rm A}\sigma_{\rm pp}^{\rm DPS}$ due to the additional rapidity cut predicted by the `Angantyr` model could, in principle, provide a better way to control the double absorptive processes shown in Fig. 7.1 a).

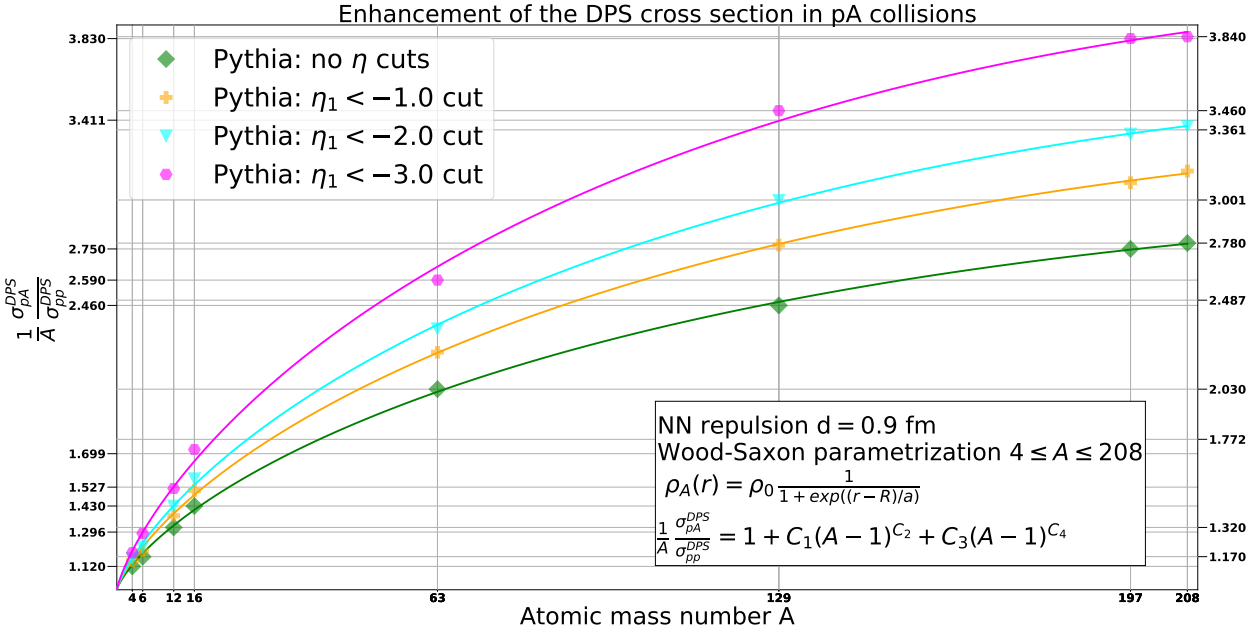

Figure 7.4: Dependence of the enhancement factor $\sigma_{\rm pA}^{\rm DPS}/{\rm A}\sigma_{\rm pp}^{\rm DPS}$ on η cuts. Predictions of `Pythia` (`Angantyr`). Here orange, cyan and magenta curves correspond to four jet DPS simulations with at least one jet with η smaller than -1, -2 and -3 correspondingly.

7.5 Conclusions

We have demonstrated that the `Angantyr` model of pA collisions in `Pythia 8` predicts the A-dependence of a DPS enhancement factor $\sigma_{\rm pA}^{\rm DPS}/{\rm A}\sigma_{\rm pp}^{\rm DPS}$ which agrees with the one predicted in the pioneering paper of Strikman and Treleani [213] at a qualitative level. This result can be seen as

[3] In our simulations we choose a pseudo rapidity axis to run in direction from a nucleus to a proton.

an additional validation of the Angantyr's approach to double absorbtive processes as described in section 7.2. Furthermore, the correct A-dependence in the Angantyr model means that, apart from "standard" applications, one can use Angantyr for standalone studies of the DPS in pA collisions. In this case users can benefit not only from evaluation of a total cross section, but also from the power of most of the models implemented in Pythia, *e. g.* ISR and FSR models, colour reconnections and hadronization models *etc.*

We also have studied how (pseudo)rapidity cuts affect the number of MPIs in a given event and therefore the behaviour of $\sigma_{\rm pA}^{\rm DPS}/{\rm A}\sigma_{\rm pp}^{\rm DPS}$. The growth of $\sigma_{\rm pA}^{\rm DPS}/{\rm A}\sigma_{\rm pp}^{\rm DPS}$ is a natural consequence of (pseudo)rapidity dependence of activity in pA collisions predicted by the "wounded nucleon model" [285] - [287] and is built into the Angantyr model. We also argue that the experimental verification of the enhancement of the dependence of the $\sigma_{\rm pA}^{\rm DPS}/{\rm A}\sigma_{\rm pp}^{\rm DPS}$ ratio could provide a way to better control the number of secondary absorptive interaction in pA collisions.

Due to the various conceptual differences between Angantyr and Strikman & Treleani models one should not expect to obtain exact agreement between their predictions. A complexity of the problem of DPS in pA collisions requires a detailed study of various non-trivial effects like partonic correlations, cold nuclear matter effects and additional DPS contributions, as it was pointed out in [216]. Therefore, in the absence of experimental studies of DPS in pA collisions, a comparison between predictions of Angantyr and improved Strikman & Treleani model (for example, with included correlations in x-space) may help us to identify key ingredients essential for correct modelling of DPS in pA collisions which, in its turn, would lead to a better understanding of proton's structure and the dynamics of its constituents.

Finally, we shall note that, as it was proposed in [290], the contribution from DPS (MPI) in pA collision may be necessary to explain the collected experimental data. Therefore, the application of the model of [290] together with the Angantyr model to the available data on pA collisions can be beneficial for the studies of DPS (MPI) phenomena in pA collisions. We also should stress that in the experimental studies of pA collisions one usually expresses measurable quantities, *e. g.* charged multiplicity distributions, as functions of *centrality* which, in turn, is a function of the distance between an incident proton and a center of a nucleus in a given pA collision. In practice it is performed with the help of so called *Glauber modelling*, see [292]. Therefore, a Monte Carlo event generators for pA collisions, has to support Glauber modelling, in order to be able to simulate events for different values of centrality. Since, as we have demonstrated in this chapter, the Angantyr model of pA collisions can reproduce results of Strikman & Treleani and because Angantyr includes a facility for Glauber modelling we consider Angantyr as a perspective Monte Carlo tool for the future studies of DPS (MPI) in pA collisions.

Before closing the discussion we shall also mentioned that recently results on combination of Strikman & Treleani model together with Glauber modelling were published by Alvioli *et al.* [291]. The detailed comparison between the predictions of Angantyr and the results of [291] can, therefore, be useful for the modelling of the DPS processes in pA collision.

Chapter 8

Summary and outlook

In this thesis we have studied the four-jet DPS production in pp and pA collisions within different theoretical frameworks.

We have started by giving in Chapter 1 a short introduction to the main concepts of QCD. Then, in Chapter 2 we have provided a brief historical review of the theoretical and experimental studies of the DPS phenomena. We have also discussed the state-of-the-art in the theoretical description of the DPS processes in pp and pA collisions including evolution of dPDFs, connection between DPS cross section and two-parton correlation functions, existing problems in the formulation of DPS in terms of collinear dPDFs and solutions to them proposed by different authors. In Chapter 3 we have given a pedagogical introduction to the Monte Carlo algorithms we use to simulate the four-jet DPS production processes.

In Chapter 4 we have performed a phenomenological study of the four-jet DPS production in pp collisions. In order to do that we have developed a standalone Monte Carlo code supporting the work with different models of dPDFs. With its help we have studied how different models of dPDFs affect the four-jet DPS production. As a baseline for our DPS simulations we have used the simple factorized product of single collinear PDFs multiplied by the step function to preserve conservation of longitudinal momentum ("naive" dPDFs). The differential DPS distributions generated with the "naive" dPDFs have been compared against corresponding distributions obtained with Gaunt & Stirling dPDFs (GS09 dPDFs) [173]. It has been found that the leading jet $p_\perp$ DPS distributions demonstrate a modest dependence on the choice of the dPDFs. However, we have demonstrated that the distributions in maximal rapidity difference $\Delta Y = \max|y_i - y_j|$ obtained with GS09 dPDFs significantly differ from the distributions obtained with "naive" dPDFs at high values of ΔY. We have also studied the interplay between DPS and SPS contributions to the four-jet production and confirmed earlier results on four-jet DPS production obtained by Maciuła and Szczurek [230].

Our Monte Carlo code supports generation of colour charges of particles produced in DPS within the leading colour approximation which is required for the correct modelling of the colour coherence phenomena in parton showering processes. This, together with modifications of the LHEF standard [81] and the `Pythia` code [255] - [257] described in Appendix G, allows to combine our DPS code with various models implemented in the `Pythia` event generator. By combining our four-jet DPS simulations with the ISR and FSR models in `Pythia` we have improved the analysis of [230]. Namely, we have studied the impact of the ISR and FSR effects on our parton-level simulations and found that parton shower effects do not spoil the separation of the DPS and SPS events produced at

low-$p_\perp$ or high-ΔY values predicted in [234]. Furthermore, incorporation of the ISR and FSR effects into our simulations also gave us a possibility to study the effects due to the GS09 dPDFs not only for the leading jet $p_\perp$ and $\Delta Y = \max|y_i - y_j|$ distributions but also for other DPS-sensitive variables based upon transverse momenta imbalance and the azimuthal angles of produced jets as listed in Appendix E. We have found that GS09 effects in four-jet DPS production significantly affect only DPS distributions in ΔY.

The DPS processes in pA collisions demonstrate different dependence on the atomic mass number A as the SPS processes [114], [213], [215], [216]. In Chapter 5 we have extended our simulation of the four-jet DPS production from pp to pA collisions within the framework proposed by Treleani and Strikman [213]. We have argued that the study of the four-jet DPS production in pA collisions for the set of jet cuts as we have used in Chapter 4 leads to a strong separation between DPS signal and SPS background even for the collision energies smaller than hadronic LHC collision energies. We also have studied the overall impact of *cold nuclear matter effects* encapsulated in the nPDFs on our DPS simulations within the Treleani & Strikman framework. The impact of the nPDFs has been found to be very modest.

In Chapter 6 we have performed a detailed comparison between GS09 and `Pythia` models of dPDFs. It has been found that dPDFs in the `Pythia` model obey the same sum rules as GS09 dPDFs (GS sum rules) [173]. The comparison between DPS distributions simulated with GS09, `Pythia` and "naive" dPDFs shows that the GS sum rules induce important correlations in momentum and flavour which manifest themselves for the four-jet DPS production at high values of ΔY.

In Chapter 7 we have studied the four-jet DPS production within the `Angantyr` model [271] being used in the `Pythia` event generator to simulate pA collisions. We have shown that the way `Angantyr` models MPI in pA collisions leads to the enhancement of the DPS cross section similar to the one predicted by Treleani and Strikman in [213]. We have also found that the `Angantyr` model predicts the strong dependence of the number of the DPS processes on the chosen rapidity cuts. This dependence, being verified experimentally, could help to study the DPS phenomena in pA collisions.

Before finishing this thesis, we would like to make several comments on future possible directions of our research. The modifications to the `Pythia` code and the LHEF standard [81] described in Appendix G allow `Pythia` read DPS events from Les-Houches files and to add various effects, *e. g.* ISR and FSR effects, hadronization and decay of produced hadrons *etc*, on top of them. This approach is beneficial for the DPS modelling since it allows to combine `Pythia` with various models of dPDFs without implementing them into `Pythia`'s code. During the work on this theses we have developed a standalone code to produce DPS events for the four-jet DPS production. The structure of our DPS code allows users to work with different models of dPDFs and easily implement new types of DPS processes, *e. g.* three-jet plus photon DPS production, heavy-flavour DPS production *etc*. This opens new directions for our future research. For example, recently, non-trivial correlations between electrons due to the heavy-flavour hadron decays were observed in Monte Carlo simulations performed with the `Pythia` code [212]. It was argued in [212] that the strength of predicted effects is affected by multiplicity of interactions in MPI events. The combination of the `Pythia` event generator with our DPS code allows to simulate the production of electrons due to the decays of heavy-flavour hadrons produced via DPS processes with different models of dPDFs. Such analysis

would help to find how strongly the results of [212] are affected by different models of dPDFs which, in turn, can be beneficial for experimental studies of heavy-flavour production.

In this thesis we have studied three different models of dPDFs, namely GS09, "naive" and `Pythia` dPDFs. Among these three models only GS09 model accounts for the evolution of dPDFs due to the dDGLAP evolution equations. The GS09 dPDFs were produced under the assumption of factorization of gPDFs into collinear and transverse pieces. However, the theoretical study performed by Gaunt in [191] and by Diehl *et al.* in [192], [193] has demonstrated that the assumption about factorization of gPDFs into longitudinal and transverse pieces is inconsistent with the field-theoretical formulation of DPS and leads to incorrect description of DPS in kinematic regions in which two partons inside a proton originate from the perturbative splitting of a single parton. A solution to this problem, which allows for the definition of dPDF as operator matrix elements in a proton, and which can be used at higher orders in perturbation theory was proposed by Diehl, Gaunt and Schönwald in [200]. However, to the best of our knowledge, no phenomenological studies within the framework of [200] were performed. The phenomenological applications of the results of Diehl, Gaunt and Schönwald imply the usage of gPDFs which cannot be factorized into a product of collinear and transverse pieces and obey a system of *homogeneous* dDGLAP evolution equations. Therefore, a combination of our DPS code with a numerical tool to solve both homogeneous and inhomogeneous dDGLAP evolution equations for different non-perturbative inputs will result in a multi-task package which can be interfaced to `Pythia` to perform various studies of DPS phenomena in pp and pA collisions. In particular, it will allow to perform phenomenological studies of DPS within the framework of Diehl, Gaunt and Schönwald which, in turn, will improve DPS simulations for the aforementioned problematic regions of a DPS phase space. Our preliminary results on solution of dDGLAP evolution equation are given in Appendix J. We have studied in detail two approaches to solve dDGLAP evolution equations. Namely, the approach based upon Chebyshev polynomial approximation which was used in [180] and the approached based upon combination of Runge-Kutta and Newton–Cotes methods which was used in [173]. However, our code requires some optimisation and improvement of precision which we leave for future work.

The aforementioned problem of correct treatment of DPS processes in kinematic regions in which two partons inside a proton originate from the perturbative splitting of a single parton is inextricably connected with the modelling of ISR effects in DPS processes. Therefore, our approach to study the impact of ISR effects on our DPS simulations can be seen only as an approximation since it does not include a correct backward evolution for the "$1v2$" DPS processes. Recently, the first results on the modelling of the ISR for "$1v2$" DPS processes within the framework of Diehl, Gaunt and Schönwald were reported [211]. The comparison between our DPS simulations and the results of [211] would help to estimate the error due to the approximate modelling of the ISR effects in our DPS simulations as well as the strength of effects due to the "$1v2$" splitting processes.

Another interesting topic is the application of the `Angantyr` model of pA collisions in the analysis of the experimental data, since, as it was argued in [290], the contribution from DPS (MPI) processes in pA collision may be necessary to explain some of the existing measurements. Therefore, the application of the model of [290] together with the `Angantyr` model to the available data on pA collisions can be beneficial for the studies of DPS (MPI) phenomena in pA collisions. As we have demonstrated in Chapter 7, the `Angatyr` model gives predictions very similar to the results obtained

by Treleani and Strikman in [213] which is essential for the correct modelling of DPS processes in pA collisions. However, apart from that, `Angantyr` offers a possibility to build complete exclusive hadronic final states which makes it a perspective and powerful tool for future studies of both DPS and MPI phenomena in pA collisions.

Appendix A

SU(N) symmetry group

The SU(3) group is a particular case of SU(N) group (a group of $N \times N$ linearly independent unitary matrices with det(U) = 1). The generators of SU(N) are traceless $\mathrm{tr}\left\{t^i\right\} = 0$. There are $N^2 - 1$ linearly independent matrices satisfying these conditions.

Here we list the basic SU(3) properties. The SU(3) generators t^i (i = 1, 2, ..., 8) are hermitian, traceless matrices which obey

$$\left[t^i, t^j\right] = i f^{ijk} t^k, \tag{A.1}$$

where f^{ijk} are the group structure constants.

They also obey the *Jacobi identity*

$$\left[t^i, \left[t^j, t^k\right]\right] + \left[t^k, \left[t^i, t^j\right]\right] + \left[t^j, \left[t^k, t^i\right]\right] = 0,$$

which is a general property of a *Lie algebra*.

In general one can find a basis where all group generators are given by block-diagonal matrices. Such representations are of particular importance and called *irreducible representations*. The following equation fixes the normalization of group generators

$$\mathrm{tr}\left\{t_r^i t_r^j\right\} = \mathrm{T_R}\delta^{ij} \tag{A.2}$$

where $\mathrm{T_R}$ is a constant for each irreducible representation. An irreducible representation of the SU(N) symmetry group given by traceless *Hermitian* $N \times N$ matrices is called *fundamental representation*. In the following we denote SU(N) generators in the fundamental representation as t_N^i.

As soon as the normalization is fixed one can determine the structure constants which are given by

$$f^{ijk} = -\frac{i}{\mathrm{T_R}} \mathrm{tr}\left\{\left[t^i, t^j\right] t^k\right\}, \tag{A.3}$$

which implies that f^{ijk} is antisymmetric under permutations of i, j and k indices.

Another very important example of irreducible representations is so called *adjoint representation*

given by $\left(N^2-1\right)\times\left(N^2-1\right)$ matrices defined as

$$\left(t_G^j\right)_{ik} = if^{ijk}, \tag{A.4}$$

where a subscript G was to use label this particular case of irreducible representation. One can show that a gauge field acting on a field in the adjoint representation is

$$(D_\mu\phi)_i = \partial_\mu\phi_i - igA_\mu^j\,(t_G^i)_{ik}\,\phi_k = \partial_\mu\phi_i + gf^{ijk}\,A_\mu^j\,\phi_k. \tag{A.5}$$

Let us consider the operator t^2 defined as $t^2 \equiv t^i\,t^i$. It is easy to show that

$$\left[t^j, t^2\right] = \left[t^j, t^i t^i\right] = if^{jik}\left\{t^k, t^i\right\} = 0, \tag{A.6}$$

due to the antisymmetry of f^{ijk}. It implies that t^2 is invariant of a Lie algebra and hence takes a constant value for each irreducible representation.

Therefore, for the aforementioned fundamental and ajoint representations we express t^2 as

$$t_N^i t_N^i = C_F, \tag{A.7}$$

$$f^{ikl}f^{jkl} = C_A\delta^{ij}, \tag{A.8}$$

where constants C_F and C_A are called *quadratic Casimir operators.*

In this thesis we choose normalization of the group generator such that $\mathrm{T_R} = 1/2$ which leads to[1]

$$\begin{aligned} C_F &= \frac{N^2-1}{2N}, \\ C_A &= N. \end{aligned} \tag{A.9}$$

[1]For the derivation see, for example, [5].

Appendix B

Mandelstam variables

Consider a $2 \to 2$ scattering process

$$p + p' \to k + k', \tag{B.1}$$

where p and p' are four momenta of particles in initial state and k, k' are four momenta of particles in a final state. In order to describe such process one may form different Lorentz-invariant combinations our of four momenta of scattering particles. A common choice is to consider the following invariants

$$\begin{aligned} \hat{s} &= \left(p + p'\right)^2 = \left(k + k'\right)^2, \\ \hat{t} &= \left(k - p\right)^2 = \left(k' - p'\right)^2, \\ \hat{u} &= \left(k' - p\right)^2 = \left(k - p'\right)^2. \end{aligned}$$

These variables have an important property

$$\hat{s} + \hat{t} + \hat{u} = \sum_i m_i^2, \tag{B.2}$$

where m_i is a mass of i-th particle.

Appendix C

Light-cone coordinates

Here we briefly sketch the properties of the light-cone variables discussed in [293].

Let us define x^+ and x^- as

$$x^+ = \frac{x^0 + x^3}{\sqrt{2}},$$
$$x^- = \frac{x^0 - x^3}{\sqrt{2}}.$$

In these new coordinates a four-vector $x^\mu = \{x^0, x^1, x^2, x^3\}$ is written as $x^\mu = \{x^+, x^-, \boldsymbol{x}\}$, where

$$\boldsymbol{x} = \{x^1, x^2\}. \tag{C.1}$$

In the light-cone coordinates the metric tensor $\eta^{\mu\nu}$ has the following non-zero components

$$\eta_{01} = \eta_{10} = 1, \tag{C.2}$$
$$\eta_{22} = \eta_{33} = -1, \tag{C.3}$$

which implies that a scalar product of two four-vectors a^μ and b_μ now reads

$$a^\mu b_\mu = a^- b^+ + a^+ b^- - \boldsymbol{a} \cdot \boldsymbol{b}. \tag{C.4}$$

If $a^\mu = b_\mu = x_\mu$ a scalar product $a^\mu b_\mu$ reduces to

$$x^\mu x_\mu = 2x^- x^+ - \boldsymbol{x}^2. \tag{C.5}$$

A boost along x_3-axis

$$x^0 = \frac{x^0 + vx^3}{\sqrt{1 - v^2}}$$
$$x^3 = \frac{vx^0 + x^3}{\sqrt{1 - v^2}},$$

then in the light-cone coordinates is written as

$$x^+ = \frac{1+u}{\sqrt{1-v^2}}v^+ = \frac{\sqrt{1+v}}{\sqrt{1-v}}v^+ = e^{\psi}v^+,$$
$$x^- = \frac{1-u}{\sqrt{1-v^2}}v^+ = \frac{\sqrt{1-v}}{\sqrt{1-v}}v^+ = e^{-\psi}v^-,$$

where

$$\psi = \frac{1}{2}\log\left(\frac{1+v}{1-v}\right). \tag{C.6}$$

Appendix D

Leading order $2 \to 2$ QCD cross sections

Here we list all $2 \to 2$ LO QCD processes being used as building blocks to construct DPS events.

Process	Cross section
$g\,g \to g\,g$	$\frac{d\sigma}{d\hat{t}} = \frac{9\pi\alpha_s^2}{2\hat{s}^2}\left(3 - \frac{\hat{t}\hat{u}}{\hat{s}^2} - \frac{\hat{s}\hat{u}}{\hat{t}^2} - \frac{\hat{s}\hat{t}}{\hat{u}^2}\right)$
$q\,g \to q\,g$	$\frac{d\sigma}{d\hat{t}} = \frac{4\pi\alpha_s^2}{8\hat{s}^2}\left(\frac{9}{4}\frac{\hat{s}^2+\hat{u}^2}{\hat{t}^2} - \frac{\hat{u}}{\hat{s}} - \frac{\hat{s}}{\hat{u}}\right)$
$q_i\,q_j \to q_i\,q_j,\ q_i \neq q_j$	$\frac{d\sigma}{d\hat{t}} = \frac{4\pi\alpha_s^2}{9\hat{s}^2}\left(\frac{\hat{s}^2+\hat{u}^2}{\hat{t}^2}\right)$
$g\,g \to q\,\bar{q}$	$\frac{d\sigma}{d\hat{t}} = \frac{4\pi\alpha_s^2}{9\hat{s}^2}\left(\frac{\hat{u}}{\hat{t}} + \frac{\hat{t}}{\hat{u}} - \frac{9}{4}\frac{\hat{t}^2+\hat{u}^2}{\hat{s}^2}\right)$
$q\,\bar{q} \to q\,\bar{q}$	$\frac{d\sigma}{d\hat{t}} = \frac{4\pi\alpha_s^2}{9\hat{s}^2}\left(\frac{\hat{s}^2+\hat{u}^2}{\hat{t}^2} + \frac{\hat{t}^2+\hat{u}^2}{\hat{s}^2} - \frac{2}{3}\frac{\hat{u}^2}{\hat{s}\hat{t}}\right)$
$q\,q \to q\,q$	$\frac{d\sigma}{d\hat{t}} = \frac{4\pi\alpha_s^2}{9\hat{s}^2}\left(\frac{\hat{u}^2+\hat{s}^2}{\hat{t}^2} + \frac{\hat{t}^2+\hat{s}^2}{\hat{u}^2} - \frac{2}{3}\frac{\hat{s}^2}{\hat{u}\hat{t}}\right)$
$q\,\bar{q} \to g\,g$	$\frac{d\sigma}{d\hat{t}} = \frac{32\pi\alpha_s^2}{27\hat{s}^2}\left(\frac{\hat{u}}{\hat{t}} + \frac{\hat{t}}{\hat{u}} - \frac{9}{4}\frac{\hat{t}^2+\hat{u}^2}{\hat{s}^2}\right)$
$q_i\,\bar{q}_i \to q_j\,\bar{q}_j,\ q_i \neq q_j$	$\frac{d\sigma}{d\hat{t}} = \frac{4\pi\alpha_s^2}{9\hat{s}^2}\left(\frac{\hat{t}^2+\hat{u}^2}{\hat{s}^2}\right)$

Table D.1: List of $2 \to 2$ LO QCD processes contributing to $pp \xrightarrow{\text{DPS}} 4j$ process. Here all quarks are considered to be massless.

Appendix E

DPS-sensitive variables

In this section we are going to list the DPS sensitive variables, experimental cuts and jet reconstruction algorithms being used in the measurements of the four-jet DPS production performed by the ATLAS collaboration [145]

Variable	Definition
$\Delta_{ij} = \frac{\lvert \vec{p}^{\,i}_{\perp} + \vec{p}^{\,j}_{\perp} \rvert}{p^{i}_{\perp} + p^{j}_{\perp}}$	Transverse momentum imbalance $i, j = 1, 2, 3, 4$
$\Delta\phi_{ij} = \lvert \phi_i - \phi_j \rvert$	Azimuthal angle difference $i, j = 1, 2, 3, 4$
$\Delta y_{ij} = \lvert y_i - y_j \rvert$	Rapidity difference $i, j = 1, 2, 3, 4$
$\lvert \phi_{1+2} - \phi_{3+4} \rvert$, $\lvert \phi_{1+3} - \phi_{2+4} \rvert$, $\lvert \phi_{1+4} - \phi_{2+3} \rvert$	The term ϕ_{i+j} denotes the azimuthal angle of the four-vector obtained by the sum of jets i and j

Table E.1: List of DPS sensitive variables used in [145].

Parameter	Value
$\sqrt{S}$	7 TeV
set A	$N_{jet} \geq 2$ $p_{\perp 1} > 20$ GeV $p_{\perp 2} > 20$ GeV
set B	$N_{jet} \geq 2$ $p_{\perp 1} > 42.5$ GeV $p_{\perp 2} > 20$ GeV
set Four-jet	$N_{jet} \geq 4$ $p_{\perp 1} > 42.5$ GeV $p_{\perp 2,3,4} > 20$ GeV
$\lvert \eta \rvert$	< 4.4
Jet reconstruction algorithm	anti-k_T
Jet radius	0.6

Table E.2: Scenario in [145].

The complete DPS events were built using di-jet events from sets A and B.

Appendix F

List of DPS processes studied in the literature

In Table F.1 we list phenomenological studies for various DPS production processes.

Process	Reference
$pp \xrightarrow{\text{DPS}} \pi^0\pi^0$; $dA \xrightarrow{\text{DPS}} \pi^0\pi^0$	[222]
$pA \xrightarrow{\text{DPS}} c\bar{c}c\bar{c}$, $b\bar{b}c\bar{c}$, $b\bar{b}b\bar{b}$	[228]
$pA \xrightarrow{\text{DPS}} W^+W^+$, W^-W^-	[223], [225]
$AA \xrightarrow{\text{DPS}} J/\psi + J/\psi$	[224]
$pA\,(AA) \xrightarrow{\text{DPS}} W^+W^+$, W^-W^-, $pA\,(AA) \xrightarrow{\text{DPS}} J/\psi + J/\psi, J/\psi + \Upsilon$, $pA\,(AA) \xrightarrow{\text{DPS}} J/\psi + W, J/\psi + Z$, $pA\,(AA) \xrightarrow{\text{DPS}} \Upsilon + \Upsilon, \Upsilon + W, \Upsilon + Z$	[225]
$pp \xrightarrow{\text{DPS}} 4j$	[119], [121], [122], [229], [230], [231], [232], [233]
$pp \xrightarrow{\text{DPS}} 2\gamma + 2j$	[239]
$pp \xrightarrow{\text{DPS}} D^0B^+$, B^+B^+	[226]
$pp \xrightarrow{\text{DPS}} b\bar{b}b\bar{b}$	[227]
$pp \xrightarrow{\text{DPS}} b\bar{b}b\bar{b}$, $c\bar{c}c\bar{c}$, $c\bar{c}b\bar{b}$	[228]
$pp \xrightarrow{\text{DPS}} c\bar{c} + 2j$, $pp \xrightarrow{\text{DPS}} D^0 + 2j$ and $pp \xrightarrow{\text{DPS}} D^0\bar{D}^0 + 2j$	[234]
$pp \xrightarrow{\text{DPS}} J/\psi + J/\psi$	[235], [236]
$pp \xrightarrow{\text{DPS}} J/\psi + J/\psi \to \mu^-\mu^+ + \mu^-\mu^+$, $pp \xrightarrow{\text{DPS}} \gamma^\star + \gamma^\star \to \mu^-\mu^+ + \mu^-\mu^+$	[237]
$pp \xrightarrow{\text{DPS}} W^+W^+$, W^-W^-	[242], [238], [243], [209]
$pp \xrightarrow{\text{DPS}} W + jj$, $Z + jj$	[243]
$pp \xrightarrow{\text{DPS}} W^\pm(Z) + H$	[240]
$pp \xrightarrow{\text{DPS}} b\bar{b} + H$	[241]

Table F.1: Phenomenological studies for various DPS production processes.

Appendix G

Modifications of the Pythia code and the LHEF standard

Here we describe modifications to the `Pythia` code and the LHEF standard necessary to read and "shower" DPS events from LHE files. The checks of these modifications are given in Chapter 4.9. The modifications of the `Pythia` code described in this section are to appear in the next public release of the `Pythia` event generator[1].

The `Pythia` event generator supports work with the LHEF standard [81]. Therefore, in order to add parton shower effects to our DPS simulations, one would first generate LHE files with DPS events and then supply them to `Pythia` for showering using `SecondHard:generate = on` and `PartonLevel:MPI = off` settings. However, there are some technical difficulties which do not allow to apply this approach directly. First of all the `Pythia` code earlier than 8.240 does not support the output of DPS events into LHE files[2]. Starting from the version 8.240 a possibility to output DPS events according to the extended LHEF standard was added, see [104]. An example of the DPS event record created by `Pythia` according to a modified LHEF standard is shown in Fig. G.1. The unmodified LHEF standard is explained in Fig. 3.5. By comparing the modified LHEF output in Fig. G.1 with the standard LHEF output shown in Fig. 3.5 we see that some important modifications were introduced. We see that two di-jet events, namely $gg \to c\bar{c}$ and $cu \to cu$ are now stacked in the same event[3]. The extension of the LHEF standard to the DPS events also requires the correct mother-daughter information as it is shown in Fig. G.1. Namely, the parent indices 1 and 2 of the c, $\bar{c}$ pair tell us that it originates from two initial-state gluons (first and second lines in the event record) and the parent indices 5 and 6 of the c, u pair tell us that it originates from the initial-state c, u pair (fifth and sixth lines in the event record)[4]. In addition to the aforementioned changes a new line starting with the key-word `#scaleShowers` was added. It contains factorization scales for the first and second hard interactions correspondingly.

[1] At the moment of writing of this thesis the most recent `Pythia` release is `Pythia` 8.240.

[2] More precisely, an attempt to output DPS events into an LHE file in the `Pythia` with version < 8.240 would lead to the wrong mother-daughter information between partons produced in the second hard interaction. Moreover, the LHEF standard does not allow to output information about the second factorization scale and, therefore, has to be extended.

[3] In LHE files different particles are distinguished according to their Particle Data Group (PDG) codes [82]. For example, for g, d, u, s, c, b the corresponding PDG codes are given by 21, 1, 2, 3, 4. The PDG codes of anti-quarks are equal to the PDG codes of corresponding quarks taken with a negative sign.

[4] Note that the numbering of lines between `<event>` and `</event>` tags starts from zero.

```
<LesHouchesEvents version="1.0">
<event>
8  9999  1.000000e+00  2.218709e+01  7.694236e-03  1.675694e-01
   21  -1  0  0   101   102   0.0   0.0   171.0  171.0  0.  0. 9.
   21  -1  0  0   103   101   0.0   0.0    -6.2    6.2  0.  0. 9.
    4   1  1  2   103     0 -16.0 -15.3    17.3   28.1  1.5 0. 9.
   -4   1  1  2     0   102  16.0  15.3    14.8   14.9  1.5 0. 9.
    4  -1  0  0   104     0   0.0   0.0     2.8    2.8  0.  0. 9.
    2  -1  0  0   105     0   0.0   0.0  -944.7  944.7  0.  0. 9.
    4   1  5  6   105     0  22.5  12.5   -61.0   66.3  1.5 0. 9.
    2   1  5  6   104     0 -22.5 -12.5  -880.9  881.3  0.3 0. 9.
#pdf   21   21  2.637e-02  9.601e-04  2.219e+01  3.618e+00  2.938e+01
#scaleShowers  2.218709e+01  2.575019e+01
</event>
</LesHouchesEvents>
```

Figure G.1: An extension of the Les-Houches version="1.0" standard to the DPS events. In order to ease the reading we keep only one digit after comma for the components of the four-momenta.

We also should note here that even though `Pythia` version = "8.240" can generate and output DPS events into LHE files, as shown in Fig. G.1, it cannot "shower" them correctly. Several important modifications have to be added. Namely, in the file `Pythia.cc` after the line "`event.scale( process.scale() );`" one also has to add
"`event.scaleSecond(process.scaleSecond());`" inside of the `Pythia::next()` method. One also has to include the same two lines in the file `Pythia.cc` after each block of the code is executed if the logical conditions `if (!doPartonLevel)` or `if (!doHadronLevel)` are true. In addition to it one has to modify the files `PartonLevel.cc` and `ProcessContainer.cc`. In the file `PartonLevel.cc` one hast to replace the condition "`if (doSecondHard)`" by "`if (twoHard)`" in the method `PartonLevel::next`, see Fig. G.2. This replacement is necessary to set the scales of ISR, FSR and MPI evolution properly while reading LHE files with DPS events since the boolean variable `twoHard` is set to `true` if during the initialization of `Pythia` we set
`SecondHard:generate = on`. Moreover, in the file `ProcessContainer.cc` one has to add changes as shown in Fig. G.3. The reason is that in the `Pythia` event generator one can assign the MPI, ISR and FSR evolution scales to each parton individually.

One also has to keep in mind that the production of the resonances requires a different scales of the MPI, ISR and FSR evolution[5]. While reading DPS events out of the LHE files these scales have to be initialized properly. After introducing the aforementioned modifications the MPI, ISR and FSR scales of the first (second) hard process are set to the factorization scale of the first (second) hard process and the scale of the resonance production is set to the mass of the resonance, see Fig. G.3.

Before closing this section we also need to stress that for the correct work of the aforementioned modifications to `Pythia` version = "8.240" the LHE events have to be written as in Fig. G.1 with a necessary tag `<LesHouchesEvents version="1.0">`. If instead one will try to use `<LesHouchesEvents version="3.0">` then `Pythia` will still read and shower DPS events but in

[5]In our analysis we do not have a production of resonances. Therefore, the modifications of the `Pyhia` code related to the correct setting of the MPI, ISR and FSR scales for resonances while reading DPS events from the LHE files are not necessary for our four-jet DPS study

```
if (doSecondHard) {
    pTscaleRad        = max( pTscaleRad, process.scaleSecond() );
    pTscaleMPI        = min( pTscaleMPI, process.scaleSecond() );
}
```

```
if (twoHard) {
    pTscaleRad        = max( pTscaleRad, process.scaleSecond() );
    pTscaleMPI        = min( pTscaleMPI, process.scaleSecond() );
}
```

Figure G.2: Logical condition to set the ISR, FSR and MPI scales in the method `PartonLevel::next` of the class `PartonLevel.cc`. Upper block of code: implementation in `Pythia` 8.240. Lower block of code: necessary changes to initialize DPS model properly while reading LHE events.

a wrong way. The reason is that the reading of the LHE version = "1" files and the LHE version = "3" files in the `Pythia` code is performed by different routines in the `LesHouches.cc` and `LHEF3.cc` files correspondingly. Whereas the reader of the LHE version = "1" files was adopted for the DPS events the reader of the LHE version = "3" files still requires important modifications. Therefore, the usage of the tag `<LesHouchesEvents version="3.0">` will invoke reading routines from the file `LHEF3.cc` which will lead to the wrong assignment of the mother-daughter labels and MPI, ISR and FSR scales.

```
// Find scale from which to begin MPI/ISR/FSR evolution.
scalup = lhaUpPtr->scale();
scale  = scalup;
double scalePr = (scale < 0.) ? sqrt(Q2Fac()) : scale;
process.scale( scalePr);
if (twoHard) process.scaleSecond( scalePr);

// For resonance decay products use resonance mass as scale.
double scaleNow = scalePr;
if (mother1 > 4 && !useStrictLHEFscales) scaleNow = process[mother1].m();
if (scaleShow >= 0.0) scaleNow = scaleShow;
```

```
// Find scale from which to begin MPI/ISR/FSR evolution.
scalup = lhaUpPtr->scale();
scale  = scalup;
double scalePr = (scale < 0.) ? sqrt(Q2Fac()) : scale;
process.scale( scalePr);
if (twoHard) process.scaleSecond( scalePr);

if ( lhaUpPtr->scaleShowersIsSet() ) {
    process.scale( lhaUpPtr->scaleShowers(0) );
    process.scaleSecond( lhaUpPtr->scaleShowers(1) );
}

double scalePr2 = process.scaleSecond();


// For resonance decay products use resonance mass as scale.
double scaleNow = (iIn < 3) ? scalePr : scalePr2;
int motherBeg = (iIn < 3) ? 4 : 4 + nOffsetSecond;
if (mother1 > motherBeg && !useStrictLHEFscales)
    scaleNow = process[mother1].m();
if (scaleShow >= 0.0) scaleNow = scaleShow;
```

Figure G.3: Logical condition to set the ISR, FSR and MPI scales in the method `ProcessContainer::constructProcess` of the class `ProcessContainer`. Upper block of code: current implementation in `Pythia` 8.240. Lower block of code: necessary changes to initialize the DPS model properly while reading LHE events.

Appendix H

Accessing dPDFs being used in the Pythia event generator

The standard usage of the `Pythia` event generator does not allow the user to access dPDFs being used to simulate DPS processes. However, using the methods of the class `BeamParticle` one calculate the value of the PDF being used for the second hard interaction $f_{Mod}^{id_2}(x_2, Q_2^2)$ which is modified according to the value of the PDF $f_{Raw}^{id_1}(x_1, Q_1^2)$ being used for the first hard interaction. The corresponding dPDF, therefore, is given by the product

$$D_{id_1,id_2}(x_1, x_2, Q_1^2, Q_2^2) = f_{Raw}^{id_1}(x_1, Q_1^2)\, f_{Mod}^{id_2}(x_2, Q_2^2). \tag{H.1}$$

In Fig. H we provide an example of a C++ function which allows to get access to modified PDFs being used to produce second hard process. As arguments it takes the reference *beam* to the object of the `BeamParticle` type and the PDG id number id_1 (id_2), Bjorken x x_1 (x_2) and factorization scale squared Q_1^2 (Q_2^2) of the first (second) initial state parton. One can get the reference to the beam object by setting `BeamParticle &beam = pythia.beamA;` in the analysis code after the initialization of the `Pythia` object.

```
double second_xPDF (BeamParticle &beam, int id1, int id2,
                    double x1, double x2,
                    double Q12, double Q22) {
    double res = 0.;

    if (x1 + x2 < 1.) {

        int ida = (id1 == 0) ? 21 : id1;
        int idb = (id2 == 0) ? 21 : id2;

        beam.clear();
        beam.append ( 0, ida, x1 );
        beam.xfISR  ( 0, ida, x1, Q12 );

        if (ida == 1 || ida == 2) beam.pickValSeaComp();
        res = beam.xfMPI ( idb, x2, Q22 );
        }
    return res;}
```

Appendix I

Stability checks

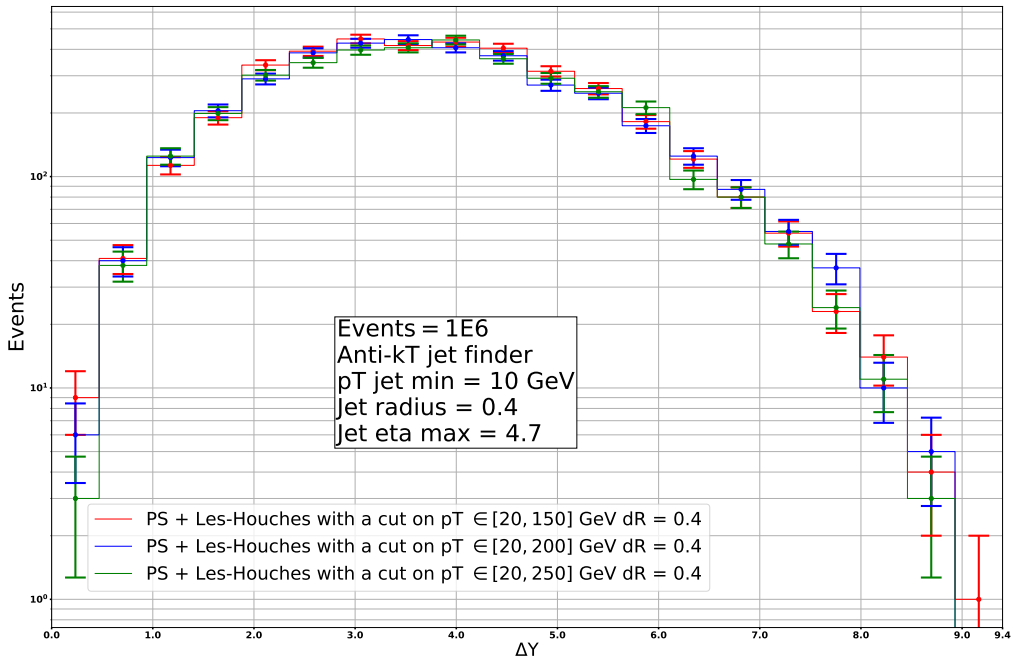

Figure I.1: Test of stability of the leading jet ΔY distributions under the variation of $p_{\perp}^{\max}$ cut. Four-jet DPS simulation performed for the collision energy $\sqrt{S} = 13TeV$ with naive dPDFs constructed out of MSTW2008 LO PDFs [298]. Factorization and renormalization scales are equal to $Q_1 = p_{1\perp}$, $Q_2 = p_{2\perp}$, where $p_{1\perp}$ and $p_{2\perp}$ are equal to the absolute value of a jet transverse momentum in a first and second hard processes in a given DPS event. Statistical errors are given by $\sqrt{N_{\text{bin}}}$ where N_{bin} is a number of events in a given bin. Here we plot ΔY distributions of the jets with $p_{\perp} \in [35, 100]$ GeV produced by adding ISR and FSR effects to the parton level DPS simulations performed with $p_{\perp}^{\max} = 150$ GeV, $p_{\perp}^{\max} = 200$ GeV and $p_{\perp}^{\max} = 250$ GeV.

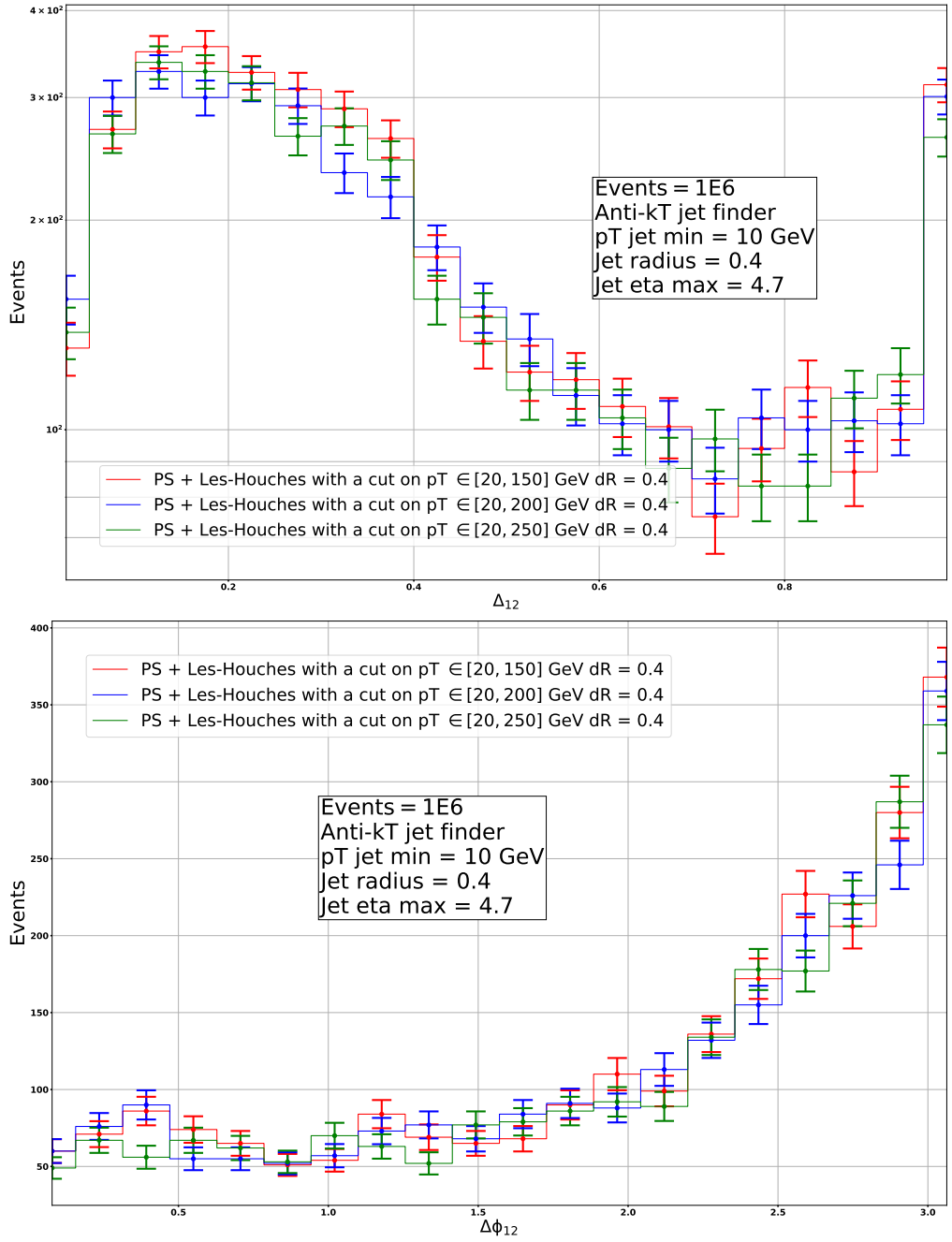

Figure I.2: Test of stability of the DPS distributions under the variation of $p_{\perp}^{\max}$ cut. Four-jet DPS simulation performed for the collision energy $\sqrt{S} = 13TeV$ with naive dPDFs constructed out of MSTW2008 LO PDFs [298]. Factorization and renormalization scales are equal to $Q_1 = p_{1\perp}$, $Q_2 = p_{2\perp}$, where $p_{1\perp}$ and $p_{2\perp}$ are equal to the absolute value of a jet transverse momentum in a first and second hard processes in a given DPS event. Statistical errors are given by $\sqrt{N_{\text{bin}}}$ where N_{bin} is a number of events in a given bin. Here we plot ΔY distributions of the jets with $p_{\perp} \in [35, 100]$ GeV produced by adding ISR and FSR effects to the parton level DPS simulations performed with $p_{\perp}^{\max} = 150$ GeV, $p_{\perp}^{\max} = 200$ GeV and $p_{\perp}^{\max} = 250$ GeV. Upper panel: distribution in terms of $p_{\perp}$ momenta imbalance of two hardest jets Δ_{12}. Lower panel: distribution in terms of difference in the azimuthal angle of two hardest jets ϕ_{12}.

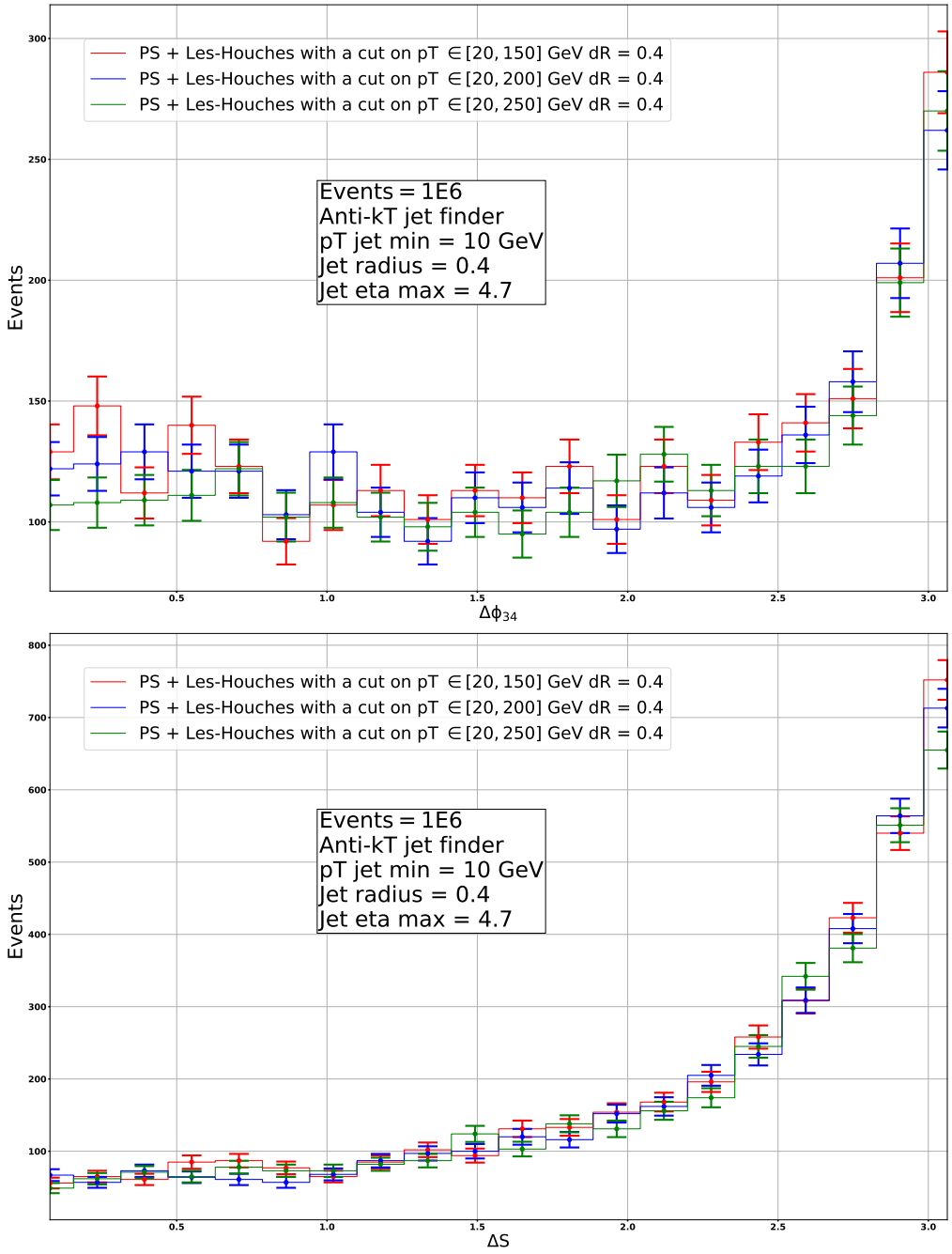

Figure I.3: Test of stability of the DPS distributions under the variation of $p_{\perp}^{\max}$ cut. Four-jet DPS simulation performed for the collision energy $\sqrt{S} = 13TeV$ with naive dPDFs constructed out of MSTW2008 LO PDFs [298]. Factorization and renormalization scales are equal to $Q_1 = p_{1\perp}$, $Q_2 = p_{2\perp}$, where $p_{1\perp}$ and $p_{2\perp}$ are equal to the absolute value of a jet transverse momentum in a first and second hard processes in a given DPS event. Statistical errors are given by $\sqrt{N_{\text{bin}}}$ where N_{bin} is a number of events in a given bin. Here we plot ΔY distributions of the jets with $p_{\perp} \in [35, 100]$ GeV produced by adding ISR and FSR effects to the parton level DPS simulations performed with $p_{\perp}^{\max} = 150$ GeV, $p_{\perp}^{\max} = 200$ GeV and $p_{\perp}^{\max} = 250$ GeV. Upper panel: distribution in terms of $p_{\perp}$ momenta imbalance of two softest jets Δ_{34}. Lower panel: distribution in terms of ΔS. For the definition of ΔS, see Eq. 4.31

Appendix J

Methods to solve double DGLAP evolution equations

Here we discuss different methods to solve DGLAP and double DGLAP evolution equations.

J.1 Method Chebyshev polynomial approximation

We start with the discussion of Chebyshev polynomial method[1] which was applied to solve double DGLAP evolution equations in [178] - [180]. We use a system of single DGLAP evolution equations as an example. In the case of double DGLAP evolution equations one gets a similar system of matrix equations of a higher rank, see [180].

The system of DGLAP evolution equations at LO can be written as

$$\begin{aligned}
\partial_t q_i(x,t) &= \frac{\alpha(t)}{2\pi}\left[\int_x^1 \frac{dz}{z} P_{qq}(z)\left\{q_i(x/z,t) - z^2 q_i(x,t)\right\} - q_i(x,t)\int_0^x dz z P_{qq}(z)\right] \\
&+ \frac{\alpha(t)}{2\pi}\left[\int_x^1 \frac{dz}{z} P_{qG}(z)\, G(x/z,t) - q_i(x,t)\int_0^1 dz\, P_{Gq}(z)\right], \qquad \text{(J.1)} \\
\partial_t G(x,t) &= \frac{\alpha(t)}{2\pi}\left[\int_x^1 \frac{dz}{z} P_{GG}(z)\left\{G(x/z,t) - z^2 G(x,t)\right\} - G(x,t)\int_0^x dz z P_{GG}(z)\right] \\
&+ \frac{\alpha(t)}{2\pi}\left[\int_x^1 \frac{dz}{z} P_{Gq}(z)\,\Sigma(x/z,t) - 2N_f(t)\, G(x,t)\int_0^1 dz\, P_{qG}(z)\right], \qquad \text{(J.2)}
\end{aligned}$$

where $N_f(t)$ is a number of flavours[2] and

$$\Sigma(x,t) = \sum_{i=1}^{N_f}\left[q_i(x,t) + \bar{q}_i(x,t)\right], \qquad \text{(J.3)}$$

see [180].

It is convenient to write Eq. J.1 and Eq. J.2 in terms of PDFs multiplied by their arguments as $\tilde{q}_i(x,t) = x\, q_i(x,t)$ and $\tilde{G}(x,t) = x\, G(x,t)$ which allows to write the DGLAP evolution equations

[1] For the description of the Chebyshev polinomial method see, for example, [308].

[2] The way the number of flavours N_f depends on the evolution parameter t depends on a scheme chosen to solve DGLAP evolution equations.

as

$$\begin{aligned}
\frac{2\pi}{\alpha(t)}\,\partial_t\,\tilde{q}_i(x,t) &= \int_x^1 dz\,P_{qq}(z)\,\{\tilde{q}_i(x/z,t)-z\,\tilde{q}_i(x,t)\}-\tilde{q}_i(x,t)\int_0^x dz\,z\,P_{qq}(z)\\
&+ \int_x^1 dz\,P_{qG}(z)\,\tilde{G}(x/z,t)-\tilde{q}_i(x,t)\int_0^1 dz\,P_{Gq}(z)\,, \qquad \text{(J.4)}\\
\frac{2\pi}{\alpha(t)}\,\partial_t\,G(x,t) &= \int_x^1 dz\,P_{GG}(z)\left\{\tilde{G}(x/z,t)-z\,\tilde{G}(x,t)\right\}-\tilde{G}(x,t)\int_0^x dz\,z\,P_{GG}(z)\\
&+ \int_x^1 dz\,P_{Gq}(z)\,\tilde{\Sigma}(x/z,t)-2N_f(t)\,\tilde{G}(x,t)\int_0^1 dz\,P_{qG}(z)\,, \qquad \text{(J.5)}
\end{aligned}$$

where integrals over the splitting functions may be computed analytically. In order to simplify Eq. J.4 and Eq. J.5 we introduce the following integrals

$$\begin{aligned}
F_q(x) &= \int_0^x dz\,z\,P_{qq}(z)+\int_0^1 dz\,z\,P_{Gq}(z)\,, \qquad \text{(J.6)}\\
F_g^1(x) &= \int_0^x dz\,z\,P_{GG}(z)\,, \qquad \text{(J.7)}\\
F_g^2(t) &= 2N_f(t)\int_0^1 dz\,z\,P_{qG}(z)\,. \qquad \text{(J.8)}
\end{aligned}$$

Using Eq. J.6 - J.8 we can write the system of DGLAP evolution equations as

$$\begin{aligned}
\frac{2\pi}{\alpha(t)}\,\partial_t\,\tilde{q}_i(x,t) &= \int_x^1 dz\,P_{qq}(z)\,\{\tilde{q}_i(x/z,t)-z\,\tilde{q}_i(x,t)\}-\tilde{q}_i(x,t)\,F_q(x)\\
&+ \int_x^1 dz\,P_{qG}(z)\,\tilde{G}(x/z,t)\,, \qquad \text{(J.9)}\\
\frac{2\pi}{\alpha(t)}\,\partial_t\,G(x,t) &= \int_x^1 dz\,P_{GG}(z)\left\{\tilde{G}(x/z,t)-z\,\tilde{G}(x,t)\right\}-\tilde{G}(x,t)\,F_g^1(x)\\
&+ \int_x^1 dz\,P_{Gq}(z)\,\tilde{\Sigma}(x/z,t)-\tilde{G}(x,t)\,F_g^2(t)\,. \qquad \text{(J.10)}
\end{aligned}$$

The decomposition into Chebyshev series will turn the system of DGLAP evolution equations into a set of linear differential equations of the first order. For the function $f(x)$ defined in the region $x\in[-1,1]$ the decomposition into Chebyshev series reads

$$\begin{aligned}
f(x) &= \sum_{k=0}^{N}\nu_k\,c_k\,T_k\,(x)\,, \qquad \text{(J.11)}\\
c_k &= \frac{2}{N+1}\sum_{j=0}^{N}f(x_j)\,T_k\,(x_j)\,, \qquad \text{(J.12)}\\
x_j &= \cos\left[(j+1/2)\,\pi/(N+1)\right]. \qquad \text{(J.13)}
\end{aligned}$$

In order to expand the function defined in the range $\tilde{x}\in[a,b]$ we have to use decomposition in

terms of "shifted" Chebyshev polynomials yielding

$$f(\tilde{x}) = \sum_{k=0}^{N} \nu_k \, c_k \, T_k \left(\mathcal{H}^{-1}(\tilde{x})\right), \tag{J.14}$$

$$c_k = \frac{2}{N+1} \sum_{j=0}^{N} f\left(\mathcal{H}(x_j)\right) T_k(x_j), \tag{J.15}$$

$$\mathcal{H}^{-1}(\tilde{x}) = \frac{2\tilde{x} - (a+b)}{b-a} = x, \tag{J.16}$$

$$\mathcal{H}(x) = \frac{1}{2}\left[(b-a)\,x + (a+b)\right] = \tilde{x}, \tag{J.17}$$

where $\nu_0 = 1/2$, $\nu_k = 1$ if $l \neq 0$. By applying Eq. J.14 - J.17 to Eq. J.9 - J.10 we get the following system of matrix equations

$$\partial_t \, c_k^i(t) = \frac{\alpha(t)}{2\pi} \hat{M}_{kl} \, c_l^i(t) + \frac{\alpha(t)}{2\pi} \hat{C}_{kl}^0 \, b_l(t), \tag{J.18}$$

$$\partial_t \, b_k(t) = \frac{\alpha(t)}{2\pi} \hat{M}_{kl}^0 \, b_l(t) + \frac{\alpha(t)}{2\pi} \sum_i \hat{C}_{kl} \, c_l^i(t) - \frac{\alpha(t)}{2\pi} F_g^2(t) \; b_k(t), \tag{J.19}$$

where the summation over all repeated indices is assumed, $c_k^i(t)$ is the k'th coefficient in Chebyshev expansion of quark PDFs and $b_k(t)$ is the k'th coefficient in Chebyshev expansion of gluon PDF. Equations J.18 and J.19 contain the following matrices:

$$\hat{M}_{kl} = \hat{A}_{kl} + \hat{B}_{kl}, \tag{J.20}$$

$$\hat{M}_{kl}^0 = \hat{A}_{kl}^0 + \hat{B}_{kl}^0, \tag{J.21}$$

$$\hat{A}_{kl} = \frac{2}{N+1} \nu_l \sum_{j=0}^{N} \int_{\tilde{x}_j}^{1} dz \, P_{qq}(z) \left\{ T_l\left(\mathcal{H}^{-1}(\tilde{x}_j/z)\right) T_k(x_j) - z \, T_k(x_j) \, T_l(x_j) \right\}, \tag{J.22}$$

$$\hat{B}_{kl} = -\frac{2}{N+1} \nu_l \sum_{j=0}^{N} F_q(\tilde{x}_j) \, T_k(x_j) \, T_l(x_j), \tag{J.23}$$

$$\hat{A}_{kl}^0 = \frac{2}{N+1} \nu_l \sum_{j=0}^{N} \int_{\tilde{x}_j}^{1} dz \, P_{GG}(z) \left\{ T_l\left(\mathcal{H}^{-1}(\tilde{x}_j/z)\right) T_k(x_j) - z \, T_k(x_j) \, T_l(x_j) \right\}, \tag{J.24}$$

$$\hat{B}_{kl}^0 = -\frac{2}{N+1} \nu_l \sum_{j=0}^{N} F_g^1(\tilde{x}_j) \, T_k(x_j) \, T_l(x_j), \tag{J.25}$$

$$\hat{C}_{kl} = \frac{2}{N+1} \nu_l \sum_{j=0}^{N} \int_{\tilde{x}_j}^{1} dz \, P_{Gq}(z) \left\{ T_l\left(\mathcal{H}^{-1}(\tilde{x}_j/z)\right) T_k(x_j) \right\}, \tag{J.26}$$

$$\hat{C}_{kl}^0 = \frac{2}{N+1} \nu_l \sum_{j=0}^{N} \int_{\tilde{x}_j}^{1} dz \, P_{qG}(z) \left\{ T_l\left(\mathcal{H}^{-1}(\tilde{x}_j/z)\right) T_k(x_j) \right\}. \tag{J.27}$$

As we have discussed in Chapter 1.5 PDFs rapidly grow at small values of x and rapidly decrease at high values of x, see Fig. 1.15. It means that in order to get a good precision in the decomposition of PDFs into Chebyshev series one may need to include to many terms. However, this problem can

be solved by switching from the linear to the logarithmic scale which implies the following change of variables

$$x \rightarrow \exp(x), \tag{J.28}$$

$$z \rightarrow \exp(z). \tag{J.29}$$

Our results of numerical solution of the single DGLAP evolution equations are given in Fig. J.1 where we compare the MSTW2008 LO PDFs evolved from $Q^2 = 30\,\mathrm{GeV}^2$ up to $Q^2 = 10^4\,\mathrm{GeV}^2$. The ratios in Fig. J.1 are given by the ratios of the MSTW2008 PDFs provided with the LHAPDF6 library and the output of our evolution code. Since the MSTW2008 set contains u, d, s, c and b quarks, for the testing purposes, we have set the staring evolution scale to $Q^2 = 30\,\mathrm{GeV}^2$. The choice of the staring evolution scale above the mass of the b quark allows to set the number of flavour to the constant which simplifies the checks of the evolution algorithm we use.

In Fig. J.2 we show a check of our implementation of the method of Chebyshev polynomials to solve the system of double DGLAP evolution equations as it was proposed in [178] - [180]. In order to test our implementation we use the GS09 set of dPDFs [173] as initial conditions at $Q^2 = 1\,\mathrm{GeV}^2$. In order to check the error propagation in our code we use the GS09 dPDFs to decouple the system of double DGLAP evolution equations. Namely, during the solution of the system of the double DGLAP evolution equations we take all dPDFs from the GS09 set apart from the D_{uu} dPDF. Effectively it reduces a system of double DGLAP evolution equations to a single evolution equation for the D_{uu} dPDF. After performing the evolution for D_{uu} we compare it against D_{uu} from the GS09 set. The result of this comparison is given in the lower panel of Fig. J.2.

J.2 Combination of the Runge-Kutta and Newton-Cotes methods

Another commonly used approach to solve the system of DGLAP evolution equations is based upon combination of Runge-Kutta and Newton-Cotes methods[3]. This approach was used by Gaunt and Stirling in [173] to produce GS09 set of dPDFs.

Here we describe the way we use Runge-Kutta and Newton-Cotes methods to solve a system of double DGLAP evolution equations. First of all let's write the system of double DGLAP equations as in [180]

$$\begin{aligned}
&\frac{2\pi}{\alpha(t)}\partial_t D_{f_1 f_2}(x_1, x_2, t) = \\
&\sum_{f'}\left\{\int_{\frac{x_1}{1-x_2}}^1 \frac{dz}{z} P^0_{f_1 f'}(z)\; D_{f' f_2}(x_1/z, x_2, t) - D_{f_1 f_2}(x_1, x_2, t)\int_0^1 dz z P^0_{f' f_1}\right\} + \\
&\sum_{f'}\left\{\int_{\frac{x_2}{1-x_1}}^1 \frac{dz}{z} P^0_{f_2 f'}(z)\; D_{f_1 f'}(x_1, x_2/z, t) - D_{f_1 f_2}(x_1, x_2, t)\int_0^1 dz z P^0_{f' f_2}\right\} + \\
&\sum_{f'}\frac{1}{x_1+x_2} P_{f'\rightarrow f_1 f_2}\left(\frac{x_1}{x_1+x_2}\right) f_{f'}(x_1+x_2, t).
\end{aligned} \tag{J.30}$$

Now let us write these these equations for different dPDFs. We start with $D_{q_i q_i}(x_1, x_2, t)$ which

[3]For the description of the Runge-Kutta and Newton-Cotes methods see, for example, [308].

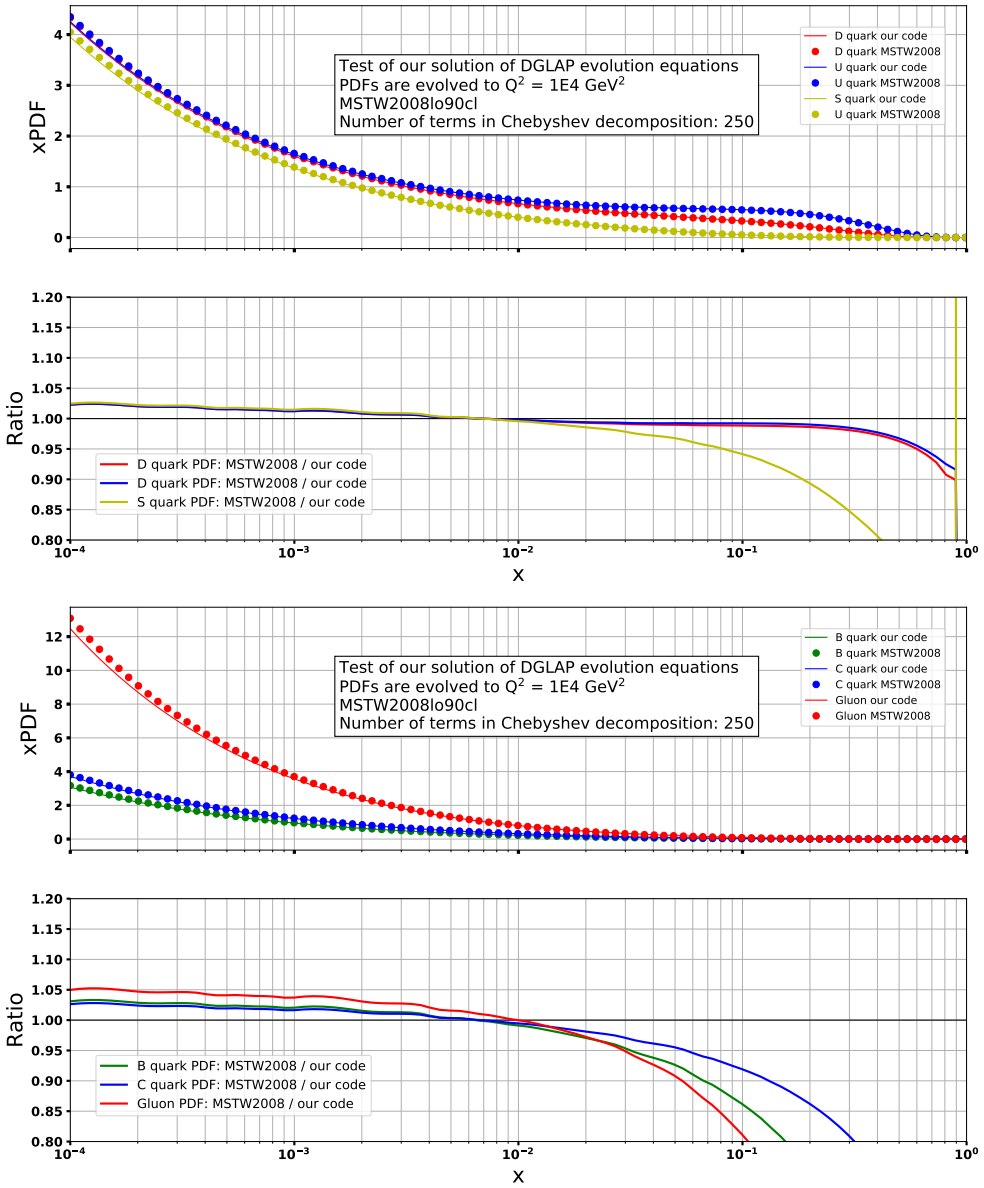

Figure J.1: Our solution of the single DGLAP evolution equations. Upper panel: light flavour PDF are evolved from 30 GeV^2 to 10^4 GeV^2 250 terms in Chebyshev expansion, 2000 evolution steps. Lower panel: heavy flavour and gluon PDF are evolved from 30 GeV^2 to 10^4 GeV^2 250 terms in Chebyshev expansion, 2000 evolution steps.

can be written as

$$
\begin{aligned}
&\frac{2\pi}{\alpha(t)}\partial_t D_{q_iq_i}(x_1,x_2,t) = \\
&\int_{\frac{x_1}{1-x_2}}^1 \frac{dz}{z} P_{qq}(z)\left\{D_{q_iq_i}(x_1/z,x_2,t) - z^2 D_{q_iq_i}(x_1,x_2,t)\right\} \\
&+\int_{\frac{x_1}{1-x_2}}^1 \frac{dz}{z} P_{qG}(z)\; D_{Gq_i}(x_1/z,x_2,t) - D_{q_iq_i}(x_1,x_2,t)\left\{\int_0^{\frac{x_1}{1-x_2}} dz\, z\, P_{qq}(z) + \int_0^1 dz\, z\, P_{Gq}(z)\right\} \\
&+\int_{\frac{x_2}{1-x_1}}^1 \frac{dz}{z} P_{qq}(z)\left\{D_{q_iq_i}(x_1,x_2/z,t) - z^2 D_{q_iq_i}(x_1,x_2,t)\right\} \\
&+\int_{\frac{x_2}{1-x_1}}^1 \frac{dz}{z} P_{qG}(z)\; D_{q_iG}(x_1,x_2/z,t) - D_{q_iq_i}(x_1,x_2,t)\left\{\int_0^{\frac{x_2}{1-x_1}} dz\, z\, P_{qq}(z) + \int_0^1 dz\, z\, P_{Gq}(z)\right\}.
\end{aligned}
$$

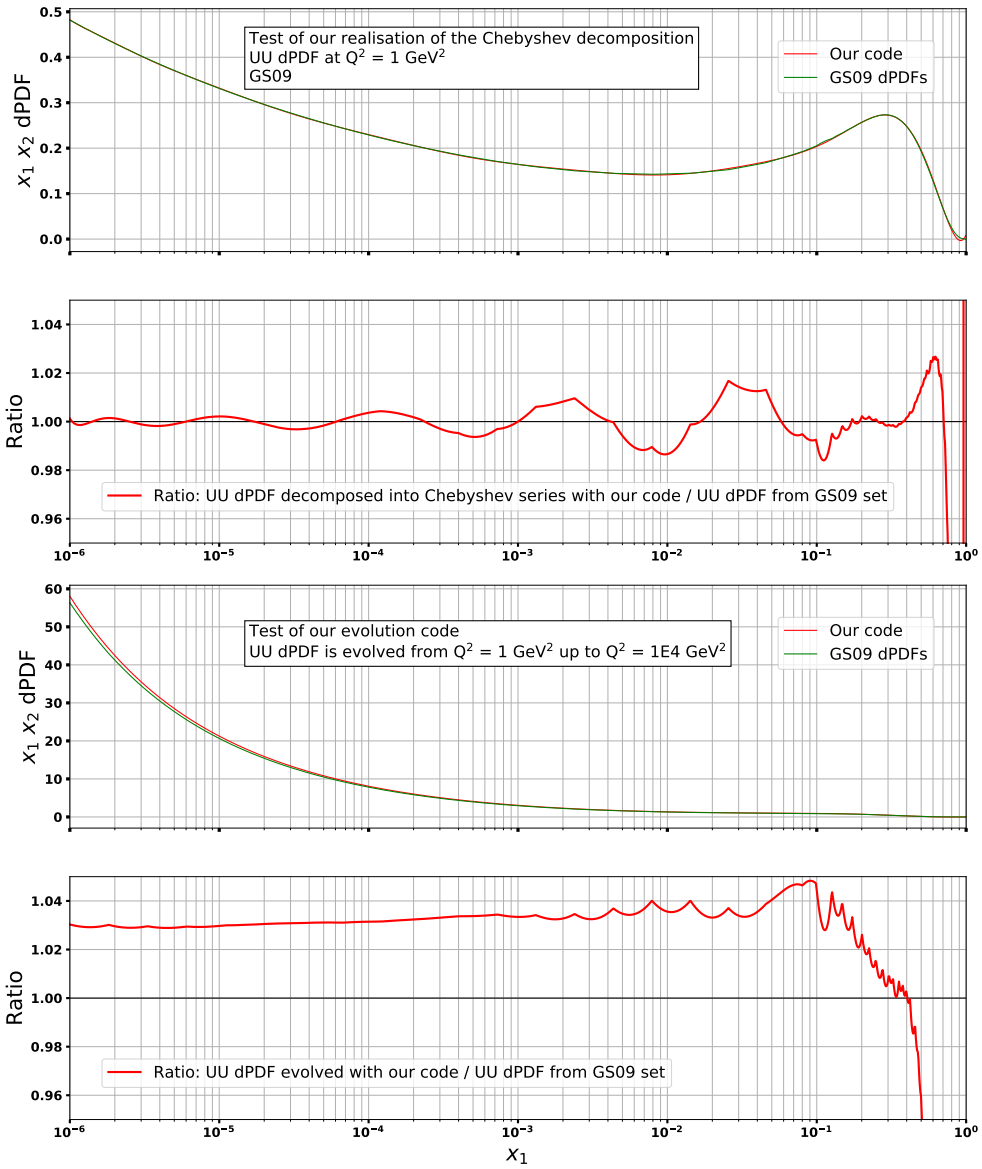

Figure J.2: Test of the evolution of the D_{uu} dPDF. Upper panel: test of the decomposition of the D_{uu} dPDF into Chebyshev series at $Q^2 = 1\,\mathrm{GeV}^2$. Lower panel: comparison between D_{uu} dPDF evolved with our evolution code against GS09 D_{uu} dPDF at $Q^2 = 10^4\,\mathrm{GeV}^2$.

The evolution equation for $D_{q_i q_i}(x_1, x_2, t)$ can be written in a more compact form by introducing the integral over DGLAP splitting functions $F_{qq}(x_1, x_2)$ defined as

$$F_{qq}(x_1, x_2) = \left\{ \int_0^{\frac{x_1}{1-x_2}} dz\, z\, P_{qq}(z) + \int_0^1 dz\, z\, P_{Gq}(z) \right\}. \tag{J.31}$$

Using Eq. J.31 we can write the evolution equation for $D_{q_iq_i}(x_1,x_2,t)$ as

$$\begin{aligned}
&\frac{2\pi}{\alpha(t)}\partial_t D_{q_iq_i}(x_1,x_2,t) = \\
&\int_{\frac{x_1}{1-x_2}}^1 \frac{dz}{z} P_{qq}(z)\left\{D_{q_iq_i}(x_1/z,x_2,t) - z^2 D_{q_iq_i}(x_1,x_2,t)\right\} + \\
&\int_{\frac{x_1}{1-x_2}}^1 \frac{dz}{z} P_{qG}(z)\, D_{Gq_i}(x_1/z,x_2,t) + \int_{\frac{x_2}{1-x_1}}^1 \frac{dz}{z} P_{qG}(z)\, D_{q_iG}(x_1,x_2/z,t) + \\
&\int_{\frac{x_2}{1-x_1}}^1 \frac{dz}{z} P_{qq}(z)\left\{D_{q_iq_i}(x_1,x_2/z,t) - z^2 D_{q_iq_i}(x_1,x_2,t)\right\} - \\
&D_{q_iq_i}(x_1,x_2,t)\left\{F_{qq}(x_1,x_2) + F_{qq}(x_2,x_1)\right\}.
\end{aligned} \tag{J.32}$$

In a similar way we can write down the evolution equations for other dPDFs. The equation for D_{q_iG} reads

$$\begin{aligned}
&\frac{2\pi}{\alpha(t)}\partial_t D_{q_iG}(x_1,x_2,t) = \\
&\int_{\frac{x_1}{1-x_2}}^1 \frac{dz}{z} P_{qq}(z)\left\{D_{q_iG}(x_1/z,x_2,t) - z^2 D_{q_iG}(x_1,x_2,t)\right\} + \\
&\int_{\frac{x_1}{1-x_2}}^1 \frac{dz}{z} P_{qG}(z)\, D_{GG}(x_1/z,x_2,t) + \int_{\frac{x_2}{1-x_1}}^1 \frac{dz}{z} P_{Gq}(z)\, \Sigma_{ij}(x_1,x_2/z,t) + \\
&\int_{\frac{x_2}{1-x_1}}^1 \frac{dz}{z} P_{GG}(z)\left\{D_{q_iG}(x_1,x_2/z,t) - z^2 D_{q_iG}(x_1,x_2,t)\right\} - \\
&D_{q_iG}(x_1,x_2,t)\left\{F^a_{qG}(x_1,x_2) + F^b_{qG}(x_1,x_2,t)\right\} + \\
&\frac{1}{x_1+x_2} P_{q_i\to g_iG}\left(\frac{x_1}{x_1+x_2}\right) f_{q_i}(x_1+x_2,t),
\end{aligned} \tag{J.33}$$

where we have defined

$$F^a_{qG}(x_1,x_2) = \int_0^{\frac{x_1}{1-x_2}} dz\, z\, P_{qq}(z) + \int_0^1 dz\, z P_{Gq}(z), \tag{J.34}$$

$$F^b_{qG}(x_1,x_2,t) = \int_0^{\frac{x_2}{1-x_1}} dz\, z\, P_{GG}(z) + 2N_f(t)\int_0^1 dz\, z P_{qG}(z), \tag{J.35}$$

$$\Sigma_{ij}(x_1,x_2/z,t) = \sum_j D_{q_iq_j}(x_1,x_2/z,t), \tag{J.36}$$

and the sum in Eq. J.36 runs over all quark and antiquark species.

The evolution equation for D_{GG} reads

$$\begin{aligned}
&\frac{2\pi}{\alpha(t)}\partial_t D_{GG}(x_1,x_2,t) = \\
&\int_{\frac{x_1}{1-x_2}}^1 \frac{dz}{z} P_{GG}(z)\left\{D_{GG}(x_1/z,x_2,t) - z^2 D_{GG}(x_1,x_2,t)\right\} + \\
&\int_{\frac{x_1}{1-x_2}}^1 \frac{dz}{z} P_{Gq}(z)\sum_j D_{q_jG}(x_1/z,x_2,t) + \int_{\frac{x_2}{1-x_1}}^1 \frac{dz}{z} P_{Gq}(z)\sum_j D_{Gq_j}(x_1,x_2/z,t) + \\
&\int_{\frac{x_2}{1-x_1}}^1 \frac{dz}{z} P_{GG}(z)\left\{D_{GG}(x_1,x_2/z,t) - z^2 D_{GG}(x_1,x_2,t)\right\} - \\
&D_{GG}(x_1,x_2,t)\left\{F_{GG}(x_1,x_2,t) + F_{GG}(x_2,x_1,t)\right\} + \\
&\frac{1}{x_1+x_2} P_{G\to GG}\left(\frac{x_1}{x_1+x_2}\right) f_G(x_1+x_2,t),
\end{aligned} \tag{J.37}$$

where

$$F_{GG}(x_1,x_2,t) = \int_0^{\frac{x_1}{1-x_2}} dz\, z\, P_{GG}(z) + 2N_f(t)\int_0^1 dz\, z P_{qG}(z), \tag{J.38}$$

and the index j in Eq. J.37 runs over all quark and antiquark species.

Finally, the evolution equation for $D_{q_iq_j}$ reads

$$\begin{aligned}
&\frac{2\pi}{\alpha(t)}\partial_t D_{q_iq_j}(x_1,x_2,t) = \\
&\int_{\frac{x_1}{1-x_2}}^1 \frac{dz}{z} P_{qq}(z)\left\{D_{q_iq_j}(x_1/z,x_2,t) - z^2 D_{q_iq_j}(x_1,x_2,t)\right\} + \\
&\int_{\frac{x_1}{1-x_2}}^1 \frac{dz}{z} P_{qG}(z)\, D_{Gq_j}(x_1/z,x_2,t) + \int_{\frac{x_2}{1-x_1}}^1 \frac{dz}{z} P_{qG}(z)\, D_{q_iG}(x_1,x_2/z,t) + \\
&\int_{\frac{x_2}{1-x_1}}^1 \frac{dz}{z} P_{qq}(z)\left\{D_{q_iq_j}(x_1,x_2/z,t) - z^2 D_{q_iq_j}(x_1,x_2,t)\right\} - \\
&D_{q_iq_j}(x_1,x_2,t)\left\{F_{qq}(x_1,x_2) + F_{qq}(x_2,x_1)\right\} + \\
&\frac{1}{x_1+x_2} P_{G\to q\bar{q}}\left(\frac{x_1}{x_1+x_2}\right) f_G(x_1+x_2,t),
\end{aligned} \tag{J.39}$$

where

$$F_{qq}(x_1,x_2,t) = \int_0^{\frac{x_1}{1-x_2}} dz\, z\, P_{qq}(z) + 2N_f(t)\int_0^1 dz\, z P_{Gq}(z), \tag{J.40}$$

and the splitting term is non-zero only for the $D_{q\bar{q}}$ distribution functions. One can see that equation for $D_{q_iq_i}$ emerge from the equation for $D_{q_iq_j}$ by setting $i=j$. Equations J.33, J.37 and J.40 form a closed system of integro-differential equations which describes the evolutions of dPDF[4].

Before solving the system of double DGLAP evolution equations we write them in a form

[4]Equations for D_{q_iG} and D_{Gq_i} dPDFs are not independent and related through the symmetry of dPDFs under the interchange of the partons $D_{q_iG}(x_1,x_2,t) = D_{Gq_i}(x_2,x_1,t)$

suitable for numerical solution. Consider, for example, $D_{q_iq_i}$. In the same way as in Appendix J.1 we introduce $\widetilde{D}_{q_iq_i} = x_1x_2D_{q_iq_i}$ which gives the following evolution for $\widetilde{D}_{q_iq_i}$

$$\begin{aligned}
&\frac{2\pi}{\alpha(t)}\partial_t\widetilde{D}_{q_iq_i}(x_1,x_2,t) = \\
&\int_{\frac{x_1}{1-x_2}}^1 dz\,P_{qq}(z)\,\left\{\widetilde{D}_{q_iq_i}(x_1/z,x_2,t) - z\widetilde{D}_{q_iq_i}(x_1,x_2,t)\right\} + \\
&\int_{\frac{x_1}{1-x_2}}^1 dz\,P_{qG}(z)\,\widetilde{D}_{Gq_i}(x_1/z,x_2,t) + \int_{\frac{x_2}{1-x_1}}^1 dz\,P_{qG}(z)\,\widetilde{D}_{q_iG}(x_1,x_2/z,t) + \\
&\int_{\frac{x_2}{1-x_1}}^1 dz\,P_{qq}(z)\,\left\{\widetilde{D}_{q_iq_i}(x_1,x_2/z,t) - z\widetilde{D}_{q_iq_i}(x_1,x_2,t)\right\} - \\
&\widetilde{D}_{q_iq_i}(x_1,x_2,t)\left\{F_{qq}(x_1,x_2) + F_{qq}(x_2,x_1)\right\}.
\end{aligned} \tag{J.41}$$

Now we relabel variables as $x_1 = x$, $x_2 = y$

$$\begin{aligned}
&\frac{2\pi}{\alpha(t)}\partial_t\widetilde{D}_{q_iq_i}(x,y,t) = \\
&\int_{\frac{x}{1-y}}^1 dz\,P_{qq}(z)\,\left\{\widetilde{D}_{q_iq_i}(x/z,y,t) - z\widetilde{D}_{q_iq_i}(x,y,t)\right\} + \\
&\int_{\frac{x}{1-y}}^1 dz\,P_{qG}(z)\,\widetilde{D}_{Gq_i}(x/z,y,t) + \int_{\frac{y}{1-x}}^1 dz\,P_{qG}(z)\,\widetilde{D}_{q_iG}(x,y/z,t) + \\
&\int_{\frac{y}{1-x}}^1 dz\,P_{qq}(z)\,\left\{\widetilde{D}_{q_iq_i}(x,y/z,t) - z\widetilde{D}_{q_iq_i}(x,y,t)\right\} - \\
&\widetilde{D}_{q_iq_i}(x,y,t)\left\{F_{qq}(x,y) + F_{qq}(y,x)\right\},
\end{aligned} \tag{J.42}$$

and switch to the logarithmic scale

$$\begin{aligned}
x &= \exp(\tilde{x}), \\
y &= \exp(\tilde{y}), \\
z &= \exp(\tilde{z}),
\end{aligned}$$

which yields

$$\begin{aligned}
&\frac{2\pi}{\alpha(t)}\partial_t D^*_{q_iq_i}(\tilde{x},\tilde{y},t) = \\
&\int_{\tilde{x}-\log(1-\exp(\tilde{y}))}^0 d\tilde{z}\,P_{qq}(\exp(\tilde{z}))\,\left\{D^*_{q_iq_i}(\tilde{x}-\tilde{z},\tilde{y},t) - \exp(\tilde{z})\,D^*_{q_iq_i}(\tilde{x},\tilde{y},t)\right\} + \\
&\int_{\tilde{x}-\log(1-\exp(\tilde{y}))}^0 dz\,P_{qG}(\exp(\tilde{z}))\,D^*_{Gq_i}(\tilde{x}-\tilde{z},\tilde{y},t), + \\
&\int_{\tilde{y}-\log(1-\exp(\tilde{x}))}^0 dz\,P_{qG}(\exp(\tilde{z}))\,D^*_{q_iG}(\tilde{x},\tilde{y}-\tilde{z},t) + \\
&\int_{\tilde{y}-\log(1-\exp(\tilde{x}))}^0 dz\,P_{qq}(\exp(\tilde{z}))\,\left\{D^*_{q_iq_i}(\tilde{x},\tilde{y}-\tilde{z},t) - \exp(\tilde{z})\,D^*_{q_iq_i}(\tilde{x},\tilde{y},t)\right\} - \\
&D^*_{q_iq_i}(\tilde{x},\tilde{y},t)\left\{F_{qq}(\exp(\tilde{x}),\exp(\tilde{y})) + F_{qq}(\exp(\tilde{y}),\exp(\tilde{x}))\right\}.
\end{aligned} \tag{J.43}$$

Expression for the others dPDFs can be easily obtained in the same way.

The test of our numerical code to solve double DGLAP evolution equations is given in Fig. J.3. In our implementation we use the two step Runge-Kutta method for the evolution in t and the seven-point Newton-Cotes rule for the numerical integration as it is described in [308]. We also use cubic spline interpolation routines from the GSL library [294] to interpolate dPDFs between different grid points. In order to check our code we take the D_{GG} dPDFs from the GS09 set and evolve it from the c quark mass up to the b quark mass. In the same was as in Appendix J.1 we use GS09 dPDFs to decouple the evolution of D_{GG} from the others dPDFs. After performing the evolution of D_{GG} we compare the output of our code against D_{GG} dPDF from the GS09 set.

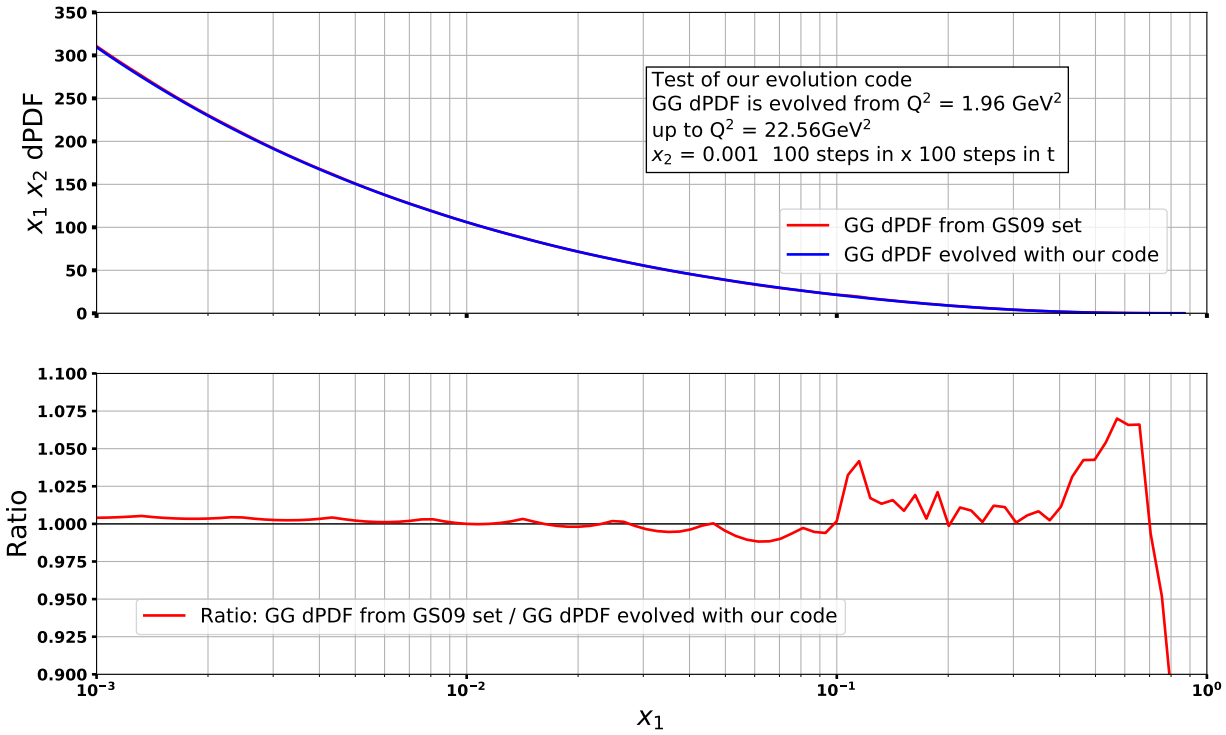

Figure J.3: Test of the evolution of the D_{GG} dPDF. Here we evolve D_{GG} dPDF given by GS09 set. The initial evolution scale is set to the c quark mass (1.40 GeV) and the final evolution scale is set to the b quark mass (4.75 GeV). We have used 100×100 grid in x-space and performed 100 steps in the evolution parameter t. In the lower panel we give the ratio between the D_{GG} evolved to the b quark mass against D_{GG} from GS09 set.

J.3 Conclusions

In Appendix J.1 and Appendix J.2 we have briefly described the method of Chebyshev polynomials and the combination of Runge-Kutta and Newton-Cotes methods which were used in [178] - [180] and in [173] to solve the system of double DGLAP evolution equations. We also presented the checks of our implementation of these methods shown in Fig. J.1 - J.3. However, the checks we have performed demonstrate that PDFs and dPDFs evolved with our code deviate from the MSTW2008 PDFs and GS09 dPDFs at small and high values of x. Therefore, we leave the improvement of our evolution code for the future work.

Bibliography

[1] J. Collins, "Foundations of perturbative QCD", Camb. Monogr. Part. Phys. Nucl. Phys. Cosmol. **32** (2011) 1.

[2] R. K. Ellis, W. J. Stirling and B. R. Webber, "QCD and collider physics", Camb. Monogr. Part. Phys. Nucl. Phys. Cosmol. **8** (1996) 1.

[3] T. Muta, "Foundations of Quantum Chromodynamics: An Introduction to Perturbative Methods in Gauge Theories, (3rd ed.)".

[4] J. C. Collins, "Renormalization : An Introduction to Renormalization, The Renormalization Group, and the Operator Product Expansion", doi:10.1017/CBO9780511622656

[5] M. E. Peskin and D. V. Schroeder, "An Introduction to quantum field theory".

[6] C. N. Yang and R. L. Mills, "Conservation of Isotopic Spin and Isotopic Gauge Invariance", Phys. Rev. **96** (1954) 191.

[7] H. Fritzsch, M. Gell-Mann and H. Leutwyler, "Advantages of the Color Octet Gluon Picture", Phys. Lett. **47B** (1973) 365.

[8] R. P. Feynman, "Quantum theory of gravitation", Acta Phys. Polon. **24** (1963) 697.

[9] B.S. De Witt, Relativity, groups and topology. (Blackie and Son Ltd 1964) pp 587-820.

[10] L. D. Faddeev and V. N. Popov, "Feynman Diagrams for the Yang-Mills Field", Phys. Lett. B **25** (1967) 29.

[11] N. Nakanishi and I. Ojima, "Covariant operator formalism of gauge theories and quantum gravity", World Sci. Lect. Notes Phys. **27** (1990) 1.

[12] R. D. Peccei, "The Strong CP problem and axions", Lect. Notes Phys. **741** (2008) 3 [hep-ph/0607268].

[13] H. Lehmann, K. Symanzik and W. Zimmermann, "On the formulation of quantized field theories", Nuovo Cim. **1** (1955) 205.

[14] F. J. Dyson, "The S matrix in quantum electrodynamics", Phys. Rev. **75** (1949) 1736.

[15] C. G. Callan, Jr., "Broken scale invariance in scalar field theory", Phys. Rev. D **2** (1970) 1541.

[16] A. Petermann, "La normalisation des constantes dans la théorie des quanta," Helv. Phys. Acta **26** (1953) 499.

[17] G. 't Hooft and M. J. G. Veltman, "Regularization and Renormalization of Gauge Fields", Nucl. Phys. B **44** (1972) 189.

[18] M. Gell-Mann and F. E. Low, "Quantum electrodynamics at small distances", Phys. Rev. **95** (1954) 1300.

[19] K. Symanzik, "Small distance behavior in field theory and power counting", Commun. Math. Phys. **18** (1970) 227.

[20] H. D. Politzer, "Reliable Perturbative Results for Strong Interactions?", Phys. Rev. Lett. **30** (1973) 1346.

[21] D. J. Gross and F. Wilczek, "Asymptotically Free Gauge Theories - I", Phys. Rev. D **8** (1973) 3633.

[22] S. Weinberg, "The quantum theory of fields. Vol. 2: Modern applications."

[23] S. Bethke, "Experimental tests of asymptotic freedom", Prog. Part. Nucl. Phys. **58** (2007) 351 [hep-ex/0606035].

[24] A. Deur, S. J. Brodsky and G. F. de Teramond, "The QCD Running Coupling", Prog. Part. Nucl. Phys. **90** (2016) 1 [arXiv:1604.08082 [hep-ph]].

[25] I. Estermann R. Frisch and O. Stern, "Magnetic Moment of the Proton", Nature **132**, 169-170, (1933).

[26] J. DiSciacca and G. Gabrielse, "Direct Measurement of the Proton Magnetic Moment", Phys. Rev. Lett. **108** (2012) 153001 arXiv:1201.3038 [physics.atom-ph]].

[27] R. P. Feynman, "Very high-energy collisions of hadrons", Phys. Rev. Lett. **23** (1969) 1415.

[28] J. D. Bjorken and E. A. Paschos, "Inelastic Electron Proton and gamma Proton Scattering, and the Structure of the Nucleon", Phys. Rev. **185** (1969) 1975.

[29] R. E. Taylor, "Deep inelastic scattering: The Early years", Rev. Mod. Phys. **63** (1991) 573.

[30] M. Gell-Mann, "A Schematic Model of Baryons and Mesons", Phys. Lett. **8** (1964) 214.

[31] G. Zweig, CERN Preprints TH 401, 412 (1964), unpublished.

[32] O. W. Greenberg, "Spin and Unitary Spin Independence in a Paraquark Model of Baryons and Mesons", Phys. Rev. Lett. **13** (1964) 598.

[33] M. Y. Han and Y. Nambu, "Three Triplet Model with Double SU(3) Symmetry", Phys. Rev. **139** (1965) B1006.

[34] F. Tkachov, "A Contribution to the history of quarks: Boris Struminsky's 1965 JINR publication", arXiv:0904.0343 [physics.hist-ph].

[35] N.N. Bogoliubov, B.V. Struminsky and A.N. Tavkhelidze , JINR Preprint D-1968 (received 23 January 1965, in Russian);
N.N. Bogoliubov, V.A. Matveev, Nguen Van Hieu, D. Stoyanov, B.V. Struminsky, A.N. Tavkhelidze and V.P. Shelest, JINR Preprint P- 2141, Dubna, 1965 (in Russian)

[36] J. D. Bjorken, "An Inequality For Electron And Muon Scattering From Nucleons", Phys. Rev. Lett. **16** (1966) 408.

[37] J. D. Bjorken, "Asymptotic Sum Rules at Infinite Momentum", Phys. Rev. **179** (1969) 1547.

[38] T. M. Yan and S. D. Drell, "The Parton Model and its Applications", Int. J. Mod. Phys. A **29** (2014) 0071 [arXiv:1409.0051 [hep-ph]].

[39] M. N. Rosenbluth, "High Energy Elastic Scattering of Electrons on Protons", Phys. Rev. **79** (1950) 615.

[40] R. Hofstadter, H. R. Fechter and J. A. McIntyre, "Scattering of High-Energy Electrons and the Method of Nuclear Recoil", Phys. Rev. **91** (1953) 422.

[41] R. Hofstadter, "Electron scattering and nuclear structure", Rev. Mod. Phys. **28** (1956) 214.

[42] D. Griffiths, "Introduction to elementary particles", Weinheim, Germany: Wiley-VCH (2008) 454 p

[43] P. Paganini, "An introduction to the Standard Model of Particle Physics".

[44] R. L. Jaffe, "Spin, twist and hadron structure in deep inelastic processes", hep-ph/9602236.

[45] E. D. Bloom *et al.*, "High-Energy Inelastic e p Scattering at 6-Degrees and 10-Degrees", Phys. Rev. Lett. **23** (1969) 930.

[46] M. Breidenbach *et al.*, "Observed Behavior of Highly Inelastic electron-Proton Scattering", Phys. Rev. Lett. **23** (1969) 935.

[47] E. D. Bloom *et al.*, "Recent Results In Inelastic Electron Scattering", SLAC-PUB-0796, XV International Conference on High Energy Physics, Kiev, U.S.S.R.

[48] G. Miller *et al.*, "Inelastic electron-Proton Scattering at Large Momentum Transfers", Phys. Rev. D **5** (1972) 528.

[49] J. I. Friedman and H. W. Kendall, "Deep inelastic electron scattering", Ann. Rev. Nucl. Part. Sci. **22**, 203 (1972).

[50] M. Riordan, "The Discovery of Quarks," SLAC-PUB-5724, April 1992, (T/E).

[51] C. G. Callan, Jr. and D. J. Gross, "High-energy electroproduction and the constitution of the electric current", Phys. Rev. Lett. **22** (1969) 156.

[52] A. Bodek *et al.*, "Experimental Studies of the Neutron and Proton Electromagnetic Structure Functions", Phys. Rev. D **20** (1979) 1471.

[53] M. Gell-Mann and Y. Ne'eman, "Current-generated algebras", Annals Phys. **30** (1964) 360.

[54] S. L. Adler and W. K. Tung, "Breakdown of asymptotic sum rules in perturbation theory", Phys. Rev. Lett. **22** (1969) 978.

[55] R. Jackiw and G. Preparata, "Probes for the constituents of the electromagnetic current and anomalous commutators", Phys. Rev. Lett. **22** (1969) 975.

[56] D. J. Gross and F. Wilczek, "Ultraviolet Behavior of Nonabelian Gauge Theories", Phys. Rev. Lett. **30** (1973) 1343.

[57] C. G. Callan, Jr. and D. J. Gross, "Bjorken scaling in quantum field theory", Phys. Rev. D **8** (1973) 4383.

[58] D. J. Gross, "The discovery of asymptotic freedom and the emergence of QCD", Proc. Nat. Acad. Sci. **102** (2005) 9099 [Int. J. Mod. Phys. A **20** (2005) 5717] [Rev. Mod. Phys. **77** (2005) 837].

[59] G. Altarelli, "A QCD primer", AIP Conf. Proc. **631** (2002) no.1, 70 [hep-ph/0204179].

[60] Frank Wilczek, "Asymptotic Freedom", arXiv:hep-th/9609099.

[61] J. C. Collins, D. E. Soper and G. F. Sterman, "Factorization of Hard Processes in QCD", Adv. Ser. Direct. High Energy Phys. **5** (1989) 1 [hep-ph/0409313].

[62] V. A. Smirnov, "Applied asymptotic expansions in momenta and masses", Springer Tracts Mod. Phys. **177** (2002) 1.

[63] T. Ahmed *et al.* [H1 Collaboration], "A Measurement of the proton structure function f2 (x, Q**2)", Nucl. Phys. B **439** (1995) 471 [hep-ex/9503001].

[64] W. A. Bardeen, A. J. Buras, D. W. Duke and T. Muta, "Deep Inelastic Scattering Beyond the Leading Order in Asymptotically Free Gauge Theories", Phys. Rev. D **18** (1978) 3998.

[65] C. F. von Weizsäcker Z. Phys. **88** (1934) 612;
E. J. Williams, Phys. Rev. **45** (1934) 729;
P. Kessel, Nuovo Cimento **16** (1960) 809;
V. N. Baier, V. S. Fadin and V. A. Khoze, Nucl. Phys. B**65** (1973) 381;
N. Cabibo and P. Rocca, CERN report TH(1972), unpublished;
M. S. Chen and P. Zervas, Phys. Rev. D**12** (1975) 187.

[66] Y. L. Dokshitzer, "Calculation of the Structure Functions for Deep Inelastic Scattering and e+ e- Annihilation by Perturbation Theory in Quantum Chromodynamics.", Sov. Phys. JETP **46** (1977) 641 [Zh. Eksp. Teor. Fiz. **73** (1977) 1216].

[67] V. N. Gribov and L. N. Lipatov, "Deep inelastic e p scattering in perturbation theory", Sov. J. Nucl. Phys. **15** (1972) 438 [Yad. Fiz. **15** (1972) 781].

[68] G. Altarelli and G. Parisi, "Asymptotic Freedom in Parton Language", Nucl. Phys. B **126** (1977) 298.

[69] S. D. Drell and T. M. Yan, "Massive Lepton Pair Production in Hadron-Hadron Collisions at High-Energies", Phys. Rev. Lett. **25** (1970) 316 Erratum: [Phys. Rev. Lett. **25** (1970) 902].

[70] G. T. Bodwin, "Factorization of the Drell-Yan Cross-Section in Perturbation Theory", Phys. Rev. D **31** (1985) 2616 Erratum: [Phys. Rev. D **34** (1986) 3932].

[71] J. C. Collins, D. E. Soper and G. F. Sterman, "Factorization for Short Distance Hadron - Hadron Scattering", Nucl. Phys. B **261** (1985) 104.

[72] J. C. Collins, D. E. Soper and G. F. Sterman, "Soft Gluons and Factorization", Nucl. Phys. B **308** (1988) 833.

[73] G. Watt, "Parton distribution function dependence of benchmark Standard Model total cross sections at the 7 TeV LHC", JHEP **1109** (2011) 069 [arXiv:1106.5788 [hep-ph]].

[74] A. Papaefstathiou, "How-to: Write a parton-level Monte Carlo event generator", arXiv:1412.4677 [hep-ph].

[75] K. Hagiwara, J. Kanzaki, N. Okamura, D. Rainwater and T. Stelzer, "Calculation of HELAS amplitudes for QCD processes using graphics processing unit (GPU)", Eur. Phys. J. C **70** (2010) 513 [arXiv:0909.5257 [hep-ph]].

[76] K. Hagiwara and Y. Takaesu, "Generating QCD amplitudes in the color-flow basis with MadGraph", Eur. Phys. J. C **71** (2011) 1668 [arXiv:1010.0748 [hep-ph]].

[77] A. Buckley *et al.*, "General-purpose event generators for LHC physics", Phys. Rept. **504** (2011) 145 [arXiv:1101.2599 [hep-ph]].

[78] S. Höche, "Introduction to parton-shower event generators", arXiv:1411.4085 [hep-ph].

[79] Michael E. Peskin, "How to turn a hep-ph paper into a simulation".

[80] Malin Sjödahl, "The Magic of Color".

[81] J. Alwall *et al.*, "A Standard format for Les Houches event files", Comput. Phys. Commun. **176** (2007) 300 [hep-ph/0609017].

[82] K. Hagiwara *et al.* [Particle Data Group], "Review of particle physics. Particle Data Group", Phys. Rev. D **66** (2002) 010001.

[83] A Doxygen representation of the Pythia's code.

[84] Pythia event generator, online manual.

[85] G. C. Fox and S. Wolfram, "A Model for Parton Showers in QCD", Nucl. Phys. B **168** (1980) 285.

[86] R. Odorico, "Exclusive Calculations for QCD Jets in a Monte Carlo Approach", Nucl. Phys. B **172** (1980) 157 Erratum: [Nucl. Phys. B **178** (1981) 545].

[87] C.-H. Lai, J.L. Petersen, T.F. Walsh Nucl. Phys., B173 (1980), p. 141

[88] K. Kajantie and E. Pietarinen, "Improved Evolution Equations for QCD", Phys. Lett. **93B** (1980) 269.

[89] T. D. Gottschalk, "A Realistic Model for e+ e- Annihilation Including Parton Bremsstrahlung Effects", Nucl. Phys. B **214** (1983) 201.

[90] G. Marchesini and B. R. Webber, "Simulation of QCD Jets Including Soft Gluon Interference", Nucl. Phys. B **238** (1984) 1.

[91] B. R. Webber, "A QCD Model for Jet Fragmentation Including Soft Gluon Interference", Nucl. Phys. B **238** (1984) 492.

[92] T. Sjostrand, "A Model for Initial State Parton Showers", Phys. Lett. **157B** (1985) 321.

[93] G. Marchesini and B. R. Webber, "Monte Carlo Simulation of General Hard Processes with Coherent QCD Radiation", Nucl. Phys. B **310** (1988) 461.

[94] H. U. Bengtsson, "The Lund Monte Carlo for High p_T Physics", Comput. Phys. Commun. **31** (1984) 323.

[95] F. Maltoni, K. Paul, T. Stelzer and S. Willenbrock, "Color Flow Decomposition of QCD Amplitudes", Phys. Rev. D **67** (2003) 014026 [hep-ph/0209271].

[96] W. Kilian, T. Ohl, J. Reuter and C. Speckner, "QCD in the Color-Flow Representation", JHEP **1210** (2012) 022 [arXiv:1206.3700 [hep-ph]].

[97] R. K. Ellis, G. Marchesini and B. R. Webber, "Soft Radiation in Parton Parton Scattering", Nucl. Phys. B **286** (1987) 643 Erratum: [Nucl. Phys. B **294** (1987) 1180].

[98] A. Bassetto, M. Ciafaloni and G. Marchesini, "Jet Structure and Infrared Sensitive Quantities in Perturbative QCD", Phys. Rept. **100** (1983) 201.

[99] G. 't Hooft, "A Planar Diagram Theory for Strong Interactions", Nucl. Phys. B **72** (1974) 461.

[100] Z. Nagy and D. E. Soper, "Parton showers with quantum interference", JHEP **0709** (2007) 114 [arXiv:0706.0017 [hep-ph]].

[101] S. Hoeche, F. Krauss, M. Schonherr and F. Siegert, "A critical appraisal of NLO+PS matching methods", JHEP **1209** (2012) 049 [arXiv:1111.1220 [hep-ph]].

[102] S. Platzer and M. Sjodahl, "Subleading N_c improved Parton Showers", JHEP **1207** (2012) 042 [arXiv:1201.0260 [hep-ph]].

[103] L. Lönnblad, "Fooling Around with the Sudakov Veto Algorithm", Eur. Phys. J. C **73** (2013) no.3, 2350 [arXiv:1211.7204 [hep-ph]].

[104] Update History of the Pythia event generator.

[105] P. J. Mulders, A. W. Schreiber and H. Meyer, "The Convolution approach in deep inelastic scattering", Nucl. Phys. A **549** (1992) 498.

[106] H. Merabet, J. F. Mathiot, J. Dolejsi and H. J. Pirner, "Modification of the gluon structure function and J / psi leptoproduction by nuclear Fermi motion", Phys. Lett. B **307** (1993) 177.

[107] K. J. Eskola, H. Paukkunen and C. A. Salgado, "EPS09: A New Generation of NLO and LO Nuclear Parton Distribution Functions", JHEP **0904** (2009) 065 [arXiv:0902.4154 [hep-ph]].

[108] S. Chatrchyan *et al.* [CMS Collaboration], "Measurement of four-jet production in proton-proton collisions at $\sqrt{s} = 7$ TeV", Phys. Rev. D **89** (2014) no.9, 092010 [arXiv:1312.6440 [hep-ex]].

[109] J. Pumplin, D. R. Stump, J. Huston, H. L. Lai, P. M. Nadolsky and W. K. Tung, "New generation of parton distributions with uncertainties from global QCD analysis", JHEP **0207** (2002) 012 [hep-ph/0201195].

[110] Z. Kunszt, "Four - Jet Production At The Proton Anti-proton Collider", Phys. Lett. **145B** (1984) 132.

[111] P. V. Landshoff and J. C. Polkinghorne, "Calorimeter Triggers for Hard Collisions", Phys. Rev. D **18** (1978) 3344.

[112]

[112] F. Takagi, "Multiple Production of Quark Jets Off Nuclei", Phys. Rev. Lett. **43** (1979) 1296.

[113] A. Donnachie and P. V. Landshoff, "Elastic Scattering at Large t", Z. Phys. C **2** (1979) 55 Erratum: [Z. Phys. C **2** (1979) 372].

[114] C. Goebel, F. Halzen and D. M. Scott, "Double Drell-Yan Annihilations in Hadron Collisions: Novel Tests of the Constituent Picture", Phys. Rev. D **22** (1980) 2789.

[115] H. D. Politzer, "Power Corrections at Short Distances", Nucl. Phys. B **172** (1980) 349.

[116] N. Paver and D. Treleani, "Multi - Quark Scattering and Large p_T Jet Production in Hadronic Collisions", Nuovo Cim. A **70** (1982) 215.

[117] M. Mekhfi, "Multiparton Processes: An Application To Double Drell-Yan", Phys. Rev. D **32** (1985) 2371.

[118] N. Paver and D. Treleani, "Relevance of Scale Breaking Terms in Large p_T Calorimeter Measurements", Nuovo Cim. A **73** (1983) 392.

[119] N. Paver and D. Treleani, "Multiple Parton Interactions and Multi - Jet Events at Collider and Tevatron Energies", Phys. Lett. **146B** (1984) 252.

[120] B. Humpert, "Are There Multi - Quark Interactions?", Phys. Lett. **131B** (1983) 461.

[121] B. Humpert and R. Odorico, "Multiparton Scattering and QCD Radiation as Sources of Four Jet Events", Phys. Lett. **154B** (1985) 211.

[122] L. Ametller, N. Paver and D. Treleani, "Possible Signature of Multiple Parton Interactions in Collider Four Jet Events", Phys. Lett. **169B** (1986) 289.

[123] F. Halzen, P. Hoyer and W. J. Stirling, "Evidence for Multiple Parton Interactions From the Observation of Multi - Muon Events in Drell-Yan Experiments", Phys. Lett. B **188** (1987) 375.

[124] J. Badier *et al.* [NA3 Collaboration], "$\psi\psi$ Production and Limits on Beauty Meson Production From 400-GeV/c Protons", Phys. Lett. **158B** (1985) 85.

[125] J. Badier *et al.* [NA3 Collaboration], "Upper Limits on Beauty Meson Production in π^- Collisions at 280-GeV/c", Phys. Lett. **124B** (1983) 535.

[126] N. Paver and D. Treleani, "Multiple Parton Processes In The Tev Region", Z. Phys. C **28** (1985) 187.

[127] M. L. Mangano, "Four Jet Production at the Tevatron Collider" Z. Phys. C **42** (1989) 331.

[128] T. Akesson *et al.* [Axial Field Spectrometer Collaboration], "Double Parton Scattering in pp Collisions at $\sqrt{s} = 63$-GeV", Z. Phys. C **34** (1987) 163.

[129] J. Alitti *et al.* [UA2 Collaboration], "A Study of multi - jet events at the CERN anti-p p collider and a search for double parton scattering", Phys. Lett. B **268** (1991) 145.

[130] F. Abe *et al.* [CDF Collaboration], "Study of four jet events and evidence for double parton interactions in $p\bar{p}$ collisions at $\sqrt{s} = 1.8$ TeV", Phys. Rev. D **47** (1993) 4857.

[131] F. Abe *et al.* [CDF Collaboration], "Measurement of double parton scattering in $\bar{p}p$ collisions at $\sqrt{s} = 1.8$ TeV", Phys. Rev. Lett. **79** (1997) 584.

[132] F. Abe *et al.* [CDF Collaboration], "Double parton scattering in $\bar{p}p$ collisions at $\sqrt{s} = 1.8$TeV", Phys. Rev. D **56** (1997) 3811.

[133] V. M. Abazov *et al.* [D0 Collaboration], "Double parton interactions in γ+3 jet events in pp^- bar collisions $\sqrt{s} = 1.96$ TeV.", Phys. Rev. D **81** (2010) 052012 [arXiv:0912.5104 [hep-ex]].

[134] M. Aaboud *et al.* [ATLAS Collaboration], "Measurement of the prompt J/ ψ pair production cross-section in pp collisions at $\sqrt{s} = 8$ TeV with the ATLAS detector", Eur. Phys. J. C **77** (2017) no.2, 76 [arXiv:1612.02950 [hep-ex]].

[135] R. Aaij *et al.* [LHCb Collaboration], "Observation of double charm production involving open charm in pp collisions at $\sqrt{s} = 7$ TeV", JHEP **1206** (2012) 141 Addendum: [JHEP **1403** (2014) 108] [arXiv:1205.0975 [hep-ex]].

[136] G. Aad *et al.* [ATLAS Collaboration], "Measurement of hard double-parton interactions in $W(\rightarrow l\nu)$+ 2 jet events at $\sqrt{s}$=7 TeV with the ATLAS detector", New J. Phys. **15** (2013) 033038 [arXiv:1301.6872 [hep-ex]].

[137] S. Chatrchyan *et al.* [CMS Collaboration], "Study of double parton scattering using W + 2-jet events in proton-proton collisions at $\sqrt{s} = 7$ TeV", JHEP **1403** (2014) 032 [arXiv:1312.5729 [hep-ex]].

[138] V. M. Abazov *et al.* [D0 Collaboration], "Observation and studies of double J/ψ production at the Tevatron", Phys. Rev. D **90** (2014) no.11, 111101 [arXiv:1406.2380 [hep-ex]].

[139] V. M. Abazov *et al.* [D0 Collaboration], "Double Parton Interactions in $\gamma + 3$ Jet and $\gamma + b/cjet + 2$ Jet Events in $p\bar{p}$ Collisions at $\sqrt{S} = 1.96\,\text{TeV}$", Phys. Rev. D **89** (2014) no.7, 072006 [arXiv:1402.1550 [hep-ex]].

[140] G. Aad *et al.* [ATLAS Collaboration], "Observation and measurements of the production of prompt and non-prompt J/ψ mesons in association with a Z boson in pp collisions at $\sqrt{s} = 8$ TeV with the ATLAS detector," Eur. Phys. J. C **75** (2015) no.5, 229 [arXiv:1412.6428 [hep-ex]].

[141] R. Aaij *et al.* [LHCb Collaboration], "Production of associated Y and open charm hadrons in pp collisions at $\sqrt{s} = 7$ and 8 TeV via double parton scattering", JHEP **1607** (2016) 052 [arXiv:1510.05949 [hep-ex]].

[142] V. M. Abazov *et al.* [D0 Collaboration], "Evidence for simultaneous production of J/ψ and Υ mesons", Phys. Rev. Lett. **116** (2016) no.8, 082002 [arXiv:1511.02428 [hep-ex]].

[143] V. M. Abazov *et al.* [D0 Collaboration], "Study of double parton interactions in diphoton + dijet events in $p\bar{p}$ collisions at $\sqrt{s} = 1.96$ TeV", Phys. Rev. D **93** (2016) no.5, 052008 [arXiv:1512.05291 [hep-ex]].

[144] CMS Collaboration [CMS Collaboration], "Study of double parton scattering in photon + 3 jets final state in proton-proton collisions at 7TeV", CMS-PAS-FSQ-12-017.

[145] M. Aaboud *et al.* [ATLAS Collaboration], "Study of hard double-parton scattering in four-jet events in pp collisions at $\sqrt{s} = 7$ TeV with the ATLAS experiment", JHEP **1611** (2016) 110 [arXiv:1608.01857 [hep-ex]].

[146] A. M. Sirunyan *et al.* [CMS Collaboration], "Constraints on the double-parton scattering cross section from same-sign W boson pair production in proton-proton collisions at $\sqrt{s} = 8$ TeV", JHEP **1802** (2018) 032 [arXiv:1712.02280 [hep-ex]].

[147] V. Khachatryan *et al.* [CMS Collaboration], "Event generator tunes obtained from underlying event and multiparton scattering measurements", Eur. Phys. J. C **76** (2016) no.3, 155 [arXiv:1512.00815 [hep-ex]].

[148] G. Calucci and D. Treleani, "Mini - jets and the two-body parton correlation", Phys. Rev. D **57** (1998) 503 [hep-ph/9707389].

[149] G. Calucci and D. Treleani, "Proton structure in transverse space and the effective cross-section", Phys. Rev. D **60** (1999) 054023 [hep-ph/9902479].

[150] L. Frankfurt, M. Strikman and C. Weiss, "Dijet production as a centrality trigger for pp collisions at CERN LHC", Phys. Rev. D **69** (2004) 114010 [hep-ph/0311231].

[151] G. Calucci and D. Treleani, "Multi-parton correlations and 'exclusive' cross sections", Phys. Rev. D **79** (2009) 074013 [arXiv:0901.3089 [hep-ph]].

[152] S. Domdey, H. J. Pirner and U. A. Wiedemann, "Testing the Scale Dependence of the Scale Factor sigma(eff) in Double Dijet Production at the LHC", Eur. Phys. J. C **65** (2010) 153 [arXiv:0906.4335 [hep-ph]].

[153] T. C. Rogers and M. Strikman, "Multiple Hard Partonic Collisions with Correlations in Proton-Proton Scattering", Phys. Rev. D **81** (2010) 016013 [arXiv:0908.0251 [hep-ph]].

[154] G. Calucci and D. Treleani, "Disentangling correlations in Multiple Parton Interactions", Phys. Rev. D **83** (2011) 016012 [arXiv:1009.5881 [hep-ph]].

[155] C. Flensburg, G. Gustafson, L. Lonnblad and A. Ster, "Correlations in double parton distributions at small x", JHEP **1106** (2011) 066 [arXiv:1103.4320 [hep-ph]].

[156] B. Blok, Yu. Dokshitzer, L. Frankfurt, M. Strikman, "Origins of parton correlations in nucleon and multi-parton collisions", [arXiv:1206.5594 [hep-ph]].

[157] M. H. Seymour and A. Siodmok, "Extracting $\sigma_{\text{effective}}$ from the LHCb double-charm measurement", arXiv:1308.6749 [hep-ph].

[158] B. Blok, Y. Dokshitzer, L. Frankfurt and M. Strikman, "Perturbative QCD correlations in multi-parton collisions", Eur. Phys. J. C **74** (2014) 2926 [arXiv:1306.3763 [hep-ph]].

[159] M. Diehl, T. Kasemets and S. Keane, "Correlations in double parton distributions: effects of evolution", JHEP **1405** (2014) 118 [arXiv:1401.1233 [hep-ph]].

[160] M. Rinaldi and F. A. Ceccopieri, "Hadronic structure from double parton scattering", Phys. Rev. D **97** (2018) no.7, 071501 [arXiv:1801.04760 [hep-ph]].

[161] M. Diehl, "Correlation effects in multiple hard scattering", PoS DIS **2013** (2013) 074 [arXiv:1306.6480 [hep-ph]].

[162] B. Blok and P. Gunnellini, "Dynamical approach to MPI four-jet production in Pythia", Eur. Phys. J. C **75** (2015) no.6, 282 [arXiv:1503.08246 [hep-ph]].

[163] B. Blok and P. Gunnellini, "Dynamical approach to MPI in W+dijet and Z+dijet production within the PYTHIA event generator", Eur. Phys. J. C **76** (2016) no.4, 202 [arXiv:1510.07436 [hep-ph]].

[164] R. Kirschner, "Generalized Lipatov-Altarelli-Parisi Equations and Jet Calculus Rules", Phys. Lett. **84B** (1979) 266.

[165] M. J. Puhala, "Some Comments on Two Particle Correlations in the Jet Calculus of Kuv", Phys. Rev. D **22** (1980) 1087.

[166] U. P. Sukhatme and K. E. Lassila, "Q^2 Evolution of Multi - Hadron Fragmentation Functions", Phys. Rev. D **22** (1980) 1184.

[167] V. P. Shelest, A. M. Snigirev and G. M. Zinovev, "The Multiparton Distribution Equations in QCD", Phys. Lett. **113B** (1982) 325.

[168] G. M. Zinovev, A. M. Snigirev and V. P. Shelest, "Equations For Many Parton Distributions In Quantum Chromodynamics", Theor. Math. Phys. **51** (1982) 523 [Teor. Mat. Fiz. **51** (1982) 317].

[169] A. M. Snigirev, "Double parton distributions in the leading logarithm approximation of perturbative QCD", Phys. Rev. D **68** (2003) 114012 [hep-ph/0304172].

[170] J. Gaunt, "Double parton scattering in proton-proton collisions", doi:10.17863/CAM.16589

[171] V. L. Korotkikh and A. M. Snigirev, "Double parton correlations versus factorized distributions", Phys. Lett. B **594** (2004) 171 [hep-ph/0404155].

[172] E. Cattaruzza, A. Del Fabbro and D. Treleani, "Fractional momentum correlations in multiple production of W bosons and of $b\bar{b}$ pairs in high energy pp collisions", Phys. Rev. D **72** (2005) 034022 [hep-ph/0507052].

[173] J. R. Gaunt and W. J. Stirling, "Double Parton Distributions Incorporating Perturbative QCD Evolution and Momentum and Quark Number Sum Rules", JHEP **1003** (2010) 005 [arXiv:0910.4347 [hep-ph]].

[174] Jonathan R. Gaunt, "The GS09 double parton distribution functions", [arXiv:1006.1118v1].

[175] F. A. Ceccopieri, "An update on the evolution of double parton distributions", Phys. Lett. B **697** (2011) 482 [arXiv:1011.6586 [hep-ph]].

[176] F. A. Ceccopieri, "A second update on double parton distributions", Phys. Lett. B **734** (2014) 79 [arXiv:1403.2167 [hep-ph]].

[177] M. Diehl, P. Plößl and A. Schäfer, "Proof of sum rules for double parton distributions in QCD", Eur. Phys. J. C **79** (2019) no.3, 253 [arXiv:1811.00289 [hep-ph]].

[178] K. Golec-Biernat, E. Lewandowska, M. Serino, Z. Snyder and A. M. Stasto, "Constraining the double gluon distribution by the single gluon distribution", Phys. Lett. B **750** (2015) 559 [arXiv:1507.08583 [hep-ph]].

[179] K. Golec-Biernat and E. Lewandowska, "How to impose initial conditions for QCD evolution of double parton distributions?", Phys. Rev. D **90** (2014) no.1, 014032 [arXiv:1402.4079 [hep-ph]].

[180] E. Lewandowska, "Processes with a hard scale at the LHC as a signature of partonic structure of the proton", PhD thesis.

[181] E. Elias, K. Golec-Biernat and A. M. Staśto, "Numerical analysis of the unintegrated double gluon distribution", JHEP **1801** (2018) 141 [arXiv:1801.00018 [hep-ph]].

[182] G. S. Bali *et al.*, "Two-current correlations in the pion on the lattice", JHEP **1812** (2018) 061 [arXiv:1807.03073 [hep-lat]].

[183] M. Rinaldi, S. Scopetta, M. Traini and V. Vento, "Double parton correlations and constituent quark models: a Light Front approach to the valence sector", JHEP **1412** (2014) 028 [arXiv:1409.1500 [hep-ph]].

[184] M. Rinaldi and F. A. Ceccopieri, "Relativistic effects in model calculations of double parton distribution function", Phys. Rev. D **95** (2017) no.3, 034040 [arXiv:1611.04793 [hep-ph]].

[185] F. A. Ceccopieri, M. Rinaldi and S. Scopetta, "Parton correlations in same-sign W pair production via double parton scattering at the LHC", Phys. Rev. D **95** (2017) no.11, 114030 [arXiv:1702.05363 [hep-ph]].

[186] M. Rinaldi and F. A. Ceccopieri, "Double parton scattering and the proton transverse structure at the LHC", arXiv:1812.04286 [hep-ph].

[187] H. M. Chang, A. V. Manohar and W. J. Waalewijn, "Double Parton Correlations in the Bag Model", Phys. Rev. D **87** (2013) no.3, 034009 [arXiv:1211.3132 [hep-ph]].

[188] M. Traini, M. Rinaldi, S. Scopetta and V. Vento, "The effective cross section for double parton scattering within a holographic AdS/QCD approach", Phys. Lett. B **768** (2017) 270 [arXiv:1609.07242 [hep-ph]].

[189] K. Konishi, A. Ukawa and G. Veneziano, "Jet Calculus: A Simple Algorithm for Resolving QCD Jets", Nucl. Phys. B **157** (1979) 45.

[190] J. R. Gaunt and W. J. Stirling, "Double Parton Scattering Singularity in One-Loop Integrals", JHEP **1106** (2011) 048 [arXiv:1103.1888 [hep-ph]].

[191] J. R. Gaunt, "Single Perturbative Splitting Diagrams in Double Parton Scattering", JHEP **1301** (2013) 042 [arXiv:1207.0480 [hep-ph]].

[192] M. Diehl and A. Schafer, "Theoretical considerations on multiparton interactions in QCD", Phys. Lett. B **698** (2011) 389 [arXiv:1102.3081 [hep-ph]].

[193] M. Diehl, D. Ostermeier and A. Schafer, "Elements of a theory for multiparton interactions in QCD", JHEP **1203** (2012) 089 [arXiv:1111.0910 [hep-ph]].

[194] B. Blok, Y. Dokshitzer, L. Frankfurt and M. Strikman, "The Four jet production at LHC and Tevatron in QCD", Phys. Rev. D **83** (2011) 071501 [arXiv:1009.2714 [hep-ph]].

[195] B. Blok, Y. Dokshitser, L. Frankfurt and M. Strikman, "pQCD physics of multiparton interactions", Eur. Phys. J. C **72** (2012) 1963 [arXiv:1106.5533 [hep-ph]].

[196] B. Blok, Y. Dokshitzer, L. Frankfurt and M. Strikman, "Origins of Parton Correlations in Nucleon and Multi-Parton Collisions", arXiv:1206.5594 [hep-ph].

[197] M. G. Ryskin and A. M. Snigirev, "A Fresh look at double parton scattering", Phys. Rev. D **83** (2011) 114047 [arXiv:1103.3495 [hep-ph]].

[198] M. G. Ryskin and A. M. Snigirev, "Double parton scattering in double logarithm approximation of perturbative QCD", Phys. Rev. D **86** (2012) 014018 [arXiv:1203.2330 [hep-ph]].

[199] A. V. Manohar and W. J. Waalewijn, "What is Double Parton Scattering?", Phys. Lett. B **713** (2012) 196 [arXiv:1202.5034 [hep-ph]].

[200] M. Diehl, J. R. Gaunt and K. Schönwald, "Double hard scattering without double counting", JHEP **1706** (2017) 083 [arXiv:1702.06486 [hep-ph]].

[201] M. Cacciari, G. P. Salam and S. Sapeta, "On the characterisation of the underlying event", JHEP **1004** (2010) 065 [arXiv:0912.4926 [hep-ph]].

[202] M. Diehl and J. R. Gaunt, "Double parton scattering theory overview", Adv. Ser. Direct. High Energy Phys. **29** (2018) 7 [arXiv:1710.04408 [hep-ph]].

[203] L. Frankfurt and M. Strikman, "Two gluon form-factor of the nucleon and J / psi photoproduction", Phys. Rev. D **66** (2002) 031502 [hep-ph/0205223].

[204] R. D. Tangerman and P. J. Mulders, "Intrinsic transverse momentum and the polarized Drell-Yan process", Phys. Rev. D **51** (1995) 3357 [hep-ph/9403227].

[205] X. Ji, J. w. Qiu, W. Vogelsang and F. Yuan, "Single Transverse-Spin Asymmetry in Drell-Yan Production at Large and Moderate Transverse Momentum", Phys. Rev. D **73** (2006) 094017 [hep-ph/0604023].

[206] A. Bacchetta, D. Boer, M. Diehl and P. J. Mulders, "Matches and mismatches in the descriptions of semi-inclusive processes at low and high transverse momentum", JHEP **0808** (2008) 023 [arXiv:0803.0227 [hep-ph]].

[207] M. Mekhfi, "Correlations in Color and Spin in Multiparton Processes", Phys. Rev. D **32** (1985) 2380.

[208] M. Mekhfi and X. Artru, "Sudakov Suppression of Color Correlations in Multiparton Scattering", Phys. Rev. D **37** (1988) 2618.

[209] S. Cotogno, T. Kasemets and M. Myska, "A spin on same-sign W-boson pair production", arXiv:1809.09024 [hep-ph].

[210] M. Diehl, J. R. Gaunt, P. Ploessl and A. Schafer, "Two-loop splitting in double parton distributions", arXiv:1902.08019 [hep-ph].

[211] B. Cabouat, "Talk at 18th MCnet meeting", Louvain-la-Neuve, Belgium, 2018.

[212] F. Hernman, "Poster at Quark Matter Conference", Venice, Italy, 2018.

[213] M. Strikman and D. Treleani, "Measuring double parton distributions in nucleons at proton nucleus colliders", Phys. Rev. Lett. **88** (2002) 031801 [hep-ph/0111468].

[214] A. Del Fabbro and D. Treleani, "b anti-b b anti-b production in proton nucleus collisions at the LHC", hep-ph/0301175.

[215] L. Frankfurt, M. Strikman and C. Weiss, "3D parton imaging of the nucleon in high-energy pp and pA collisions", Annalen Phys. **13** (2004) 665 [hep-ph/0410307].

[216] B. Blok, M. Strikman and U. A. Wiedemann, "Hard four-jet production in pA collisions", Eur. Phys. J. C **73** (2013) no.6, 2433 [arXiv:1210.1477 [hep-ph]].

[217] L. L. Frankfurt and M. I. Strikman, "High-Energy Phenomena, Short Range Nuclear Structure and QCD", Phys. Rept. **76** (1981) 215.

[218] R. D. Woods and D. S. Saxon, "Diffuse Surface Optical Model for Nucleon-Nuclei Scattering", Phys. Rev. **95** (1954) 577.

[219] M. Rybczynski, G. Stefanek, W. Broniowski and P. Bozek, "GLISSANDO 2 : GLauber Initial-State Simulation AND mOre..., ver. 2", Comput. Phys. Commun. **185** (2014) 1759 [arXiv:1310.5475 [nucl-th]].

[220] M. Cacciari, G. P. Salam and G. Soyez, "FastJet User Manual", Eur. Phys. J. C **72** (2012) 1896 [arXiv:1111.6097 [hep-ph]].

[221] M. Cacciari, G. P. Salam and G. Soyez, "The anti-k_t jet clustering algorithm", JHEP **0804** (2008) 063 [arXiv:0802.1189 [hep-ph]].

[222] M. Strikman and W. Vogelsang, "Multiple parton interactions and forward double pion production in pp and dA scattering", Phys. Rev. D **83** (2011) 034029 [arXiv:1009.6123 [hep-ph]].

[223] D. d'Enterria and A. M. Snigirev, "Same-sign WW production in proton-nucleus collisions at the LHC as a signal for double parton scattering", Phys. Lett. B **718** (2013) 1395 [arXiv:1211.0197 [hep-ph]].

[224] D. d'Enterria and A. M. Snigirev, "Enhanced J/Ψ-pair production from double parton scatterings in nucleus-nucleus collisions at the Large Hadron Collider", Phys. Lett. B **727** (2013) 157 [arXiv:1301.5845 [hep-ph]].

[225] D. d'Enterria and A. M. Snigirev, "Pair production of quarkonia and electroweak bosons from double-parton scatterings in nuclear collisions at the LHC", Nucl. Phys. A **931** (2014) 303 [arXiv:1408.5172 [hep-ph]].

[226] R. Maciula, "Simultaneous production of D and B mesons", Acta Phys. Polon. B **49** (2018) 1257 [arXiv:1803.09061 [hep-ph]].

[227] A. Del Fabbro and D. Treleani, "Double parton scatterings in b quark pairs production at the CERN LHC", Phys. Rev. D **66** (2002) 074012 [hep-ph/0207311].

[228] E. R. Cazaroto, V. P. Goncalves and F. S. Navarra, "Heavy quark production and gluon saturation in double parton scattering at the LHC", Phys. Rev. D **88** (2013) no.3, 034005 [arXiv:1306.4169 [hep-ph]].

[229] E. L. Berger, C. B. Jackson and G. Shaughnessy, "Characteristics and Estimates of Double Parton Scattering at the Large Hadron Collider", Phys. Rev. D **81** (2010) 014014 [arXiv:0911.5348 [hep-ph]].

[230] R. Maciula and A. Szczurek, "Searching for and exploring double-parton scattering effects in four-jet production at the LHC", Phys. Lett. B **749**, 57 (2015) [arXiv:1503.08022 [hep-ph]].

[231] K. Kutak, R. Maciuła, M. Serino, A. Szczurek and A. van Hameren, "Search for optimal conditions for exploring double-parton scattering in four-jet production: k_t-factorization approach", Phys. Rev. D **94** (2016) no.1, 014019 [arXiv:1605.08240 [hep-ph]].

[232] K. Kutak, R. Maciula, M. Serino, A. Szczurek and A. van Hameren, "Four-jet production in single- and double-parton scattering within high-energy factorization", JHEP **1604** (2016) 175 [arXiv:1602.06814 [hep-ph]].

[233] R. Maciula and A. Szczurek, "Double-parton scattering contribution to production of jet pairs with large rapidity separation at the LHC", Phys. Rev. D **90** (2014) no.1, 014022 [arXiv:1403.2595 [hep-ph]].

[234] R. Maciula and A. Szczurek, "Double-parton scattering effects in associated production of charm mesons and dijets at the LHC", Phys. Rev. D **96** (2017) no.7, 074013 [arXiv:1707.08366 [hep-ph]].

[235] C. H. Kom, A. Kulesza and W. J. Stirling, "Pair Production of J/psi as a Probe of Double Parton Scattering at LHCb", Phys. Rev. Lett. **107** (2011) 082002 [arXiv:1105.4186 [hep-ph]].

[236] C. Borschensky and A. Kulesza, "Double parton scattering in pair production of J/ψ mesons at the LHC revisited", Phys. Rev. D **95** (2017) no.3, 034029 [arXiv:1610.00666 [hep-ph]].

[237] C. H. Kom, A. Kulesza and W. J. Stirling, "Prospects for observation of double parton scattering with four-muon final states at LHCb", Eur. Phys. J. C **71** (2011) 1802 [arXiv:1109.0309 [hep-ph]].

[238] J. R. Gaunt, C. H. Kom, A. Kulesza and W. J. Stirling, "Same-sign W pair production as a probe of double parton scattering at the LHC", Eur. Phys. J. C **69** (2010) 53 [arXiv:1003.3953 [hep-ph]].

[239] J. Q. Tao, S. J. Zhang, Y. Q. Shen, J. W. Fan, G. M. Chen and H. S. Chen, "Production of $\gamma\gamma$+2 jets from double parton scattering in proton-proton collisions at the LHC", Chin. Phys. C **39** (2015) no.12, 121001 [arXiv:1504.04469 [hep-ph]].

[240] M. Y. Hussein, "A Double parton scattering background to associate WH and ZH production at the LHC", Nucl. Phys. Proc. Suppl. **174** (2007) 55 [hep-ph/0610207].

[241] M. Y. Hussein, "Double parton scattering in associate Higgs boson production with bottom quarks at hadron colliders", In *Karlsruhe 2007, SUSY 2007* 474-477 [arXiv:0710.0203 [hep-ph]].

[242] A. Kulesza and W. J. Stirling, "Like sign W boson production at the LHC as a probe of double parton scattering", Phys. Lett. B **475** (2000) 168 [hep-ph/9912232].

[243] Q. H. Cao, Y. Liu, K. P. Xie and B. Yan, "Double parton scattering of weak gauge boson productions at the 13 TeV and 100 TeV proton-proton colliders", Phys. Rev. D **97** (2018) no.3, 035013 [arXiv:1710.06315 [hep-ph]].

[244] A. H. Mueller and H. Navelet, "An Inclusive Minijet Cross-Section and the Bare Pomeron in QCD", Nucl. Phys. B **282** (1987) 727.

[245] V. Del Duca and C. R. Schmidt, "Dijet production at large rapidity intervals", Phys. Rev. D **49** (1994) 4510 [hep-ph/9311290].

[246] W. J. Stirling, "Production of jet pairs at large relative rapidity in hadron hadron collisions as a probe of the perturbative pomeron", Nucl. Phys. B **423** (1994) 56 [hep-ph/9401266].

[247] V. Del Duca and C. R. Schmidt, "BFKL versus O (alpha-s**3) corrections to large rapidity dijet production", Phys. Rev. D **51** (1995) 2150 [hep-ph/9407359].

[248] V. T. Kim and G. B. Pivovarov, "BFKL QCD pomeron in high-energy hadron collisions: Inclusive dijet production", Phys. Rev. D **53** (1996) 6 [hep-ph/9506381].

[249] J. R. Andersen, V. Del Duca, S. Frixione, C. R. Schmidt and W. J. Stirling, "Mueller-Navelet jets at hadron colliders", JHEP **0102** (2001) 007 [hep-ph/0101180].

[250] Z. Bern *et al.*, "Four-Jet Production at the Large Hadron Collider at Next-to-Leading Order in QCD", Phys. Rev. Lett. **109** (2012) 042001 [arXiv:1112.3940 [hep-ph]].

[251] S. Badger, B. Biedermann, P. Uwer and V. Yundin, "NLO QCD corrections to multi-jet production at the LHC with a centre-of-mass energy of $\sqrt{s} = 8$ TeV", Phys. Lett. B **718** (2013) 965 [arXiv:1209.0098 [hep-ph]].

[252] A. Kardos, P. Nason and C. Oleari, "Three-jet production in POWHEG", JHEP **1404** (2014) 043 [arXiv:1402.4001 [hep-ph]].

[253] M. L. Mangano, M. Moretti, F. Piccinini, R. Pittau and A. D. Polosa, "ALPGEN, a generator for hard multiparton processes in hadronic collisions", JHEP **0307** (2003) 001 [hep-ph/0206293].

[254] J. Alwall *et al.*, "The automated computation of tree-level and next-to-leading order differential cross sections, and their matching to parton shower simulations", JHEP **1407** (2014) 079 [arXiv:1405.0301 [hep-ph]].

[255] T. Sjostrand, S. Mrenna and P. Z. Skands, "PYTHIA 6.4 Physics and Manual", JHEP **0605** (2006) 026 [hep-ph/0603175].

[256] T. Sjostrand, S. Mrenna and P. Z. Skands, "A Brief Introduction to PYTHIA 8.1", Comput. Phys. Commun. **178** (2008) 852 [arXiv:0710.3820 [hep-ph]].

[257] T. Sjöstrand *et al.*, "An Introduction to PYTHIA 8.2", Comput. Phys. Commun. **191** (2015) 159 [arXiv:1410.3012 [hep-ph]].

[258] T. Sjostrand, "Multiple Parton-Parton Interactions in Hadronic Events", FERMILAB-PUB-85-119-T.

[259] T. Sjostrand and M. van Zijl, "A Multiple Interaction Model for the Event Structure in Hadron Collisions", Phys. Rev. D **36** (1987) 2019.

[260] T. Sjostrand and P. Z. Skands, "Multiple interactions and the structure of beam remnants," JHEP **0403** (2004) 053 [hep-ph/0402078].

[261] R. Corke and T. Sjostrand, "Multiparton Interactions and Rescattering", JHEP **1001** (2010) 035 [arXiv:0911.1909 [hep-ph]].

[262] R. Corke and T. Sjostrand, "Multiparton Interactions with an x-dependent Proton Size", JHEP **1105** (2011) 009 [arXiv:1101.5953 [hep-ph]].

[263] T. Sjöstrand, "The Development of MPI Modeling in Pythia," Adv. Ser. Direct. High Energy Phys. **29** (2018) 191 [arXiv:1706.02166 [hep-ph]].

[264] J. Bellm *et al.*, "Herwig 7.0/Herwig++ 3.0 release note", Eur. Phys. J. C **76** (2016) no.4, 196 [arXiv:1512.01178 [hep-ph]].

[265] M. Bahr, S. Gieseke and M. H. Seymour, "Simulation of multiple partonic interactions in Herwig++", JHEP **0807** (2008) 076 [arXiv:0803.3633 [hep-ph]].

[266] S. Gieseke, F. Loshaj and P. Kirchgaeßer, "Soft and diffractive scattering with the cluster model in Herwig", Eur. Phys. J. C **77** (2017) no.3, 156 [arXiv:1612.04701 [hep-ph]].

[267] T. Gleisberg, S. Hoeche, F. Krauss, M. Schonherr, S. Schumann, F. Siegert and J. Winter, "Event generation with SHERPA 1.1", JHEP **0902** (2009) 007 [arXiv:0811.4622 [hep-ph]].

[268] A. D. Martin, H. Hoeth, V. A. Khoze, F. Krauss, M. G. Ryskin and K. Zapp, "Diffractive Physics", PoS QNP **2012** (2012) 017 [arXiv:1206.2124 [hep-ph]].

[269] H. L. Lai *et al.* [CTEQ Collaboration], "Global QCD analysis of parton structure of the nucleon: CTEQ5 parton distributions", Eur. Phys. J. C **12** (2000) 375 [hep-ph/9903282].

[270] C. Bierlich, G. Gustafson and L. Lonnblad, "Diffractive and non-diffractive wounded nucleons and final states in pA collisions", JHEP **1610** (2016) 139 [arXiv:1607.04434 [hep-ph]].

[271] C. Bierlich, G. Gustafson, L. Lonnblad and H. Shah, "The Angantyr model for Heavy-Ion Collisions in PYTHIA8", JHEP **1810** (2018) 134 [JHEP **2018** (2020) 134] [arXiv:1806.10820 [hep-ph]].

[272] T. Pierog, I. Karpenko, J. M. Katzy, E. Yatsenko and K. Werner, "EPOS LHC: Test of collective hadronization with data measured at the CERN Large Hadron Collider", Phys. Rev. C **92** (2015) no.3, 034906 [arXiv:1306.0121 [hep-ph]].

[273] Z. W. Lin, C. M. Ko, B. A. Li, B. Zhang and S. Pal, "A Multi-phase transport model for relativistic heavy ion collisions", Phys. Rev. C **72** (2005) 064901 [nucl-th/0411110].

[274] X. N. Wang and M. Gyulassy, "HIJING: A Monte Carlo model for multiple jet production in p p, p A and A A collisions", Phys. Rev. D **44** (1991) 3501.

[275] B. Andersson, G. Gustafson and B. Nilsson-Almqvist, "A Model for Low p(t) Hadronic Reactions, with Generalizations to Hadron - Nucleus and Nucleus-Nucleus Collisions", Nucl. Phys. B **281** (1987) 289.

[276] A. H. Mueller, "Soft gluons in the infinite momentum wave function and the BFKL pomeron", Nucl. Phys. B **415** (1994) 373.

[277] A. H. Mueller and B. Patel, "Single and double BFKL pomeron exchange and a dipole picture of high-energy hard processes", Nucl. Phys. B **425** (1994) 471 [hep-ph/9403256].

[278] E. Avsar, G. Gustafson and L. Lonnblad, "Small-x dipole evolution beyond the large-N(c) limit", JHEP **0701** (2007) 012 [hep-ph/0610157].

[279] E. Avsar, G. Gustafson and L. Lonnblad, "Energy conservation and saturation in small-x evolution", JHEP **0507** (2005) 062 [hep-ph/0503181].

[280] C. Flensburg, G. Gustafson and L. Lonnblad, "Inclusive and Exclusive Observables from Dipoles in High Energy Collisions", JHEP **1108** (2011) 103 [arXiv:1103.4321 [hep-ph]].

[281] Z. Koba, H. B. Nielsen and P. Olesen, "Scaling of multiplicity distributions in high-energy hadron collisions", Nucl. Phys. B **40** (1972) 317.

[282] S. Navin, "Diffraction in Pythia", arXiv:1005.3894 [hep-ph].

[283] R. Corke and T. Sjostrand, "Interleaved Parton Showers and Tuning Prospects", JHEP **1103** (2011) 032 [arXiv:1011.1759 [hep-ph]].

[284] G. Ingelman and P. E. Schlein, "Jet Structure in High Mass Diffractive Scattering", Phys. Lett. **152B** (1985) 256.

[285] A. Bialas, M. Bleszynski and W. Czyz, "Multiplicity Distributions in Nucleus-Nucleus Collisions at High-Energies", Nucl. Phys. B **111** (1976) 461.

[286] N. N. Nikolaev and S. Pokorski, "Quark Dynamics in Soft Hadronic Collisions and Fragmentation on Nuclear Targets," Phys. Lett. **80B** (1979) 290.

[287] N. N. Nikolaev, "Quarks in High-energy Interactions of Hadrons, Photons, and Leptons With Nuclei", Sov. Phys. Usp. **24** (1981) 531 [Usp. Fiz. Nauk **134** (1981) 369].

[288] W. Busza, J. E. Elias, D. F. Jacobs, P. A. Swartz, C. C. Young and M. R. Sogard, "Charged Particle Multiplicity in pi- Nucleus Interactions at 100-GeV/c and 175-GeV/c.", Phys. Rev. Lett. **34** (1975) 836.

[289] G. Aad *et al.* [ATLAS Collaboration], "Measurement of the centrality dependence of the charged-particle pseudorapidity distribution in proton-lead collisions at $\sqrt{s_{\rm NN}} = 5.02$ TeV with the ATLAS detector", Eur. Phys. J. C **76** (2016) no.4, 199 [arXiv:1508.00848 [hep-ex]].

[290] P. Christiansen, "Ideas for a data driven model for dN/deta and high pT production in pPb collisions based on pp data", Proton and Photon-induced nuclear collisions at the LHC, 6.07.2016 - 8.07.16, CERN

[291] M. Alvioli, M. Azarkin, B. Blok, M. Strikman. "Revealing minijet dynamics via centrality dependence of the double parton interactions in proton-nucleus interactions", [arXiv:1901.11266].

[292] M. L. Miller, K. Reygers, S. J. Sanders and P. Steinberg, "Glauber modeling in high energy nuclear collisions", Ann. Rev. Nucl. Part. Sci. **57** (2007) 205 [nucl-ex/0701025].

[293] J. C. Collins, "Light cone variables, rapidity and all that", hep-ph/9705393.

[294] M. Galassi et al, "GNU Scientific Library Reference Manual", (3rd Ed.), ISBN 0954612078

[295] G. P. Lepage, "A New Algorithm for Adaptive Multidimensional Integration", J. Comput. Phys. **27** (1978) 192.

[296] A. Buckley, J. Ferrando, S. Lloyd, K. Nordström, B. Page, M. Rüfenacht, M. Schönherr and G. Watt, "LHAPDF6: parton density access in the LHC precision era", Eur. Phys. J. C **75** (2015) 132 [arXiv:1412.7420 [hep-ph]].

[297] J. R. Gaunt, private communications.

[298] A. D. Martin, W. J. Stirling, R. S. Thorne and G. Watt, "Parton distributions for the LHC", Eur. Phys. J. C **63** (2009) 189 [arXiv:0901.0002 [hep-ph]].

[299] S. Dulat *et al.*, "New parton distribution functions from a global analysis of quantum chromodynamics", Phys. Rev. D **93** (2016) no.3, 033006 [arXiv:1506.07443 [hep-ph]].

[300] K. Kovarik *et al.*, "nCTEQ15 - Global analysis of nuclear parton distributions with uncertainties in the CTEQ framework", Phys. Rev. D **93** (2016) no.8, 085037 [arXiv:1509.00792 [hep-ph]].

[301] K. J. Eskola, P. Paakkinen, H. Paukkunen and C. A. Salgado, "EPPS16: Nuclear parton distributions with LHC data", Eur. Phys. J. C **77** (2017) no.3, 163 [arXiv:1612.05741 [hep-ph]].

[302] H. Paukkunen, "Nuclear PDFs Today", arXiv:1811.01976 [hep-ph].

[303] L. Frankfurt and M. Strikman, "Diffraction at HERA, color opacity and nuclear shadowing", Eur. Phys. J. A **5** (1999) 293 [hep-ph/9812322].

[304] D. Binosi and L. Theussl, "JaxoDraw: A Graphical user interface for drawing Feynman diagrams", Comput. Phys. Commun. **161** (2004) 76 [hep-ph/0309015].

[305] J. D. Hunter, "Matplotlib: A 2D Graphics Environment", Comput. Sci. Eng. **9** (2007) no.3, 90.

[306] Travis E, Oliphant, "A guide to NumPy", USA: Trelgol Publishing, (2006).

[307] Jones E, Oliphant E, Peterson P, *et al*, "SciPy: Open Source Scientific Tools for Python".

[308] W. H. Press, B. P. Flannery, S. A. Teukolsky and W. T. Vetterling, "Numerical Recipes in C: The Art of Scientific Computing", 1988, Cambridge University Press, New York, NY, USA.